Faster than Nyquist Transmission over Continuous-Time Channels: Capacity Analysis and Coding

YONG JIN DANIEL KIM

Department of Electrical and Computer Engineering
McGill University
Montréal, Canada

August 2013

A thesis submitted to McGill University in partial fulfillment of the requirements of the degree of Doctor of Philosophy.

Abstract

Future telecommunication systems and infrastructure must support large data rates in order to meet the growing demand for data-intensive multimedia contents and applications. Practical communication systems operate on *continuous-time* bandlimited communication channels, transmitting symbols over such channels at the Nyquist rate that is proportional to the channel bandwidth. Nyquist rate transmission has been traditionally motivated by the simple transmitter and receiver architectures, as it avoids introducing intersymbol-interference (ISI). This dissertation explores the benefits of transmitting data *faster* than the Nyquist rate of the continuous-time bandlimited channel. This alternative data transmission approach has been explored in the literature, but it causes severe intersymbol-interference which makes design of practical communication systems challenging.

The main goal of this work is to quantify the fundamental merits and identify potential applications of the faster than Nyquist (FTN) signaling. Using tools from information theory and channel coding, this dissertation demonstrates that, in some scenarios, systems based on the FTN signaling can have capacity benefits over conventional Nyquist rate systems. First, FTN is shown to have competitive capacity benefits in point-to-point digital communications systems that employ finite-alphabet modulation symbols and practical modulating pulses. Moreover, the concept of FTN signaling is extended to a single-hop network, known as Gaussian broadcast channels, where FTN signaling is proved to be capacity-wise optimal and able to outperform traditional time- or frequency-division broadcasting schemes. Consequently, low-complexity FTN coding architectures are proposed and implemented in order to explore the practical feasibility of achieving this improved capacity. Furthermore, appropriate precoding strategies at the FTN transmitter are derived and shown to enable significant capacity improvements over non-precoded FTN transmission. Overall, presented results indicate that the FTN technology has significant potential for the next generation wireless cellular systems, digital TV broadcasting, and fiber-optic communication networks.

Sommaire

Les systèmes de télécommunication futurs doivent supporter d'importants taux de débit de données afin de répondre à la demande croissante d'applications et contenus à grosse échelle dans le domaine du multimédia. Des systèmes de communication pratiques fonctionnent sur des canaux de communications à bande limitée en temps continu, transmettant des symboles sur ces canaux au taux de Nyquist qui est proportionnel à la largeur du spectre du canal. La transmission de la fréquence de Nyquist a traditionnellement été motivée par l'architecture simple de l'émetteur et du récepteur. Cette thèse explore les avantages de la transmission de données plus rapide que le taux de Nyquist du canal à bande limitée en temps continu. Cette approche alternative pour la transmission de données a été explorée dans la littérature, mais elle provoque une interférence inter-symbole significative qui rend la conception de systèmes de communication difficile en pratique.

L'objectif principal de ce travail est de quantifier les mérites fondamentaux et identifier les applications potentielles pour la signalisation plus rapide que Nyquist (FTN). En utilisant les outils de la théorie de l'information et du codage, la thèse démontre que la signalisation FTN peut avoir des avantages au niveau de la capacité sur les systèmes au taux de Nyquist classiques dans plusieurs scénarios envisagés. Tout d'abord, FTN démontre des avantages de la capacité concurrentielle sur les systèmes de communication classiques point à point numériques qui utilisent un alphabet fini de symboles de modulation et les impulsions pratiques de modulation. En outre, le concept de signalisation FTN est étendu à un réseau à un bond connu sous le nom de canaux à diffusion gaussienne, dans lesquels il est prouvé que la capacité optimale est atteinte et qu'elle surpasse les systèmes traditionnels de la diffusion à temps partagé ou des systèmes par répartition en fréquence. Par conséquent, les architectures de codage FTN à faible complexité sont proposées pour explorer la possibilité d'atteindre cette capacité améliorée à une large gamme d'efficacité spectrale. En outre, les stratégies de précodage appropriées à l'émetteur FTN sont dérivées et de permettre l'amélioration significative des capacités au-delà de la transmission FTN sans précodage. Globalement, les résultats présentés indiquent que FTN a un potentiel important pour les systèmes cellulaires sans fil de prochaine génération, la télédiffusion digitale et les systèmes de communication par fibre optique.

Acknowledgments

First and foremost, I would like to thank Prof. Jan Bajcsy, my Ph.D. advisor, for his excellent mentorship, supervision, and guidance throughout the course of my Ph.D. research. I still remember the day when he approached me and passionately introduced me to the concept of faster than Nyquist signaling (although the terminology was unknown to us at that time). His passion and belief on the research topic have been the main fuel for us to get to this point. This thesis wouldn't have been possible without his continuous support, encouragements, and guidance.

I would like to thank the members of my Ph.D. committee, Prof. Richard Rose and Prof. Dennis Giannacopoulos for their valuable feedback and helpful suggestions over the course of my Ph.D. work. Their alternative viewpoints on my research have greatly helped improving the research and making it more complete. I would also like to express my gratitude to my thesis examiners, Prof. James J. Clark and Prof. Steve Hranilovic, for kindly reviewing this dissertation and finding time in their busy schedules. I would like to also thank my Ph.D. defense committee members, Prof. Ioannis Psaromiligkos, Prof. Sofiène Affes, and Prof. Michael Hilke, for their time and helpful suggestions on my thesis work. I would like to acknowledge generous financial support by the National Science and Engineering Research Council (NSERC), Faculty of Engineering at McGill University, and my advisor that made my Ph.D. work possible.

Simple words cannot fully express all the gratitude and appreciation for my colleagues and friends. For many years, Aminata Garba has been a friend, a mentor, and a role model for me as a Ph.D. I would like to thank Yi Feng for his friendly support over the years and for numerous reviews/suggestions on my research. I would like to also thank Salman Khan for suggestions, Sami El-Dabbagh for French translations on multiple occasions, and Kwame Amoako for helping me plotting the minimum Euclidean distance. I would like to also extend my thanks to Bilal Riaz, Prasad Pisharodi, and Hye Won Suk for being special friends of mine. Special thanks to Bharathram Sivasubramanian for introducing me to the term faster than Nyquist signaling, which became the starting point of my literature search.

Lastly, I would like to thank my parents, brother, sister-in-law, and two lovely nephews for all their love, encouragements, and patience during my time in Montreal. I would like finally to thank Hyeyeon Gong for sharing all the moments together. It is to them I dedicate this thesis.

Table of Contents

List of Figures

List of Tables

Acronyms

AWGN	Additive white Gaussian noise
BCJR	Bahl-Cocke-Jelinek-Raviv
BER	Bit error rate
DEMUX	Demultiplexer
E_b/N_0	Energy-per-bit to noise power spectral density ratio
EXIT	Extrinsic information transfer chart
FDMA	Frequency-division-multiple-access
FPGA	Field-programmable gate array
FTN	Faster than Nyquist
i.i.d.	Independent and identically distributed
i.n.i.d.	Independent and non-identically distributed
ISI	Intersymbol interference
LDPC	Low density parity check
LTI	Linear time-invariant
MAP	Maximum a posteriori
MATLAB	Matrix laboratory
MIMO	Multiple-input-multiple-output
MUX	Multiplexer
OFDM	Orthogonal frequency-division multiplexing
PAM	Pulse amplitude modulation
PAPR	Peak-to-average power ratio
PSD	Power spectral density
PSK	Phase shift keying
$\mathbf{PW}^2$	Paley-Wiener space

QAM	Quadrature amplitude modulation
SINR	Signal to interference plus noise ratio
SISO	Soft-in-soft-out
SNR	Signal-to-noise ratio
VLSI	Very-large-scale integration
WCDMA	Wideband code division multiple access
WSS	Wide-sense stationary

Chapter 1

Introduction

1.1 Developments and Trends in Communication Systems

During the past few decades, various technological innovations in the telecommunication industries have transformed our society. Led by technological breakthroughs such as the Internet, cellular phones, advances in digital signal processing, and emergence of spectrally efficient data communication techniques, we are now constantly connected with peers on the Internet, search daily online for news/information, stream live videos for entertainment, and upload and share personal stories in near real-time.

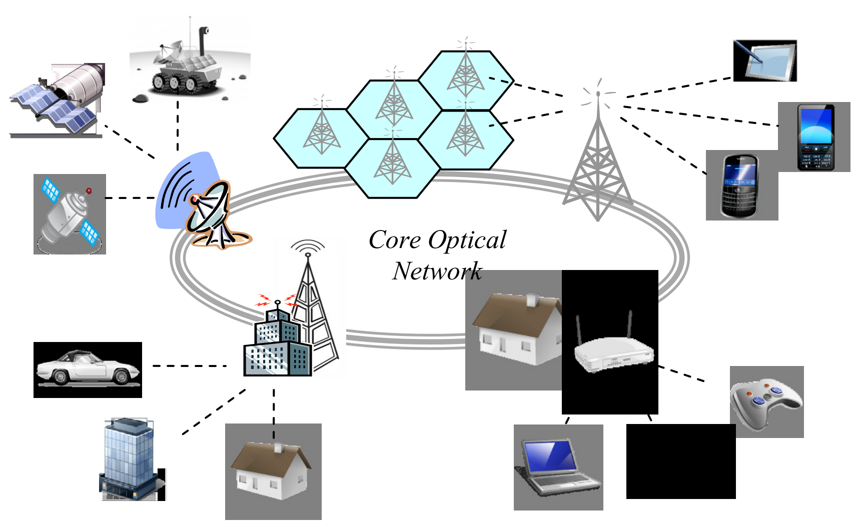

Figure 1.1 **Illustration of today's telecommunication networks; showing that large portion of the "last mile" links are wireless including (clockwise from top) mobile cellular networks, wireless local area networks, radio broadcasting, and satellite links**

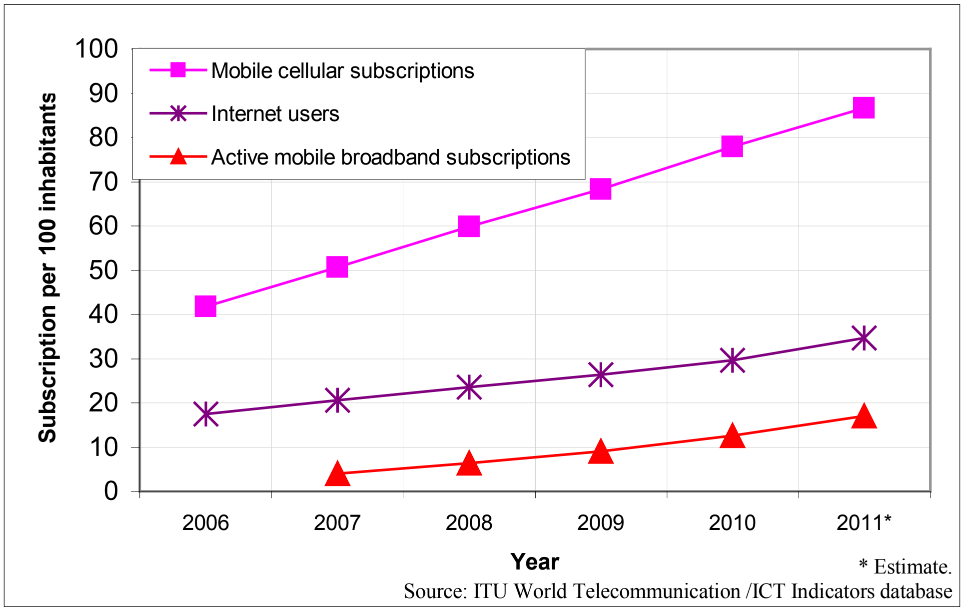

Figure 1.2 Worldwide trend in information and communication technology [68]

One of the major emerging trends in the telecommunications sector is the development of ubiquitous *wireless mobile networks* that provide seamless connectivity to the core network anywhere and at anytime. Figure 1.1 depicts today's telecommunication network infrastructure illustrating that a significant portion of the "last mile" communication is now done over wireless links. As Google also proclaims *"the time for mobile is now"* (2011) [137], the mobile smartphones (e.g., iPhones, Blackberries, Androids, etc.) and tablet computers (e.g., iPads, Galaxy Notes, etc.) caused the recent explosive growth of mobile cellular and broadband subscriptions worldwide. Figure 1.2 shows the fast growth in worldwide broadband penetrations (subscriptions per 100 inhabitants) from 2006 to 2011, showing a startling increase in mobile cellular subscriptions in the recent years. This trend is expected to continue, as evident from recent progress in the emerging markets (most notably China, India, Russia, and Brazil).

A closer look at the types of mobile media that consumers typically access, shown in Figure 1.3, reveals increasing usage of data-intensive contents including, but not limited to, live streaming video or TV, social networking, and web browsing. One of the notable trends in Figure 1.3 is the increase in the real-time entertainment (e.g., Youtube, Netflix,

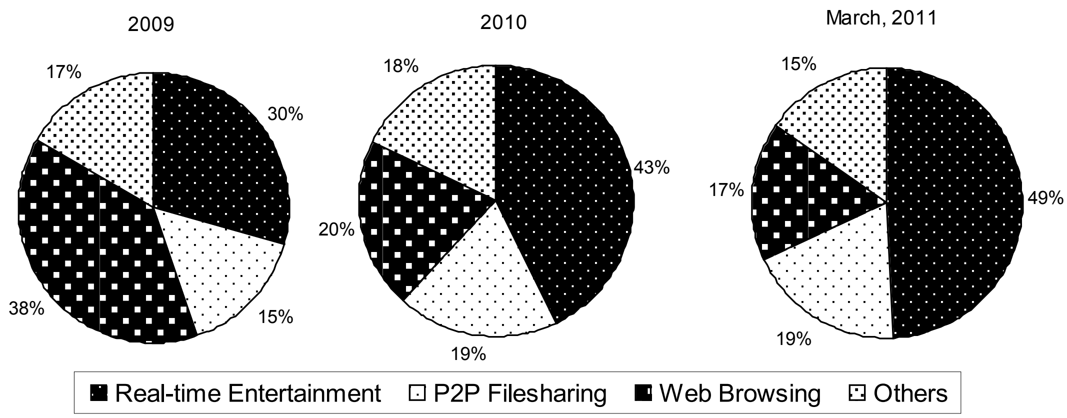

Source: Sandvine Network Demographics

Figure 1.3 Peak period aggregate traffic composition (North America, fixed access); *Real-time Entertainment* refers to applications and protocols that allow "on-demand" entertainment that is consumed (viewed or heard) as it arrives (e.g., Youtube, Netflix, Pandora, PPStream, etc.) [54]

Pandora, etc.) from 30% in 2009 to near 50% in March, 2011, indicating that multimedia contents are beginning to dominate the data traffic in wireless systems and over the Internet.

These data-heavy applications must operate in real-time and can put a heavy traffic load on the wireless networks. Most smartphones and tablet PCs available today already require data rates that exceed the networks' capabilities and, given the chance, "[they] can choke their wireless networks to death" [110]. The wireless service providers now face a grand challenge of making enough spectral resources available to accommodate the fast growing number of data-hungry broadband subscribers.

Currently, many wireless and Internet service providers are proposing ambitious plans in offering order-of-magnitude increase in the data rates. For instance, the so-called 'pre-4G' networks using Long Term Evolution (LTE) technology promise peak download rates of 100 Mb/s [140], which is more than 100 times faster than the rates of some of the early third generation (3G) standards. The proposed technologies that should enable this enormous capacity increase include multiple-antenna technology (MIMO), advanced coding and multiplexing, and addition of infrastructure to improve coverage and signal quality.

Even with these promising technologies, however, the offered data rates are still far short of the IMT-Advanced (International Mobile Telecommunications-Advanced) requirements of 1 Gb/s for stationary user in a cell for the true fourth generation (4G) systems [121]. Furthermore, due to the proliferation of mobile devices and rapidly growing wireless applications [137], the offered data rates may not keep up with the exploding customer demands on the multimedia communications in the near future. Consequently, major global telecommunication companies are already in the process of developing fifth generation (5G) wireless cellular systems [44] and the innovative technologies that can further offer order of magnitude higher spectrum utilization are keenly anticipated by researchers and industries alike.

1.2 Traditional Digital Communication Systems

Initially, the digital communication systems had been severely constrained by limited memory, available hardware capabilities and coding techniques. Recent advancements in both hardware capabilities and communication systems theory are driving the need for more spectrally efficient communication techniques beyond traditional digital communication systems.

1.2.1 Recent Advancements in Memory, Hardware and Coding

The wireless spectrum has become a premium commodity due to its increasing scarcity, while thanks to the recent advancements in the silicon technology, the memory and signal processing units have become inexpensive and abundant in quantities. For instance, the number of transistors on integrated circuit has been observed to be doubling in every 18 months − the phenomenon also known as the Moore’s law [103]. In addition, the density of the memory storage has been observed to be increasing even at a faster rate − known as the Kryder’s law [157]. Consequently, we now have significantly more hardware processing power in a small handheld device (e.g., a smartphone) than in some of the bulky supercomputers used in early 1970s. Today, this available data and signal processing ability allows us to practically implement advanced error-correcting-codes that were too complex to build earlier.

The advancements in error-control-coding also amend limited energy storage capabilities of mobile devices. It has been observed that battery technologies have not kept pace with the exponential increase in the processing abilities [4]. Using better error-control-coding techniques, the mobile devices can reduce power consumptions required for communications at a given data rate. The saved battery power can readily be used for a wide array of other applications and leads to increased lifespan of mobile devices.

Moreover, there have been significant developments in the fields of information theory and coding in the recent years. Since Shannon's landmark information theory paper in 1948 [132], channel capacity has become a practical benchmark for reliable communications over many practical bandlimited communication channels. However, it was only after 40 years since the birth of the information theory when practical error-correcting-codes including Turbo codes and the low density parity check (LDPC) codes were designed to perform close to the capacity limits of practical channels [47]. These advances in the information theory and coding techniques have not only drastically improved the practical performances of digital communication systems, but have also established the channel capacity limit as one of the key benchmarks in communication system performance.

1.2.2 Nyquist Rate Modulation and Demodulation

The common assumptions made on the modern digital communication systems stem from the pioneering works of Nyquist in 1924 and 1928 [105], [106], who formulated a general baseband model for data transmission over continuous-time bandlimited channel. In particular, one can express the baseband transmission signal by

$$x(t) = \sum_{n \in \mathbb{Z}} x[n] s(t - nT), \tag{1.1}$$

where $x(t)$ is a continuous-time baseband signal to be transmitted over the communication channel and $\{x[n]\}$ are modulation symbols (or information) mapped onto continuous-time

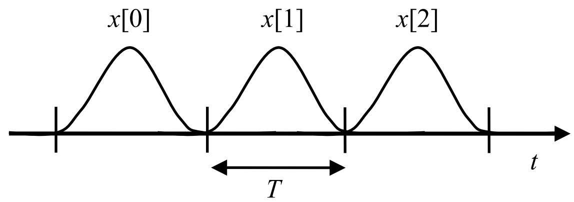

Figure 1.4 **Conceptual illustration of traditional Nyquist rate signaling without intersymbol interference between modulation symbols $\{x[n]\}$**

modulating pulses …, $s(t+T)$, $s(t)$, $s(t-T)$, $s(t-2T)$, … that are assumed to be bandlimited to W Hertz. The model in (1.1) also has an interpretation of sending information carrying pulses at every T seconds as illustrated in Figure 1.4. We note that these pulses may significantly overlap in time, as long as they remain orthogonal to one another.

Nyquist showed that the maximal signaling rate $1/T$, such that the pulses do not cause intersymbol interference (ISI) over a bandlimited communication channel with a bandwidth W Hertz, is given by $2W$ pulses per second. This so-called *Nyquist rate signaling* of $2W$ symbols per second is now the de-facto standard in the modern communication systems − motivated mainly by the simple receiver architecture based on a matched filter and a sampler [163], [13]. The receiver front-end is commonly equipped with a matched filter, that is matched to the modulation pulse shape, followed by a Nyquist rate sampler, which are known to maximize the received signal-to-noise ratio (SNR) in the additive white Gaussian noise (AWGN) channel. Most current digital communication systems are built with these assumptions of the Nyquist rate signaling at the transmitter and the Nyquist rate sampling at the receiver.[1]

1.3 Faster than Nyquist Rate Transmission

Following Nyquist's work on zero-ISI transmission over bandlimited channels, many researchers (notably from the Bell Labs) have contemplated whether signaling *faster* than

[1] The Nyquist rate signaling may be considered as a dual of the Nyquist sampling theorem (also named after Whittaker [161], Shannon [133], or Kotel'nikov [89] in different literatures). The Nyquist sampling theorem states that any continuous-time signal with bandwidth W Hertz is completely determined by an infinite sequence of its samples spaced $1/(2W)$ seconds apart, i.e., the Nyquist rate samples (see also [70] for a tutorial review). Albeit intricately related, we note that the Nyquist rate *sampling* and the Nyquist rate *signaling* are two separate concepts, where the latter deals with communication over a bandlimited channel.

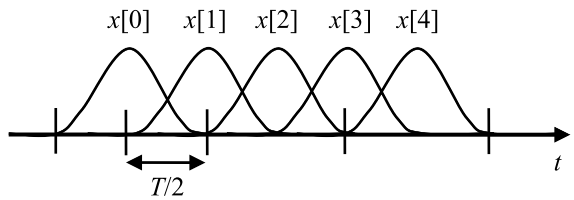

Figure 1.5 **Conceptual illustration of faster than Nyquist rate signaling with its inherent intersymbol interference between transmitted symbols in a continuous-time bandlimited channel**

the channel Nyquist rate has any practical merit. (This approach is conceptually shown in Figure 1.5. Note that the overlapped pulses are no longer orthogonal in FTN.) The question of whether *faster-than-Nyquist rate signaling* has any merit beyond the Nyquist rate signaling has been pondering many communication engineers for years, as it is evident from some of the early references, including papers by Landau [91], Saltzberg [129], Lucky [98], Mazo [99], Salz [130], Foschini [49] and others. However, this topic has not received a widespread attention in the literature and practical systems until very recently. The key problem can be mainly attributed to the complex processing necessary to deal with the cumbersome intersymbol-interference (ISI) [49] − a byproduct of the faster than Nyquist transmission.

Today, due to the escalating cost of wireless bandwidth and declining cost of memory and processing units, the importance of spectral efficiency of communication far outweighs the amount of processing required. Furthermore, recent advances in memory and hardware capabilities allow us to implement some of the powerful equalization and coding techniques that can practically deal with the severe ISI. Consequently, we are now in a perfect position to revisit the concept of faster than Nyquist transmission as a potential method to trading processing complexity for improved spectral efficiency.

1.4 Thesis Contributions and Structure

This dissertation is motivated by the following long-standing open question in digital communications: *What are the practical merits of faster than Nyquist* (*FTN*) *signaling in continuous-time bandlimited channels*? In order for the FTN signaling to have any competitive advantages over the conventional below-Nyquist rate signaling, the benefit of data rate increase beyond the Nyquist rate must outweigh potential information loss incurred by FTN-induced ISI. The goal of this dissertation is to study the FTN signaling with a strong emphasis on the information theoretic analysis of FTN in various channel setups. The information theoretic tools allow us to analyze the *channel capacity* of the FTN signaling, which shows the maximal rate of information transfer at which reliable recovery after the channel is possible. Subsequently, the dissertation focuses on coding designs that allow practically approaching the FTN capacity limits. Finally, the potential merits of FTN signaling over various communication channels will be identified with consideration of practicality, and potential applications of FTN are also presented.

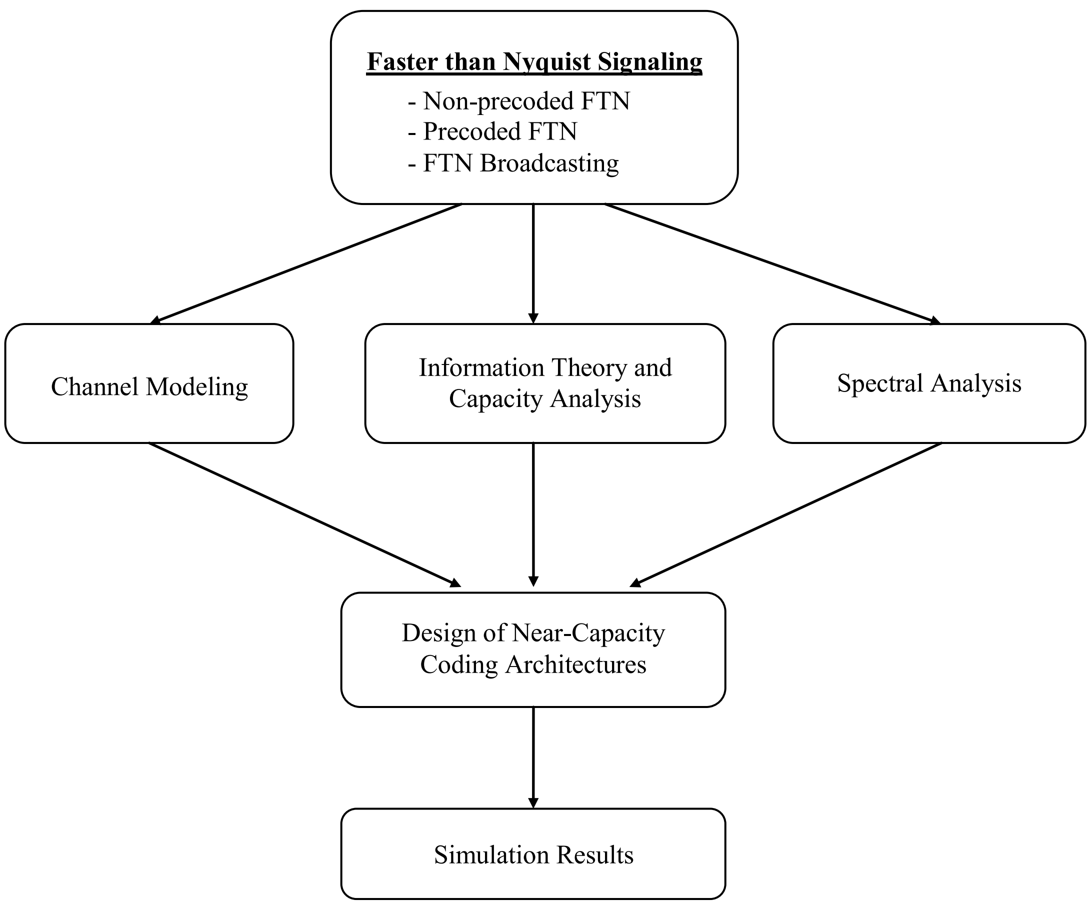

Figure 1.6 Concept map of this dissertation

The main contributions of this dissertation work are described below [2] and, for convenience, a concept map of this thesis is presented in Figure 1.6:

1. ***FTN Channel Models, Power Constraints and Spectral Analysis:***
   - Discrete-time channel models of general FTN signaling (precoded and non-precoded with generalized waveforms) are formulated, highlighting all underlying assumptions.
   - FTN power transmission constraint is derived for the first time to allow proper assessment of the transmission power for non-*i.i.d.* (precoded) FTN signals.
   - The power spectral density (PSD) of FTN signals is analytically derived for non-*i.i.d.* (pre-coded) FTN signals, showing potential increase in transmission bandwidth.
2. ***FTN Channel Capacity Analysis:***
   - The channel capacity of non-precoded FTN signaling is derived (for the first time) for independent non-identically distributed (*i.n.i.d.*) FTN signals.
   - Channel capacity of previously considered convolutionally precoded FTN signaling is derived for the first time.
   - A closed-form capacity expression and capacity-wise optimal precoding are derived for FTN signaling. This highlights the benefit of precoding in the FTN systems and reveals the information theoretic potential of FTN signaling,
   - FTN channel capacity analysis is extended to linear time-invariant Gaussian channels, showing that the capacity admits the classical water-filling solution.
3. ***FTN Broadcasting:***
   - A novel concept of FTN broadcasting is proposed for the first time, extending the concept of the FTN signaling to a single-hop network setting.
   - The corresponding channel capacity region is derived for FTN broadcasting which can achieve the capacity boundaries of Gaussian broadcast channel.
4. ***Design and Simulation of Coded FTN Systems with Near-Capacity Performance:***
   - A low-complexity iterative receiver is designed for non-precoded FTN signaling using Gaussian approximation and successive cancellation of the FTN-induced ISI.[3]
   - Two FTN broadcasting transceiver architectures are proposed and shown to perform close to the capacity boundaries of the Gaussian broadcast channel.

---

[2] Please note that this work has been published in [74]-[85] and is being prepared for publication in [86],[87].

[3] This design alleviates the use of any complex equalizer and hence offers significant complexity savings at high spectral efficiencies, when compared to the prior coded FTN system receivers in the literature.

The rest of the dissertation is structured as follows. Chapter 2 provides a chronological literature survey of the FTN signaling followed by an overview of important concepts, results and techniques in information theory, coding, and matrix algebra that will be useful in studying the FTN signaling. Chapter 3 describes the discrete-time channel models, their properties, and spectral analysis of the FTN signaling. In Chapter 4, the capacity analysis of non-precoded FTN signaling is derived, followed by a design and simulation of a low-complexity near-capacity coded FTN system. Chapter 5 presents capacity analysis of precoded FTN signaling and highlights merits of data precoding in FTN systems. In Chapter 6, a novel concept of FTN broadcasting is introduced along with the development of FTN-based transceiver architectures for the broadcast channel communications. Finally, Chapter 7 provides a summary of research achievements and directions for future work.

Chapter 2

Preliminaries

The main objective of this chapter is to provide preliminary background and relevant techniques for studying faster than Nyquist (FTN) signaling. First in section 2.1, a chronological literature survey on the FTN signaling is given, starting from the early developments to the current state-of-the-art. Several relevant concepts from the information theory are then reviewed in section 2.2 as well as some of the results from the coding theory in section 2.3 (especially on the maximum a posteriori (MAP) symbol detection for intersymbol interference (ISI) channels and the Turbo coding). In section 2.4, selected results from matrix algebra are reviewed as these will be useful in the later chapters. The study of the FTN signaling cannot be complete without a proper review of the Nyquist theorem and we revisit the concept and provide a simple proof in section 2.5. In addition, the definitions of continuous-time channel bandwidth and the power spectral density are carefully reviewed in section 2.5. Finally, section 2.6 gives a useful insight into the FTN signaling by introducing the concept of signaling dimensions for FTN.

2.1 Review of Past Literature on Faster than Nyquist Signaling

The faster than Nyquist rate transmission makes its first appearance in the literature in the mid 1960s. Despite its 50 year history, there seems to be only handful number of papers regarding on the FTN transmission up until very recently. In this section, this literature is classified in three chronological periods, and the general theme of research in each period is highlighted. The focus will be placed exclusively on the *data transmission problem* when the signaling rate exceeds the Nyquist rate of the bandlimited continuous channel.

Early Days of FTN (1960s ~ 1985):

The research in this early telecommunication era was mainly motivated by the Bell Labs' interests with the possibility of transmitting faster than the Nyquist rate of a band-limited communication channel, for better utilization of their communication infrastructure. However, a general conclusion was that minor benefit of FTN exists for practical usage. The reason was that the equalization techniques available at the time could not sufficiently deal with the inter-symbol interference (ISI) once the transmission rate becomes significantly faster than the Nyquist rate.

To the best of our knowledge, first published reference on FTN dates back to 1965, when Tufts, of Harvard University, extended Nyquist's pulse transmission results and showed that "it is possible to transmit a *finite* sequence of real numbers at an arbitrarily high rate through any linear, time invariant, *noiseless* transmission medium" [149]. As for noisy channels, Tufts derived an analytical framework for designing minimum mean square error equalization for his FTN scheme, but its use was limited to transmission of very short burst of pulses and he did not consider any error-control-coding. In 1967, Landau from Bell Labs defined a concept of *stable sampling* and argued that "data cannot be transmitted as (stable) samples at a rate higher than the Nyquist" [91]. Tufts soon challenged Landau's claim in 1968 by arguing that "it is possible to transmit any finite number of data elements at rates faster than the Nyquist rate" [150]. On the other hand, Saltzberg in 1968 attempted reducing the channel bandwidth below the Nyquist band (hence simulating an effective FTN transmission) and observed that "the system bandwidth can be reduced slightly below the Nyquist band without catastrophic results" [129].

In 1970, Lucky from Bell Labs argued in his short paper [98] that despite advances in equalization, ISI caused by FTN signaling cannot be sufficiently removed by decision feedback equalization (which was relatively new in communications at the time) to guarantee any practical merit to FTN. In 1973, Salz also from Bell Labs analyzed mean-square decision feedback equalizers and, as a special case, considered such equalizers for FTN transmission [130]. However, he concluded that FTN transmission causes increased mean-square error after the decision feedback equalizer, thus worsening the overall communication system performance.

It was only in 1975, when the first significant result appeared on the FTN transmission. In his landmark paper [99], Mazo from Bell Labs showed for the first time that the *minimum Euclidean distance*[4] can be preserved even when the signaling rate exceeds the Nyquist rate by up to 25% (see Figure 2.1).

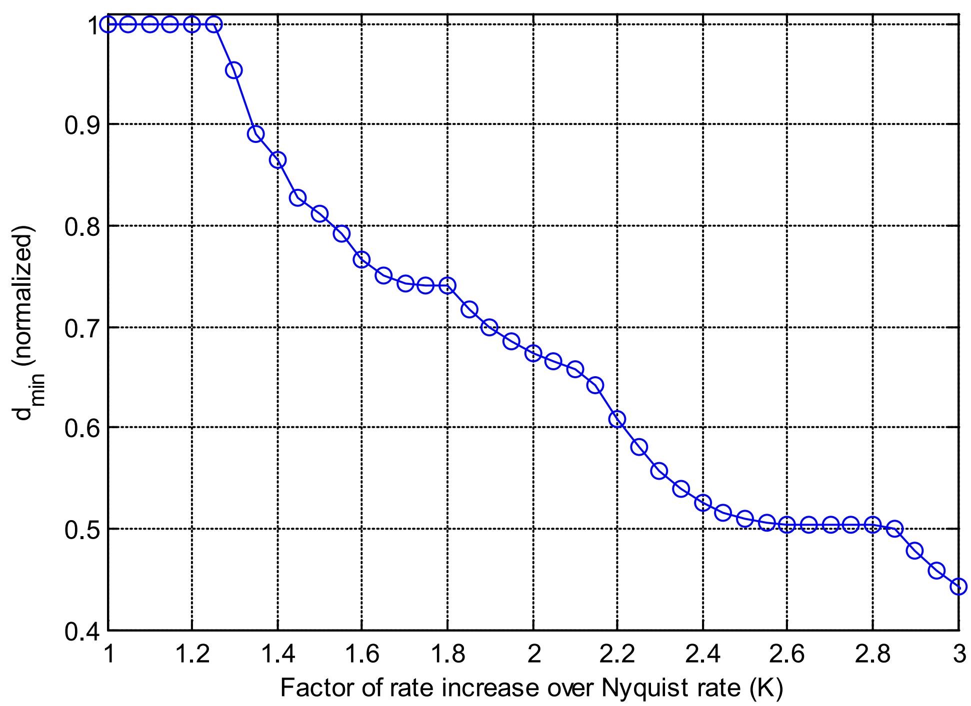

Figure 2.1 Normalized minimum Euclidean distance of FTN signaling with increasing signaling rates; Note that the minimum Euclidean distance stays constant until *K* = 1.25 (i.e., 25% faster than the Nyquist rate)

Considering that the minimum Euclidean distance is one of the important metrics for measuring performance of communication systems, Mazo's findings seemed to imply that FTN transmission can increase the rate of communication up to 25% without incurring any

[4] Euclidean distance between two signals is defined as $\int|s_a(t) - s_b(t)|^2 dt$. It is closely related to the probability of mistaking transmitted singal $s_a(t)$ for some other signal $s_b(t)$.

loss in the communication performance.[5] Mazo's paper, however, focused little on transceiver architecture and considered only the idealized *sinc*-type modulating pulses[6]. Also, channel capacity, rather than the minimum Eucldean distance, becomes a more relavant metric for measuring communication performance when advanced error-control-coding techniques such as Turbo codes and LDPC codes are used as in the 3G and 4G wireless standards. Nevertheless, Mazo's work opened the door and spurred much of the later research in this direction, as highlighted in the next chronological period.

On the other hand, Foschini in 1984 conducted for the first time a thorough feasibility study and comparative analysis on the FTN signaling with standard quadrature amplitude modulation (QAM) techniques [49]. His conclusion was that FTN signaling using binary symbols offers only minor gains over QAM, mainly due to the significant spectral sidelobes inherent in FTN signaling and the large implementation complexity of the ISI equalizer. The comparisons were made by using pulses that maximize the minimum Euclidean distance under some constraints in complexity and out-of-band energy (OBE). Foschini's work, however, was limited to FTN signaling using only binary symbols and this was compared to the high-level QAM techniques [45]. Furthermore, Foschini briefly mentions at the end of his paper that one "cannot dismiss (FTN signaling using *multi-level symbols*)" and "(such) systems may have some value (over QAM)" [49].

Marked by the paper by Foschini, the once looming curiosity over the FTN signaling within Bell Labs seems to be put to an end, as most of the authors have moved on to different research topics. Mazo, on the other hand, motivated by independent work by Hajela [59]-[63], has followed up on his work with a joint paper along with Landau in 1988 [100], but did not seem to publish any further results on the FTN signaling.

[5] For example, the error probability of M-ary signaling on additive white Gaussian noise (AWGN) channels can be tightly upper-bounded by a function of minimum Euclidean distance in high signal-to-noise ratio (SNR). In addition, the error probability of a maximum-likelihood sequence estimator (MLSE) in high SNR is closely related to the minimum Euclidean distance between signal sequences or codewords [155].

[6] sinc(t) is defined as $\sin(\pi t)/(\pi t)$. They are strictly bandlimited in the frequency domain.

Later Days of FTN (mid 1980s ~ early 2000s):

While the genuine interests in the FTN signaling seemed to have faded within Bell Labs by mid 1980's, other researchers subsequently have picked up the topic and started contributing in different ways. The main direction of the research in this chronological period had been in extending Mazo's work on the minimum Euclidean distance calculation while using more practical modulating pulses. In addition, more practical system designs incorporating advanced channel coding techniques were proposed, showing that ISI resulting from FTN signaling can be effectively removed in practice (this addressed the concerns raised by Lucky [98], Salz [130], and Foschini [49]). Unfortunately, papers in this period appear very sparsely from various independent groups and most of these groups did not seem to follow up on their work after their initial publication.

Mazo's work on the invariance of minimum Euclidean distance up to 25% above the Nyquist rate was first made mathematically rigorous by Hajela, who published a series of papers on the topic between 1987-1992 [59]-[63]. Hajela's main contributions were first mathematically formulating the problem of finding minimum Euclidean distance (of FTN signaling using *sinc* pulses), and then showing that about 25% above Nyquist rate, as shown numerically by Mazo, is indeed the best possible result. Liveris and Georghiades in 2003 [96] subsequently extended Mazo's minimum distance analysis from the *sinc* pulses to more practical raised cosine pulses, and showed numerically that similar rate increase is possible (although less than 25%).

Aside from the theoretical work, practical pulses and coding designs were also proposed by various authors. In 1995, Wang and Lee [158] proposed a 5-step iterative procedure to modify realizable FTN transmit filter response (equivalently, modulating pulse) in order to increase the minimum Euclidean distance in a multi-level FTN[7]. In addition, they proposed using approximate whitened matched filter at the receiving front-end followed by an adaptive Viterbi algorithm to combat ISI, although no simulation results were reported. On the other hand, Liveris and Georghiades in 2003 [96] designed constrained coding to keep minimum Euclidean distance constant for higher signaling

[7] Unfortunately, some key technical flaws in [158] were later pointed out by Rusek and Anderson [126].

rates, at the expense of small rate loss, and also considered iterative Turbo equalization. Their simulation results show that, using advanced coding and equalizers, ISI resulting from FTN signaling can be effectively removed in practice. Their FTN coding system, however, still performed many decibels away from the capacity limit of the FTN signaling.

The concept of faster than Nyquist signaling has also inspired some other notable designs. For instance, the pulse-code modulation (PCM) modem of the International Telecommunications Union (ITU)-T V.92 Recommendations (which specifies the government approved protocols for modem communications over telephone networks) employs signaling slightly faster than the Nyquist rate of the channel bandwidth (see e.g., [147], [9], [8], [93]). Strictly speaking, however, the V.92 modem is not an FTN system as it only signals 7 out of 8 time slots, keeping the overall symbol rate less than the Nyquist rate. Furthermore, Wu and Feher in 1985 [164] used a transmit filter with cutoff frequency slightly below the Nyquist frequency to achieve a similar effect as the FTN signaling, and reported 3% rate increase above the Nyquist rate with 0.4 dB degradation in performance.

Recent FTN Work (mid 2000s ~ present):

The recent research activities in the FTN signaling have been driven strongly by the escalating cost of channel bandwidth and declining cost of memory and processing units. Furthermore, due to the advances in precoding and equalization techniques allowing practical reduction of FTN-caused intersymbol interference, the FTN signaling is now being considered as a method of trading processing complexity for potential of improving spectral efficiency. Recently, the concept of FTN signaling has been extended to multicarrier communication systems based on the orthogonal frequency-division multiplexing (OFDM) technology, long-haul fiber-optic communication links, and underwater acoustic channels. The FTN signaling is currently a vibrant on-going research area with many open problems and potentials for improvements.

Considerate amounts of the research in the past decade have been made by Rusek and Anderson from Lund University in Sweden, initially as a part of Rusek's Ph. D. thesis work [122]. They (recently with some other collaborators) have taken up various approaches to examine the FTN signaling in a great detail, including analysis of constrained channel capacity, extension of FTN to frequency dimension, design of practical coding systems, and more recently, implementation on FPGA hardware.

Most notably, in 2009, Rusek and Anderson have analyzed the capacity of FTN signaling when the modulation symbols are constrained to be independent and identically distributed (*i.i.d.*) [127]. They showed that the capacity of the *i.i.d.* FTN signaling can be greater than that of traditional orthogonal signaling, but this capacity gain comes from using excess transmission bandwidth (if available). That is, when the modulating pulse is strictly bandlimited, the FTN capacity reduces back to the Shannon capacity of continuous-time bandlimited channel for their FTN transmission approach. Also, their *i.i.d.* FTN transmission prohibits any type of precoding since it introduces symbol correlations, although precoding has been used in coded FTN systems.

In [123], [124], [128], Rusek and Anderson extended the FTN concept to two dimensions, in time and frequency as illustrated in Figure 2.2, similar to the non-orthogonal frequency division multiplexing. Furthermore, they generalized Mazo's work on the invariance of minimum Euclidean distance of FTN signaling to the two dimensions in time and frequency for root-raised cosine pulses and Gaussian pulses. Their simulation results showed that the two-dimensional FTN can achieve the same error performance as the conventional OFDM at high SNR, while using only half of the time-bandwidth product of OFDM. This work showed that the concept of FTN can be potentially used to improve the conventional OFDM, which is the backbone technology for the upcoming 4G wireless networks.

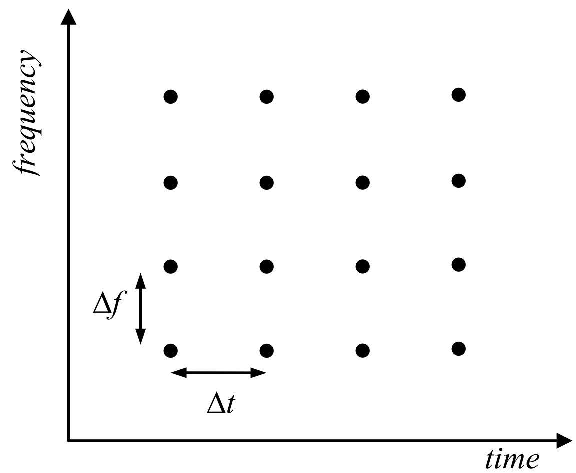

Figure 2.2 Two dimensional FTN signaling in time and frequency; Dots represent locations of modulating pulses in the time-frequency plane that are separated by Δt and Δf

Rusek and Anderson (with other collaborators) also conducted a significant amount of research on the design of practical coding systems (see e.g., [112], [125], [126] and the references therein). In one design [112], they considered FTN transmitters using the root-raised cosine pulse and rate one recursive convolutional precoder. The FTN receivers were based on the Turbo equalization using the BCJR decoders. In addition, they used extrinsic information transfer (EXIT) chart analysis [144] to study the convergence of their Turbo equalizers. The overall system performed around 0.5dB away from the Shannon capacity limit on the additive white Gaussian noise (AWGN) channel in the low SNR regime. Furthermore, their FTN transceiver architecture was recently synthesized in both 65nm complementary metal-oxide-semiconductor (CMOS) and field-programmable gate array (FPGA), thus demonstrating that FTN systems can be efficiently implemented in practice (see e.g., [32]-[34]).

In the last decade, the topic of FTN signaling has also been considered by many other researchers. For instance, the FTN signaling has been considered in long-haul fiber-optic communication links as a means to increase the spectral efficiency without having to use high-order modulation formats (see e.g., [136], [25], [22], [94]). In particular, Colavolpe et al. in 2011 [25] proposed using the FTN signaling with low-order modulation symbols in optical transmission, as opposed to using traditional Nyquist-rate signaling with higher-order modulation formats. Their claim was that FTN signaling using low-order modulation can be more robust against the optical nonlinearities. Also, non-orthogonal multicarrier modulation techniques, which are similar to the two-dimensional (time-and-frequency) FTN signaling, have been considered in the literature (see e.g., Spectrally-Efficient FDM [118], [73], [69], High Compaction Multicarrier-Communication [64], Overlapped FDM [71], and Weyl-Heisenberg frame transmission [65]). These techniques commonly aim to increase the spectral efficiencies of the multicarrier systems via reduced spacing between the modulating pulses in time and/or in frequency.

In addition, Yoo and Cho in 2010 [165] proved that the FTN signaling using binary modulation symbols can achieve the capacity of *i.i.d.* Gaussian FTN signaling as signaling rates tends to infinity. This work implies that the binary FTN can be asymptotically optimal in the capacity sense when compared to Nyquist rate signaling using Gaussian-distributed modulation symbols. On the other hand, Erez, Wornell, and Trott in 2004 [43] used the concept of FTN to design low-complexity rateless coding for the case when the transmitter does not know when the decoding will begin. Their FTN rateless coding scheme was recently considered in underwater acoustic channel transmission [42], [43]. Furthermore, McGuire and Sima in 2010 [101] reformulated the discrete-time channel model for FTN signaling, for the purpose of designing a low-complexity FTN receiver. Their simulation results indicate that the FTN receiver can achieve ISI-free performance at high SNR − a result that is consistent with the Mazo's result on the minimum Euclidean distance of the FTN signaling. All these recent vibrant research developments indicate that there is now a growing interest in the topic of FTN signaling and its potentials are beginning to be recognized in the research community.

2.2 Selected Information Theory Concepts

Selected concepts from the information theory are reviewed in this section. Subsection 2.2.1 reviews definitions and properties of Gaussian vector, entropy, and mutual information, while subsection 2.2.2 reviews selected capacity results of additive Gaussian channels. These concepts will be used in the capacity analysis of FTN signaling from Chapter 4 to Chapter 6.

2.2.1 Gaussian Vector, Entropy, and Mutual Information

Some relevant definitions and lemmas are first given in the following.

Definition 2.1 (Complex multivariate Gaussian vector): *An n-by-*1 *complex random vector* $\mathbf{z} \equiv \mathbf{x} + i\mathbf{y} \in \mathbb{C}^n$, *is said to be Gaussian distributed if the real n-by-*1 *vectors* $\mathbf{x}$ *and* $\mathbf{y}$ *are jointly Gaussian.*

Definition 2.2 (Circularly symmetric complex multivariate Gaussian vector): *The complex Gaussian vector* $\mathbf{z}$ *is further said to be circularly symmetric if the real random vector* $\tilde{\mathbf{z}} \equiv [\mathbf{x}^T, \mathbf{y}^T]^T \in \mathbb{R}^{2n}$ *has covariance matrix of the form*

$$E\left\{\left(\tilde{\mathbf{z}} - E\{\tilde{\mathbf{z}}\}\right)\left(\tilde{\mathbf{z}} - E\{\tilde{\mathbf{z}}\}\right)^{\dagger}\right\} = \frac{1}{2}\begin{bmatrix} \Re e\left(K_z\right) & -\Im m\left(K_z\right) \\ \Im m\left(K_z\right) & \Re e\left(K_z\right) \end{bmatrix}, \tag{2.1}$$

where K_z *is the covariance matrix of* $\mathbf{z}$ *and the superscript* $(\cdot)^{\dagger}$ *denotes the complex conjugate transpose operator (also called the Hermitian operator). The circularly symmetric complex Gaussian vector is completely characterized by its mean* $\boldsymbol{\mu}$ *and covariance* K_z, *and its probability density function is given [162] by*[8]

$$f\left(\mathbf{z}\right) = \frac{\pi^{-n}}{\det K_z} \exp\left(-\left(\mathbf{z} - \boldsymbol{\mu}\right)^{\dagger} K_z^{-1}\left(\mathbf{z} - \boldsymbol{\mu}\right)\right). \tag{2.2}$$

Lemma 2.1 (Affine transformation of Gaussian): *If* $\mathbf{z}$ *is circularly symmetric complex Gaussian with mean* $\boldsymbol{\mu}$ *and covariance* K_z, *then any affine transformation* $A\mathbf{z} + \mathbf{b}$ *results in another circularly-symmetric complex random vector with mean* $A\boldsymbol{\mu} + \mathbf{b}$ *and covariance matrix* $AK_zA^{\dagger}$.

Proof: By the linearity of the expectation, $E\{A\mathbf{z} + \mathbf{b}\} = A\boldsymbol{\mu} + \mathbf{b}$. Also by the definition of the covariance matrix,

[8] Note that the covariance matrix K_z is nonnegative definite and may not be always invertible. In such a case, the probability distribution (2.2) cannot be used as K_z^{-1} is undefined and $\det(K_z) = 0$. A more general definition of circularly symmetric multivariate Gaussian can be used in that case (see e.g., [115]), but we do not consider such generalizations here since it would unnecessarily complicate the following analysis.

$$K_{Az+b} \equiv E\left\{(A\mathbf{z}+\mathbf{b}-E\{A\mathbf{z}+\mathbf{b}\})(A\mathbf{z}+\mathbf{b}-E\{A\mathbf{z}+\mathbf{b}\})^{\dagger}\right\} \tag{2.3}$$

$$= E\left\{A(\mathbf{z}-\boldsymbol{\mu})(\mathbf{z}-\boldsymbol{\mu})^{\dagger} A^{\dagger}\right\} \tag{2.4}$$

$$= A \cdot E\left\{(\mathbf{z}-\boldsymbol{\mu})(\mathbf{z}-\boldsymbol{\mu})^{\dagger}\right\} \cdot A^{\dagger} = AK_{z}A^{\dagger}, \tag{2.5}$$

where (2.5) is due to the matrix A being deterministic (i.e., non-random). This completes the proof of Lemma 2.1. ■

Next some information theoretic quantities and results are introduced as they will be used throughout this dissertation. We use base 2 logarithms to express the following quantities in bits.

Definition 2.3 (Differential entropy): *The differential entropy* $h(\mathbf{x})$ *of a continuous random vector* $\mathbf{x} = [x[0], x[1], \cdots, x[n-1]]^T$ *with joint probability density function* $p(\mathbf{x})$ = $p(x[0], x[1], \cdots, x[n\text{-}1])$ *is defined as*

$$h(\mathbf{x}) \equiv -\int p(\mathbf{x}) \log_2 p(\mathbf{x})\, d\mathbf{x}. \tag{2.6}$$

Definition 2.4 (Conditional differential entropy): *If continuous random vectors* $\mathbf{x}$ *and* $\mathbf{y}$ *have a joint density function* $p(\mathbf{x},\mathbf{y})$*, the conditional differential entropy* $h(\mathbf{x}|\mathbf{y})$ *is defined as*

$$h(\mathbf{x}|\mathbf{y}) \equiv -\int\int p(\mathbf{x},\mathbf{y}) \log_2 p(\mathbf{x}|\mathbf{y})\, d\mathbf{x}d\mathbf{y}. \tag{2.7}$$

Definition 2.5 (Mutual information): *The mutual information between random vectors* $\mathbf{x} = [x[0], x[1], \cdots, x[n-1]]^T$ *and* $\mathbf{y} = [y[0], y[1], \cdots, y[m-1]]^T$ *is the relative entropy between their joint distribution and the product of distributions* $p(\mathbf{x})p(\mathbf{y})$ *and is defined as:*

$$I(\mathbf{x};\mathbf{y}) \equiv \int\int p(\mathbf{x},\mathbf{y}) \log_2 \frac{p(\mathbf{x},\mathbf{y})}{p(\mathbf{x})\,p(\mathbf{y})}\, d\mathbf{x}d\mathbf{y} \tag{2.8}$$

$$= h(\mathbf{y}) - h(\mathbf{y}|\mathbf{x}) = h(\mathbf{x}) - h(\mathbf{x}|\mathbf{y}) = I(\mathbf{y};\mathbf{x}). \tag{2.9}$$

Definition 2.6 (Conditional mutual information): *The mutual information between two random vectors* $\mathbf{x} = [x[0], x[1], \cdots, x[n-1]]^T$ *and* $\mathbf{y} = [y[0], y[1], \cdots, y[m-1]]^T$ *when conditioned on another random vector* $\mathbf{z} = [z[0], z[1], \cdots, z[l-1]]^T$ *is defined as:*

$$I(\mathbf{x};\mathbf{y}|\mathbf{z}) \equiv \int\int\int p(\mathbf{x},\mathbf{y},\mathbf{z}) \log_2 \frac{p(\mathbf{x},\mathbf{y}|\mathbf{z})}{p(\mathbf{x}|\mathbf{z})\, p(\mathbf{y}|\mathbf{z})} d\mathbf{x} d\mathbf{y} d\mathbf{z} \tag{2.10}$$

$$= h(\mathbf{x}|\mathbf{z}) - h(\mathbf{x}|\mathbf{y},\mathbf{z}) = h(\mathbf{y}|\mathbf{z}) - h(\mathbf{y}|\mathbf{x},\mathbf{z}) = I(\mathbf{y};\mathbf{x}|\mathbf{z}), \tag{2.11}$$

when the joint probability distribution $p(\mathbf{x},\mathbf{y},\mathbf{z})$ *and conditional probability distribution* $p(\mathbf{x}|\mathbf{z})$, $p(\mathbf{y}|\mathbf{z})$, *etc. are well defined.*

The mutual information satisfies a chain rule as shown below:

Lemma 2.2 (Chain rule of mutual information): *Let* $\mathbf{y}$, $\mathbf{x}_1$, $\mathbf{x}_2$ *be any column random vectors (possibly of different sizes). Then the mutual information satisfies the chain rule:* $I(\mathbf{y};(\mathbf{x}_1,\mathbf{x}_2)) = I(\mathbf{y};\mathbf{x}_1) + I(\mathbf{y};\mathbf{x}_2|\mathbf{x}_1)$.

Proof**:** By the definition of mutual information, $I(\mathbf{y};(\mathbf{x}_1,\mathbf{x}_2)) = h(\mathbf{y}) - h(\mathbf{y}|(\mathbf{x}_1,\mathbf{x}_2))$ $= h(\mathbf{y}) - h(\mathbf{y}|\mathbf{x}_1) + h(\mathbf{y}|\mathbf{x}_1) - h(\mathbf{y}|(\mathbf{x}_1,\mathbf{x}_2))$ $= I(\mathbf{y};\mathbf{x}_1) + I(\mathbf{y};\mathbf{x}_2|\mathbf{x}_1)$. This completes the proof of Lemma 2.2. ■

In the following lemmas, the differential entropy of a Gaussian vector $\mathbf{z}$ and the entropy maximizing distribution under an average power constraint are determined.

Lemma 2.3 (Differential entropy of Gaussian): *The differential entropy of a circularly symmetric complex Gaussian vector* $\mathbf{z}$ *with invertible covariance matrix* K_z *is* $h(\mathbf{z}) = \log_2((\pi e)^n \det K_z)$.

Proof**:** Proof can be found in Appendix A. ■

Lemma 2.4 (Gaussian as entropy maximizing distribution): *Let* $\mathbf{x}$ *be a circularly symmetric complex Gaussian vector with* $n \times n$ *covariance matrix* K_x. *Also let* $\mathbf{y}$ *be another random vector, not necessarily Gaussian, with the same covariance. Then* $h(\mathbf{y}) \leq h(\mathbf{x})$ *with equality if and only if* $\mathbf{y}$ *is also circularly symmetric Gaussian.*

Proof**:** Proof can be found in Appendix A. ■

The following lemma shows that translation does not change the differential entropy.

Lemma 2.5 (Translation invariance of differential entropy): *Let* **x** *be any* $n\times 1$ *complex random vector and* **c** *be any deterministic (non-random) vector. Then* $h(\mathbf{x}+\mathbf{c}) = h(\mathbf{x})$.

Proof**:** Proof can be found in Appendix A. ■

2.2.2 Selected Channel Capacity Results

One of the most celebrated accomplishments of the information theory is the explicit characterization of the quantity known as *channel capacity*, which refers to the maximal information rate for which a reliable communication is possible over the channel [132].

Definition 2.7 (Channel capacity): *Let* **x** *be an input sequence of length n and* **y** *be the output sequence of a discrete channel characterized by the conditional probability density function p(***y***|***x***). Then the channel capacity is defined by*[9]*:*

$$C = \lim_{n\to\infty} \sup_{p(\mathbf{x})\in S} \frac{1}{n} I(\mathbf{x};\mathbf{y}) \text{ in bits per channel use,} \tag{2.12}$$

where S is the set of allowed probability distribution of **x** *reflecting a possible constraint on the input to the channel and I(***x***;***y***) is the mutual information between* **x** *and* **y**.

Shannon's celebrated channel coding theorem [132], [31] states that when the data (information) rate R is below the capacity C of the channel, i.e., $R < C$, there exists a coding scheme that can achieve the communication with arbitrarily small probability of error. Conversely, if $R > C$, i.e., if information rate is greater than the channel capacity, the probability of error of the communication must be bounded away from zero. Consequently, the channel capacity C is a tight upperbound on the amount of information that can be transmitted reliably over a communication channel.

[9] The channel capacity definition (2.12) generally holds for the *information stable channels*. Loosely speaking, the communication channel is called *information stable* if $\lim_{n\to\infty}\sup_{\mathbf{x}} n^{-1} I(\mathbf{x};\mathbf{y}) = \sup_{\mathbf{x}} \lim_{n\to\infty} n^{-1} I(\mathbf{x};\mathbf{y})$, i.e., the order of limit and supremum operations can be interchanged without any ambiguity. The precise definition of information stability is much more involved and can be found in Chapter 6 in reference [23]. Most practical channels of interests are information stable, including the considered bandlimited AWGN channels and frequency-selective channels considered in this thesis.

The explicit capacity expression for the bandlimited additive white Gaussian noise (AWGN) channel is well known and is often praised as "one of the most famous formulae of information theory" [31].

Theorem 2.1 (Capacity of bandlimited Gaussian channel [132], [31]): *The capacity of an additive white Gaussian noise (AWGN) channel with noise power spectral density $N_0/2$ watts/Hertz, and transmission power P watts is given by*

$$C_{AWGN} = \frac{1}{2T}\log_2\left(1+\frac{PT}{N_0/2}\right) \text{ bits per second,} \tag{2.13}$$

where T is the symbol period in seconds. When the Gaussian channel is strictly bandlimited to [−W, W] Hertz with the Nyquist rate signaling of 1/T = 2W, the corresponding capacity of the bandlimited Gaussian channel is given by

$$C_{AWGN} = W\log_2\left(1+\frac{P}{N_0 W}\right) \text{ bits per second.} \tag{2.14}$$

Proof**:** The proof can be found in chapter 11 of [31]. For completeness of this thesis, the proof is also presented in Appendix A. ■

In general, the communication channel may impose more broad spectral constraints in the form of the spectral masks (e.g., the spectral masks for ultra-wideband (UWB) communications, frequency-division-multiple-access (FDMA), etc.). In such cases, the transmission power spectral density (PSD) is restricted to fall under the mask. Generally, the transmit spectral constraint is given by

$$\mathsf{S}_x(f) \le \mathsf{S}(f) \text{ for all } f, \tag{2.15}$$

where $\mathsf{S}_x(f)$ and $\mathsf{S}(f)$ are the transmission PSD and the given spectral mask, respectively. The corresponding capacity of the Gaussian channel subject to the spectral constraint (2.15) is given in the following:

Theorem 2.2 (Capacity as a function of PSD): *The capacity of a Gaussian channel with the spectral constraint (2.15) is given by*

$$C_{PSD} = \frac{1}{2}\int_{-\infty}^{\infty}\log_2\left(1+\frac{\mathsf{S}(f)}{N_0/2}\right)df \text{ bits per second.} \tag{2.16}$$

Summary of proof [12]: We shall use the idea similar to the Riemann sum for approximating an integral. First, partition the frequency axis into $\{f_i\}_{i=-\infty}^{\infty}$, such that for all i, $f_{i+1} - f_i = \Delta f$. In each partition $f \in [f_i, f_{i+1}]$, denote the maximal and the minimal values of the spectral mask $\mathsf{S}(f)$ by m_i and M_i, respectively. Furthermore, construct two new spectral masks by $\mathsf{L}(f) = \sum_{i=-\infty}^{\infty} m_i \mathbf{1}_{[f_i, f_{i+1}]}(f)$ and $\mathsf{U}(f) = \sum_{i=-\infty}^{\infty} M_i \mathbf{1}_{[f_i, f_{i+1}]}(f)$, where $\mathbf{1}_{[f_i, f_{i+1}]}(f)$ denotes the indicator function (i.e., $\mathbf{1}_{[f_i, f_{i+1}]}(f)$ =1 for $f \in [f_i, f_{i+1}]$ and 0 otherwise). Then, it's easy to see that $\mathsf{L}(f) \le \mathsf{S}(f) \le \mathsf{U}(f)$.

The spectral mask $\mathsf{L}(f)$ comprises of a set of multiple rectangular bands of widths Δf Hz and hence the capacity with the spectral mask $\mathsf{L}(f)$ may be easily derived by a simple sum of (2.14):

$$C\left(\mathsf{L}(f)\right) = \sum_{i=-\infty}^{\infty} \frac{\Delta f}{2} \log_2\left(1 + \frac{m_i \Delta f}{N_0 \cdot \Delta f/2}\right) = \sum_{i=-\infty}^{\infty} \frac{\Delta f}{2} \log_2\left(1 + \frac{m_i}{N_0/2}\right), \tag{2.17}$$

where the *two-sided* bandwidth $2W$ is replaced by Δf, and the power P in the frequency band $f \in [f_i, f_{i+1}]$ is given by $m_i \Delta f$ (since area under PSD corresponds to the power). Similarily, we can show that, for $\mathsf{U}(f)$:

$$C\left(\mathsf{U}(f)\right) = \sum_{i=-\infty}^{\infty} \frac{\Delta f}{2} \log_2\left(1 + \frac{M_i}{N_0/2}\right). \tag{2.18}$$

The sought-out capacity C_{PSD} can then be bounded as

$$C\left(\mathsf{L}(f)\right) \le C_{PSD} \le C\left(\mathsf{U}(f)\right), \tag{2.19}$$

due to $\mathsf{L}(f) \le \mathsf{S}(f) \le \mathsf{U}(f)$. Finally, by letting $\Delta f \to 0$, we can show by using calculus that

$$\lim_{\Delta f \to 0} C\left(\mathsf{L}(f)\right) = \lim_{\Delta f \to 0} C\left(\mathsf{U}(f)\right) = \frac{1}{2} \int_{-\infty}^{\infty} \log_2\left(1 + \frac{\mathsf{S}(f)}{N_0/2}\right) df\,, \tag{2.20}$$

which, with (2.19), leads to the desired expression. This completes the proof. ■

We note that the capacity expression (2.16) as a function of PSD is a generalized form of the classical Shannon formula (2.14). In practical cases where the bandwidth is ill-defined (e.g., when transmitting pulses that are non-strictly bandlimited), the generalized capacity expression (2.16) can be a more appropriate capacity benchmark.

In some scenarios, one may be interested in the maximal achievable rate when some *fixed* input probability distribution $p(\mathbf{x})$ is used that is not necessarily the capacity-wise optimal. The resulting maximal achievable rate with the fixed $p(\mathbf{x})$ is known as *an information rate*:

Definition 2.8 (Information rate): *An information rate in bits per second is defined as [109], [132]*

$$\overline{C} = \lim_{N\to\infty} \frac{1}{NT} I(\mathbf{x};\mathbf{y}) \text{ bits per second,} \tag{2.21}$$

(without supremum or maximum) for some specific probability distribution of $\mathbf{x}$.

The information rate usually gives a lower-bound to the true channel capacity due to the assumption of a specific channel input probability distribution $p(\mathbf{x})$ that is in general not capacity-achieving.

2.3 Review of Selected Channel Coding Techniques

Selected concepts from coding and equalization are reviewed in this section. In particular, the BCJR algorithm (named after its four inventors Bahl, Cocke, Jelinek, and Raviv) on a trellis representation of convolutional code is reviewed in subsection 2.3.1. Moreover, maximum a-posteriori (MAP) symbol detection for an intersymbol interference (ISI) channel is reviewed in subsection 2.3.2. Finally, the capacity-approaching Turbo code and Turbo equalization are reviewed in subsection 2.3.3. Many of these concepts will be used in designing FTN coding architectures in section 4.3 and section 6.4.

2.3.1 BCJR Algorithm on a Trellis

Error-correcting-codes enable error detection and correction by adding redundancies to the transmissions for reliable data communication over noisy channels. C*onvolutional codes* are one important class of error-correcting-codes, which encode its input message by continually feeding the message bits into a finite-state machine, as shown in Figure 2.3 as an example. The finite state machine consists of registers, denoted by *D* in Figure 2.3, that are initialized to 0 and binary modulo 2 adders, denoted by $\oplus$.

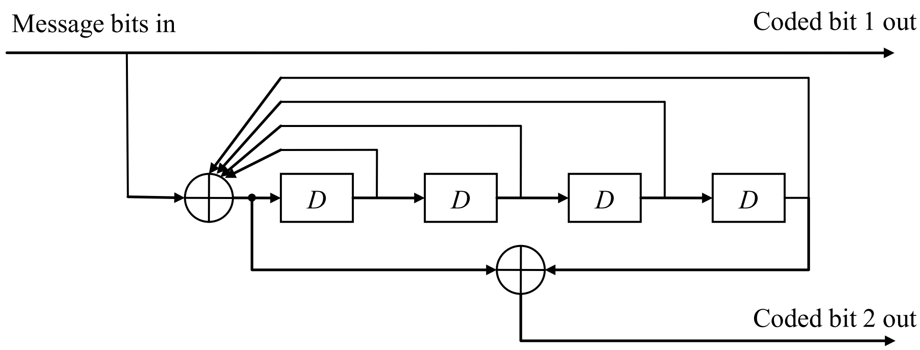

Figure 2.3 Rate 1/2 - memory 4 - recursive systematic convolutional code used by Berrou *et al.* [18]

The convolutional code can also be conveniently represented by a trellis diagram, which describes the encoded bits in a layered directed graph. As an example, the trellis representation of the convolutional code from Figure 2.3 is shown in Figure 2.4. In the trellis diagram, the set of vertices on the left-hand-side denotes all possible states of the convolutional encoder at the *n*-th stage, whereas the set of vertices on the right hand side denotes the possible states at the (*n*+1)-th stage. The transition from one state to another is possible only if there is an edge connecting the two states, and is triggered by incoming message bits while simultaneously generating the coded bits as outputs.

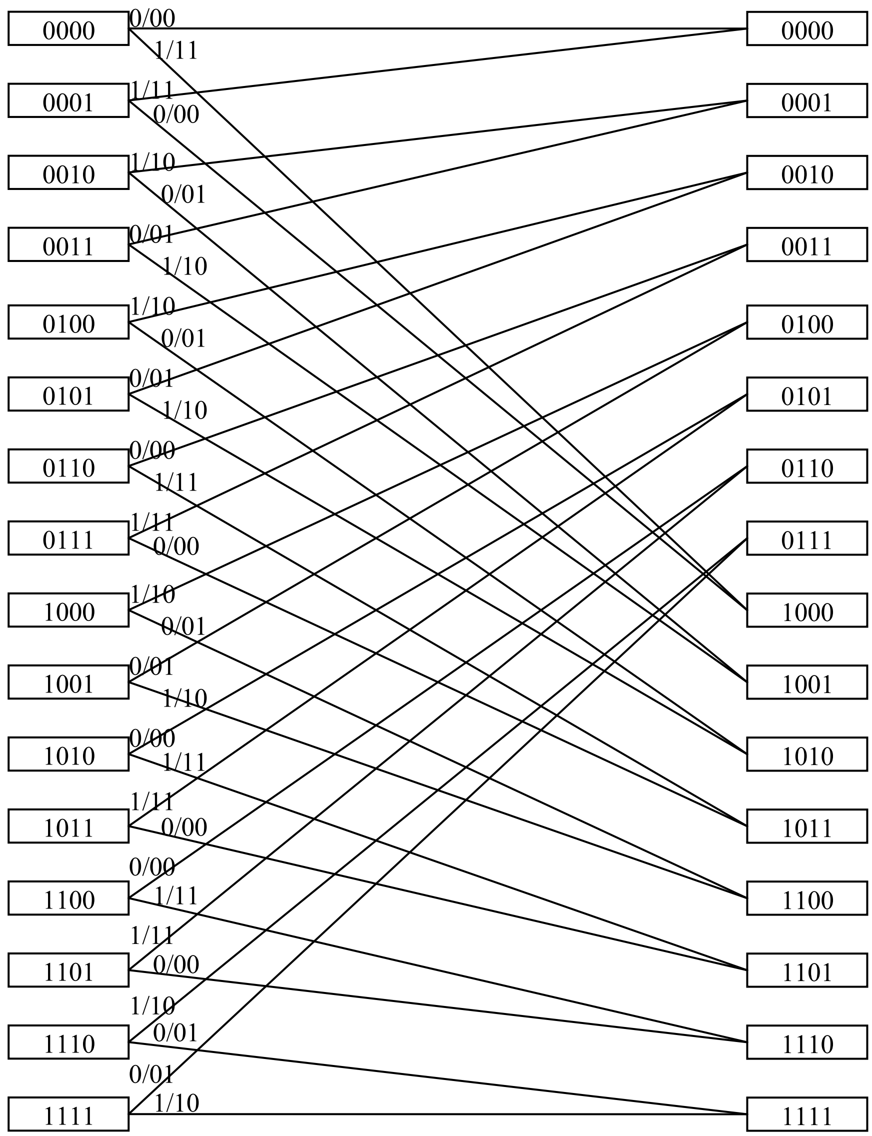

Figure 2.4 One trellis stage of the recursive convolutional code from Berrou *et al.* [18]; Input and output symbols are denoted by in/out labels at each trellis edge

Having such a trellis representation allows efficient probabilistic (soft-in-soft-out) decoding of the convolutional encoder. The goal of the probabilistic decoding of an error-correcting-code is to find the probability of n-th message bit, $m[n]$, given a received noisy version of the corresponding codewords, $\mathbf{r}$, i.e., the a-posteriori probabilities $p(m[n]|\mathbf{r})$. These can be efficiently computed by the BCJR algorithm [10], [11] (also known as the forward-backward, a posteriori probability (APP), or MAP algorithm) applied on to the trellis representation of the convolutional encoder.

The BCJR algorithm is described below. First let S be a set of all states in the trellis and $s_n \in \mathsf{S}$ be one of the states at n-th stage of the trellis. Given a state pair (s_n, s_{n+1}), the BCJR algorithm computes the probability of traversing the trellis edge connecting the state pair given received sequence **r**, by the factorization:

$$p(s_n = s, s_{n+1} = s') = \alpha_n(s)\gamma_n(s,s')\beta_{n+1}(s'), \tag{2.22}$$

where $\alpha_n(s)$ is called the forward metric of the state s at the n-th trellis stage, $\beta_{n+1}(s')$ is called the backward metric of the state s' at the (n+1)-th stage, and $\gamma_n(s, s')$ is called the metric of the edge connecting the state pair (s, s'). The edge metric $\gamma_n(s, s')$ is given by

$$\gamma_n(s,s') = p(m[n])\, p(r[n] \| c[n]), \tag{2.23}$$

where $p(m[n])$ is a-priori probability of the n-th message bit and $p(r[n]|c[n])$ is the likelihood probability of receiving $r[n]$ when the codeword $c[n]$ was transmitted at the n-th stage. For example, in the conventional additive Gaussian channel where $r[n] = c[n] + z[n]$ with $z[n] \sim \mathsf{N}(0,\sigma^2)$, the edge metric can be computed as

$$\gamma_n(s,s') = p(m[n])(2\pi\sigma^2)^{-1/2} \exp\left(-\frac{(r[n]-c[n])^2}{2\sigma^2}\right). \tag{2.24}$$

On the other hand, the forward metric and the backward metric are computed recursively in forward and backward sweeps over the trellis, respectively, according to

$$\alpha_{n+1}(s) = \sum_{\sigma} \alpha_n(s)\gamma_n(s,s') \text{ and} \tag{2.25}$$

$$\beta_n(s') = \sum_{\sigma'} \beta_{n+1}(s')\gamma_n(s,s'), \tag{2.26}$$

where $\alpha_0(s)$ and $\beta_N(s')$ are initialized to 1 for the beginning state s of the trellis and the ending state s' of the trellis (and $\alpha_n(s)$ and $\beta_{n+1}(s')$ for all the other states at each trellis stage are initialized to zero by default).

Finally, the sought-out a-posteriori probabilities $p(m[n]=0|\mathbf{r})$ and $p(m[n]=1|\mathbf{r})$ can be obtained by noting that these are precisely equal to the probability of traversing the one of the trellis edges having the input labels of $m[n]$=0 and $m[n]$=1, respectively, at the n-th trellis stage. Therefore,

$$p(m[n]=0|\mathbf{r}) = \sum_{\substack{(s,s') \text{ with} \\ \text{input label } m[n]=0}} p(s_n = s, s_{n+1} = s') \text{ and} \tag{2.27}$$

$$p(m[n]=1|\mathbf{r}) = \sum_{\substack{(s,s') \text{ with} \\ \text{input label } m[n]=1}} p(s_n = s, s_{n+1} = s') . \tag{2.28}$$

We note that the BCJR algorithm can be applied to other codes including non-binary codes, block codes, or other codes that has a trellis representation. It can also be used to perform a posteriori probability decoding for intersymbol interference channels (since such channels can also be represented by an appropriate trellis diagram).

2.3.2 MAP Symbol Detection for Ungerboeck Observation Model

The objective of this subsection is to develop a posteriori symbol detection/decoding for the FTN systems, which have a particular intersymbol interference (ISI) pattern with a specific noise correlation structure known as *Ungerboeck observation model* [151], using the BCJR algorithm discussed in subsection 2.3.1.

Intersymbol interference (ISI) refers to a form of distortion of signals that causes a data symbol interfering with other data symbols. Such ISI typically arises in channels with memory, such as multipath fading or frequency selective channels, but also appears in the considered FTN signaling due to the inherent non-orthogonality of the signals that are spaced closer than the Nyquist interval. Although it has been traditionally considered as an undesired phenomenon to communications, ISI has recently been shown to be beneficial in some scenarios, such as in multiple-input-multiple-output (MIMO) channels where multipath propagation improves statistical independence on each communication path [141], [53] and in partial-response signaling where a controlled amount of ISI is deliberately introduced into the signal to allow reshaping of the spectrum or achieving the ideal Nyquist signaling rate while using practical time-limited pulses [72].

The typical ISI observation model is given in the following:

$$y[n] = \sum_{l=-L}^{L} h_l x[n-l] + z[n] , \tag{2.29}$$

where $y[n]$ is the n-th observation from the ISI channel, $x[n]$ is the desired n-th data symbol, $z[n]$ is the additive noise, and $\{h_l\}$ for $l \in \{-L, -L+1, \cdots, 0, \cdots, L\}$ is a set of real numbers that corresponds to the ISI pattern. The integer parameter L determines the memory length of ISI and can be appropriately chosen depending on the values of h_l. Let the noise $z[n]$ be modeled as a *correlated* Gaussian with 0 mean and an autocorrelation function $E\{z[n]z^*[m]\} = (N_0/2)h_{m-n}$, $n, m \in \mathbb{Z}$ where $N_0/2$ is the two-sided noise power spectral density [151]. The resulting model (2.29), with the noise correlation being proportional to the ISI coefficients $\{h_l\}$, is known as the *Ungerboeck observation model* [151], which can model selected ISI channels including the considered FTN systems[10].

One of the key methods to combat the effects of ISI is by using an equalizer at the receiver. In this subsection, we describe a design of the *optimal* equalizer based on the maximum a-posteriori (MAP) symbol detection for the *Ungerboeck observation model* [24]. This equalizer can be used with the considered FTN systems, as will be discussed in the later chapters[11].

The MAP symbol detector attempts to find the symbol probabilities of $x[n]$ given the sequence of observations $\mathbf{y}$ (i.e., a-posteriori probabilities), which can be written as (by using the Bayes' rule):

$$p(x[n] \| \mathbf{y}) = c_1 \cdot p(\mathbf{y} | x[n]) p(x[n]), \tag{2.30}$$

where c_1 is a normalization constant that can be easily computed by the law of total probability. By the law of total probability, we can express the a-posteriori probabilities as

$$p(x[n] \| \mathbf{y}) = c_1 \cdot \sum_{\substack{\mathbf{x} \\ \text{with } x[n] \text{ fixed}}} p(\mathbf{y} | \mathbf{x}) p(\mathbf{x}), \tag{2.31}$$

[10] Another popular model for ISI channels is the *Forney observation model*, which is obtained by designing a whitened matched filter at the receiver, leading to a white Gaussian noise vector. The Forney and Ungerboeck models are known to be equivalent in the way what one model can be transformed to the other without any loss in information.

[11] Instead, one could use *suboptimal*, reduced complexity equalizers (e.g., zero-forcing, MMSE, decision-feedback, etc.). There have been numerous reports on the good performances of these suboptimal detectors in many special scenarios, and these may be preferred in practical coding systems due to their significant complexity reduction.

where the summation is over all possible combinations of **x** with the n-th symbol $x[n]$ fixed. Noting that **y** conditioned on **x** is Gaussian distributed in the considered Ungerboeck observation model, we can express the likelihood function $p(\mathbf{y}|\mathbf{x})$ as [151]

$$p(\mathbf{y}|\mathbf{x}) = c_2 \cdot \prod_k \exp\left(\frac{2}{N_0}\left(x[k]y[k] - \frac{1}{2}x^2[k]h_0 - \sum_{l=1}^{L} x[k]x[k-l]h_l\right)\right), \tag{2.32}$$

where c_2 is a normalization constant that can be computed by the law of total probability. Finally substituting the likelihood function $p(\mathbf{y}|\mathbf{x})$ into (2.31) yields

$$p(x[n]|\mathbf{y}) = c \cdot \sum_{\substack{\mathbf{x} \\ \text{with } x[n] \text{ fixed}}} \prod_k p(x[k]) \exp\left(\frac{2}{N_0}\left(x[k]y[k] - \frac{1}{2}x^2[k]h_0 - \sum_{l=1}^{L} x[k]x[k-l]h_l\right)\right), \tag{2.33}$$

where we have used the assumption that input symbols $x[n]$ are independent and c is another normalization constant that can be computed by the law of total probability.

These a-posteriori probabilities can be efficiently computed by the BCJR algorithm, described in subsection 2.3.1, applied on to the trellis representation of the observation model (2.29). In the case of the Ungerboeck observation model, the edge metrics used to compute (2.22) is given by [24]

$$\gamma_n(\sigma, \sigma') = p(x[n]) \exp\left(\frac{2}{N_0}\left(x[n]y[n] - \frac{1}{2}x^2[n]h_0 - \sum_{l=1}^{L} x[n]x[n-l]h_l\right)\right), \tag{2.34}$$

which can be derived from the a-posteriori probabilities (2.33). Due to the summation term appearing in (2.34), we need L past symbols values $x[n\text{-}L]$, $x[n\text{-}L+1]$, …, $x[n\text{-}1]$ at the n-th trellis stage. Consequently, the number of states required to implement this BCJR algorithm is M^L for M-ary symbols (e.g., 2^L for binary symbols). Consequently, the overall implementation complexity of the equalizer based on the MAP symbol detection is on the order of M^L.

2.3.3 Turbo Coding and Turbo Equalization

Since Shannon's landmark paper [132], which established the concept of channel capacity, many coding techniques have been devised to close the gap between the practical performance of digital communications and the channel capacity benchmark. In 1993, Turbo code emerged as one of the first practical codes to closely approach the capacity of AWGN channel within a fraction of a decibel [18] and has since revolutionized the field of digital communications. Presently, it has been adopted in various communications standards including, but not limited to, 3G and 4G standards such as IMT2000, UMTS, HSPA, LTE [146], [145], and satellite communication systems such as DVB-RCS [38], [35]. In this subsection, we briefly highlight the structures of Turbo codes and its important variation known as the Turbo equalization for ISI channels.

Turbo codes are comprised of either parallel or serial concatenation of two (or more) constituent codes that are separated by an interleaver, and are decoded by iterative decoding of the constituent codes. The classical parallel Turbo code [18] is first illustrated in Figure 2.5. At the encoding-end, *encoder* 1 encodes message bits m to produce coded bits c_1, while *encoder* 2 encodes *interleaved* message bits m_π to produce another set of coded bits c_2.[12] The two sets of the coded bits (c_1, c_2) are subsequently modulated and sent to the communication channel.

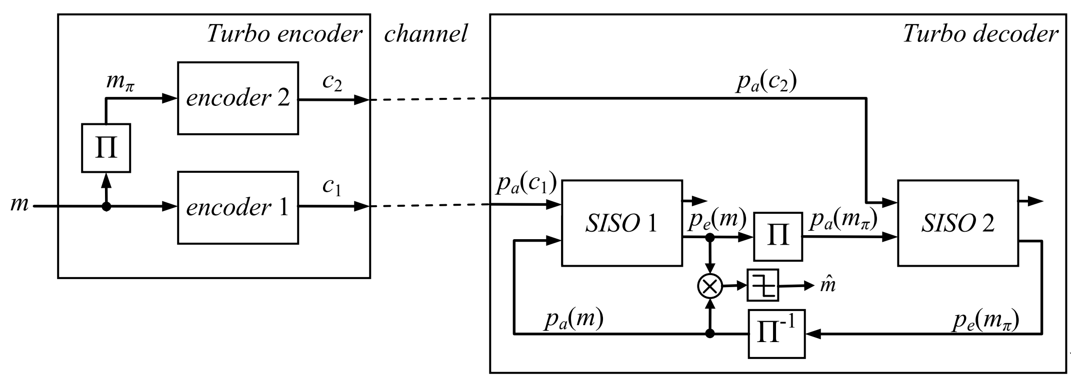

Figure 2.5 Encoder and decoder structures of a parallel Turbo code; Π and Π^{-1} denote interleaver and deinterleaver, respectively; *SISO* denotes a soft-input-soft-output module

Given the channel observations, the demodulator at the receiver first computes a-posteriori probabilities $p(c_1)$ and $p(c_2)$ of the coded bits and passes these information to the

[12] In typical parallel Turbo code, *encoder* 1 is usually a systematic recursive convolutional code, which includes its encoder input as the output sequence, whereas *encoder* 2 is typically a non-systematic recursive convolutional code that does not include its encoder input as the output sequence.

Turbo decoder for further processing. The Turbo decoder is comprised of two soft-input-soft-output (SISO) modules computing the reverse operations of the *encoder* 1 and *encoder* 2 at the Turbo encoder. The SISO module, illustrated in Figure 2.6, accepts a-priori probabilities about the codeword c and the message m and as its two inputs and computes a-posteriori probabilities about c and m, using the BCJR algorithm, described in subsection 2.3.1. The a-posteriori probabilities are then divided by the corresponding a-priori probabilities, as also shown in Figure 2.6, to produce *extrinsic information* $p_e(c)$ and $p_e(m)$ about c and m.[13] The purpose of this so-called *extrinsic information processing* is to extract only the information that are newly learnt from the BCJR decoding. It is accomplished by removing from the a-posteriori probability of each BCJR decoded symbol the contributions of the a-priori probability of this symbol and known extrinsic information about this symbol that was at the input of this decoder.

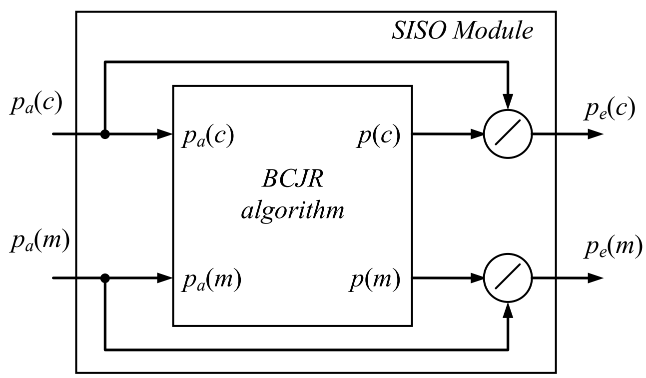

Figure 2.6 Illustration of the soft-input-soft-output (SISO) module of the Turbo decoder that is implemented using the BCJR algorithm; also includes the extrinsic information processing

The *SISO* 1 module of the Turbo decoder in Figure 2.5 first computes the extrinsic information about the message, $p_e(m)$. These are then interleaved, using the same interleaver used at the Turbo encoder, and are input to the *SISO* 2 module as a-priori

[13] Note that, instead of the probabilities $p(c)$ and $p(m)$, the log-likelihood ratios (LLRs) defined by $\Lambda(c) \equiv \log(p(c=1)/p(c=0))$ or $\Lambda(m) \equiv \log(p(m=1)/p(m=0))$ may be computed and exchanged between the two constituent decoders in Turbo code. Then, the SISO module in Figure 2.6 will accept two LLRs $\Lambda_a(c) \equiv \log(p_a(c=1)/p_a(c=0))$ and $\Lambda_a(m) \equiv \log(p_a(m=1)/p_a(m=0))$ as inputs. Furthermore, the output extrinsic information is generated by simply subtracting the LLRs by $\Lambda_e(c) = \Lambda(c)-\Lambda_a(c)$ and $\Lambda_e(m) = \Lambda(m)-\Lambda_a(m)$. Note that either using probabilities or LLRs lead to an equivalent operation in Turbo code.

probabilities about the interleaved message bits m_π. The *SISO* 2 module then computes the extrinsic information about the interleaved message bits m_π, using the a-posteriori probabilities $p(c_2)$ from the demodulator as the a-priori information about c_2. The extrinsic information $p_e(m_\pi)$ are then de-interleaved back to the format of m, which are fed back to the *SISO* 1 module as an updated a-priori probabilities about the message bits m. These steps continue for a prescribed number of iterations or until some convergence is reached. At the last iteration, the estimates about the message bits $\hat{m}$ are obtained by multiplying $p_e(m)$ by $p_a(m)$ after the *SISO* 1 module, followed by a hard-decision device, as illustrated in Figure 2.5.

Similarily, the serial Turbo code [14] is illustrated in Figure 2.7. The encoding of message bits m is now done in two stages in serial, with an interleaver in between. Note that the *encoder* 2 now does not encode the message bits m directly, but instead encodes the interleaved version of the codeword c_1, denoted by $c_{1\pi}$. Consequently, at the Turbo decoder, the *SISO* 2 module treats $c_{1\pi}$ as its message bits and outputs the extrinsic information about $c_{1\pi}$. The rest of the operations follow similarly as in the parallel case.

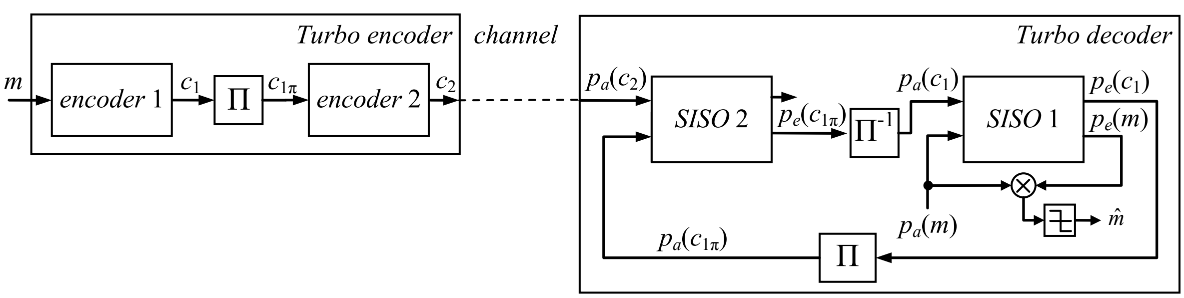

Figure 2.7 Encoder and decoder structures of a serial Turbo code; Π and Π^{-1} denote interleaver and deinterleaver, respectively; *SISO* denotes a soft-input-soft-output module

Turbo codes have been originally applied to the memoryless AWGN channels and were shown to perform near the capacity limit (e.g., 0.1 dB within the capacity limit reported in [142]). Within only few years of its invention, Turbo code has been successfully extended to intersymbol interference (ISI) channels (and branded as *Turbo equalization* [37], [88]) which was shown to be able to iteratively remove ISI and perform close to the ISI channel capacity limit. In the Turbo equalization, the ISI channel is treated as a constituent code of the serial Turbo code by modeling it as a tapped-delay line as illustrated in Figure 2.8. The receiver first needs to estimate the ISI channel tap coefficients $h_{-L}, \ldots, h_L$, which can be achieved by sending training or pilot sequences. The (soft-input-soft-output) *SISO symbol detector* at the Turbo equalizer then calculates a-posteriori probabilities about each modulation symbol x, which can be implemented by the MAP symbol detector as explained in subsection 2.3.2. This is followed by the de-mapper (symbols to bits), which reverses the mapping function of the *mapper* (bits to symbols) used at the encoder, and computes the extrinsic information $p_e(c_\pi)$ about the interleaved codewords c_π. The rest of the iterative processing is the same as in the serial Turbo decoder from Figure 2.7.

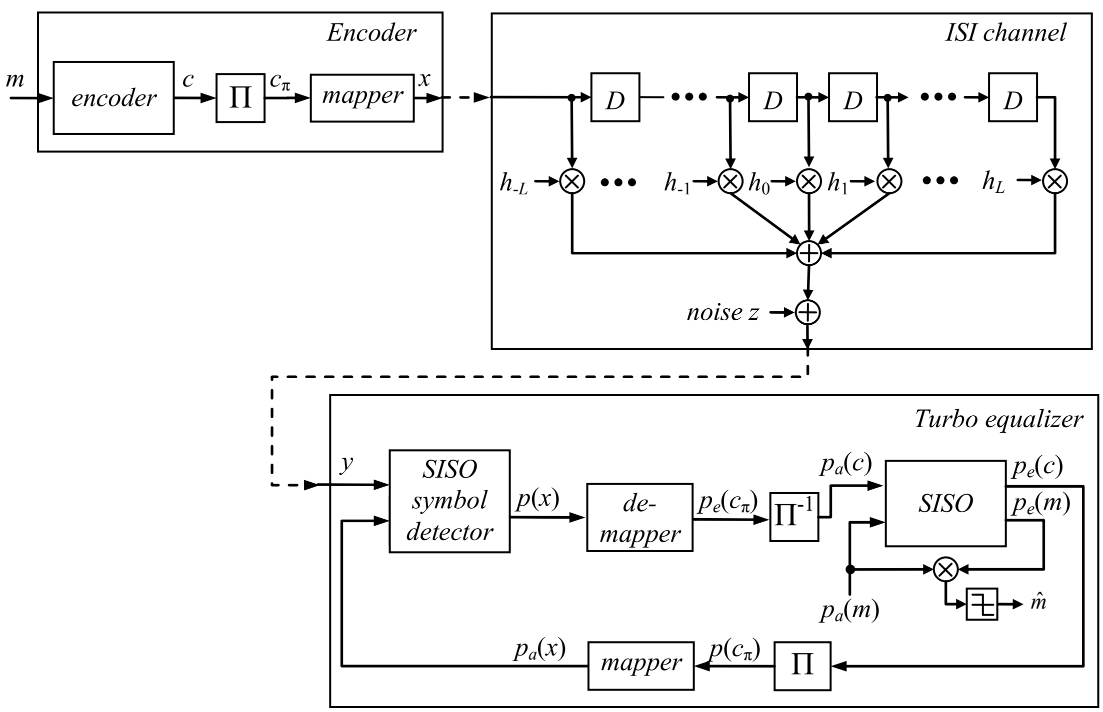

Figure 2.8 Turbo equalization in ISI channels

The performance of the Turbo equalizer depends on which (error-correcting) *encoder* is being used at the transmitter. When it is a simple convolutional code, the Turbo equalizer can successfully remove the adverse effects of ISI, but does not perform near the capacity limit of the ISI channel [88]. This is primarily due to the ISI channel being equivalent to a *non-recursive* code, which is known to have a poor convergence when used as a constituent code of Turbo code [15]. In order to approach the capacity limit of the ISI channel, either the *encoder* at the transmitter must be a Turbo code (parallel or serial) by itself, leading to a three-stage iterative decoding at the Turbo equalizer [116], [159], or an additional recursive precoder must be used right before the ISI channel in order to make the overall effects of the precoder and the ISI channel *recursive* [104], [92]. For instance, when the *encoder* block at the transmitter is by itself a parallel Turbo code, the corresponding Turbo equalizer was reported to perform less than 1 dB away from the ISI channel capacity [116].

2.4 Some Concepts and Results from Matrix Algebra

This dissertation uses extensively the following concepts and results from matrix algebra, which are reviewed in this section for completeness. (Please refer to [55] for proofs of these results.) In particular, we first define some special types of matrices:

Definition 2.9 (Unitary matrix): *A square complex matrix U of size $n\times n$ is called Unitary if it satisfies $UU^{\dagger} = U^{\dagger}U = I_n$, where $(\cdot)^{\dagger}$ denotes matrix transpose followed by complex conjugation of the matrix entries and I_n denotes the $n\times n$ identity matrix.*

Definition 2.10 (Hermitian matrix): *An $n\times n$ square complex matrix A is called Hermitian if it satisfies $A = A^{\dagger}$.*

Definition 2.11 (Hermitian positive and negative definite matrices): *An $n\times n$ Hermitian matrix A is said to be:*

- *positive definite if* $\mathbf{x}^{\dagger}A\mathbf{x} > 0$
- *non-negative definite if* $\mathbf{x}^{\dagger}A\mathbf{x} \geq 0$
- *non-positive definite if* $\mathbf{x}^{\dagger}A\mathbf{x} \leq 0$
- *negative definite if* $\mathbf{x}^{\dagger}A\mathbf{x} < 0$

for all non-zero complex $n\times 1$ vectors $\mathbf{x}$.

One special property of the Hermitian matrices is that they can be further decomposed into a product of matrices involving unitary matrices and a diagonal matrix:

Theorem 2.3 (Eigenvalue decomposition or eigendecomposition): *For any $n \times n$ complex Hermitian matrix A, there exist an $n \times n$ complex unitary matrix U and an $n \times n$ diagonal matrix Λ with real diagonal entries such that*

$$A = U \Lambda U^{\dagger} . \tag{2.35}$$

In addition, the column vectors of U, $\mathbf{u}_0$, $\mathbf{u}_1$, ..., $\mathbf{u}_{n-1}$, are called eigenvectors of A and the real diagonal entries of matrix Λ, λ_0, λ_1, …, λ_{n-1}, are called eigenvalues of A.

The eigenvalue decomposition expresses the Hermitian matrix A as an n-dimensional vector $[\lambda_0, \lambda_1, \ldots, \lambda_{n-1}]$ in the space spanned by the eigenvectors of A. This is similar to the well-known Gram-Schmidt orthonormalization process in linear algebra.

The sign of the real eigenvalues $\lambda_0, \lambda_1, \ldots, \lambda_{n-1}$ of Hermitian matrix A depends on the positive definiteness of A.

Lemma 2.6 (Sign of eigenvalues of Hermitian matrix): *A Hermitian matrix A is positive definite, non-negative definite, non-positive definite, or negative definite if and only if all of its real eigenvalues are positive, non-negative, non-positive, or negative, respectively.*

In the following, two special matrices known as Toeplitz and Gramian are defined.

Definition 2.12 (Toeplitz matrix): *An $n \times n$ square matrix A is called Toeplitz if it can be expressed as*

$$A = \begin{bmatrix} a_0 & a_{-1} & a_{-2} & \cdots & a_{-(n-1)} \\ a_1 & a_0 & a_{-1} & & a_{-(n-2)} \\ a_2 & a_1 & a_0 & & a_{-(n-3)} \\ \vdots & & & \ddots & \vdots \\ a_{n-1} & a_{n-2} & a_{n-3} & \cdots & a_0 \end{bmatrix}, \tag{2.36}$$

where the entries $\{a_i\}$ are complex numbers.

Toeplitz matrices naturally arise in many applications including image processing and signal processing as well as in the considered FTN signaling. If Toeplitz matrix is further Hermitian, then its eigenvalues are also well characterized by Szegö's theorem [57], [56]. (More details about this theorem are given in Appendix D.)

The Gramian matrix is defined in the following.

Definition 2.13 (Gramian or Gram matrix): *The Gramian matrix of non-zero complex finite energy functions $r_0(t)$, $r_1(t)$, ..., $r_{n-1}(t)$ is a matrix of their inner products, defined as*

$$G\left(r_0\left(t\right),\cdots,r_{n-1}\left(t\right)\right)\equiv\begin{bmatrix}\langle r_0,r_0\rangle & \langle r_0,r_1\rangle & \langle r_0,r_2\rangle & \cdots & \langle r_0,r_{n-1}\rangle \\ \langle r_1,r_0\rangle & \langle r_1,r_1\rangle & \langle r_1,r_2\rangle & \cdots & \langle r_1,r_{n-1}\rangle \\ \langle r_2,r_0\rangle & \langle r_2,r_1\rangle & \langle r_2,r_2\rangle & \cdots & \langle r_2,r_{n-1}\rangle \\ \vdots & \vdots & \vdots & \ddots & \vdots \\ \langle r_{n-1},r_0\rangle & \langle r_{n-1},r_1\rangle & \langle r_{n-1},r_2\rangle & \cdots & \langle r_{n-1},r_{n-1}\rangle\end{bmatrix}, \tag{2.37}$$

where inner product of $r_i(t)$ and $r_j(t)$ is defined as

$$\langle r_i,r_j\rangle\equiv\int_{-\infty}^{\infty}r_i\left(t\right)r_j^*\left(t\right)dt\,. \tag{2.38}$$

One important result related to the invertibility of the Gramian matrix is given below:

Lemma 2.7 (Gram's criterion [51]): *Let $r_0(t)$, $r_1(t)$, ..., $r_{n-1}(t)$ be non-zero complex finite energy functions with a finite support in the closed interval $[\alpha, \beta]$. Then, the Gramian matrix $G(r_0(t),\ldots, r_{n-1}(t))$ as defined in (2.37) has a nonzero determinant, thus is invertible, if and only if the set of functions $\{r_0(t), r_1(t), \ldots, r_{n-1}(t)\}$ is linearly independent.*

In the following, we present some matrix identities involving matrix trace $tr(\cdot)$, which is equal to a sum of main diagonal entries of $n\times n$ square matrix.

Lemma 2.8 (Cyclic invariance of matrix trace): *The trace of a matrix is commutative, i.e., for any $n\times m$ matrix A and $m\times n$ matrix B,*

$$tr(AB)=tr(BA)\,, \tag{2.39}$$

where $tr(A)=\sum_{i=0}^{n-1}a_{ii}$, where a_{ii} denotes (i,i)th entry (or i-th diagonal entry) of A.

Lemma 2.9 (Trace of Hermitian matrix): *The trace of Hermitian matrix A of size $n\times n$ is the sum of the eigenvalues of A, i.e.*

$$tr(A)=\sum_{i=0}^{n-1}\lambda_i\,, \tag{2.40}$$

where λ_0, λ_1, ..., λ_{n-1}, are the real eigenvalues of the Hermitian matrix A.

Moreover, some matrix algebra results involving matrix determinant det(·) are presented below.

Lemma 2.10 (Properties of determinant): *Let A and B be square matrices of size n×n and c be any real constant. Then, the matrix determinant satisfies the following:*

$$\det(A) = \det(A^T) \tag{2.41}$$

$$\det(A^{-1}) = 1/\det(A) \text{ (for an invertible A)} \tag{2.42}$$

$$\det(AB) = \det(A)\det(B) = \det(BA) \tag{2.43}$$

$$\det(cA) = c^n \det(A)\,. \tag{2.44}$$

Lemma 2.11 (Sylvester's determinant identity): *If A and B are matrices of size n×m and m×n, respectively, then*

$$\det(I_n + AB) = \det(I_m + BA)\,, \tag{2.45}$$

where I_n and I_m are identity matrices of size n×n and m×m, respectively.

Lemma 2.12 (Hadamard's inequality): *The determinant of an n×n Hermitian non-negative definite define matrix A is equal or less than the product of the diagonal elements, i.e.,*

$$\det(A) \le \prod_{i=0}^{n-1} a_{ii}\,, \tag{2.46}$$

where a_{ii} is the (i,i)th entry (or i-th diagonal entry) of A.

Lemma 2.13 (Concavity of log-determinant [20]): *The function f(A) = $\log_2(\det(A))$ is concave on the set of non-negative definite matrices A.*

The Kronecker product of matrices is also defined below:

Definition 2.14 (Kronecker product): *If A and B are m×n and p×q matrices, respectively, then the Kronecker product $A \otimes B$ is an mp×nq matrix defined as*

$$A \otimes B \equiv \begin{bmatrix} a_{11}B & \cdots & a_{1n}B \\ \vdots & \ddots & \vdots \\ a_{m1}B & \cdots & a_{mn}B \end{bmatrix}. \tag{2.47}$$

Lastly, we review the concept of *conditioning* of non-singular (invertible) $n\times n$ matrices. A classical problem in the linear algebra is to solve a linear equation $A\mathbf{x} = \mathbf{b}$ about an $n\times 1$ vector $\mathbf{x}$ given $m\times n$ matrix A and $m\times 1$ vector $\mathbf{b}$ that are a priori known or obtained through some observation or measurements. When this equation is solved using a computer, we are interested in how accurate the computed solution $\hat{\mathbf{x}}$ will be, when compared to the analytically obtained solution $\mathbf{x}$. From the classical perturbation analysis [148], the accuracy of the results from the linear equation solution (such as matrix inversion) is proportional to the degree of *conditioning* of the matrix A, defined as follows:

Definition 2.15 (Conditioning or condition number for a matrix): *The condition number of a nonsingular matrix A is defined by $\kappa(A) \equiv ||A^{-1}||\cdot||A||$, where $||A||$ is the induced matrix norm*[14].

By the perturbation analysis, given a perturbed matrix equation $(A+\delta A)(\mathbf{x}+\delta\mathbf{x}) = (\mathbf{b}+\delta\mathbf{b})$, the relative error in the solution (i.e., $\|\delta\mathbf{x}\|/\|\mathbf{x}\|$) can be upper-bound by

$$\frac{\|\delta\mathbf{x}\|}{\|\mathbf{x}\|} \le \frac{\kappa(A)}{1-\kappa(A)\left(\|\delta\mathbf{x}\|/\|\mathbf{x}\|\right)}\left(\frac{\|\delta\mathbf{x}\|}{\|\mathbf{x}\|}+\frac{\|\delta b\|}{\|b\|}\right). \tag{2.48}$$

This implies that if the condition number $\kappa(A)$ is not close to 1, then small relative error in A or $\mathbf{b}$ can be roughly magnified by up to $\kappa(A)$, to give the relative error in the solution. Essentially, the *conditioning number* of a matrix measures the sensitivity of the solution of a system of linear equations to perturbations in the data.

The following lemma shows that the condition number of the Hermitian matrix is particularly easy to compute, as it is inversely proportional to the minimum absolute value of an eigenvalue of this matrix.

Lemma 2.14 (Condition number of Hermitian matrix): *When an $n\times n$ nonsingular matrix A is Hermitian, its condition number can be expressed as*

$$\kappa\left(A\right) = \left|\lambda_{\max}(A)/\lambda_{\min}(A)\right|, \tag{2.49}$$

[14] In this dissertation, we use the convention that $||\mathbf{a}||$ for an $n\times 1$ vector $\mathbf{a}$ is a vector norm, whereas, $||A||$ for an $n\times n$ matrix A is the induced matrix norm that is defined as $\|A\| \equiv \max_{\mathbf{x}\neq 0}\|A\mathbf{x}\|/\|\mathbf{x}\|$.

where $\lambda_{max}(A)$ and $\lambda_{min}(A)$ are the maximal and the minimal (in absolute value) eigenvalues of A, respectively.

2.5 Continuous-time Channels and the Nyquist Rate

The FTN signaling deals with continuous-time bandlimited channels and is intricately related to the Nyquist theorem for zero-ISI signal transmission. In this section, we carefully review the definition of Nyquist rate signaling, signal and channel bandwidth, power spectral density (PSD) of noise and transmitted signal, and signal-to-noise ratio (SNR) on continuous-time channels.

2.5.1 Nyquist Rate Signaling

Dr. Nyquist, in his seminal paper on data transmission over bandlimited channel [106], considered what would be the maximal signaling rate over such channels without causing intersymbol interference (ISI). He showed that this maximal signaling rate is directly proportional to the channel bandwidth. Throughout this dissertation, this maximal signaling rate without ISI will be refered to as *Nyquist rate* and PAM transmissions with signaling rate equal to the Nyquist rate will be referred to as *Nyquist rate signaling*.

We review, in following two theorems (in Theorem 2.4 and Theorem 2.5), two key results regarding on the Nyquist rate signaling. In this subsection, we consider standard pulse-amplitude modulation (PAM) baseband transmission model, given by $\sum_{n=0}^{N-1} x[n]s\left(t-nT\right)$ where $s(t)$ is a modulating pulse (typically assumed to be bandlimited to W Hertz), N is a signaling block length, and $\{x[n]\}$ are modulation symbols. The signaling rate of such PAM transmission scheme is $1/T$ symbols per second. After channel and matched filter receiver with impulse responses $c(t)$ and $g(t)$, respectively, received noisy signal is given by $y(t)=\sum_{n=0}^{N-1} x[n]r\left(t-nT\right)+z(t)$, where $z(t)$ is a noise signal and $r(t)$ is given by a convolution of $s(t)$, $c(t)$, and $g(t)$, denoting the combined response of transmit filter, channel, and receive filter. Sampling this received signal at $t = nT$ yields

$$y(nT) = x[n]r(0) + \sum_{\substack{m=0 \\ m \neq n}}^{N-1} x[m]r\left((n-m)T\right) + z(nT), \tag{2.50}$$

where the summation term represents an ISI term to the desired symbol $x[n]$ [113]. Consequently, a necessary and sufficient condition for zero ISI is $r((n-m)T) = 0$ for $m \neq n$ and $r(0) \neq 0$. Without loss of generality, we may assume that $r(0)=1$ by normalizing the pulse $r(t)$. Then, in order to remove the effect of ISI, $r(t)$ should satisfy

$$r(nT) = \begin{cases} 1, & n = 0 \\ 0, & n \neq 0. \end{cases} \tag{2.51}$$

Dr. Nyquist has derived a following necessary and sufficient condition for $\hat{r}(f)$ (Fourier transform of $r(t)$) such that (2.51) is satisfied.

Theorem 2.4 (Nyquist condition for zero ISI [106]): *A necessary and sufficient condition for* $\hat{r}(f)$*, to satisfy (2.51) is*

$$\sum_{k=-\infty}^{\infty} \hat{r}\left(f + k/T\right) = T. \tag{2.52}$$

Proof : This version of proof is reproduced from section 8.3.1 of [113] for completeness. First, by inverse Fourier transform:

$$r(t) = \int_{-\infty}^{\infty} \hat{r}(f) e^{j2\pi ft} df \text{ , and} \tag{2.53}$$

$$r(nT) = \int_{-\infty}^{\infty} \hat{r}(f) e^{j2\pi fnT} df, \tag{2.54}$$

where j denotes an imaginary unit. We further rewrite (2.54) as

$$r(nT) = \sum_{k=-\infty}^{\infty} \int_{(2k-1)/(2T)}^{(2k+1)/(2T)} \hat{r}(f) e^{j2\pi fnT} df \tag{2.55}$$

$$= \sum_{k=-\infty}^{\infty} \int_{-1/(2T)}^{1/(2T)} \hat{r}\left(f + \frac{k}{T}\right) e^{j2\pi fnT} df \tag{2.56}$$

$$= \int_{-1/(2T)}^{1/(2T)} \left(\sum_{k=-\infty}^{\infty} \hat{r}\left(f + \frac{k}{T}\right) \right) e^{j2\pi fnT} df \tag{2.57}$$

$$= \int_{-1/(2T)}^{1/(2T)} \hat{r}_{folded}(f) e^{j2\pi fnT} df, \tag{2.58}$$

where $\hat{r}_{folded}(f)$ is defined by

$$\hat{r}_{folded}(f) \equiv \sum_{k=-\infty}^{\infty} \hat{r}\left(f + \frac{k}{T}\right). \tag{2.59}$$

Note that $\hat{r}_{folded}(f)$ is a periodic function with period $1/T$, and hence it has a Fourier series expansion:

$$\hat{r}_{folded}(f) = \sum_{n=-\infty}^{\infty} r_n e^{j2\pi nfT}, \tag{2.60}$$

where its Fourier series coefficients r_n are given by

$$r_n = T\int_{-1/(2T)}^{1/(2T)} \hat{r}_{folded}(f) e^{-j2\pi nfT} df . \tag{2.61}$$

Comparing equations (2.61) and (2.58) we obtain

$$r_n = T \cdot r(-nT) . \tag{2.62}$$

Therefore, the necessary and sufficient condition for (2.51) to be satisfied is that

$$r_n = \begin{cases} T, & n = 0 \\ 0, & n \neq 0 \end{cases}. \tag{2.63}$$

Substituting into equation (2.60) finally yields

$$\hat{r}_{folded}(f) = \sum_{k=-\infty}^{\infty} \hat{r}\left(f + \frac{k}{T}\right) = T . \tag{2.64}$$

This completes the proof of Theorem 2.4. ∎

One important consequence of Theorem 2.4 is that when $1/T > 2W$ (representing faster-than-Nyquist signaling over strictly bandlimited channel with bandwidth W Hz), the ISI cannot be avoided in any way. This is because the channel frequency response $\hat{c}(f)$ will be equal to zero for $|f| > W$ for strictly bandlimited channel and hence $\hat{r}(f) = 0$ also for $|f| > W$. Consequently, $\sum_k \hat{r}(f + k/T)$ will have non-overlapping replicas of $\hat{r}(f)$ and thus there is no choice for $\hat{r}(f)$ to ensure the condition $\sum_k \hat{r}(f + k/T) = T$ in this case.

In strictly bandlimited channel with one-sided bandwidth of W Hz, Dr. Nyquist proved that the Nyquist rate (i.e., maximal signaling rate without ISI) is explicitly given by twice the channel bandwidth, i.e. $1/T = 2W$. In the following, a simple proof of this result is given, which provides some insights into the various tradeoffs associated with increasing the signaling rates beyond the Nyquist rate.

Theorem 2.5 (Nyquist rate in strictly bandlimited channel): *If the modulating pulse s(t) is strictly band-limited to [-W,W] where W is some fixed frequency in Hz, the smallest T without intersymbol interference (ISI) is T=1/(2W), otherwise known as the Nyquist symbol period.*

Proof: We first define $p(t) \equiv \sum_{n=0}^{N-1} x[n]\delta(t-nT)$. Then

$$p(t)*s(t) = \int_{-\infty}^{+\infty} p(\tau)s(t-\tau)\,d\tau = \sum_{n=0}^{N-1} x[n]\int \delta(\tau-nT)s(t-\tau)\,d\tau \tag{2.65}$$

$$= \sum_{n=0}^{N-1} x[n]s(t-nT), \tag{2.66}$$

where $a(t)*b(t) \equiv \int a(\tau)b(t-\tau)d\tau$ denotes the convolution. This shows that the PAM baseband transmission signal is a convolution of $p(t)$ and $s(t)$. By taking the Fourier transform, the frequency response is shown below:

$$\mathcal{F}\left\{p(t)*s(t)\right\} = \hat{p}(f)\hat{s}(f) = \left(\sum_{n=0}^{N-1} x[n]e^{-j2\pi fnT}\right)\hat{s}(f), \tag{2.67}$$

where $\hat{p}(f)$ and $\hat{s}(f)$ are the Fourier transforms of $p(t)$ and $s(t)$, respectively. Note that $\hat{p}(f) = \sum_{n=0}^{N-1} x[n]e^{-j2\pi fnT}$ is periodic with $1/T$. But, if $\hat{s}(f)$ is band-limited to [-W, W], the frequency components of $\hat{p}(f)$ that are outside [$-W$, W] will be clipped off due to due to the multiplication with $\hat{s}(f)$ in (2.67). Figure 2.9 illustrates the case when the period of $\hat{p}(f)$, $1/T$, is greater than $2W$.

Due to the periodicity of $\hat{p}(f)$, the data symbols $\{x[n]\}$ can be completely inferred from only one period of $\hat{p}(f)$ (and the rest are redundant replicas). Therefore, a sufficient condition for full data recovery (i.e., without intersymbol interference) is $1/T \leq 2W$, or $T \geq 1/(2W)$, which is known as the Nyquist rate. This completes the proof of Theorem 2.5. ■

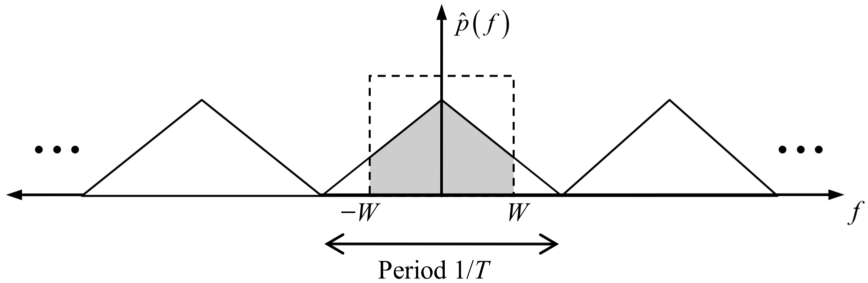

Figure 2.9 Spectrum of baseband transmission signal; only the shaded portion of $\hat{p}(f)$ is transmitted

The above proof of the Nyquist's theorem allows further insights into what happens in the faster than Nyquist rate signaling. With the Nyquist rate signaling (i.e., $1/T = 2W$), the one complete period of $\hat{p}(f)$ is captured within the transmission bandwidth $[-W, W]$ and hence the full data is transmitted over the band-limited channel. On the other hand, as for the FTN signaling, part of the spectrum gets necessarily truncated as seen in Figure 2.9, due to the symbol rate of $1/T$ being greater than the channel bandwidth $2W$.

This does not necessarily mean that the data are lost, as the increased symbol rate in FTN can be exploited in the time domain to add redundancies in the data to recover the information contained in the lost spectrum by means of error control coding. Therefore, the FTN signaling can be considered as a means to trading off amount of data encoding in either spectrum domain or in time domain.

2.5.2 Bandwidth, Power, and Power Spectral Density

There is no single universal definition of bandwidth. Bandwidth is typically defined by the frequency support of the Fourier transform of a signal, but this may not be always satisfactory because mathematically no signal can be both strictly band-limited and strictly time-limited, except the zero energy signals (see Appendix B for the reasoning). In other words, any strictly band-limited signal must have an infinite time-support, which is physically unrealizable. Consequently, the Nyquist rate of $2W$ pulses per second can be an *ill-defined* quantity, since there is no single definition of the bandwidth W for non-strictly bandlimited signals. This may give rise to discrepancies and confusions in signal analysis.

In this dissertation, therefore, we consider a more universal description of the spectrum called the power spectral density (PSD) of a random process, which describes how the power is distributed over all range of frequencies. Many of the common definitions of bandwidth can easily be derived from the PSD expression [2]. First, we formally define power of a random process below:

Definition 2.16: *The (average) power*[15] *of a random process $x(t)$ are defined as*

$$P \equiv E\left[\lim_{T\to\infty}\frac{1}{T}\int_{-T/2}^{T/2}|x(t)|^2\,dt\right], \tag{2.68}$$

where $E[\cdot]$ denotes the statistical expectation (or average) with respect to the probability distribution of the process $x(t)$.

The above definition also has an interpretation of how the power is distributed over *time*. Alternatively, the power can also be thought to be distributed over some range of *frequencies*. This gives rise to the following definition:

Definition 2.17 (Power spectral density): *Let $x(t)$ be a random process and define a time-truncated random process $x_T(t)$ by*

$$x_T(t) = \begin{cases} x(t), & |t| < T/2 \\ 0, & otherwise. \end{cases} \tag{2.69}$$

The power spectral density $\mathsf{S}_x(f)$ of the random process $x(t)$ is a non-negative function of frequency such that

$$\mathsf{S}_x(f) \equiv \lim_{T\to\infty}\frac{1}{T}E\left[|\hat{x}_T(f)|^2\right], \tag{2.70}$$

where $\hat{x}_T(f)$ denotes the Fourier transform of the time-truncated process $x_T(t)$.[16] *Furthermore, the power spectral density $\mathsf{S}_x(f)$ satisfies:*

$$\int_{-\infty}^{\infty}\mathsf{S}_x(f)df = P, \tag{2.71}$$

[15] The average power of a signal P corresponds to the physical power delivered by the signal when the signal is interpreted as a voltage or current source feeding 1 ohm resistor [113].

[16] Note that the time-truncation ensures that any sample function of $x_T(t)$ is square integrable and hence its Fourier transform is well defined.

where P is the average power of x(t).

Note that the power spectral density $\mathsf{S}_x(f)$ of a random process $x(t)$ describes how the average power P is distributed over range of frequencies. For instance, if P_0 denotes the power allocated to the frequency band $f \in [f_0, f_1]$, then PSD $\mathsf{S}_x(f)$ satisfies

$$\int_{f_0}^{f_1} \mathsf{S}_x(f)df = P_0 . \tag{2.72}$$

For (wide-sense) stationary random signals, PSD can be simply obtained by taking a Fourier transform of the autocorrelation function of $x(t)$, $R_x(\tau) = E[x(t)x^*(t+\tau)]$ where $(\cdot)^*$ denotes the complex conjugation, due to the well-known *Wiener-Khinchin theorem* [113], [26].

Theorem 2.6 (Wiener-Khinchin theorem [113], [26]): *Let $x(t)$ be a wide-sense stationary process with an absolutely integrable autocorrelation function $R_x(\tau)$ and*

$$\int_{-T/2}^{T/2}\int_{-T/2}^{T/2} \frac{1}{T} E\left[\left|x(t_1)x^*(t_2)\right|\right]dt_1 dt_2 < \infty , \tag{2.73}$$

for all finite $T > 0$. Then, the power spectral density $\mathsf{S}_x(f)$ for this $x(t)$ is given by

$$\mathsf{S}_x(f) = \mathsf{F}\left[R_x(\tau)\right], \tag{2.74}$$

where $\mathsf{F}[\cdot]$ denotes the Fourier transform.

The power spectral density of the considered non-precoded and precoded FTN signals will be derived rigorously in section 3.4.

2.5.3 Definitions of *SNR* and E_b/N_0

The common definitions of the signal-to-noise ratio (SNR) in the additive white Gaussian channels is $SNR = P/(N_0/2)$ or P/N_0. These definitions are mostly suited for discrete-time channel models as these do not involve time or bandwidth. For continuous-time channels, the definition $SNR = P/(N_0W)$ is typically used to take into account of the channel bandwidth of W Hertz. As discussed in subsection 2.5.2, however, the bandwidth W may be an ill-defined quantity for many practical scenarios.

Alternatively, the SNR definition in terms of time (instead of bandwidth) is given by $E_s/(N_0/2) = PT/(N_0/2)$, where T is the symbol period in seconds, $E_s = PT$ is the symbol energy in watts·second (i.e., Joules), and $N_0/2$ is the two-sided power spectral density of the white Gaussian noise in watts/Hz or watts·second. This definition of SNR naturally arises from the Shannon capacity expression (2.13) and it becomes the usual $P/(N_0W)$ in the strictly bandlimited channels using the Nyquist rate transmissions (T=1/(2W)). This definition of SNR seems especially appropriate for the considered FTN system as the FTN signaling is a time-domain technique and will be the default definition throughout the dissertation, unless otherwise specified.

Definition 2.18 (SNR): *The signal-to-noise ratio (SNR) for communication over Gaussian channels with $N_0/2$ additive white Gaussian noise power spectral density is defined by*

$$SNR \equiv \frac{PT}{N_0/2}, \tag{2.75}$$

where P is the total available power and T is the symbol period in seconds.

In addition, E_b/N_0 (the energy-per-bit to noise power spectral density ratio) is defined conventionally as $(P/R)/N_0$ where R is the communication rate in information bits per second.

Definition 2.19 (E_b/N_0): *Let R denote the communication rate in information bits per second and $x(t)$ denote the information-bearing transmission signal. Then, the energy-per-bit E_b (in watts·second per information bit or Joules per information bit) is defined by*

$$E_b \equiv P/R, \tag{2.76}$$

where P is the average power of the transmission signal $x(t)$ in watts. Moreover, E_b/N_0 in Gaussian channels with $N_0/2$ noise power spectral density in watts·second is defined by

$$\frac{E_b}{N_0} \equiv \frac{P/R}{N_0}. \tag{2.77}$$

2.6 Faster than Nyquist Signaling in a Hilbert Space

In this section, a useful geometrical insight on the FTN signaling is presented. We establish that the FTN signaling can be viewed as a technique to insert additional signaling dimensions beyond those of the Nyquist rate signaling. First, we review the two key mathematical concepts from the theory of functional analysis, namely the Hilbert space of bandlimited signals and $2WNT$ dimensions, before turning our discussion to the FTN signaling.

Hilbert Space of Bandlimited Signals:

Hilbert space generalizes the Euclidean space of real numbers to finite energy (L^2) signals[17]. Each finite energy signal can be represented by a vector in the Hilbert space with each coordinate given by an inner product with the corresponding orthonormal basis functions. To see this, first express a finite energy signal $x(t)$ as a linear combination of the orthonormal basis functions:

$$x(t) = \sum_{n \in \mathbb{Z}} x[n] b_n(t), \tag{2.78}$$

where $b_n(t)$ is an orthonormal basis function (i.e., the inner product $\langle b_n(t), b_m(t) \rangle$ is equal to zero for any $n \neq m$ or equal to one for $n = m$) and $x[n]$ is the corresponding coefficient in the direction of the basis function $b_n(t)$. Note that any finite energy signal can be written as (2.78) with an example being the inverse Fourier series with complex exponentials as the basis functions. The coefficients $x[n]$ then can be obtained by the following inner product:

$$\langle x(t), b_n(t) \rangle = \sum_{m \in \mathbb{Z}} x[m] \langle b_m(t), b_n(t) \rangle = x[n], \tag{2.79}$$

due to the linearity of the inner product and the orthogonality of the basis functions $b_n(t)$.

This Hilbert space representation is particularly useful as it allows a complete description of time-continuous signals $x(t)$ by set of discrete values $\{x[n]\}$. In addition, it

[17] Although Hilbert spaces can be defined for more general classes of signals, for the purpose of the ensuing discussions, it suffices to consider Hilbert spaces only for the finite energy signals.

allows visualizing a continuous-time signal $x(t)$ as a vector in an n-dimensional space, as illustrated in Figure 2.10.

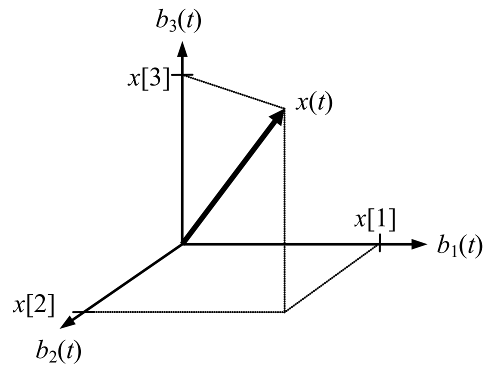

Figure 2.10 Illustration of Hilbert space (showing only up to three dimensions for brevity)

We now let the signal $x(t)$ be further strictly bandlimited; i.e., its Fourier transform $\hat{x}(f)$ has a frequency support of $f \in (-W, W)$. Such bandlimited-finite energy signals also have a Hilbert space representation, and it has a special name attached to it [40]:

Definition 2.20 (Paley-Wiener space): *The Hilbert space consisting of finite-energy (L^2) functions whose Fourier transforms are supported on $f \in (-W, W)$, where $W > 0$ and $W \in \mathbb{R}$ is called the Paley-Wiener space (PW^2).*

The Nyquist sampling theorem [70] tells us that any bandlimited signal (in the PW^2 space) can be written as

$$x(t) = \sum_{n=-\infty}^{\infty} x[n]\left(\sqrt{2W}\,\mathrm{sinc}(2W(t-nT))\right), \tag{2.80}$$

where T is the Nyquist interval T=1/(2W). Comparing (2.80) with (2.78), we can see that the orthonormal bases of PW^2 are $b_n(t) = \sqrt{2W}\,\mathrm{sinc}(2W(t-nT))$. Also by the Nyquist sampling theorem, we also know that $x[n] = T\cdot x(nT)$, i.e., the samples of $x(t)$ scaled by the factor T. Due to the completeness of the PW^2 space, the set of Nyquist rate sinc pulses $\{\mathrm{sinc}(2W(t-nT))\}_n$ is a *complete* set, i.e., *any* bandlimited signal can be written as a linear combination of these sinc pulses as in (2.80). Consequently, even the sinc pulses that do not lie at integer multiples of T, e.g., sinc($2W(t$-$nT/2)$), still lie completely in the PW^2 space, since they can be written as a linear combination of the set of Nyquist rate sinc pulses.

2WNT Dimensions:

Let us now consider sending a bandlimited signal of the form (2.80) over a band-limited channel, and let $x[n]$ be the symbol (or data) modulated on the sinc pulse $b_n(t)$. This, so called Nyquist rate signaling using the sinc function as its modulating pulse, is illustrated in Figure 2.11. Using the Nyquist rate signaling of $2W$ symbols per second, approximately $2WNT$ symbols are transmitted in NT seconds of transmission (assuming that the tails of the sinc are reasonably negligible compared to the overall duration of the transmission NT).

In the Hilbert space, the Nyquist rate signaling corresponds to sending a $2WNT$ dimensional vector within NT seconds of transmission. Furthermore, since the sinc pulses are mutually orthogonal, they do not interfere with one another. This implies that Nyquist rate signaling is capable of accessing $2WNT$ signaling dimensions within NT seconds of transmission. This statement (and its variations) is sometimes referred to as "2*WT theorem*" in the literature [133], [134], [135].

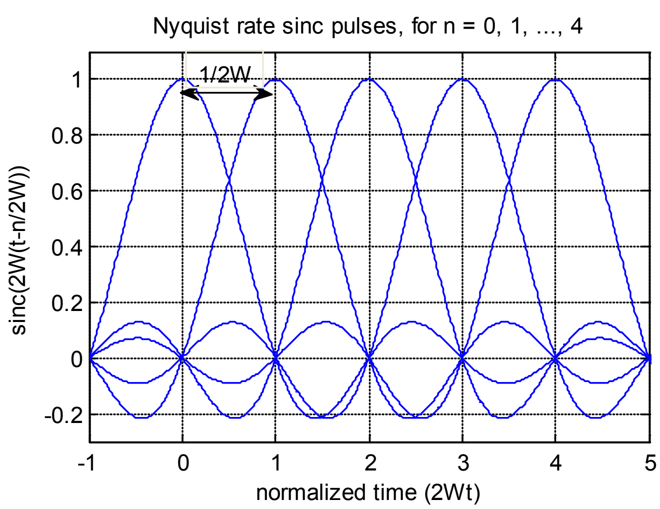

Figure 2.11 Nyquist rate sinc pulses, for n = 0,1, …, 4; W is the one-sided channel bandwidth in Hertz

Adding New Dimensions Through FTN Signaling

We now turn our attention to the faster than Nyquist signaling. Using the above two concepts, the FTN signaling will be shown to provide more signaling dimensions in the Hilbert space than $2WNT$ dimensions offered by the Nyquist rate signaling in the case of *finite-time* transmissions. As a consequence, FTN leads to higher data throughput than that of the conventional Nyquist-rate signaling in this case.

First consider a finite set of Nyquist rate sinc-pulses, denoted by $\mathsf{S}_{Nyquist}$:

$$\mathsf{S}_{Nyquist} \equiv \left\{ s_n(t) = (2W)^{1/2} \operatorname{sinc}(2W(t-nT)) \right\}, \text{ for } n = 0, 1, \ldots, 2WNT-1. \tag{2.81}$$

The number of signaling dimensions spanned by this Nyquist set $\mathsf{S}_{Nyquist}$ is $2WNT$ within approximately NT seconds of transmission. Now, consider inserting into the Nyquist set $\mathsf{S}_{Nyquist}$ a FTN sinc-pulse $s_{1/2}(t) = (2W)^{1/2} \operatorname{sinc}(2W(t-T/2))$. Applying the well-known Gram-Schmidt orthogonalization process to the newly formed set, we obtain the following orthonormal basis functions:

$$b_n(t) = s_n(t) \quad \text{for } n = 0, 1, \cdots, 2WNT-1, \tag{2.82}$$

and

$$b_{2WNT}(t) = \frac{s_{1/2}(t) - \sum_{n=0}^{2WNT-1} \left\langle s_{1/2}(t), b_n(t) \right\rangle b_n(t)}{\left\| s_{1/2}(t) - \sum_{n=0}^{2WNT-1} \left\langle s_{1/2}(t), b_n(t) \right\rangle b_n(t) \right\|}. \tag{2.83}$$

The newly formed basis function $b_{2WNT}(t)$ is plotted in Figure 2.12 and is shown to be a non-zero function due to linear independence of $s_{1/2}(t)$ and the Nyquist set. Consequently, the number of signaling dimensions spanned by the Nyquist set plus $s_{1/2}(t)$ becomes $2WNT+1$. That is, *a new signaling dimension has been introduced by the FTN signaling within NT seconds of transmission*.

Similarily, inserting another FTN rate sinc-pulse, say $s_{3/2}(t)$, into the set introduces a $(2WNT+2)^{\text{th}}$ signaling dimension. The corresponding orthonormal basis function $b_{2WNT+1}(t)$ is also plotted in Figure 2.12 and is non-zero due to linear independence of $s_{3/2}(t)$ to the Nyquist set and $s_{1/2}(t)$.

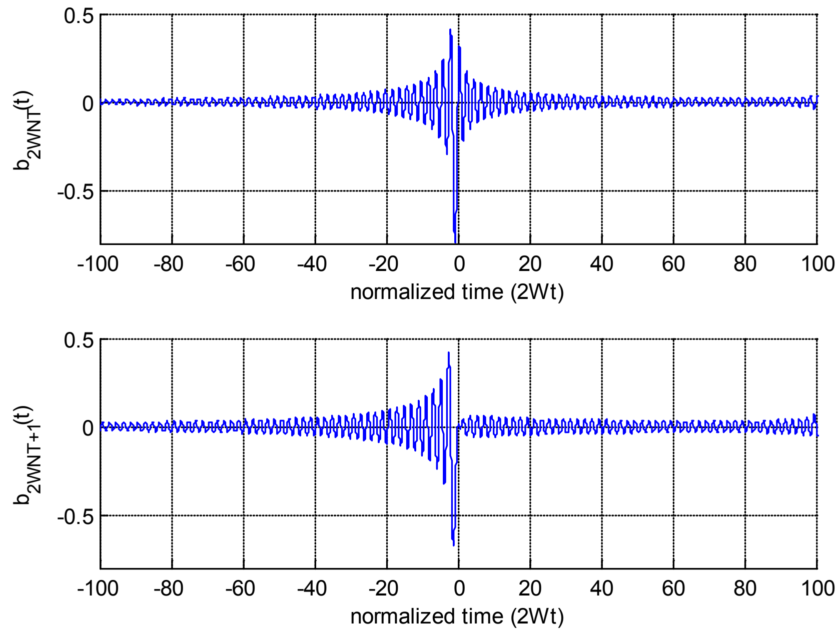

Figure 2.12 New orthonormal basis functions introduced by inserting FTN signals $s_{1/2}(t)$ and $s_{3/2}(t)$ into the Nyquist set of $\{s_0(t), s_1(t), \ldots, s_{2WNT-1}(t)\}$

In summary, when viewed from the Hilbert space, the FTN signaling provides a means to access more than $2WNT$ signaling dimensions within the NT seconds of transmission. *In other words, FTN signaling gives an access to signaling dimensions that are otherwise only accessible by signaling outside the time window in the Nyquist rate signaling.*

2.7 Chapter Summary

The main objective of this chapter has been a review of preliminary definitions and tools that are relevant to studying the FTN signaling. First, a chronological literature survey on the FTN signaling was presented. Selected definitions and theorems from the information theory were then reviewed with an emphasis on the characterization of the channel capacities in strictly bandlimited or power-spectrum confined AWGN channels. Moreover, MAP symbol detection for ISI channels (for Ungerboeck observation model) and the advanced channel coding techniques known as the Turbo coding and Turbo equalization were briefly highlighted. This was followed by the review of selected results from the matrix algebra.

In addition, continuous-time channel parameters such as the channel bandwidth, power spectral density (PSD), and channel *SNR* and E_b/N_0 were carefully defined for a fair and unambiguous analysis of the considered continuous-time FTN signaling. The Nyquist theorem was also revisited with a simple proof, and it was pointed out that data can still be recovered even if the Nyquist theorem is violated as in the faster than Nyquist signaling. Finally, a useful insight into the FTN signaling, from the signaling dimensions perspective, was presented.

Chapter 3

FTN System Models and Power Spectral Analysis

Conventional discrete-time channel models used in digital communications are generally formulated with the assumptions of Nyquist rate transmissions or orthogonality of the transmitted signals. For the considered faster than Nyquist (FTN) signaling, however, these channel models no longer apply due to the inherent non-orthogonality of FTN and hence it is imperative to re-establish the link between the actual continuous-time channel transmissions and the discrete-time channel models for an accurate analysis.

In this chapter, we develop several discrete-time FTN channel models, study their various properties, and analyze power spectral densities of the FTN signals. First, in section 3.1, the discrete-time channel models of the FTN signaling are formulated, clearly highlighting all the underlying assumptions. Some important properties of the FTN signaling are then studied and derived in section 3.2, through analysis of the FTN channel matrix H that characterizes the inter-symbol interference (ISI) patterns. Secondly, in section 3.3, a (non-trivial) power transmission constraint for the FTN signaling is derived for the first time, which allows a proper assessment of the transmission power of non-*i.i.d.* FTN signals. Finally, in section 3.4, the power spectral density (PSD) analysis of FTN signals is presented, which extends the PSD analysis of *i.i.d.* FTN signals to non-*i.i.d.* FTN signals. It is analytically shown that data precoding in FTN signaling generally increases the transmission bandwidth and sufficient conditions for preventing such bandwidth expansions are identified.

3.1 FTN Discrete-Time Channel Models

In this section, we formulate the discrete-time channel models for the considered FTN signaling. The FTN baseband transmission model, illustrated in Figure 3.1, is given by

$$x(t) = \sum_{n=0}^{KN-1} x[n] s(t - nT/K) = \sum_{n=0}^{KN-1} x[n] s(t - n\Delta t), \tag{3.1}$$

where $s(t)$ is a modulating pulse (or transmit filter response), $\{x[n]\}$ is a set of modulation symbols that may be either precoded or not, N is the packet length, and K (> 1) is a factor by which the Nyquist rate is exceeded. Then, the signaling rate (or the baud rate) is given by $1/\Delta t = K/T$ symbols per second and the total time duration taken to transmit KN symbols is $NT+(K-1)T/K$ seconds (for N sufficiently large, $NT+(K-1)T/K \cong NT$ seconds). Without any loss of generality, the modulating pulse $s(t)$ is assumed to have a unit energy by proper normalization.

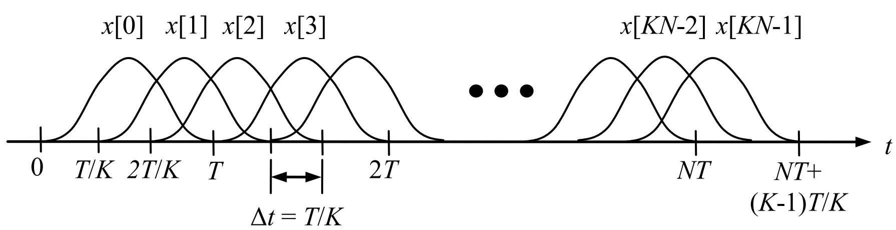

Figure 3.1 Conceptual illustration of the faster than Nyquist signaling with the signaling rate $1/\Delta t = K/T$

We consider the FTN signaling in a linear, time-invariant (LTI) channel perturbed by additive white Gaussian noise (AWGN). LTI channels are frequently encountered in practice, such as in landline and cellular telephony, microwave line-of-sight radio, satellite, and underwater acoustic [113]. Figure 3.2 shows the considered continuous-time FTN channel model, where $c(t)$ is an impulse response of LTI channel, $z(t)$ is AWGN with a two-sided power spectral density $N_0/2$ watts/Hz, and the outputs of the receiver matched filter $g(t)$ are sampled at the FTN signaling rate of $1/\Delta t$ in order to obtain an channel observation $y[n]$ for each transmitted symbol $x[n]$.

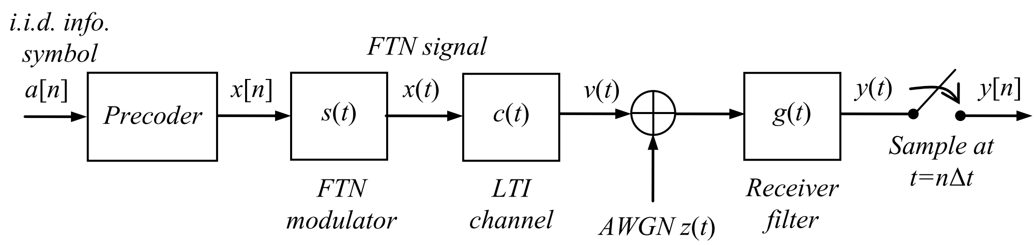

Figure 3.2 Considered FTN digital communication setup

The receiver filter may be matched to the transmit filter response only, in which case $g(t) = s^*(-t)$, or matched to the combined response of the transmit filter and the channel, in which case $g(t) = (s(t) * c(t))^*\big|_{t=-t}$, where the superscript $(\cdot)^*$ denotes the complex conjugation and the convolution operator is denoted by $a(t) * b(t) \equiv \int_{-\infty}^{\infty} a(\tau)b(t-\tau)d\tau$. Note that the latter $g(t) = (s(t) * c(t))^*\big|_{t=-t}$ is the optimal matched filtering in the sense of maximizing the received signal-to-noise ratio (SNR), but the former $g(t) = s^*(-t)$ is also being used in practice where adaptive adjustment of the receiver to varying $c(t)$ is not feasible, such as in rapidly changing channels, or where the receiver is "hardwired" and cannot be adjusted.

The n-th sampled output $y[n]$ from Figure 3.2 is given by

$$y[n] \equiv y\left(n\Delta t\right) = \underbrace{x(t) * c(t) * g(t)\big|_{t=n\Delta t}}_{\text{signal component}} + \underbrace{z(t) * g(t)\big|_{t=n\Delta t}}_{\text{noise component}} . \tag{3.2}$$

Our goal in the following is to write the above expression in a compact form involving discrete-time terms only for the considered FTN signaling. We start by substituting the expression of the FTN signal $x(t)$ from (3.1) into the signal component of (3.2), which leads to

$$x\left(t\right) * c\left(t\right) * g\left(t\right)\Big|_{t=n\Delta t} = \sum_{m=0}^{KN-1} x[m]\left(s(t) * c(t) * g(t)\big|_{t=(n-m)\Delta t}\right). \tag{3.3}$$

For notational conveniences, we define terms α and $\tilde{h}_k$ as

$$\alpha \equiv s\left(t\right) * c\left(t\right) * g\left(t\right)\Big|_{t=0} \text{ and} \tag{3.4}$$

$$\tilde{h}_k \equiv \frac{s(t)*c(t)*g(t)\big|_{t=k\Delta t}}{s(t)*c(t)*g(t)\big|_{t=0}} = \frac{1}{\alpha}\cdot s(t)*c(t)*g(t)\big|_{t=k\Delta t}, \quad k \in \mathbb{Z} . \tag{3.5}$$

Then, the signal component of the sampled outputs can be simply expressed as

$$x(t)*c(t)*g(t)\big|_{t=n\Delta t} = \alpha x[n] + \alpha \sum_{\substack{m=0 \\ m\neq n}}^{KN-1} \tilde{h}_{n-m} x[m], \tag{3.6}$$

where the first term $\alpha x[n]$ is the desired term scaled by the scalar α whereas the second term $\alpha \sum_{\substack{m=0 \\ m\neq n}}^{KN-1} \tilde{h}_{n-m} x[m]$ represents the intersymbol interference (ISI) term.

The noise component in (3.2) will be denoted by $z[n]$ for $n = 0, 1, \ldots, KN-1$:

$$z[n] \equiv z(t)*g(t)\big|_{t=n\Delta t} = \int_{-\infty}^{+\infty} z(\tau)\, g(n\Delta t - \tau)\, d\tau . \tag{3.7}$$

The filtered noise samples $\{z[n]\}$ are Gaussian distributed with zero mean and $N_0/2$ variance with the following correlations between the samples:

$$E\left\{z[n]z^*[m]\right\} = \frac{N_0}{2} \int_{-\infty}^{+\infty} g(\tau)\, g^*\left(\tau - (n-m)\Delta t\right) d\tau , \tag{3.8}$$

which is due to the properties of AWGN, i.e., due to $E\{z^*(\tau)z(\lambda)\} = (N_0/2)\delta(\tau - \lambda)$. For convenience, we define a variable φ_k by

$$\varphi_k \equiv \left\| g(t) \right\|^{-2} \int_{-\infty}^{\infty} g(\tau)\, g^*\left(\tau - k\Delta t\right) d\tau, \quad k \in \mathbb{Z} , \tag{3.9}$$

where $\|\cdot\|$ denotes the L^2 norm. Then, the noise correlation (3.8) can be rewritten as

$$E\left\{z[n]z^*[m]\right\} = \frac{N_0}{2} \left\| g(t) \right\|^2 \varphi_{n-m} . \tag{3.10}$$

Summarizing, the sampled outputs $y[n]$ (3.2) can be written as

$$y[n] = \alpha x[n] + \alpha \sum_{\substack{m=0 \\ m\neq n}}^{KN-1} \tilde{h}_{n-m} x[m] + z[n], \tag{3.11}$$

where the noise samples $\{z[n]\}$ are zero mean Gaussian distributed with the correlations given by (3.10).

Alternatively, the set of sampled outputs $\{y[n]\}$ can be conveniently expressed in a matrix form. Let $\mathbf{y} \equiv [y[0], y[1], \cdots, y[KN\text{-}1]]^T$, $\mathbf{x} \equiv [x[0], x[1], \cdots, x[KN\text{-}1]]^T$, and $\mathbf{z} \equiv$

$[z[0], z[1], \cdots, z[KN\text{-}1]]^T$, where the superscript $[\cdot]^T$ denotes the vector (matrix) transpose operator. Also define a Toeplitz matrix $\tilde{H} \equiv [\tilde{h}_{(i-j)}]_{i,j=0,1,\cdots,KN-1}$, i.e.,

$$\tilde{H} \equiv \begin{bmatrix} 1 & \tilde{h}_{-1} & \tilde{h}_{-2} & \cdots & \tilde{h}_{-(KN-1)} \\ \tilde{h}_1 & 1 & \tilde{h}_{-1} & \cdots & \tilde{h}_{-(KN-2)} \\ \tilde{h}_2 & \tilde{h}_1 & 1 & \cdots & \tilde{h}_{-(KN-3)} \\ \vdots & \vdots & \vdots & \ddots & \vdots \\ \tilde{h}_{KN-1} & \tilde{h}_{KN-2} & \tilde{h}_{KN-3} & \cdots & 1 \end{bmatrix}, \tag{3.12}$$

where $\tilde{h}_k$, as defined in (3.5), is reproduced below for convenience:

$$\tilde{h}_k \equiv \frac{1}{\alpha} \cdot s(t) * c(t) * g(t)\Big|_{t=k\Delta t}, \text{ where} \tag{3.13}$$

$$\alpha \equiv s(t) * c(t) * g(t)\Big|_{t=0}. \tag{3.14}$$

Then, the matrix equation of $\{y[n]\}$ becomes simply

$$\mathbf{y} = \alpha \tilde{H} \mathbf{x} + \mathbf{z}, \tag{3.15}$$

and the Gaussian noise vector $\mathbf{z}$ has a zero mean vector and a covariance matrix (due to the noise correlations (3.10))

$$E\{\mathbf{z}\mathbf{z}^\dagger\} = \frac{N_0}{2} \left\| g(t) \right\|^2 \Phi, \tag{3.16}$$

where $(\cdot)^\dagger$ denotes the conjugate transpose (Hermitian) operator and the $KN \times KN$ matrix Φ is defined by

$$\Phi \equiv \begin{bmatrix} 1 & \varphi_{-1} & \varphi_{-2} & \cdots & \varphi_{-(KN-1)} \\ \varphi_1 & 1 & \varphi_{-1} & \cdots & \varphi_{-(KN-2)} \\ \varphi_2 & \varphi_1 & 1 & \cdots & \varphi_{-(KN-3)} \\ \vdots & \vdots & \vdots & \ddots & \vdots \\ \varphi_{KN-1} & \varphi_{KN-2} & \varphi_{KN-3} & \cdots & 1 \end{bmatrix}, \tag{3.17}$$

where

$$\varphi_k \equiv \left\| g(t) \right\|^{-2} \int_{-\infty}^{+\infty} g(\tau) g^*(\tau - k\Delta t) \, d\tau. \tag{3.18}$$

Discrete-time channel models, that are similar to the considered FTN model (3.15), appear frequently in the ISI channel literature (e.g., see [46], [151], [131], [66]). The key differences that distinguish the FTN channel (3.15) from the other ISI channels are

1) the AWGN noise samples $\{z[n]\}$ are not *i.i.d.* as a result of sampling faster than the Nyquist rate at the receiver, and
2) significant ISI also originates from the transmitter, not only from the physical channel, due to the non-orthogonality of FTN.

As an important special case, in the *AWGN channel* where $c(t) = \delta(t)$ and $g(t) = s^*(-t)$, the discrete time FTN channel model (3.11) simplifies to

$$y[n] = x[n] + \sum_{\substack{m=0 \\ m\neq n}}^{KN-1} h_{n-m} x[m] + z[n], \tag{3.19}$$

where

$$h_k \equiv \int_{-\infty}^{+\infty} s(\tau) s^*(\tau - k\Delta t)\, d\tau, \quad k \in \mathbb{Z} . \tag{3.20}$$

Furthermore, the FTN matrix model in AWGN channel becomes simply

$$\mathbf{y} = H\mathbf{x} + \mathbf{z}, \tag{3.21}$$

where

$$H \equiv \begin{bmatrix} 1 & h_{-1} & h_{-2} & \cdots & h_{-(KN-1)} \\ h_1 & 1 & h_{-1} & \cdots & h_{-(KN-2)} \\ h_2 & h_1 & 1 & \cdots & h_{-(KN-3)} \\ \vdots & \vdots & \vdots & \ddots & \vdots \\ h_{KN-1} & h_{KN-2} & h_{KN-3} & \cdots & 1 \end{bmatrix} \tag{3.22}$$

with the covariance matrix of $\mathbf{z}$ now given by

$$E\{\mathbf{z}\mathbf{z}^\dagger\} = \frac{N_0}{2} H . \tag{3.23}$$

The matrix H (3.22) is a Toeplitz matrix with entries h_k given by the signal autocorrelations of $s(t)$ at every FTN signaling instances $k\Delta t = kT/K$, $k = 0, 1, \ldots, KN\text{-}1$. Due to its significance in the analysis of FTN in the AWGN channel, we will call this matrix the *FTN matrix H* throughout this dissertation. Some of its key properties are derived in the next section.

3.2 Properties of the FTN Channel Matrix *H*

The FTN matrix H as defined in (3.22) represents the intersymbol interference that arises from signaling faster than the Nyquist rate. This matrix is *Toeplitz* and *Hermitian* by definition and has the size $KN \times KN$. The question of whether this matrix is invertible or not and how it behaves asymptotically as the block length N tends to infinity will have important consequences in the later analysis of FTN signaling. In this section, we study two properties of the matrix H, namely its invertibility for K and N finite and its asymptotic eigenvalue distribution as N tends to infinity. The analysis here will be vital in understanding the contrasting behavior of FTN signaling at the finite block length N and at N arbitrarily large.

We first consider the invertibility of the FTN matrix H with *finite* FTN signaling rate factor K and *finite* packet size N. We prove in the following proposition that a class of finite Toeplitz matrices including the matrix H is always invertible.

***Proposition 3.1* (*Nonsingularity of some Toeplitz matrices*):** *Let $q(t)$ be any non-zero finite energy L^2 function that is either strictly band-limited to $(-W, W)$ or time-limited to (T_0, T_1). Then an $n \times n$ Toeplitz matrix*

$$Q_n \equiv \begin{bmatrix} q_0 & q_{-1} & q_{-2} & \cdots & q_{-(n-1)} \\ q_1 & q_0 & q_{-1} & \cdots & q_{-(n-2)} \\ q_2 & q_1 & q_0 & \cdots & q_{-(n-3)} \\ \vdots & \vdots & \vdots & \ddots & \vdots \\ q_{n-1} & q_{n-2} & q_{n-3} & \cdots & q_0 \end{bmatrix}, \tag{3.24}$$

where for $k \in \mathbb{Z}$,

$$q_k \equiv \int_{-\infty}^{+\infty} q(\tau) q^*(\tau - k\Delta t)\, d\tau \tag{3.25}$$

is invertible for any positive integer $n < \infty$.

The proof of the proposition involves the following two lemmas. First lemma establishes a direct relationship between linear independence of $q(t)$ and the invertibility of the matrix Q_n.

Lemma 3.1: *Let q(t) be a non-zero finite energy L^2 function either strictly band-limited to $(-W, W)$ or time-limited to (T_0, T_1). Then, matrix Q_n as defined in (3.24) is invertible if and only if the set of translates $\{q(t-k\Delta t)\}_k$ with $k = 0, \ldots, n-1$ is linearly independent.*

***Proof of Lemma 3.1*:** Recall from section 2.4 that the Gramian matrix of finite energy functions $r_0(t), r_1(t), \ldots, r_{n-1}(t)$ is defined as

$$G\left(r_0(t),\cdots,r_{n-1}(t)\right) \equiv \begin{bmatrix} \langle r_0,r_0\rangle & \langle r_0,r_1\rangle & \langle r_0,r_2\rangle & \cdots & \langle r_0,r_{n-1}\rangle \\ \langle r_1,r_0\rangle & \langle r_1,r_1\rangle & \langle r_1,r_2\rangle & \cdots & \langle r_1,r_{n-1}\rangle \\ \langle r_2,r_0\rangle & \langle r_2,r_1\rangle & \langle r_2,r_2\rangle & \cdots & \langle r_2,r_{n-1}\rangle \\ \vdots & \vdots & \vdots & \ddots & \vdots \\ \langle r_{n-1},r_0\rangle & \langle r_{n-1},r_1\rangle & \langle r_{n-1},r_2\rangle & \cdots & \langle r_{n-1},r_{n-1}\rangle \end{bmatrix},$$

where

$$\langle r_i,r_j\rangle \equiv \int_{-\infty}^{\infty} r_i(t)\,r_j^*(t)\,dt\,. \tag{3.26}$$

If $r_i(t)$ and $r_j(t)$ are both bandlimited to $(-W, W)$, then (3.26) becomes

$$\langle r_i,r_j\rangle = \int_{-W}^{W} \hat{r}_i(f)\,\hat{r}_j^*(f)\,df\,, \tag{3.27}$$

due to the generalized Parseval's theorem $\int_{-\infty}^{\infty} a(t)b^*(t)dt = \int_{-\infty}^{\infty} \hat{a}(f)\hat{b}^*(f)df$, where $\hat{r}_i(f)$ and $\hat{r}_j(f)$ denote the Fourier transforms of $r_i(t)$ and $r_j(t)$, respectively.

On the other hand, when $r_i(t)$ and $r_j(t)$ are both time-limited, the product $r_i(t)r_j^*(t)$ is also time-limited to, say (T_0, T_1), and (3.26) becomes

$$\langle r_i,r_j\rangle = \int_{T_0}^{T_1} r_i(t)\,r_j^*(t)\,dt\,. \tag{3.28}$$

We note that the matrix Q_n defined in (3.24) is also a Gramian matrix since Q_n can be re-written as

$$Q_n = G\Big(q(t),q(t-\Delta t),\cdots,q\big(t-(n-1)\Delta t\big)\Big). \tag{3.29}$$

Then by the Gram's criterion in Lemma 2.7, the Gramian matrix Q_n has a nonzero determinant, thus is invertible, if and only if the set of translates $\{q(t), \ldots, q(t-(n-1)\Delta t)\}$ is linearly independent. This completes the proof of Lemma 3.1. ■

Therefore, to ensure that the matrix Q_n is invertible, the set of translates $\{q(t-k\Delta t)\}_k$ must be linearly independent. The next lemma derives a sufficient condition for invertibility of the matrix Q_n.

Lemma 3.2 (based on Proposition 5.1.1 in [21]): *Let q_k be defined by (3.25), i.e.,*

$$q_k \equiv \int_{-\infty}^{+\infty} q(\tau)q^*(\tau-k\Delta t)\,d\tau, \quad k \in \mathbb{Z}\,, \tag{3.30}$$

where q(t) is a non-zero finite energy L^2 function that is either strictly band-limited to $(-W, W)$ or time-limited to (T_0, T_1). If $q_k \to 0$ as $k \to \infty$ then the $n \times n$ matrix Q_n given in (3.24) is non-singular for every $n \geq 1$.

The proof of this lemma is given in Appendix C.

At this point, we are finally ready to give a proof to the Proposition 3.1.

Proof of Proposition 3.1: By Lemma 3.2, the sufficient condition for the non-singularity of Q_n is $q_k \to 0$ as $k \to \infty$. When $q(t)$ is time-limited to (T_0, T_1), q_k clearly becomes zero for k sufficiently large (precisely, when $k\Delta t > (T_1-T_0)$) and hence the non-singularity of Q_n follows. Now we consider the case when $q(t)$ is strictly bandlimited to $(-W, W)$. Denoting the Fourier transform of $q(t)$ by $\hat{q}(f)$, we have for $k \in \mathbb{Z}$,

$$q_k = \int_{-\infty}^{\infty} q(\tau)q^*(\tau-k\Delta t)\,d\tau \tag{3.31}$$

$$= \int_{-\infty}^{\infty} \hat{q}(f)\hat{q}^*(f)e^{j2\pi fk\Delta t}df \tag{3.32}$$

$$= \int_{-W}^{W} \left|\hat{q}(f)\right|^2 e^{j2\pi fk\Delta t}df\,, \tag{3.33}$$

where (3.32) is due to the generalized Parseval's theorem, $\int_{-\infty}^{\infty} a(t)b^*(t)dt = \int_{-\infty}^{\infty} \hat{a}(f)\hat{b}^*(f)df$ followed by the delay property of the Fourier transform, and (3.33) is due to the finite bandwidth $f \in (-W, W)$. But by the Riemann-Lebesgue lemma[18] and by noting that $|\hat{q}(f)|^2$ is absolutely integrable or $\int_{-W}^{W} |\hat{q}(f)|^2 \, df = \|q(t)\|^2 < \infty$,

$$\lim_{|\lambda|\to\infty} \int_{-W}^{W} |\hat{q}(f)|^2 e^{j\lambda f} \, df = 0 . \tag{3.34}$$

Therefore, $q_k \to 0$ as $k \to \infty$ and the proof of Proposition 3.1 is complete. ■

Note that the FTN matrix H (as well as the noise covariance matrix Φ in (3.17)) is a special instance of the matrix Q_n in Proposition 3.1 by replacing $q(t)$ with the modulating pulse $s(t)$ and by setting $n = KN$. The invertibility (or non-singularity) of the FTN matrix H will have several important consequences in the analysis of optimal precoding and the resulting channel capacities in Chapter 5.

We now consider the behavior of the FTN matrix H as $N \to \infty$. First, we define a useful frequency-domain signal called *folded pulse spectrum* below:

Definition 3.1 (Folded pulse spectrum): *Let $\hat{s}(f)$ denote the Fourier transform of a unit energy modulating pulse $s(t)$. Then, the folded pulse spectrum $\hat{s}_{folded}(f)$ is defined by*

$$\hat{s}_{folded}(f) \equiv \sum_{k=-\infty}^{\infty} |\hat{s}(f - k/\Delta t)|^2, \quad f \in \left(-\frac{1}{2\Delta t}, \frac{1}{2\Delta t}\right). \tag{3.35}$$

The folded pulse spectrum $\hat{s}_{folded}(f)$ consists of overlapping replicas of $|\hat{s}(f)|^2$ separated by $1/\Delta t$, and the terminology "*folded spectrum*" stems from the Nyquist's work on his pulse-shaping criterion (or zero-ISI criterion) [106]. It is interesting to note that the folded pulse spectrum is absolutely integrable over the frequency range $f \in (-1/(2\Delta t), 1/(2\Delta t))$, i.e., $\int_{-1/(2\Delta t)}^{1/(2\Delta t)} |\hat{s}_{folded}(f)| \, df = \sum_{k=-\infty}^{\infty} \int_{-1/(2\Delta t)-k/\Delta t}^{1/(2\Delta t)-k/\Delta t} |\hat{s}(f)|^2 \, df = \int_{-\infty}^{\infty} |\hat{s}(f)|^2 \, df = 1$, where the last equality is due to $s(t)$ having a unit energy.

The folded pulse spectrum $\hat{s}_{folded}(f)$ is directly related to the FTN matrix H in the following way:

[18] The *Riemann-Lebesgue lemma* states that, for any absolutely integrable function $q(t)$ on $[a, b]$, the Fourier series coefficients a_k's tend to zero as $|k|\to\infty$ [119]. That is, if $\int_a^b |q(t)| \, dt < \infty$, $\lim_{|k|\to\infty} \int_a^b q(t) \exp(-jkt) \, dt = 0$.

Lemma 3.3 (Folded pulse spectrum and inverse Fourier series of FTN matrix): *Let* $h(\lambda)$ *be the inverse Fourier series of the entries of the Toeplitz FTN matrix* $H \equiv [h_{(i-j)}]_{i,j=0,1,\cdots,KN-1}$*, i.e.,*

$$h(\lambda) = \sum_{k=-\infty}^{\infty} h_k e^{jk\lambda} \;\; for \;\; \lambda \in \mathbb{R} \, , \tag{3.36}$$

where $h_k = \int_{-\infty}^{+\infty} s(\tau) s^*(\tau - k\Delta t) d\tau$ *for* $k \in \mathbb{Z}$ *. If* $\hat{s}_{folded}(f) < \infty$ *for all f, then*

$$\hat{s}_{folded}(f) = \Delta t \cdot h(-2\pi f \Delta t). \tag{3.37}$$

Proof of Lemma 3.3: We begin by evaluating $h(-2\pi f\Delta t)$ in the following:

$$h(-2\pi f \Delta t) = \sum_{k=-\infty}^{\infty} \left(\int_{-\infty}^{\infty} s(\tau) s^*(\tau - k\Delta t) d\tau \right) e^{-j2\pi f k\Delta t} \tag{3.38}$$

$$= \sum_{k=-\infty}^{\infty} \left(\int_{-\infty}^{\infty} |\hat{s}(\lambda)|^2 e^{j2\pi\lambda k\Delta t} d\lambda \right) e^{-j2\pi f k\Delta t} \tag{3.39}$$

$$= \int_{-\infty}^{\infty} |\hat{s}(\lambda)|^2 \sum_{k=-\infty}^{\infty} e^{j2\pi k\Delta t(\lambda - f)} d\lambda \tag{3.40}$$

$$= \int_{-\infty}^{\infty} |\hat{s}(\lambda)|^2 \sum_{k=-\infty}^{\infty} \delta\left(\Delta t(\lambda - f) + k\right) d\lambda \tag{3.41}$$

$$= (\Delta t)^{-1} \sum_{k=-\infty}^{\infty} |\hat{s}(f - k/\Delta t)|^2 , \tag{3.42}$$

where (3.39) is due to the generalized Parseval's theorem, $\int_{-\infty}^{\infty} a(t) b^*(t) dt$ = $\int_{-\infty}^{\infty} \hat{a}(f) \hat{b}^*(f) df$ and the delay property of the Fourier transform, (3.40) and (3.42) are due to Fubini's theorem [19], and (3.41) is due to the Poisson summation formula $\sum_{k=-\infty}^{\infty} e^{j2\pi kt} = \sum_{k=-\infty}^{\infty} \delta(t+k)$. Finally, using the definition of $\hat{s}_{folded}(f)$, we have $h(-2\pi f \Delta t) = (\Delta t)^{-1} \hat{s}_{folded}(f)$ as desired. This completes the proof of Lemma 3.3. ■

[19] To use Fubini's theorem, we go backwards from (3.42) to (3.40), establishing equalities throughout. First note that (3.42) is $(\Delta t)^{-1}\hat{s}_{folded}(f)$, which was assumed to be finite for all *f*. Since (3.42) is finite, Fubini's theorem can be applied to obtain (3.41) (by interchanging the order of the integral and the sum), and from (3.41) we can re-apply Fubini to get to (3.40).

Lemma 3.3 implies that the folded pulse spectrum $\hat{s}_{folded}(f)$ completely characterizes the FTN matrix H, by being an inverse Fourier series of the entries of H. The following proposition further establishes that the asymptotic eigenvalue distribution of the FTN matrix H as $N \to \infty$ is also completely characterized by the folded pulse spectrum. Roughly speaking, the proposition indicates that the eigenvalues of H behaves as the normalized folded pulse spectrum $(\Delta t)^{-1}\hat{s}_{folded}(f)$.

Proposition 3.2 (Asymptotic eigenvalue distribution of H): *Let $\lambda_0, \lambda_1, \lambda_2, \ldots, \lambda_{KN-1}$ be the eigenvalues of the $KN\times KN$ FTN matrix H. Define the (cumulative) eigenvalue distribution function by $D_N(\xi)$ = (number of $\lambda_i \le \xi$)/(KN) for $\xi \in \mathbb{R}$. Assume furthermore that, for all $\xi \in \mathbb{R}$,*

$$\int_{f:\,(\Delta t)^{-1}\hat{s}_{folded}(f)=\xi} df = 0\,.\text{[20]} \tag{3.43}$$

Then the limiting distribution $D(\xi) = \lim_{N\to\infty} D_N(\xi)$ exists and is given by

$$D(\xi) = \Delta t \int_{(\Delta t)^{-1}\hat{s}_{folded}(f)\le\xi} df\ . \tag{3.44}$$

(Note that fraction of eigenvalues between two values a and b (b>a) is then D(b) – D(a). The definition D(ξ) is similar to the cumulative distribution function (CDF) in probability theory.)

Proof: The following proof uses a generalized form of Szegö's theorem on the asymptotic eigenvalues of Toeplitz matrices, which is discussed in detail in Appendix D. By Lemma D.2 in Appendix D, the limiting eigenvalue distribution function $D(\xi)$ of the FTN matrix H is given by

$$D(\xi) = \frac{1}{2\pi}\int_{h(\lambda)\le\xi} d\lambda\,, \tag{3.45}$$

[20] The technical condition (3.43) may be interpreted as not allowing $\hat{s}_{folded}(f)$ to have a flat region around the point ξ. In many cases, this condition may be circumvented by approximating $\hat{s}_{folded}(f)$ by another signal, say $\tilde{\hat{s}}_{folded}(f)$, which replaces flat regions in $\hat{s}_{folded}(f)$ (if any) by small arcs with very small $\varepsilon > 0$ perpendicular distances.

where $h(\lambda)=\sum_{k=-\infty}^{\infty}h_k e^{jk\lambda}$ denotes the inverse Fourier series of the entries of *H*. By substitution of variable (setting $f=-\lambda/(2\pi\Delta t)$), (3.45) can be rewritten as

$$D(\xi)=\Delta t\int_{h(-2\pi f\Delta t)\le\xi}df\ . \tag{3.46}$$

Finally, due to Lemma 3.3, $h\left(-2\pi f\Delta t\right)$ can be replaced by the normalized folded pulse spectrum $(\Delta t)^{-1}\hat{s}_{folded}(f)$. This completes the proof of Proposition 3.2. ■

Proposition 3.2 indicates that the eigenvalues of *H*, as the packet length *N* gets large, behave as the normalized folded pulse spectrum $(\Delta t)^{-1}\hat{s}_{folded}(f)$. To help better understand the implications of Proposition 3.2, we consider two following concrete examples with two different modulating pulses *s*(*t*) and subsequently examine the eigenvalue distributions of the corresponding FTN matrices *H*.

Example 3.1 (Bandlimited modulating pulse): *The FTN matrix H when the modulating pulse is $s(t) = (2W)^{1/2}\mathrm{sinc}(2Wt)$ (which leads to a constant frequency response over $f \in(-W, W)$ and zero everywhere else) is given by $H = [sinc((i-j)/K)]_{i,\, j=0,\ldots,KN-1}$, or*

$$H=\begin{bmatrix} 1 & \mathrm{sinc}\left(\frac{1}{K}\right) & \mathrm{sinc}\left(\frac{2}{K}\right) & \cdots & \mathrm{sinc}\left(\frac{KN-1}{K}\right)\\ \mathrm{sinc}\left(\frac{1}{K}\right) & 1 & \mathrm{sinc}\left(\frac{1}{K}\right) & \cdots & \mathrm{sinc}\left(\frac{KN-2}{K}\right)\\ \mathrm{sinc}\left(\frac{2}{K}\right) & \mathrm{sinc}\left(\frac{1}{K}\right) & 1 & \cdots & \mathrm{sinc}\left(\frac{KN-3}{K}\right)\\ \vdots & \vdots & \vdots & \ddots & \vdots\\ \mathrm{sinc}\left(\frac{KN-1}{K}\right) & \mathrm{sinc}\left(\frac{KN-2}{K}\right) & \mathrm{sinc}\left(\frac{KN-3}{K}\right) & \cdots & 1 \end{bmatrix}, \tag{3.47}$$

for some integers $K > 0$ and $N > 0$. It is interesting to note that this specific matrix based on the sinc function is also known as the "Prolate matrix" in the linear algebra and applied mathematics literature (e.g., see [154]) and is noted for its extreme ill-conditioning.

Example 3.2 (Time-limited modulating pulse): *The FTN matrix H when the s(t) is a rectangular pulse, i.e., $s(t) = T^{-1/2}$ within $t\in(0, T)$ and zero everywhere else, is given by $H = [max(0, 1-|i-j|/K)]_{i,\, j=0,1,\ldots,KN-1}$, for $K>0$, $N>0$, or*

$$
H=\begin{bmatrix}
1 & \frac{K-1}{K} & \cdots & 1/K & & \mathbf{0} \\
\frac{K-1}{K} & 1 & & 2/K & \ddots & \\
\vdots & & \ddots & \vdots & & 1/K \\
1/K & 2/K & \cdots & 1 & & \\
 & & & \ddots & & 2/K \\
 & \ddots & & & \ddots & \vdots \\
\mathbf{0} & & 1/K & 2/K & \cdots & 1
\end{bmatrix}, \tag{3.48}
$$

which is a banded Toeplitz matrix with the size KN×KN.

Figure 3.3 plots the MATLAB computed eigenvalues of H from the above two examples along with the corresponding normalized folded pulse spectra.

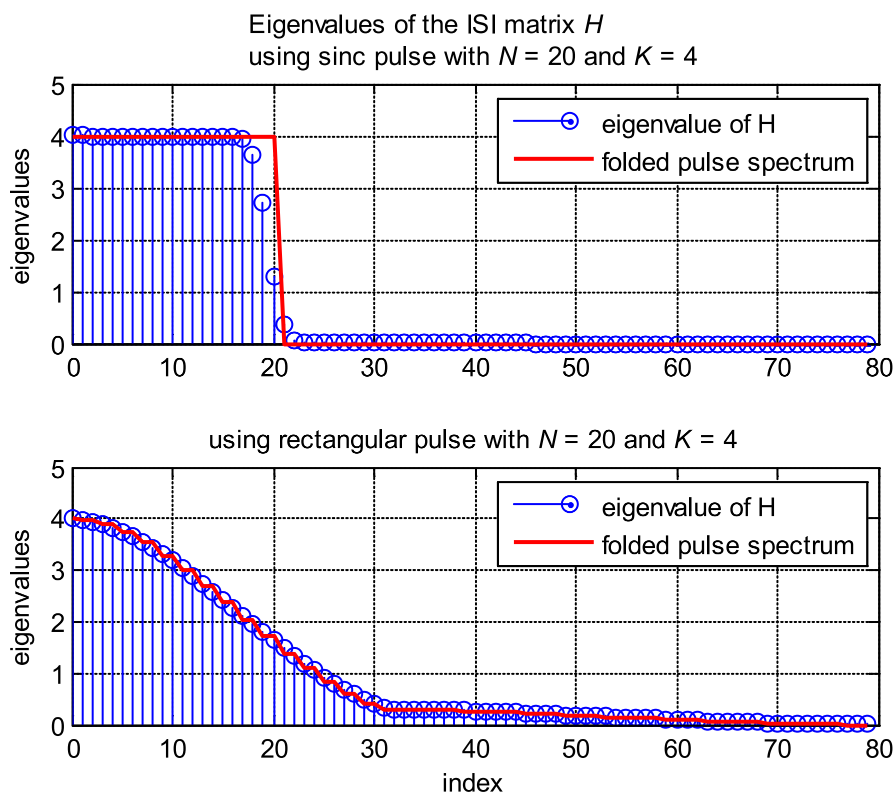

Figure 3.3 Plotting MATLAB computed eigenvalues of the FTN matrices *H* from Example 3.1 (top) and Example 3.2 (bottom); Also plotting the corresponding normalized folded pulse spectra $(\Delta t)^{-1}\hat{s}_{folded}(f_n)$ (sampled at $f_n = -1/(2\Delta t) + n/(NT)$ for n = 0, 1, …, KN-1 and sorted in the descending order); packet length N = 20 and FTN signaling rate factor K = 4 are considered in both examples.

Note that in order to compare with KN number of eigenvalues of H, the normalized folded pulse spectra $(\Delta t)^{-1}\hat{s}_{folded}(f)$ were sampled at KN uniformly spaced frequency locations over the frequency range $f \in (-1/(2\Delta t), 1/(2\Delta t))$ and plotted in the descending order in Figure 3.3. The figure shows an excellent match between the computed eigenvalues and the normalized folded pulse spectra even at the small block length $N = 20$.

One of the consequences of Proposition 3.2 is that if the modulating pulse $s(t)$ is bandlimited, the eigenvalues of H also exhibit 'bandlimited-ness'. This effect can be observed from the top plot in Figure 3.3 when the sinc modulating pulse (strictly bandlimited in frequency) is being used. Mathematically, when $s(t)$ is strictly bandlimited to $f \in (-W, W)$ as in Example 3.1, and noting that the signaling rate $1/\Delta t > 2W$ for the FTN signaling, the folded pulse spectrum simplifies to

$$\hat{s}_{folded}(f) = |\hat{s}(f)|^2, \quad f \in (-W, W). \tag{3.49}$$

Hence, the asymptotic eigenvalues of H will also be bandlimited, i.e., only about $2W/(1/NT) = 2WNT = N$ (by $T = 1/(2W)$ due to the Nyquist theorem) number of eigenvalues remain nonzero and the other $(KN–N)$ number of them converge to zero as N tends to infinity. This means that the FTN matrix H becomes asymptotically singular (or non-invertible) as $N \to \infty$. On the other hand, when the modulating pulse $s(t)$ is not strictly bandlimited as in the bottom plot of Figure 3.3, we can observe that the eigenvalues decay much more slowly.

In summary, the FTN matrix H is theoretically invertible when its size is finite (when FTN signaling rate factor K and packet size N are finite). As N tends to infinity, the asymptotic eigenvalues of the FTN matrix H follows the abovementioned folded pulse spectrum, consequences of which include 'bandlimited-ness' of the eigenvalues if the modulating pulse $s(t)$ is strictly bandlimited. This implies that the asymptotic eigenvalues of H depends on the spectrum of the modulating pulse $s(t)$ and for band-limited $s(t)$, the FTN matrix H tends asymptotically to a singular matrix.

3.3 Generalized FTN Transmission Power Constraint

All digital communication systems are practically limited in amounts of power it can use. Accordingly, many capacity analyses involve maximizing the mutual information subject to given input power and energy constraints [31]. In this section, we develop energy and power constraints fitted for the FTN communication system that allows fair comparisons with the conventional Nyquist-rate systems. These constraints turn out to be quite nontrivial due to the nonzero signal correlations inherent to the FTN signals.

Lemma 3.4 (FTN signal energy): *The energy of the continuous-time FTN signal $x(t)$ defined in (3.1) can be expressed as*

$$E\left\{\int_{-\infty}^{\infty}\left|x(t)\right|^2 dt\right\} = tr\left(K_x H\right), \tag{3.50}$$

where the left-hand side is the statistical energy average over the ensemble of transmitted FTN waveforms $x(t)$, $K_x=E\{\mathbf{x}\mathbf{x}^\dagger\}$ is the correlation matrix of the modulation symbols $x[n]$, H is the FTN matrix defined by (3.22) *that is Toeplitz, and $tr(\cdot)$ denotes the matrix trace.*

Proof: Substituting in the expression of $x(t)$ from (3.1), we have

$$E\left\{\int_{-\infty}^{\infty}\left|x(t)\right|^2 dt\right\} = E\left\{\int_{-\infty}^{\infty}\sum_{n=0}^{KN-1}\sum_{m=0}^{KN-1} x^*[n]x[m]s^*(t-n\Delta t)s(t-m\Delta t)dt\right\} \tag{3.51}$$

$$= \sum_{n=0}^{KN-1}\sum_{m=0}^{KN-1} E\left\{x^*[n]x[m]\right\} h_{(n-m)}, \tag{3.52}$$

where $h_{(n-m)} = \int_{-\infty}^{\infty} s(\tau)s^*\left(\tau-(n-m)\Delta t\right)d\tau$ by the definition (3.20)[21]. Moreover, (3.52) can be written in a matrix form:

$$\sum_{n=0}^{KN-1}\sum_{m=0}^{KN-1} E\left\{x^*[n]x[m]\right\} h_{(n-m)} = E\left\{\mathbf{x}^\dagger H\mathbf{x}\right\}, \tag{3.53}$$

[21] As a side note, if the set of time-translates $\{s(t-k\Delta t)\}_k$ is an orthonormal set, then $h_{(m-n)} = \delta(m-n)$ and the energy expression (3.50) simplifies to $\sum_n E\{|x[n]|^2\}$, which is the commonly-used energy expression in the orthogonal systems. Unfortunately, the orthogonality condition on $\{s(t-k\Delta t)\}_k$ is never satisfied for the FTN systems and the energy must now include the signal correlation terms $h_{(n-m)}$.

Since $\mathbf{x}^{\dagger} H\mathbf{x}$ is a scalar, the matrix trace $tr(\cdot)$ can be applied, and by the trace identity $tr(AB) = tr(BA)$:

$$E\left\{\mathbf{x}^{\dagger} H\mathbf{x}\right\} = E\left\{tr\left(\mathbf{x}^{\dagger} H\mathbf{x}\right)\right\} = E\left\{tr\left(\mathbf{x}\mathbf{x}^{\dagger} H\right)\right\}. \tag{3.54}$$

Furthermore, by the linearity of the trace and the expectation operators, the order can be interchanged as follows:

$$E\left\{tr(\mathbf{x}\mathbf{x}^{\dagger} H)\right\} = tr\left(E\{\mathbf{x}\mathbf{x}^{\dagger}\}H\right) = tr\left(K_x H\right), \tag{3.55}$$

where $K_x = E\{\mathbf{x}\mathbf{x}^{\dagger}\}$ denotes the correlation matrix of the modulation symbols $\{x[n]\}$. This completes the proof of Lemma 3.4. ■

We can normalize the FTN signal energy from (3.50) by either the total number of transmitted symbols (KN symbols) to get an average FTN energy in Joules per symbol. Alternatively, it can be normalized by total time duration taken to transmit KN symbols (NT seconds in FTN plus $(K-1)T/K$ which is negligible for N sufficiently large, see Figure 3.1) for a power constraint in Joules per second (i.e., watts). We will consider the latter since the capacity derivations in this dissertation deal with bits per second. The following power constraint derived for the FTN transmission specify that the energy of individual FTN symbols $\{x[n]\}$ must scale down according to increasing FTN signaling rate factor K, in order to keep the overall transmission power fixed and independent of the signaling rate.

Proposition 3.3 (FTN transmission power constraint): *The transmission power constraint of the FTN transmission signal $x(t)$ in Joules per second (watts) is given in a matrix form by*

$$\frac{1}{NT} tr\left(K_x H\right) \leq P. \tag{3.56}$$

where P is a fixed constant in Joules per second.

Note that, regardless of the FTN signaling rate $1/\Delta t = K/T$, the maximum used power remains P. This fixed maximum power enforces stricter restrictions on the energy of individual modulation symbol $\{x[n]\}$ as the signaling rate $1/\Delta t = K/T$ is increased (i.e., as the FTN signaling rate factor K increases, the energy of $\{x[n]\}$ must scale down accordingly). The power constraint (3.56) thus allows a 'fair' comparison between the FTN systems and traditional Nyquist rate systems.

Furthermore, the constraint (3.56) allows a fair comparison between the un-precoded FTN and the precoded FTN. For un-precoded (*i.i.d.*) FTN systems, the correlation matrix becomes simply $K_x = E\{|x[n]|^2\} \cdot I_{KN}$, where I_{KN} denotes $KN \times KN$ identity matrix. Hence $tr(K_x H) = E\{|x[n]|^2\} \cdot KN$, from the power constraint (3.56), since the diagonal entries of H are all 1's, and the power constraint for the un-precoded FTN simplifies to $(\Delta t)^{-1} E\{|x[n]|^2\} \leq P$ (note that this is consistent with the constraints used in the un-precoded FTN literature, e.g., [127]).

Sometimes, it will be convenient to re-express the transmission power constraint in a different form.

***Corollary 3.1* (*Alternative transmission power constraint*):** *The transmission power constraint on FTN transmission signal x(t) can alternatively be written as*

$$\frac{1}{NT} tr\left(U^{\dagger} H^{1/2} K_x H^{1/2} U\right) \leq P, \tag{3.57}$$

with any unitary matrix U, i.e., $U^{\dagger}U = UU^{\dagger} = I$.

Proof: First let $H = H^{1/2}H^{1/2}$ by taking a matrix square root of H. Hence, we have $tr(K_x H) = tr(K_x H^{1/2} H^{1/2}) = tr(H^{1/2} K_x H^{1/2})$, where the last equality is due to the trace identity $tr(AB) = tr(BA)$. Furthermore, $tr(H^{1/2} K_x H^{1/2}) = tr(H^{1/2} K_x H^{1/2} UU^{\dagger}) = tr(U^{\dagger} H^{1/2} K_x H^{1/2} U)$, due to $UU^{\dagger} = I$ followed by the trace identity $tr(AB) = tr(BA)$. This completes the proof. ■

As an interesting side note, the derived FTN signal energy $tr(K_x H)$ may be compared to the block symbol energy $tr(K_x)$ used in the Nyquist-rate communication systems (see e.g., [66], [141]). The following corollary characterizes this relationship between the FTN signal energy and the conventional block symbol energy in the Nyquist rate systems:

Corollary 3.2 (Block symbol energy versus FTN signal energy): *The block symbol energy for transmission of KN symbols in Nyquist rate systems is given by*

$$tr\left(K_x\right)=\sum_{n=0}^{KN-1}E\left\{x^2[n]\right\}, \tag{3.58}$$

in Joules. This is related to the FTN signal energy from Lemma 3.4 by the following relationship:

$$tr\left(K_x H\right)\le\lambda_{\max}tr\left(K_x\right), \tag{3.59}$$

where λ_{max} denotes the maximum eigenvalue of the FTN matrix H. Furthermore, by exploring the structure of H, we can associate λ_{max} with the folded pulse spectrum $\hat{s}_{folded}(f)$, as defined by

$$\hat{s}_{folded}(f)\equiv\sum_{k=-\infty}^{\infty}\left|\hat{s}(f-k/\Delta t)\right|^2,\quad f\in(-1/(2\Delta t),1/(2\Delta t)), \tag{3.60}$$

where $\hat{s}(f)$ denotes the Fourier transform of s(t), and we have

$$\lambda_{\max}\le(\Delta t)^{-1}\operatorname*{ess\,sup}_{f}\hat{s}_{folded}(f), \tag{3.61}$$

which becomes an equality in the limit as N tends to infinity and ess sup denotes the essential supremum. (A rule of thumb we observed is $\lambda_{max}\approx K$ in FTN systems and $\lambda_{max}\approx 1$ in Nyquist rate systems.)

Proof**:** We use the von Neumann's inequality of trace product [102]: i.e., for any complex $n\times n$ matrices A and B,

$$\left|tr(AB)\right|\le\sum_{i=0}^{n-1}\alpha_i\beta_i, \tag{3.62}$$

where $\alpha_0\ge\alpha_1\ge\ldots\ge\alpha_{n-1}$ and $\beta_0\ge\beta_1\ge\ldots\ge\beta_{n-1}$ are the singular values of A and B, respectively. Therefore,

$$tr(K_x H)\le\sum_{i=0}^{KN-1}\sigma_i\lambda_i, \tag{3.63}$$

where $\sigma_0\ge\sigma_1\ge\ldots\ge\sigma_{KN-1}$ and $\lambda_0\ge\lambda_1\ge\ldots\ge\lambda_{KN-1}$ are the singular values of K_x and H, respectively. Note that we dropped the absolute value since K_x and H are Hermitian non-negative definite matrices and hence the trace of their product is always non-negative. Applying the Hölder's inequality on (3.63), we obtain

$$\sum_{i=0}^{KN-1} \sigma_i \lambda_i \leq \left(\sum_{i=0}^{KN-1} |\sigma_i| \right) \left(\max(|\lambda_0|, \cdots, |\lambda_{KN-1}|) \right) \tag{3.64}$$

$$= \lambda_{\max} tr(K_x), \tag{3.65}$$

where $\lambda_{\max}$ denotes the maximum singular value of H. Since H is Hermitian non-negative definite, $\lambda_{\max}$ is also the maximum eigenvalue of H by the spectral theorem.

Now to associate $\lambda_{\max}$ with $\hat{s}_{folded}(f)$, we use Lemma D.1 in Appendix D to upper-bound the eigenvalues of H by essential supremum of the inverse Fourier series of $\{h_k\}$, i.e.,

$$\lambda_i \leq \operatorname*{ess\,sup}_{\lambda} \sum_{k=-\infty}^{\infty} h_k e^{ik\lambda} = \operatorname*{ess\,sup}_{\lambda} h(\lambda). \tag{3.66}$$

By Lemma 3.3, we know that $h(-2\pi f \Delta t) = (\Delta t)^{-1} \hat{s}_{folded}(f)$. Now noting that the essential supremum of $h(\lambda)$ is equal to the essential supremum of $h(-2\pi f \Delta t)$, we arrive at (3.61). Finally, (3.66) becomes equality as N tends to infinity due to Lemma D.1. This completes the proof of Corollary 3.2. ■

As a consequence of Corollary 3.2 (and using our rule of thumb $\lambda_{\max} \approx K$), if

$$\frac{1}{NT} tr\left(K_x\right) \leq \frac{P}{K}, \tag{3.67}$$

then the transmission power constraint $(NT)^{-1} tr\left(K_x H\right) \leq P$ from Proposition 3.3 is automatically satisfied. In other words, in FTN systems, energy of each modulation symbol $x[n]$ needs to be reduced roughly by a factor of K compared to the Nyquist rate systems for the same transmission energy.

3.4 Spectral Analysis of Different FTN Signals

A common assumption accompanying the FTN signaling in the literature is that such signaling preserves the transmission bandwidth for varying signaling rates. We shall show in this section, however, that this assumption on bandwidth invariance holds always only if a perfectly band-limited modulating pulse is used or the modulation symbols are uncorrelated. Furthermore, any precoding on the modulation symbols can significantly alter the shape of the power spectrum of the FTN signals. Therefore, the exact form of the power spectrum with respect to the symbol rates and precoding is of interest in the context of FTN signaling.

The objective of this section is to analyze closed-form expressions on power spectral densities (PSDs) of various FTN signals. Specifically we consider non-precoded, convolutionally-precoded, or block-precoded FTN signals, operating over either AWGN or linear- time-invariant (LTI) channels. The analysis reveals how the power spectrum of FTN varies with 1) the FTN signaling rate $1/\Delta t$, 2) the modulating pulse spectra $\hat{s}(f)$, 3) the modulation symbol correlations $E\{x[n]x^*[m]\}$, and 4) the utilized precoding strategy. Moreover, we identify sufficient conditions on the precoding to prevent spectrum broadening of the resulting FTN signals.

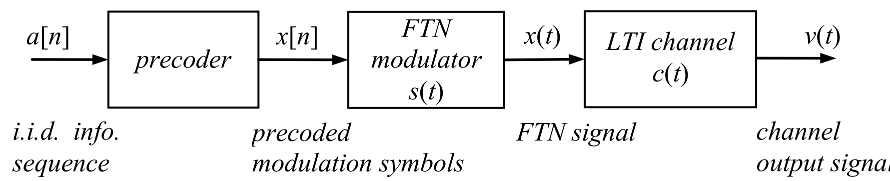

Figure 3.4 The considered precoded FTN signaling over linear, time-invariant (LTI) channel setup

We will consider the precoded FTN transmission over the linear time-invariant (LTI) channel with the impulse response $c(t)$ as introduced in section 3.1. For convenience, a schematic block diagram including only the relevant blocks is shown in Figure 3.4. The channel output signal $v(t)$ is simply the convolution of the FTN signal $x(t)$ and LTI channel response $c(t)$, i.e.,

$$v(t) = x(t) * c(t) = \sum_{n=-\infty}^{\infty} x[n]p(t - n\Delta t) \tag{3.68}$$

where $*$ denotes the convolution of continuous-time signals and $p(t) \equiv s(t) * c(t)$. Note that the overall combined ISI from LTI channel and signaling faster than Nyquist rate is determined by $p(t)$ and the FTN signaling rate $1/\Delta t$.

3.4.1 PSD of FTN for Wide-Sense Stationary Data

This subsection considers the FTN signal $x(t)$ when the modulation symbols $\{x[n]\}$ are *wide-sense stationary* (WSS) with a constant mean m_x and an autocorrelation function $R_x(n, m) = E\{x[n]x^*[m]\}$ that satisfies

$$R_x(n,m) = R_x(m-n) = R_x(k), \tag{3.69}$$

where $k \equiv m–n$. First note that the power spectral density of the pulse-amplitude modulation (PAM) signal with WSS modulation symbols (also known as cyclostationary PAM signal) is well known (see e.g., subsection 8.2.1 in [113]). Careful review of the derivation reveals that such PSD analysis does not depend on the signaling rate, and hence it can be directly applied to the considered FTN signal. This yields the following PSD expression of the FTN signal:

$$\mathsf{S}_x(f) = \frac{1}{\Delta t}\mathsf{S}_{R_x}(f)\left|\hat{s}(f)\right|^2, \tag{3.70}$$

where $\hat{s}(f)$ is the Fourier transform of $s(t)$ and $\mathsf{S}_{R_x}(f)$, called a data spectrum, is defined by

$$\mathsf{S}_{R_x}(f) \equiv \sum_{k=-\infty}^{\infty} R_x(k)e^{+j2\pi fk\Delta t}, \tag{3.71}$$

which has an interpretation of a PSD of *discrete-time* modulation symbols $\{x[n]\}$ (furthermore, note that $\mathsf{S}_{R_x}(f)$ is periodic in f with a period $1/\Delta t$). An a consequence of (3.70), the spectrum of the FTN signals can be precisely controlled by changing the modulating pulse spectra, $\hat{s}(f)$, and the second order statistics of the modulation symbols, $R_x(k)$.

3.4.2 PSD of Convolutionally Precoded FTN Signals in LTI Channels

Convolutional precoding has been considered in the FTN literature (see e.g., [158], [96], [125], [126]) to deal with the FTN-induced intersymbol interference. Precoding in general causes the FTN symbols become non-*i.i.d*, but the effects of this symbol correlation to the

PSD of precoded FTN signals have been largely ignored in the past literature. The assumption of precoders generating always uncorrelated sequences [125] is mathematically incorrect. The objective of this subsection is to properly analyze PSD of *convolutionally* precoded FTN signal over linear time-invariant (LTI) channels.

Convolutional precoding is a special class of precoding defined as follows:

Definition 3.2 (Convolutional precoding): *The modulation symbols* $\{x[n]\}$ *are called convolutionally precoded if they can be written as*

$$x[n] = \sum_{k=-\infty}^{\infty} \xi_k a[n-k], \textit{ for } n = 0, \pm 1, \pm 2, \ldots, \tag{3.72}$$

for some real precoding (weighting) coefficients $\{\xi_k\}$, *where* $\{a[n]\}$ *are zero-mean i.i.d. information sequence.*

Such precoding may model many conventional linear precodings employed in practice, such as partial response signaling, trellis coding as well as finite-impulse-response (FIR) or infinite-impulse-response (IIR) filtering. The precoding coefficients $\{\xi_k\}$ are further assumed to be absolutely summable; i.e., they satisfy the condition

$$\sum_{k=-\infty}^{\infty} |\xi_k| < \infty. \tag{3.73}$$

We note that the the above condition is always satisfied for FIR filters with finite tap coefficients and also for IIR filters that are causal and BIBO (bounded-input-bounded-output) stable. (Latter is due to the property of causal linear, time-invariant digital filters being BIBO stable if and only if the impulse response is absolutely summable [107].)

The following theorem gives PSD of the convolutionally precoded FTN signal explicitly as a function of the signaling rate $1/\Delta t$, the channel frequency response $\hat{c}(f)$ and the precoding coefficients $\{\xi_k\}$.

Theorem 3.1 (PSD of convolutionally precoded FTN signals over LTI channels): *Let the modulation symbols* $\{x[n]\}$ *be generated by precoding of a zero mean i.i.d. information sequence* $\{a[n]\}$ *according to* (3.72) *with absolutely summable precoding coefficients* $\{\xi_k\}$. *Let c(t) be an impulse response of linear time-invariant (LTI) channel and consider the* *channel setup as in Figure 3.4. Then, the power spectral densities of the convolutionally precoded FTN signal x(t) and the channel output signal v(t) are respectively given by*

$$\mathsf{S}_x(f) = \frac{\sigma_a^2}{\Delta t}\left|\mathsf{S}_\xi(f)\hat{s}(f)\right|^2 \text{ and} \tag{3.74}$$

$$\mathsf{S}_v(f) = \frac{\sigma_a^2}{\Delta t}\left|\mathsf{S}_\xi(f)\hat{s}(f)\hat{c}(f)\right|^2, \tag{3.75}$$

where $\hat{s}(f)$ and $\hat{c}(f)$ are the Fourier transforms of s(t) and c(t), respectively, σ_a^2 = $E\{|a[n]|^2\}$ is the variance (or PSD) of the i.i.d. information sequence $\{a[n]\}$, and $\mathsf{S}_\xi(f)$ is called precoding spectrum as defined by

$$\mathsf{S}_\xi(f) \equiv \sum_{k=-\infty}^{\infty} \xi_k e^{+j2\pi fk\Delta t}. \tag{3.76}$$

Proof: Note that the convolutionally precoded data symbols $\{x[n]\}$ have zero mean $m_x = E\{x[n]\} = 0$ for all n and have an autocorrelation function

$$R_x(k) = \sigma_a^2 \sum_{n=-\infty}^{\infty} \xi_n \xi_{n+k}^*. \tag{3.77}$$

Therefore, $\{x[n]\}$ are wide-sense stationary when precoding coefficients are absolutely summable, and the PSD of the corresponding FTN signal $x(t)$ is given (3.70). Now by substituting the expression for $R_x(k)$ from (3.77) to (3.71) and simplifying:

$$\mathsf{S}_{R_x}(f) = \sigma_a^2 \sum_{k=-\infty}^{\infty}\sum_{n=-\infty}^{\infty} \xi_n \xi_{n+k}^* e^{+j2\pi fk\Delta t} \tag{3.78}$$

$$= \sigma_a^2 \sum_{n=-\infty}^{\infty} \xi_n \sum_{k=-\infty}^{\infty} \xi_k^* e^{+j2\pi f(k-n)\Delta t} \tag{3.79}$$

$$= \sigma_a^2 \sum_{n=-\infty}^{\infty} \xi_n e^{-j2\pi fn\Delta t} \cdot \sum_{k=-\infty}^{\infty} \xi_k^* e^{+j2\pi fk\Delta t}, \tag{3.80}$$

which is equal to $\sigma_a^2\left|\mathsf{S}_\xi(f)\right|^2$. As for the PSD of the output signal $v(t)$, simply replace $\hat{s}(f)$ by $\hat{s}(f)\hat{c}(f)$ in the above analysis to yield the desired result. This completes the proof of Theorem 3.1. ■

The theorem gives the PSD of the FTN signal explicitly as a function of the signaling rate $1/\Delta t$, the channel frequency response $\hat{c}(f)$ and the precoding coefficients $\{\xi_k\}$. This allows a communication system designer to use appropriate precoding to shape the power spectrum of $x(t)$. Note also that due to the $1/\Delta t$ term appearing in (3.74), increasing the symbol rate of the precoded FTN signal amplifies the overall power spectrum and can also *modify* the shape of the spectrum due to dependencies of Δt in the precoding spectrum (3.76). Therefore, care must be exercised if such data precoding is to be applied to the FTN signaling. The next corollary presents sufficient conditions for preventing the spectrum broadening.

Corollary 3.3 (Sufficient conditions for preventing spectrum broadening): *The power spectral density of the convolutionally precoded FTN signal does not exhibit spectrum broadening with respect to the signaling rate $1/\Delta t$ if*

$$\sigma_a^2 \le \Delta t \ \text{and} \ \sum_{k=-\infty}^{\infty} |\xi_k| \le 1. \tag{3.81}$$

Proof: Substituting the conditions above to (3.74) (or (3.75)) yields

$$\mathsf{S}_x(f) = \frac{\sigma_a^2}{\Delta t}\left|\mathsf{S}_\xi(f)\hat{s}(f)\right|^2 \le \left|\hat{s}(f)\right|^2, \tag{3.82}$$

since $\left|\mathsf{S}_\xi(f)\right| \le \sum_k |\xi_k|$. Note that the right-hand side of (3.82) is independent of the both signaling rate $1/\Delta t$ and the precoding coefficients $\{\xi_k\}$. This completes the proof. ■

The conditions in the corollary imply that in order to avoid the spectrum broadening in the precoded FTN signaling, the power of the information sequence $\{a[n]\}$ should be scaled down accordingly with increasing FTN signaling rate and the precoding coefficients should not be chosen too big. We note that these sufficient conditions are stronger conditions than the FTN transmission power constraint in (3.56).

In order to gain further insights, several practical examples are considered below. First, we consider a precoded FTN signal using a *rectangular* modulating pulse and a *duo-binary-like* [72] precoding with the system parameters listed below:

- $\sigma_a^2 = T = 1$ μs,

- $s(t)=\begin{cases} T^{-1/2} & for\ t\in(0,T) \\ 0 & elsewhere \end{cases}$ (*rectangular modulating pulse*)
- $c(t)=\delta(t)$, (*AWGN channel*)
- $\xi_0=\xi_1=1$ and $\xi_k=0$ for $k\neq 0$ and 1. (*duo-binary-like precoding*)

By Theorem 3.1, the overall closed form PSD of this example is given by

$$\mathsf{S}_x(f)=4T(\sigma_a^2/\Delta t)\left|\mathrm{sinc}(fT)\cos(\pi f\Delta t)\right|^2, \tag{3.83}$$

where $\mathrm{sinc}(\lambda)\equiv\sin(\pi\lambda)/(\pi\lambda)$.

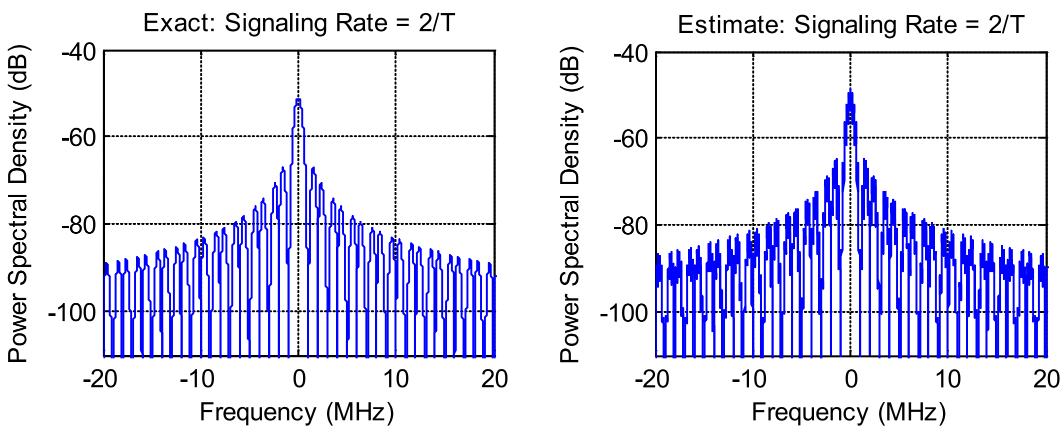

Figure 3.5 Power spectral density of FTN signal at symbol rate $1/\Delta t = 2/T$ using rectangular pulse $s(t)$; Left is the exact PSD and right is plotted using the Welch method; See text for the system parameters

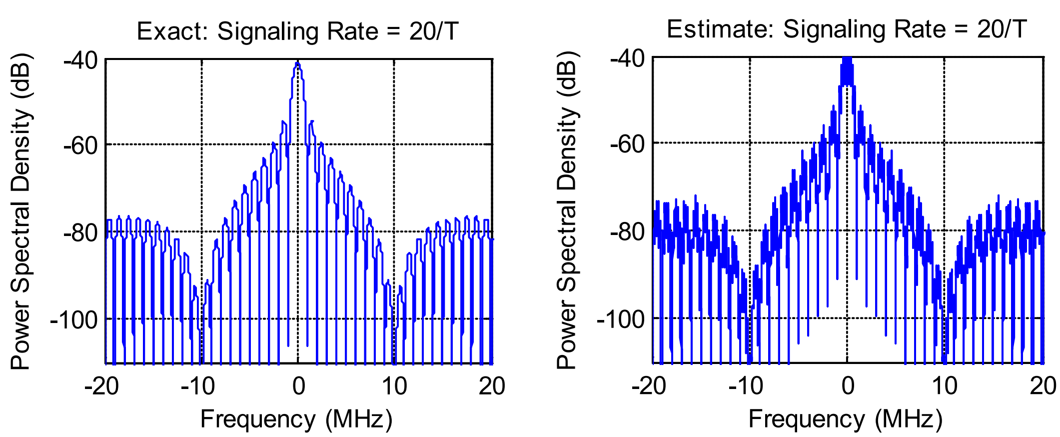

Figure 3.6 Power spectral density of FTN signal at symbol rate $1/\Delta t = 20/T$ using rectangular pulse $s(t)$; Left is the exact PSD and right is plotted using the Welch method; See text for the system parameters

Figure 3.5 and Figure 3.6 plot the PSD expressions (3.83) using signaling rates $1/\Delta t$ = $2/T$ and $20/T$, respectively, and compare them with numerically estimated PSDs using MATLAB. (Note that the left plots in Figure 3.5 and Figure 3.6 are the exact closed-form PSDs while right plot are the PSD estimates obtained by the Welch method [160], which is a variant of the periodogram-based spectral estimation technique.) From these figures, we note that the presented results show an excellent match between the analytic and the numerically estimated power spectral densities. Also, by comparing Figure 3.5 and Figure 3.6, we can see that as the signaling rate $1/\Delta t$ increases, the PSDs of the FTN signals clearly exhibit the spectrum broadening as well as shape altering.

Next, we use a different modulating pulse and investigate how precoding can impact the power spectrum. In Figure 3.7 and Figure 3.8, we consider a *raised cosine* modulating pulse $s(t)$ with a roll-off factor β = 0.22 (used in e.g., WCDMA standard) and a *long-memory* precoder. Following lists the system parameters:

- $\sigma_a^2 = T = 1$ μs,
- $s(t) = \dfrac{\sin(\pi t/T)}{\pi t/T}\left(\dfrac{\cos(\pi\beta t/T)}{1-(2\beta t/T)^2}\right)$, (*raised cosine modulating pulse*)
- $c(t) = \delta(t)$, (*AWGN channel*)
- $\xi_k = 1$ for $k = 0, \ldots, 9$ and $\xi_k = 0$ elsewhere. (*long memory precoding*)

By Theorem 3.1, PSD of the FTN signal is given by

$$\mathsf{S}_x(f) = \begin{cases} 4g(f) & \text{for } |f| \le (1-\beta)/2T \\ g(f)|q(f)|^2 & \text{for } (1-\beta)/2T \le |f| \le (1+\beta)/2T \\ 0 & \text{otherwise} \end{cases} \tag{3.84}$$

where $q(f) \equiv 1+\cos[(\pi T/\beta)(|f|-(1-\beta)/2T)]$ and $g(f) \equiv T^2(\sigma_a^2/\Delta t)|\cos(\pi f \Delta t)|^2$.

We note from Figure 3.7 and Figure 3.8 that the precoding in FTN can considerably alter the shape and amplify the overall power spectrum. In the figures, the PSD estimates exhibit long spectral 'tails', which is just an effect of time-truncating $s(t)$ to $|t|\le 6T$, the otherwise infinite duration $s(t)$, for the purpose of computer simulations. We also note that the spectrum does not broaden in this case since the raised cosine pulse is a (theoretically) strictly band-limited pulse.

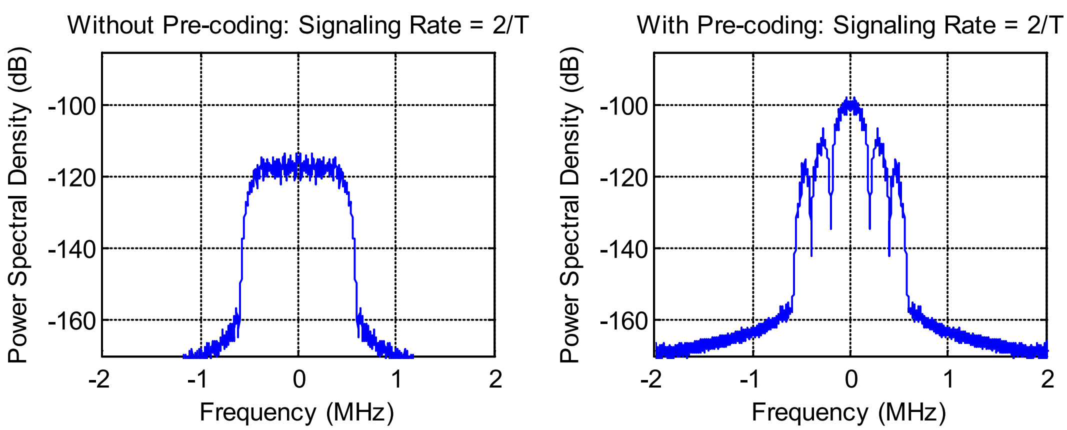

Figure 3.7 Power spectral density of FTN signaling before and after the long memory precoding; at signaling rate $1/\Delta t = 2/T$ using time-truncated raised cosine pulse $s(t)$

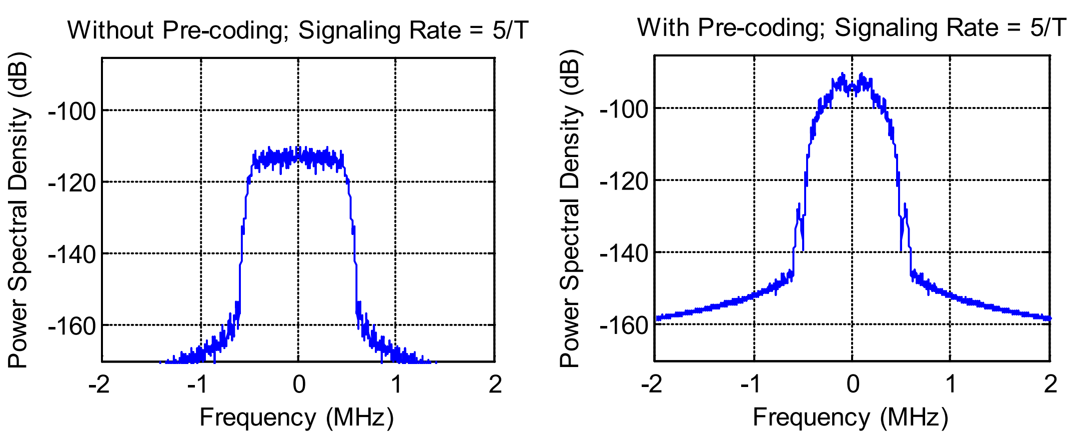

Figure 3.8 Power spectral density of FTN signaling before and after the long memory precoding; at signaling rate $1/\Delta t = 5/T$ using time-truncated raised cosine pulse $s(t)$

Finally in Figure 3.9 and Figure 3.10, we consider an impact of an LTI channel to the power spectrum of the FTN signaling. A simple realization of the two-way fading channel model $c(t)$ is considered which is given by

- $c(t) = 1 + ae^{-j2\pi f\tau}$ with $a = 0.5$ and $\tau = 3.3$ μs,

where a represents the attenuation factor of the secondary path delayed by τ seconds [120]. Figure 3.9 and Figure 3.10 plot the exact PSD of the FTN signals before and after the channel; i.e., left plots show $\mathsf{S}_x(f)$ and right plots show $\mathsf{S}_v(f)$. The system parameters are kept the same as in Figure 3.5 using rectangular pulse $s(t)$. The power spectral density after the channel $\mathsf{S}_v(f)$ is derived using Theorem 3.1 and is given by

$$\mathsf{S}_v(f) = 4T(\sigma_a^2/\Delta t)\left|\mathrm{sinc}(fT)\cos(\pi f\Delta t)(1+\alpha^2+2\alpha\cos(2\pi f\tau))\right|^2, \qquad (3.85)$$

where $\mathrm{sinc}(\lambda) \equiv \sin(\pi\lambda)/(\pi\lambda)$. The figures show that the channel introduces distortions to the original spectrum, which can be precisely determined by the spectral analysis, and if the channel is known at the transmitter, appropriate precoding can be applied to combat these channel distortions (Chapter 5 will deal with such FTN precoding in a greater detail).

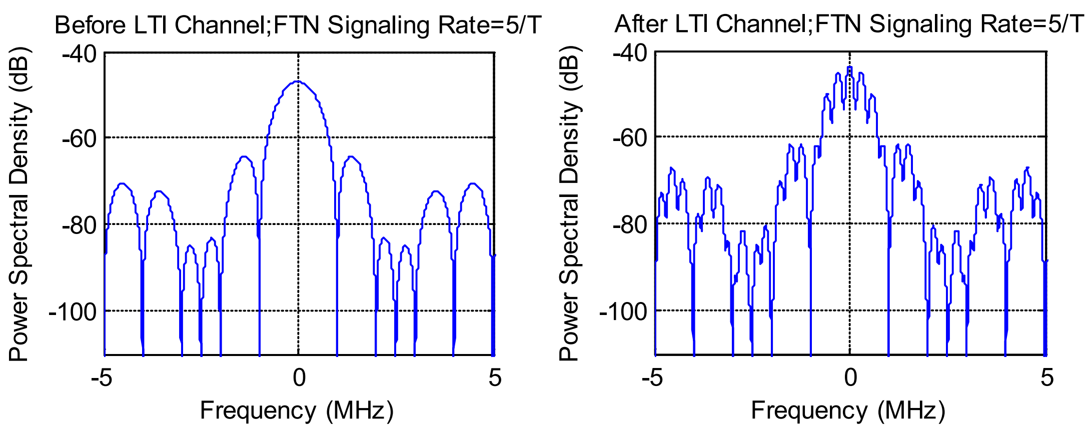

Figure 3.9 Power spectral densities of FTN signal before and after a realization of 2-way fading channel at signaling rate $1/\Delta t = 5/T$

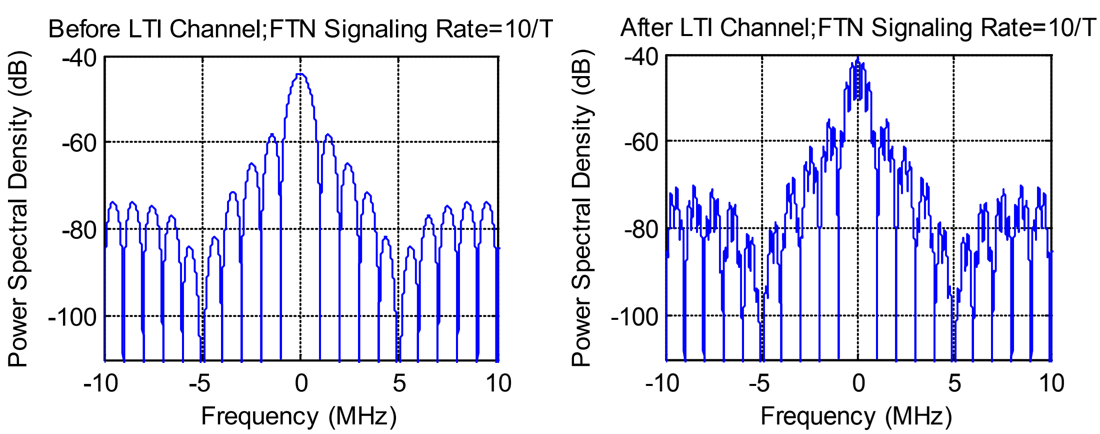

Figure 3.10 Power spectral densities of FTN signal before and after a realization of 2-way fading channel at signaling rate $1/\Delta t = 10/T$

3.4.3 PSD of General Linearly Precoded FTN Signals

As an extension to the analysis thus far, we can consider a more general linear precoding:

$$x[n] = \sum_{k=-\infty}^{\infty} \xi_{n,k} a[k], \quad for\ n = 0, \pm 1, \pm 2, \cdots, \tag{3.86}$$

for some deterministic precoding coefficients $\{\xi_{n,k}\}$. With the above general precoding, however, corresponding FTN signals $x(t)$ may become non-stationary stochastic processes with ill-defined power spectral densities or time-evolving spectra [97]. Nevertheless, when the data are parsed into packets which are sent separately, the overall FTN signal can be treated as a cyclostationary process with the period being the length of each packet. This treatment allows one to *estimate* the power spectrum of general precoded FTN signals using standard periodogram-based spectral estimation techniques[22].

We consider a special linear precoding, described by (in vector notations)

$$\mathbf{x} = (\sqrt{P\Delta t} \cdot H^{-1/2})\mathbf{a}, \tag{3.87}$$

where H is the FTN matrix defined in (3.22). It will be shown in Chapter 5 that this linear precoding is capacity-wise *optimal* for the FTN signaling. Table 3.1 lists PSD estimates of this optimally precoded FTN signals using different modulating pulses. Four modulating pulses (rectangular, root-raised cosine, prolate spheriodal wave function, and sinc-type) are considered. The rectangular and sinc modulating pulses are the two extreme cases in a sense that the former is most time compacted and the latter is most frequency compacted. The root raised cosine pulses, commonly used in modems [113], stand in between the two in terms of time-frequency compaction, whereas the prolate spheroidal wave functions have the best time-frequency energy concentrations [134], [135]. From the table, we can observe that the optimal precoding (3.87) heavily distorts the spectra and boosts the side-lobes as the signaling rate $1/\Delta t$ is increased beyond the Nyquist rate; with the exception of the case of the perfectly band-limited sinc-type pulse. The behavior of the power spectrum with respect to the optimal precoding and the signaling rate will have several important consequences in the capacity analysis of precoded FTN signaling in Chapter 5.

---

[22] Notably, there are several other techniques that can be used to *estimate* the time-varying nature of non-stationary processes; see for example, [1] using short-time Fourier analysis and [111] using evolutionary spectra. We do not pursue such directions in this dissertation.

Table 3.1 Some power spectral densities (PSDs) of optimally precoded FTN signals

<table>
<tr><th rowspan="2">Modulating Pulse Type</th><th rowspan="2">Time Domain $s(t)$</th><th colspan="3">Power spectra of optimally precoded FTN signals $x(t)$</th></tr>
<tr><th>$1/\Delta t = 1/T$ (Nyquist case)</th><th>$1/\Delta t = 2/T$ (K=2)</th><th>$1/\Delta t = 5/T$ (K=5)</th></tr>
<tr><td>*Rectangular pulse*
$s(t) = 1;$
$t \in (-1/2, 1/2)$</td>
<td>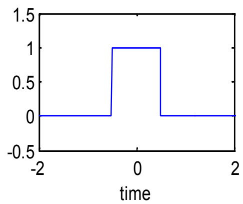</td>
<td>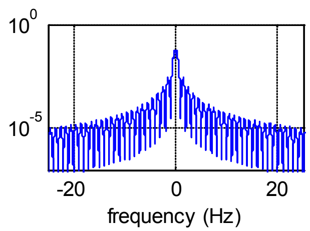</td>
<td>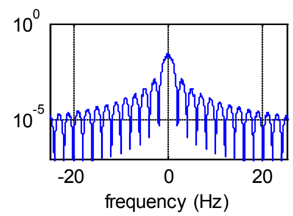</td>
<td>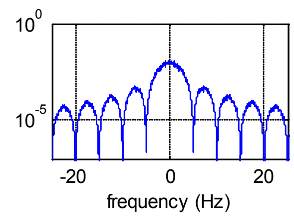</td></tr>
<tr><td>*Square-root raised cosine pulse*
Roll-off factor = 0.22</td>
<td>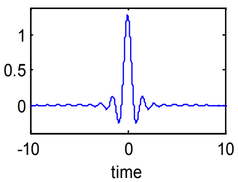</td>
<td>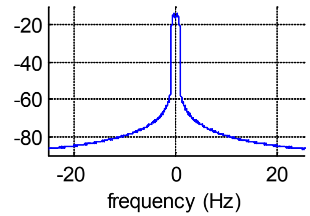</td>
<td>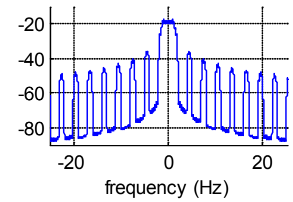</td>
<td>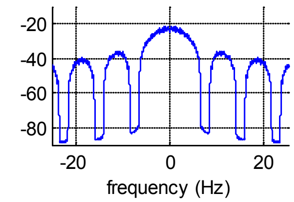</td></tr>
<tr><td>*Prolate spheroidal wave function (1^{st})*
truncated to $t \in (-2.5, 2.5)$
bandwidth ~ 1 Hz</td>
<td>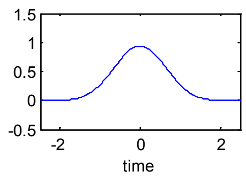</td>
<td>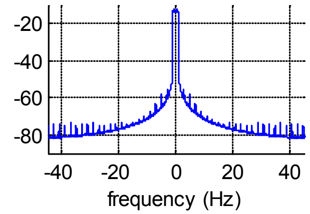</td>
<td>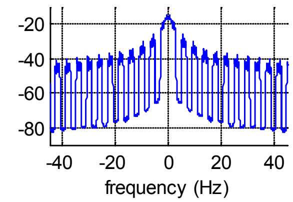</td>
<td>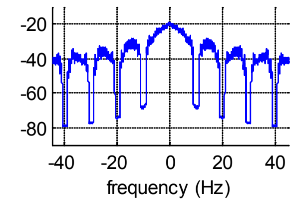</td></tr>
<tr><td>*Sinc-type pulse*
$s(t) = (2W)^{1/2}\mathrm{sinc}(2Wt);$
$W = 1$ Hz</td>
<td>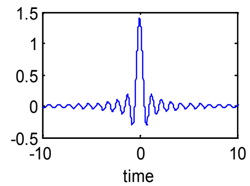</td>
<td>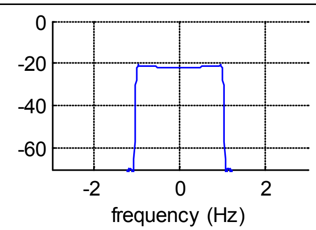</td>
<td>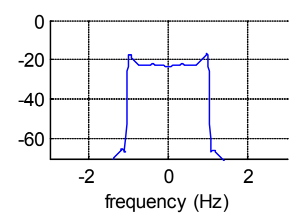</td>
<td>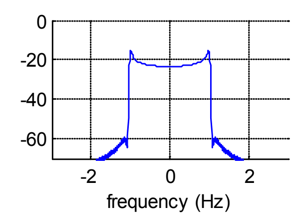</td></tr>
</table>

3.5 Chapter Summary

The main objective of this chapter has been the development of accurate FTN system models by re-establishing the link between the continuous-time communication setup and the discrete-time channel models. Due to its inherent non-orthogonality, the FTN signaling led to non-trivial discrete-time channel models that involve the intersymbol interference (ISI) and correlated noise statistics that depended on the FTN-induced ISI pattern. Based on the established FTN channel models, some of their important properties were derived, including the invertibility and eigenvalue distribution of the FTN matrix H that characterizes the ISI pattern. Furthermore, a non-trivial power transmission constraint for the FTN signaling has been derived for the first time, which allows fair comparisons of the FTN signaling with the Nyquist rate systems.

Finally, through the power spectral density (PSD) analysis, it was shown that the data precoding in the FTN signaling can both broaden and alter the shape of the original power spectrum. The result implied that the common assumption of bandwidth invariance of the FTN signaling no longer holds if the modulating pulse $s(t)$ is not strictly band-limited and the modulation symbols $\{x[n]\}$ are correlated. In addition, sufficient conditions for preventing the broadening of the power spectrum were provided. The discrete-time FTN channel models and the power spectral analysis presented in this chapter provides a foundation for more in-depth analysis on the FTN signaling in the later chapters.

Chapter 4

Non-Precoded FTN Signaling

Traditional FTN signaling assumes sending independent and identically distributed (*i.i.d.*) modulation symbols **x** that are sent without any pre-coding. Such *non-precoded* FTN signaling does not alter the transmission power spectrum (as shown in section 3.4), and allows fair and simple comparisons with other coded modulation techniques. Recent developments in the information theory have further allowed closed form evaluation of the capacity limits of the *non-precoded* FTN signaling and further enhancement of our understanding of the FTN signaling.

This chapter has the following objectives with regards to the *non-precoded* FTN:

1) Determine capacity benefits of *non-precoded* FTN signaling over conventional Nyquist rate signaling.
2) Evaluate optimality of equal power distribution for *non-precoded* FTN and quantify any capacity loss in sending FTN symbols with non-equally distributed power.
3) Design a low-complexity and spectrally efficient FTN coding system.

The above three objectives are addressed in detail in sections 4.1, 4.2, and 4.3, respectively. In short, it will be shown that there *exist* capacity benefits of non-precoded FTN signaling, when compared to the *M*-ary Nyquist rate signaling. Also a class of non-uniform power distributed modulation symbols does not incur any capacity loss, and this observation consequently leads to a design of a low-complexity FTN-based coding system that can support large signaling rates and achieve high spectral efficiencies.

4.1 Review on Capacity Benefits of *i.i.d.* FTN Signaling

This section reviews previous capacity results on FTN signaling when independent and identically distributed (*i.i.d.*) modulation symbols $\{x[n]\}$ are assumed. Two separate cases are considered for the *i.i.d.* FTN symbol alphabet, namely the Gaussian distributed modulation symbols $\{x[n]\}$ in subsection 4.1.1 and more practical finite alphabet modulation symbols such as PAM, QAM, or PSK in subsection 4.1.2.

4.1.1 Gaussian Distributed Modulation Symbols

Consider FTN signaling over AWGN channel: $\mathbf{y} = H\mathbf{x} + \mathbf{z}$ from (3.21), where the modulation symbol vector $\mathbf{x}$ is assumed to be *i.i.d.* In order to satisfy the FTN transmission power constraint (3.56), the covariance matrix of $\mathbf{x}$ under the *i.i.d.* constraint is given by $K_x = (P\Delta t)\cdot I_{KN}$, where I_{KN} denotes the $KN\times KN$ identity matrix, P is the total available transmission power in watts, and Δt is the FTN signaling interval ($\Delta t \equiv T/K$). Furthermore, recall from Definition 3.1 that the folded pulse spectrum $\hat{s}_{folded}(f)$ is defined as

$$\hat{s}_{folded}(f) \equiv \sum_{k=-\infty}^{\infty} \left|\hat{s}(f - k/\Delta t)\right|^2, \quad f \in \left(-\frac{1}{2\Delta t}, \frac{1}{2\Delta t}\right), \tag{4.1}$$

where $\hat{s}(f)$ is the Fourier transform of the modulating pulse $s(t)$.

The capacity of the *i.i.d. FTN signaling* was first presented and rigorously proved by Rusek and Anderson in [127] and the statement of this result is given below.

Theorem 4.1 (Capacity of i.i.d. FTN signaling over AWGN channel [127]): *Let the FTN modulation symbols* $x[0], x[1], \ldots, x[KN-1]$ *be chosen to be i.i.d, with a variance* $P\Delta t$ *that satisfies the FTN transmission power constraint (3.56). Then the capacity of this i.i.d. FTN signaling in AWGN channel with the signaling rate* $1/\Delta t$ *symbols per second is given by*

$$C_{i.i.d.}^{FTN} = \int_{-1/(2\Delta t)}^{1/(2\Delta t)} \log_2\left(1 + \frac{P}{N_0/2}\hat{s}_{folded}(f)\right) df \ \ \textit{bits per second,} \tag{4.2}$$

and it is achieved by Gaussian-distributed FTN modulation symbols.

Proof: Please refer to [127] for the proof. We will also extend this theorem to a more general setting (for convolutionally precoded FTN signaling) in Chapter 5 where the proof of this theorem will be presented as a special case (see Corollary 5.1). ■

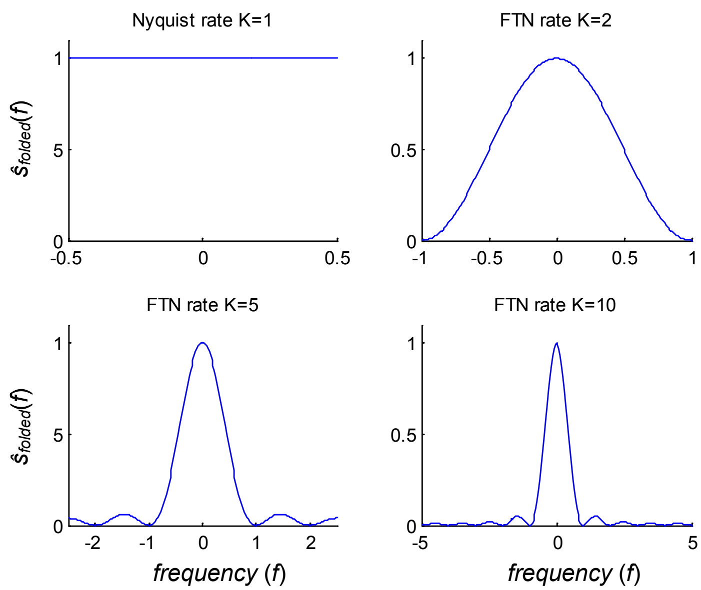

Figure 4.1 The folded pulse spectra $\hat{s}_{folded}(f)$ plotted for the frequency range $f \in (-1/(2\Delta t), 1/(2\Delta t))$ with varying FTN rates $K = 1, 2, 5$, and 10; The rectangular pulse $s(t) = 1$ for $t \in (-1/2, 1/2)$ and 0 elsewhere is used in this example (where $T = 1$)

As an example, the folded pulse spectra $\hat{s}_{folded}(f)$ for varying FTN rates K are plotted in Figure 4.1 when the rectangular pulse $s(t)$ is used. The capacity expression (4.2) is given by an integral of (or an area under) a non-negative logarithm function of $\hat{s}_{folded}(f)$ and the signal-to-noise power ratio. Note that the integral in (4.2) extends over the frequency range $f \in (-1/(2\Delta t), 1/(2\Delta t))$ and this range expands with the increasing FTN signaling rate $1/\Delta t$. Consequently, if $\hat{s}_{folded}(f)$ is not strictly zero outside the frequency range $f \in (-1/(2\Delta t), 1/(2\Delta t))$, there exists a capacity benefit in signaling faster than the Nyquist rate. In contrast, the conventional Nyquist rate transmissions with $1/T$ symbols per second will not be able to recover any information residing in the frequency range outside $f \in (-1/(2T), 1/(2T))$.

The following corollary deals with asymptotic case when FTN signaling rate $1/\Delta t$ tends to infinity.

Corollary 4.1 (Asymptotic K [127]): *The capacity of i.i.d. FTN signaling as the signaling rate tends to infinity (or as $\Delta t = T/K \to 0$) is given by*

$$C_{i.i.d.}^{FTN} \xrightarrow[\Delta t \to 0]{} \int_{-\infty}^{\infty} \log_2\left(1+\frac{P}{N_0/2}\left|\hat{s}(f)\right|^2\right)df \tag{4.3}$$

$$= \int_{-\infty}^{\infty} \log_2\left(1+\frac{\mathsf{S}_x(f)}{N_0/2}\right)df\ , \tag{4.4}$$

where $\mathsf{S}_x(f) = P\left|\hat{s}(f)\right|^2$ *denotes the transmission power spectral density (PSD) of the i.i.d. FTN signal x(t) and* $N_0/2$ *is the two-sided Gaussian noise PSD.*

***Proof*:** Please refer to [127] for the proof. ■

Above corollary shows that the *i.i.d.* FTN signaling has the capability to recover information residing over all spectral range, $f \in (-\infty, \infty)$, including all spectral side-lobes of the transmission power spectrum. We also note that the capacity expression (4.4) is the same as the generalized Shannon capacity written as a function of PSD (i.e., C_{PSD} from Theorem 2.2), meaning that the *i.i.d.* FTN signaling can asymptotically achieve the capacity benchmark C_{PSD} for any given transmission PSD[23].

There are some limitations, however, in the practical usage of the capacity expression above. The capacity from Theorem 4.1 does not take into account of interfering users (if any) present in the adjacent frequency bands. These neighboring spectrum users may cause or may be negatively affected by inter-channel-interference if the FTN transmission PSD extends to these frequency bands. Therefore, in a conventional multi-user setting, nearly bandlimited modulating pulses are typically used in order to minimize such inter-channel-interference. However, the capacity benefits of the *i.i.d.* FTN signaling diminishes quickly with the increasing 'bandlimited-ness' of the modulating pulse $s(t)$, and it completely disappears at the extreme case when $s(t)$ is a strictly bandlimited (e.g., sinc pulse), as shown in the following corollary:

[23] The *i.i.d.* FTN capacity expression (4.4) is in fact two times C_{PSD} from Theorem 2.2. This factor of two comes from allowing complex signals (by allowing complex modulation symbols and complex modulating pulses) in the FTN capacity analysis.

***Corollary 4.2 (Special case using sinc modulating pulse [127])**: Let the modulating pulse $s(t)$ be a unit energy sinc pulse with bandwidth of W Hz, i.e., $s(t) = (2W)^{1/2} sinc(2Wt) = (2W)^{1/2} sin(2\pi Wt)/(2\pi Wt)$. Its Fourier transform is given by*

$$\hat{s}(f) = \begin{cases} (2W)^{-1/2} & f \in (-W, W) \\ 0 & \textit{otherwise.} \end{cases}$$

Furthermore, let the modulation symbols $\{x[n]\}$ be chosen i.i.d. Then the capacity of the i.i.d. FTN signaling in AWGN channel for all K becomes

$$C_{i.i.d.}^{FTN} = 2W \log_2\left(1 + P/(N_0 W)\right) \textit{ bits per second,} \tag{4.5}$$

which is equivalent to the classical Shannon capacity of Nyquist rate transmission over bandlimited complex AWGN channel (see Theorem 2.1).

Proof: Using the sinc pulse, the Nyquist interval T is simply $T = 1/(2W)$. Note also that the folded pulse spectrum $\hat{s}_{folded}(f)$ simplifies to

$$\hat{s}_{folded}(f) = \sum_{k=-\infty}^{\infty} \left|\hat{s}(f - k(2WK))\right|^2 \tag{4.6}$$

$$= \left|\hat{s}(f)\right|^2, \tag{4.7}$$

over the frequency range $f \in \left(-W, W\right)$, due to $s(t)$ being strictly bandlimited. Substituting these to Theorem 4.1 and simplifying:

$$C_{i.i.d.}^{FTN} = \int_{-1/(2\Delta t)}^{1/(2\Delta t)} \log_2\left(1 + \frac{P}{N_0/2}\left|\hat{s}\left(f\right)\right|^2\right) df \tag{4.8}$$

$$= 2W \log_2\left(1 + \frac{P}{N_0 W}\right), \tag{4.9}$$

after setting $\Delta t = T/K$ and $T = 1/(2W)$. This completes the proof. ■

The implication of the corollary is as follows. For strictly bandlimited transmissions with the *i.i.d.* Gaussian modulation symbols, the conventional Nyquist rate transmission is indeed optimal and the FTN capacity is equal to the Shannon capacity with Nyquist signaling. On the other hand, considering that strictly bandlimited pulses cannot be realized in practice (due to its infinite time support, see Appendix B), the FTN signaling will always provide additional capacity benefits when compared to the Nyquist rate counterpart. The capacity benefits of FTN can be explained due to its ability to recover information residing over all spectral range (even though the gain may be small if the spectral side-lobes are small in magnitude). On the other hand, traditional Nyquist rate transmit signaling with a Nyquist rate matched filtering, corresponding to the case $\Delta t = T = 1/(2W)$, can only recover information within frequency range $f \in (-1/(2T), 1/(2T)) = (-W, W)$.

4.1.2 Finite Alphabets Modulation Symbols

Thus far, we have assumed using Gaussian distributed modulation symbols, as these lead to achieving FTN capacity in Theorem 4.1. In practice, however, finite constellations such as PAM, PSK and QAM are used, and the specific channel input alphabet limits the achievable capacities of a digital communication system. In Figure 4.2, the capacity curves of various (Nyquist rate) PAM transmissions are plotted with respect to the Shannon capacity $\log_2(1+P/(N_0W))$ in bits/s/Hz. Figure 4.2 reveals that the PAM capacities eventually level off as SNR increases due to the input alphabet constraints. This well-known fact implies that, at high SNR, the number of modulation levels should be increased in order to perform close to the Shannon limit.

In some channels, however, increasing the number of modulation levels may lead to undesirable effects. For example, in long haul optical links, higher modulation levels lead to increased sensitivity to nonlinear effects [25], whereas in ISI channels, it leads to (order of magnitude) increase in implementation complexity of the equalizer. In these channels, design of alternative signaling schemes would be of interest.

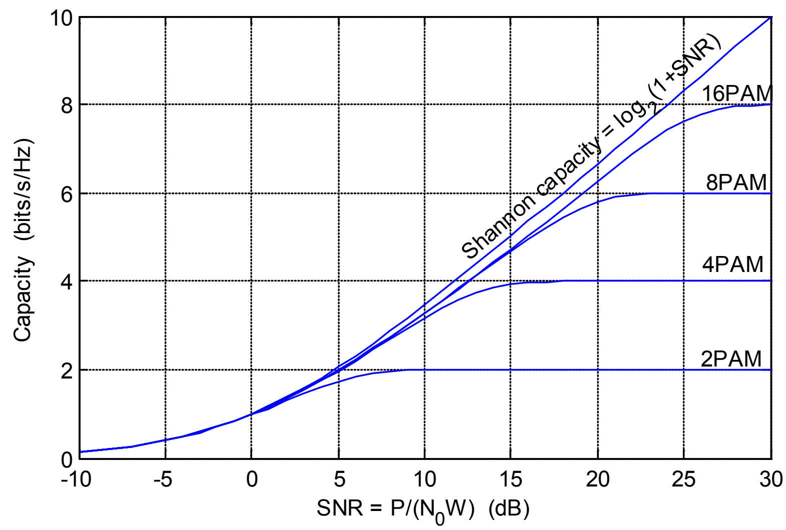

Figure 4.2 Input-constrained capacities of (Nyquist rate) equiprobable *M*-PAM transmissions

A key benefit of the *i.i.d.* FTN signaling lies in its capability to attain the capacities of the high-order (*M*-ary) modulation while employing only the binary modulation formats at the transmitter. That is, instead of increasing the modulation order (e.g., from 2-PAM to 8-PAM), FTN obtains similar capacity gains by increasing its signaling rate (e.g., from K=1 to K=3). This ability of FTN can be easily understood by considering a following example. Consider a binary antipodal FTN signaling using a rectangular modulating pulse $s(t)$, as illustrated in Figure 4.3b. As opposed to traditional binary Nyquist rate signal shown in Figure 4.3a, the FTN signal in Figure 4.3b can attain increased number of signal levels {−2, 0, +2} while employing only the binary antipodal modulation $x[n] \in \{-1, +1\}$. We also note that the FTN receiver only needs to execute binary demodulation, not the full *M*-ary demodulation (at the price of having to remove FTN-induced ISI).

In 2010, Yoo and Cho [165] made this argument mathematically rigorous by showing that the capacity of binary antipodal FTN signaling converges to that of the *i.i.d.* Gaussian FTN signaling (4.2) as the FTN signaling rate tends to infinity.

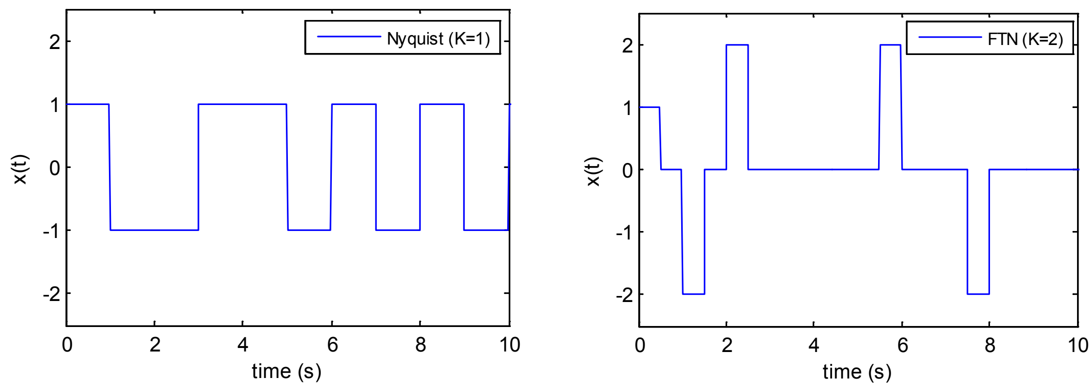

(*a*) (*b*)

Figure 4.3 Comparing a generic (a) Nyquist rate signal and (b) a faster than Nyquist rate signal with *K*=2: For binary antipodal modulation {-1,+1} and rectangular modulating pulse with symbol period *T*=1

Theorem 4.2 (Asymptotic optimality of binary FTN signaling [165]): *As the FTN signaling rate tends to infinity (i.e., as* $1/\Delta t \to \infty$ *or* $K \to \infty$*), the capacity of binary antipodal i.i.d. FTN signaling converges to the capacity of the i.i.d. Gaussian FTN in (4.2).*

Proof: Please refer to [165] for the proof. ■

In other words, the FTN signaling with binary modulation suffices to achieve the *i.i.d.* FTN capacity limit (4.2) for all values of SNR, which, with the conventional Nyquist rate signaling, is achieved only by using Gaussian-distributed modulation symbols (or as a limiting case of M-ary modulation, as $M\to\infty$, with additional signal shaping [48], [90]). Consequently, the FTN signaling may be more desirable than the Nyquist rate signaling in applications where high spectral efficiencies are needed, yet increasing the number of modulation levels is not desired (such as in fiber-optical links [25], [136]). In this sense, *the i.i.d. FTN signaling can be an important competing technology to non-binary (M-ary) Nyquist rate communications.* Moreover, this result calls for a low-complexity design of high rate FTN systems, but this is still an open problem [165] due to the large implementation complexity associated with the equalizer. We will address this complexity issue in section 4.3 by proposing a low-complexity FTN coding architecture that can support moderate to large FTN rates and operate at high spectral efficiencies.

4.2 Capacity Analysis of FTN with Non-Uniform Power Allocation

The purpose of this section is to determine what happens to the capacity of FTN signaling when we send independent modulation symbols with *non-uniform power distribution*. We will show that, for a specific class of non-uniform power allocation, its capacity is always equal or greater than that of the Nyquist rate siganling. The non-uniform power allocation will eventually lead to a design of low-complexity FTN-based coding architecture in section 4.3 that can support large spectral efficiencies.

Consider the FTN signaling over AWGN channel: $\mathbf{y} = H\mathbf{x} + \mathbf{z}$ from (3.21), where the signaling rate is $1/\Delta t = K/T$ (i.e., K times faster than the Nyquist rate) and $x[n]$ are now allowed to have unequal power allocations but still independently distributed. We consider one such class of $\mathbf{x}$ with the covariance matrix K_x given by

$$K_x = I_N \otimes diag(P_1T, P_2T, \cdots, P_KT)\,, \tag{4.10}$$

where $\otimes$ denotes the Kronecker product of matrices (Definition 2.14), $diag(\cdot)$ denotes a diagonal matrix with diagonal entries given by its arguments, and the maximum available power P is divided into K non-negative parts, P_1, P_2, …, P_K, such that $\sum_{k=1}^{K} P_k = P$. Such signaling has an interpretation of multiplexing of K Nyquist rate signal streams, each with different delay and power assignment, as illustrated Figure 4.4 for $K = 3$.

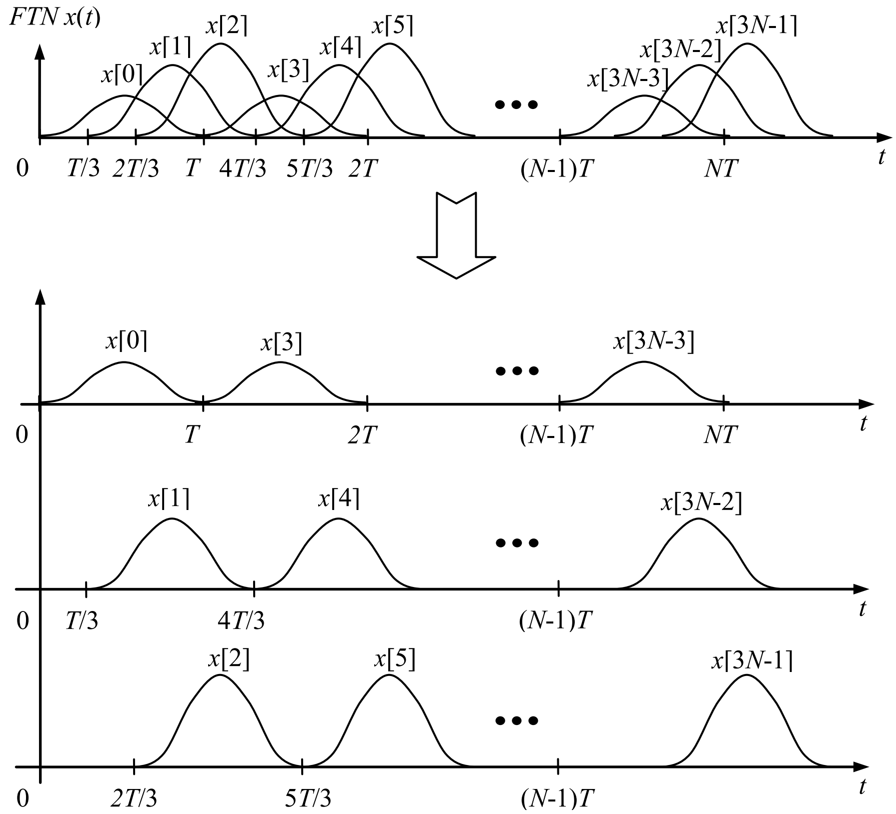

Figure 4.4 Illustration of non-uniform power distributed faster than Nyquist signal $x(t)$ as multiplexing of K Nyquist rate signal streams, each with different delay and power assignment (K=3 illustrated)

We now show our own result that such non-uniform power distributed FTN signaling does not incur any capacity loss regardless of the power distribution $P_1, P_2, \ldots, P_K$, when compared to the capacity of bandlimited complex AWGN channel C_{AWGN}.

Theorem 4.3 (Capacity of FTN signaling over AWGN channel with unequal power assignment): *Consider the case of non-equal power distribution when FTN modulation symbol vector* $\mathbf{x}$ *has the covariance matrix* K_x *defined in (4.10). The capacity of such independent and non-identically distributed (i.n.i.d.) FTN signaling over AWGN channel* $C_{i.n.i.d.}^{FTN}$ *is greater than or equal to the Shannon capacity of complex AWGN channel* C_{AWGN}*, i.e.,*

$$C_{i.n.i.d.}^{FTN} \geq C_{AWGN} = \frac{1}{T}\log_2\left(1+\frac{PT}{N_0/2}\right), \tag{4.11}$$

regardless of the power distribution $P_1, P_2, \ldots, P_K$ *as long as* $\sum_{k=1}^{K} P_k = P$.

Proof: Recall that $\mathbf{y} = H\mathbf{x} + \mathbf{z}$ where $\mathbf{z}$ is a zero mean Gaussian noise vector with a covariance matrix $K_z = (N_0/2)H$. Consequently, the mutual information between $\mathbf{x}$ and $\mathbf{y}$ is

$$I(\mathbf{x};\mathbf{y}) = h(\mathbf{y}) - h(\mathbf{y}|\mathbf{x}) \tag{4.12}$$

$$= h(\mathbf{y}) - h(\mathbf{z}), \tag{4.13}$$

where $h(\cdot)$ denotes the differential entropy (Definition 2.3) and (4.13) follows from $H\mathbf{x}$ being deterministic given $\mathbf{x}$, and the translation invariance of the differential entropy (Lemma 2.5) followed by independence of $\mathbf{x}$ and $\mathbf{z}$. By Lemma 2.4, equation (4.13) can be maximized by choosing $\mathbf{x}$ to be complex symmetric Gaussian distributed and the corresponding mutual information is given by

$$I(\mathbf{x};\mathbf{y}) = \log_2\left(\det(K_y)/\det(K_z)\right), \tag{4.14}$$

where K_y denotes the covariance matrix of $\mathbf{y}$ and is given by

$$K_y = HK_xH^\dagger + (N_0/2)\cdot H. \tag{4.15}$$

Therefore, the mutual information for $\mathbf{x} \sim \mathcal{N}(\mathbf{0}, K_x)$, normalized by total time duration NT seconds, is given by

$$\frac{1}{NT} I(\mathbf{x};\mathbf{y}) = \frac{1}{NT}\log_2\left(\frac{\det\left(HK_xH^\dagger + (N_0/2)\cdot H\right)}{\det\left((N_0/2)\cdot H\right)}\right), \tag{4.16}$$

$$= \frac{1}{NT}\log_2\left(\det\left((N_0/2)^{-1} K_xH + I_{KN}\right)\right), \tag{4.17}$$

where I_{KN} is a $KN\times KN$ identity matrix, and (4.17) is due to the determinant identities $\det(A)^{-1} = \det(A^{-1})$ and $\det(A)\det(B) = \det(AB)$.

For convenience, we will denote (4.17) by $\psi(\cdot)$, i.e.,

$$\psi(K_x) \equiv \frac{1}{NT}\log_2 \det\left((N_0/2)^{-1} K_xH + I_{KN}\right). \tag{4.18}$$

Furthermore, let $K_x^{(k)}$ denote the covariance matrix when all power is allocated to k-th signal stream, i.e.,

$$K_x^{(k)} \equiv I_N \otimes diag(0,\cdots,0,PT,0,\cdots,0) \text{ for } k \in \{1,2,\cdots,K\}, \tag{4.19}$$

where PT appears at the k-th entry of $diag(\cdot)$. With such a power allocation, only one Nyquist rate signal-stream is active and the FTN transmission becomes simply the conventional Nyquist-rate channel transmission with the AWGN capacity, i.e., for all k,

$$\psi\left(K_x^{(k)}\right) = C_{AWGN} = \frac{1}{T}\log_2\left(1+\frac{PT}{N_0/2}\right), \tag{4.20}$$

from Theorem 2.1.

Now for a general K_x, we will use the fact that $\psi(\cdot)$ is *concave* on the set of covariance matrices K_x. To show that $\psi(\cdot)$ is concave, first note that

$$\log\det\left(cK_x H + I\right) = \log\det\left(cH^{1/2}K_x H^{1/2} + I\right), \tag{4.21}$$

for any constant c by the identity: $\operatorname{logdet}(AB+I) = \operatorname{logdet}(BA+I)$. The concavity of $\psi(\cdot)$ then follows from the fact that the *logdet*$(\cdot)$ function is concave on the set of non-negative definite matrices (Lemma 2.13) and the mapping $K_x \to (cH^{1/2}K_x H^{1/2} + I)$ for any constant c is linear and preserves positive definiteness for any nonzero H.

Hence, by the concavity of $\psi(\cdot)$,

$$\psi\left(\sum_{k=1}^{K}\alpha_k K_x^{(k)}\right) \geq \sum_{k=1}^{K}\alpha_k \psi\left(K_x^{(k)}\right), \tag{4.22}$$

for any $\alpha_k \in [0,1]$ such that $\sum_{k=1}^{K}\alpha_k = 1$. By (4.20),

$$\psi\left(\sum_{k=1}^{K}\alpha_k K_x^{(k)}\right) \geq \sum_{k=1}^{K}\alpha_k C_{AWGN} = C_{AWGN}. \tag{4.23}$$

But by the definition of $K_x^{(k)}$ and setting $\alpha_k = P_k/P$,

$$\sum_{k=1}^{K}\alpha_k K_x^{(k)} = I_N \otimes diag\left(\alpha_1 PT, \alpha_2 PT, \cdots, \alpha_K PT\right) = K_x. \tag{4.24}$$

Hence, for all packet lengths N, (4.23) becomes

$$\psi\left(K_x\right) \geq C_{AWGN}. \tag{4.25}$$

Substituting this back to (4.17), we have thus shown that

$$(NT)^{-1} I\left(\mathbf{x};\mathbf{y}\right) \geq C_{AWGN} \tag{4.26}$$

for all N, when $\mathbf{x}$ is a zero mean complex symmetric Gaussian vector with any power assignments P_1, P_2, …, P_K. This establishes that the capacity using the considered non-identically distributed $\mathbf{x}$ is greater than or equal to the AWGN capacity C_{AWGN}. This completes the proof of Theorem 4.3. ■

When considering the FTN signaling as a multiplexing of K Nyquist rate signal streams shown in Figure 4.4, Theorem 4.3 implies that the available power P can be split to each signal stream any way we like, while ensuring that the corresponding capacity $C_{i.n.i.d.}^{FTN}$ is at least the capacity of Nyquist rate transmission over complex AWGN channel. This approach of non-uniform power allocation leads to a design of low-complexity FTN-based coding system in the next section that can support large spectral efficiencies.

When compared to the capacity of *i.i.d.* FTN signaling, however, the non-uniform power allocation in the considered *i.n.i.d.* FTN signaling can in general lead to a non-zero capacity loss, i.e., $C_{i.n.i.d.}^{FTN} \leq C_{i.i.d.}^{FTN}$. In the special case when strictly bandlimited modulating pulse $s(t)$ is used, however, the two capacities coincide and become the Shannon capacity C_{AWGN}, as shown in the following corollary.

Corollary 4.3 (Optimality of non-uniform power allocation using sinc pulse): *When the FTN modulating pulse is the strictly bandlimited sinc pulse, i.e.,* $s(t) = (2W)^{1/2}\mathrm{sinc}(2Wt)$ *with W Hertz bandwidth, the i.n.i.d. FTN capacity* $C_{i.n.i.d.}^{FTN}$ *is equal to the i.i.d. FTN capacity* $C_{i.i.d.}^{FTN}$ *as well as the Shannon capacity of bandlimited complex AWGN channel* C_{AWGN}*, i.e.,*

$$C_{i.i.d.}^{FTN} = C_{i.n.i.d.}^{FTN} = C_{AWGN}. \tag{4.27}$$

Proof: The equality $C_{i.i.d.}^{FTN} = C_{AWGN}$ is due to Corollary 4.2 for the sinc modulating pulse. Finally, the desired relation (4.27) follows by $C_{i.n.i.d.}^{FTN} \leq C_{i.i.d.}^{FTN} = C_{AWGN}$ and $C_{i.n.i.d.}^{FTN} \geq C_{AWGN}$ due to Theorem 4.3. This completes the proof of the corollary. ■

4.3 Proposed Low-Complexity FTN Coding Architecture

Section 4.1 reviewed results indicating that FTN can be a competing technology to standard M-ary Nyquist rate signaling with signal shaping in the high SNR regime since FTN can achieve the Shannon capacity while using only binary modulation symbols. Consequently, FTN signaling has been considered for potential applications in channels with moderate to high SNR including long-haul fiber-optic communication links [136], [25]. Due to the high SNR in the optical fibers, FTN systems must be designed to operate at high spectral efficiencies, yet possess manageable implementation complexity.

4.3.1 Initial Considerations

Most of the previously-known FTN coding architectures involve some form of equalizers, the purpose of which is to remove the FTN-induced intersymbol interference (ISI). Unfortunately, the implementation complexity of the optimal *maximum a-posteriori* (MAP) equalizer (described in subsection 2.3.2) is on the order of M^L where M is the modulation order and L is the length of the ISI memory which is usually multiple orders of K. For example, consider an FTN system that employs BPSK (M=2) and signaling 5-times faster then Nyquist rate (K=5), using the root raised cosine pulse with roll-off factor of 0.22 in AWGN channel. From simulations, the memory length of the ISI induced by FTN signaling was observed to be near L=50 and cosueqently the implementation complexity of the corresponding MAP equalizer is on the order of $2^{50} \approx 1\times10^{15}$. Even for a simple rectangular pulse, the complexity scales exponentially in the FTN signaling rate factor K. Given practical FTN system implementations in current state-of-the-art VLSI or FPGA hardware, this exponentially increasing complexity turns out to be prohibitive even for moderately large values of M and K. Reduced complexity equalizers have been considered in the literature (see e.g., [96], [93], [125], [128], [25]), but these still suffer from the large implementation complexity at the considered high SNRs. Consequently, practical FTN transceiver design for moderate to high transmission rates has been recently recognized as an open problem in [165].

In this section, we propose a low-complexity FTN-based coding architecture that is based on non-uniform power allocated FTN signaling and multistage decoding of the constituent Nyquist rate signals. The proposed architecture does not require any complex equalizer and has a *linear* implementation complexity on the orders of $K \cdot M$, where M is the modulation order of the modulation symbols and K is FTN signaling rate factor. The key idea is the treatment of FTN as multiplexing of K Nyquist rate signal substreams with different power assignments and delays as illustrated in Figure 4.4. At the receiver, the K Nyquist-rate signal substreams are successively decoded following an order from the most powerful substream to the least powerful substream, while canceling out the previously decoded signal substreams along the way. This architecture shares similar concepts and properties of Imai and Hirakawa's multilevel codes [67], [156] or with Cover's superposition coding [28] and may be considered as an extension of the multilevel codes in the discrete-time symbol domain to continuous-time waveform domain. Furthermore, the capability of FTN to multiplex of more than one Nyquist-rate signal substreams can be used to explitly multiplex more than one user's message in downlink broadcast channels. We develop this idea in a greater depth in Chapter 6.

4.3.2 FTN Transceiver Architecture

Figure 4.5 shows the block diagram of the proposed FTN transmitter architecture with non-uniform power assignments.

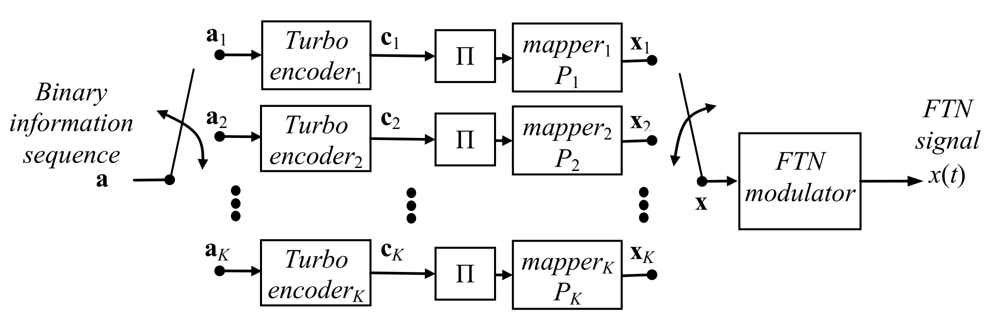

Figure 4.5 Proposed FTN transmitter architecture with power assignments P_1, P_2, …, P_K

The *i.i.d.* information sequence $\mathbf{a}$ is first demultiplexed into K subsequences $\mathbf{a}_1$, $\mathbf{a}_2$, …, $\mathbf{a}_K$ according to

$$\mathbf{a}_k \equiv \left[a[k-1], a[K+k-1], \cdots, a[K(N-1)+k-1]\right]^T \text{, for } k \in \{1,2,\cdots K\}. \quad (4.28)$$

These K subsequences are then separately Turbo-coded and bit-wise interleaved. The interleaved coded bits are then mapped to (possibly different) constellation alphabets with different power assignments, so that the resulting K mapped symbol vectors $\mathbf{x}_1$, $\mathbf{x}_2$, …, $\mathbf{x}_K$ are assigned with power P_1, P_2, …, P_K, respectively. Without loss of generality, we assume that $P_1 \leq P_2 \leq \ldots \leq P_K$. The K symbol vectors are then multiplexed to form a combined modulation symbol vector $\mathbf{x} = [x[0], x[1], \ldots, x[KN\text{-}1]]^T$ such that

$$x_k[n] = x[Kn+k-1], \quad (4.29)$$

for $k \in \{1,2,\cdots K\}$ and $n \in \{0,1,\cdots,N-1\}$. Finally, using a chosen modulating pulse shape $s(t)$, the FTN modulator constructs the FTN signal by $x(t) = \sum_{n=0}^{KN-1} x[n]s\left(t - nT/K\right)$, and sends it over the communication channel.

The proposed FTN receiver architecture and its constituent blocks are shown in Figure 4.6. The signal $y(t)$ received from the communication channel is first matched filtered to the pulse shape $s(t)$ and sampled at the FTN rate of $1/\Delta t$. The corresponding matched filter outputs $y[n] = \langle y(t), s(t-n\Delta t)\rangle$ in Figure 4.6 are then de-multiplexed into K FTN sub-stream vectors, $\mathbf{y}_1$, $\mathbf{y}_2$, …, $\mathbf{y}_K$, where $\mathbf{y}_i$ is defined by

$$\mathbf{y}_i = \left[y[i-1], y[K+i-1], \cdots, y[K(N-1)+i-1]\right]^T \text{, for } i \in \{1, 2, \ldots, K\}. \quad (4.30)$$

That is, the n-th element of $\mathbf{y}_i$ is given by $y_i[n] = y[Kn+i-1]$. Consequently, the term $y_i[n]$ can be written explicitly as a function of $x_k[n]$ as

$$y_i[n] = \sum_{j=i-K}^{i-1} \sum_{m=-\infty}^{\infty} h_{mK+j} x_{i-j}[n-m] + z\left[Kn+i-1\right], \quad (4.31)$$

which is due to the definition of $x_k[n]$ in (4.29) and $z[n] = \langle z(t), s(t-n\Delta t)\rangle$. We can simplify above further by noticing that for any T-orthogonal unit energy modulating pulses $s(t)$:

$$h_{mK} = \int_{-\infty}^{\infty} s(t)s^*(t-mT)dt = \begin{cases} 1 & \text{if } m = 0 \\ 0 & \text{if } m \neq 0 \end{cases} \quad (4.32)$$

by the definition $\{h_k\}$. Furthermore, also due to (4.32), the noise samples $z[Kn+i-1]$ for $n \in \{0, 1, \ldots, N-1\}$ become *independent* zero mean Gaussian distributed with the $N_0/2$ variance. Based on these observations, (4.31) can be simplified as

$$y_i[n] = x_i[n] + \sum_{\substack{j=i-K \\ j \neq 0}}^{i-1} \sum_{m=-\infty}^{\infty} h_{mK+j} x_{i-j}[n-m] + z_i[n], \quad (4.33)$$

where the summation terms can be interpreted as ISI terms to the desired symbol $x_i[n]$, and the noise samples denoted by $z_i[n] = z[Kn+i-1]$ for $n \in \{0, 1, \ldots, N-1\}$ are white Gaussian distributed with zero mean and $N_0/2$ variance.

The proposed FTN receiver in Figure 4.6 proceeds in K stages, decoding from the most powerful FTN substream vector ($\mathbf{y}_K$) in the top branch and gradually working its way down to the least powerful FTN substream vector ($\mathbf{y}_1$) in the bottom branch. (Without loss of generality, the depicted decoding structure assumes that the assigned powers are chosen such that $P_K \geq P_{K-1} \geq \ldots \geq P_1$.) This decoding order is chosen to minimize possible error propagation through the decoding stages.

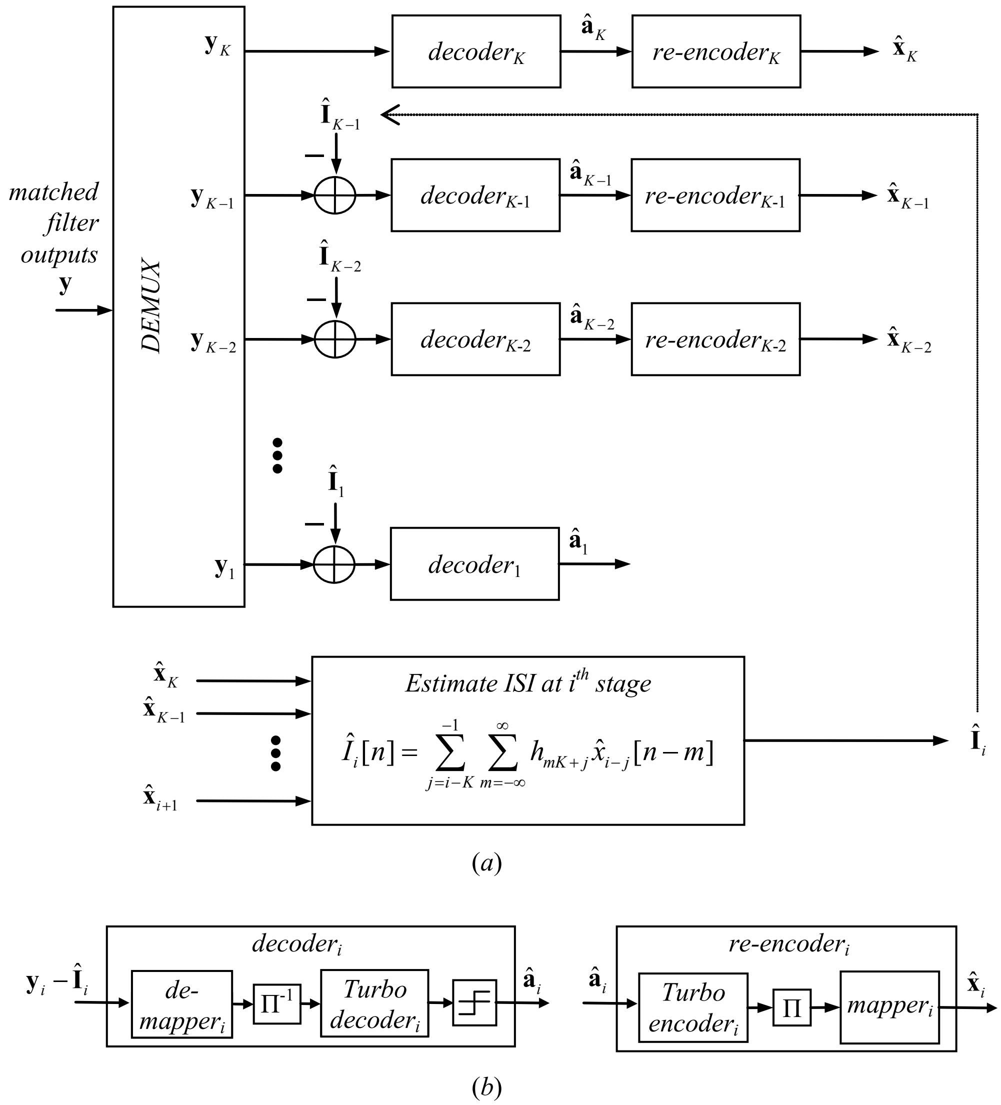

Figure 4.6 (*a*) Proposed FTN receiver architecture based on multistage decoding; (*b*) Structures of *decoder$_i$* and *re-encoder$_i$* modules of the proposed FTN receiver

The FTN receiver first processes $\mathbf{y}_K$ (in the top branch after the de-multiplexer in Figure 4.6), which represents a noisy observation about the data symbol vector $\mathbf{x}_K$. Due to (4.33), the n-th element of $\mathbf{y}_K$ is given by

$$y_K[n] = x_K[n] + \sum_{j=1}^{K-1} \sum_{m=-\infty}^{\infty} h_{mK+j} x_{K-j}[n-m] + z_K[n]. \tag{4.34}$$

The ISI term $\sum_{j=1}^{K-1}\sum_{m=-\infty}^{\infty} h_{mK+j} x_{K-j}[n-m]$ in (4.34) is approximated by a Gaussian random variable due to the *Central Limit Theorem*. Consequently, the receiver treats the

ISI term as additional noise and approximates it by a Gaussian random variable with zero mean and $\sum_{j=1}^{K-1}\sum_{m=-\infty}^{\infty}\left|h_{mK+j}\right|^2 P_{K-j}T$ variance (due to the variance of $x_k[n]$ being P_kT). Therefore, a-posteriori probabilities of K-th data symbols $x_K[n]$ can be approximately calculated by

$$\Pr\left(x_K[n]\,\middle|\,y_K[n]\right) \cong c\cdot\Pr\left(x_K[n]\right)\exp\left(-\frac{(y_K[n]-x_K[n])^2}{2\sigma_K^2}\right), \tag{4.35}$$

where c is a normalization constant, $\Pr(x_K[n])$ is a-priori probability of $x_K[n]$, and σ_K^2 denotes the variance of noise plus ISI, i.e., $\sigma_K^2 = N_0/2+\sum_{j=1}^{K-1}\sum_{m=-\infty}^{\infty}\left|h_{mK+j}\right|^2 P_{K-j}T$. Using this Gaussian approximation (4.35), the *decoder*$_K$ in Figure 4.6 computes the estimates about the K-th information subsequence $\hat{\mathbf{a}}_K$ by taking a hard decision. These are subsequently re-encoded to produce estimates about the K-th data symbols $\hat{\mathbf{x}}_K$, which will be used to recreate the corresponding ISI terms in the later decoding stages.

In general, consider the i-th stage when $y_i[n]$ is processed with regard to the i-th data $x_i[n]$. At this time, the symbol estimates $\hat{\mathbf{x}}_K$, $\hat{\mathbf{x}}_{K-1}$, …, $\hat{\mathbf{x}}_{i+1}$ are already available from the previous stages and the corresponding ISI terms can be estimated by $\sum_{j=i-K}^{-1}\sum_{m=-\infty}^{\infty} h_{mK+j}\hat{x}_{i-j}[n-m]$. These are then subtracted from $y_i[n]$ to yield (using (4.33)):

$$y_i[n]-\sum_{j=i-K}^{-1}\sum_{m=-\infty}^{\infty} h_{mK+j}\hat{x}_{i-j}[n-m] \cong x_i[n]+\sum_{j=1}^{i-1}\sum_{m=-\infty}^{\infty} h_{mK+j}x_{i-j}[n-m]+z_i[n], \tag{4.36}$$

which becomes equality if the estimates $\hat{\mathbf{x}}_K$, $\hat{\mathbf{x}}_{K-1}$, …, $\hat{\mathbf{x}}_{i+1}$ are all without errors. The residual ISI term $\sum_{j=1}^{i-1}\sum_{m=-\infty}^{\infty} h_{mK+j}x_{i-j}[n-m]$ in (4.36) is approximated by a zero mean Gaussian random variable with zero mean and $\sum_{j=1}^{i-1}\sum_{m=-\infty}^{\infty}\left|h_{mK+j}\right|^2 P_{i-j}T$ variance, again due to the *Central Limit Theorem*. Consequently, the a-posteriori probabilities of the i-th data symbols $x_i[n]$ can be approximated by

$$\Pr\left(x_i[n]\,\middle|\,y_i[n]\right) \cong c\cdot\Pr\left(x_i[n]\right)\exp\left(-\frac{(y_i[n]-x_i[n])^2}{2\sigma_i^2}\right), \tag{4.37}$$

where c is a normalization constant, $\Pr(x_i[n])$ is a-priori probability of $x_i[n]$, and σ_i^2 denotes the variance of noise plus the residual ISI, i.e., $\sigma_i^2 = N_0/2 + \sum_{j=1}^{i-1} \sum_{m=-\infty}^{\infty} \left| h_{mK+j} \right|^2 P_{i-j} T$. Using the Gaussian approximation (4.37), the *decoder*$_i$ computes estimates about the i-th information subsequence $\hat{\mathbf{a}}_i$, which are then re-encoded to produce estimates about $\hat{\mathbf{x}}_i$. These steps continue in stages from $i = K$ all the way down to $i = 1$, and the obtained $\hat{\mathbf{a}}_1$, $\hat{\mathbf{a}}_2$, …, $\hat{\mathbf{a}}_K$ are finally multiplexed to form an overall estimate about the entire information sequence $\hat{\mathbf{a}}$.

Due to the sequential nature of decoding, some amount of buffering is required for a practical implementation of the FTN receiver. To buffer the FTN substream vectors $\mathbf{y}_1$, $\mathbf{y}_2$, …, $\mathbf{y}_K$, one would need 32×KN bits or 4×KN bytes, if 32 bit single-precision floating-point format is used to represent a number. For FTN rate factor K = 5 and packet length N = 10,000, only 0.2 Megabyte of memory would be needed for buffering of the FTN substream vectors. Such memory requirement is insignificant for the state-of-the-art mobile handsets.

4.3.3 Power Assignment Rule for Finite Modulation Alphabets

The considered FTN signaling with non-uniform power allocation allows one to choose how the available power P can be split and assigned to K FTN sub-streams. The capacity analysis in section 4.2 indicates that the power can be distributed *non-uniformly* without negatively affecting the capacity when the optimal Gaussian modulation symbols are used. However, in the case of practical *finite-alphabet* modulation (e.g., PAM, QAM, and PSK), choosing appropriate power assignments among FTN sub-streams becomes crucial in achieving the performance close to the channel capacity. Furthermore, due to the multistage decoding setup of the proposed FTN receiver in subsection 4.3.2, the power assignments should take into account of the performance of individual error-correcting-codes used in each stage.

In the following, a simple power assignment rule is described that takes into account of the finite modulation alphabets and the performance of individual error-correcting-codes.

First let the error-correcting-code used in the i-th branch of the FTN transceiver in Figure 4.5 and Figure 4.6 converges at $SNR = \rho_i$ in the conventional AWGN channel (e.g., for the original Turbo code from [18], $10\log_{10}(\rho) \approx 0.7$ dB). Using the discrete-time FTN channel model given in (4.33) and the configuration of the proposed FTN multistage decoding in Figure 4.6, the i-th branch of the decoder can be modeled as an AWGN channel. In this channel, the signal energy is given by P_iT and the variance of noise plus residual ISI is given by $\sigma_z^2 + \sum_{j=1}^{i-1}\sum_{m=-\infty}^{\infty}\left|h_{mK+j}\right|^2 P_{i-j}T$. Due to the *Central Limit Theorem*, the distribution of this ISI can be approximated as a Gaussian distribution as the FTN induced ISI memory length increases.

Therefore, in order for the error-correcting-code to be able to successfully decode the information sequence at the i-th branch of the decoder, signal-to-interference-plus-noise ratio (SINR) must satisfy

$$SINR = \frac{P_iT}{\sigma_z^2 + \sum_{j=1}^{i-1}\sum_{m=-\infty}^{\infty}\left|h_{mK+j}\right|^2 P_{i-j}T} \geq \rho_i \text{, for } i = 1, 2, \ldots, K, \tag{4.38}$$

which, in addition to the power constraint $P = P_1+P_2+\ldots+P_K$, lead to K+1 equations with K+1 unknowns (i.e., P_1, P_2, …, P_K, and σ_z^2). Note that σ_z^2 signifies the noise power at which the system is expected to converge. Consequently, we obtain for i = 1, 2, …, K,

$$P_i \geq \rho_i \frac{N_0/2}{T}\left(1+\sum_{j=1}^{i-1}\left(\sum_{m=-\infty}^{\infty}\left|h_{mK+i-j}\right|^2\right)\frac{P_jT}{N_0/2}\right) \text{ such that } P = \sum_{j=1}^{K} P_j . \tag{4.39}$$

Then, the *minimum required* power P_i for all i can be obtained by taking the equality in (4.39) and recursively solving (4.39) starting from i=1. The simulation results in the next subsection follow the above power assignment rule.

4.3.4 Simulation Results and Discussions

In this subsection, we report the simulated performances of the proposed FTN transceiver. In all simulations, the modulating pulses $s(t)$ were chosen to be the bandlimited square-root raised cosine with the roll-off factor β=0.22, used in, e.g., WCDMA standard (with time-truncation to $\pm 15T$ about t=0, signaling interval T=(1+β)/(2W), and bandwidth W=1 kHz). Figure 4.7 depicts the modulating pulse $s(t)$ in time domain and the corresponding pulse correlation coefficients $h_l = \int_{-\infty}^{+\infty} s(t)\, s(t - l \cdot T/K)\, dt$ for $l \in \mathbb{Z}$.

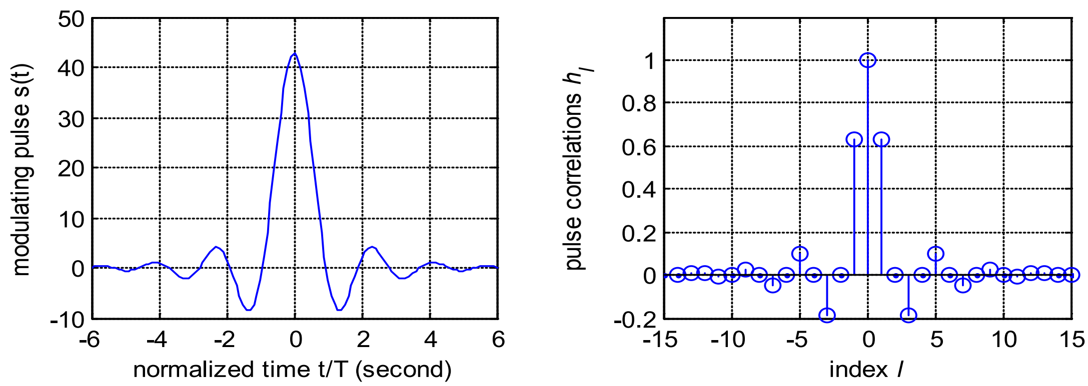

(a) (b)

Figure 4.7 Characteristics of the time-truncated square-root raised cosine modulating pulse $s(t)$ with the roll-off factor β=0.22; Normalized to have a unit energy;
(a) plotting in normalized time t/T in seconds where T=(1+β)/(2W) and W = 1 kHz;
(b) plotting the corresponding pulse correlations h_l

All interleavers were pseudorandom [24] and, unless otherwise specified, the packet lengths were N=4×10^4. With these design choices, the overall spectral efficiencies η in bits per second per Hz were calculated as

$$\eta = \frac{1}{TW} \sum_{i=1}^{K} R_{coding_i} R_{modulation_i} \quad \text{bits/s/Hz,} \tag{4.40}$$

where R_{coding_i} and $R_{modulation_i}$ denote the coding rate (in information bits per coded bit) and the modulation rate (in coded bits per modulation symbol), respectively, for the i-th message subsequence (i = 1, 2, …, K). The signaling rate (in symbols per second) for the i-th symbol subsequence $\mathbf{x}_i$ is equal to $1/T$ (note that T=(1+β)/(2W) for the root-raised cosine pulses). Motivated by the optimality of binary FTN signaling [165], binary antipodal modulation has been used for all the data symbols (although the designed architecture

[24] Turbo codes using pseudorandom interleavers have been demonstrated to perform close to the Shannon capacity of AWGN channel [18]. Using other interleavers such as S-random [36] or algebraic interleavers [139] can bring additional small performance gains including lower error-floor and better convergence with small packet length.

allows higher order modulations). Furthermore, the error correcting encoders at the proposed FTN transmitter were chosen to be a version of the rate 1/2 serial Turbo codes[25] proposed by ten Brink [143], which is known to perform very close to the capacity limit in AWGN channel.

In Figure 4.8, the achieved spectral efficiencies of the simulated FTN transceiver architecture with varying rates (K = 2 to 6) are plotted in a power-bandwidth plane for the AWGN channel. The corresponding bit-error-rate (BER) curves of the FTN systems (each after 100 Turbo iterations) are plotted in Figure 4.9. The power assignments between the K symbol subsequences $\mathbf{x}_1, \mathbf{x}_2, \ldots, \mathbf{x}_K$ were as listed in Table 4.1, which were found using the power assignment rule described in subsection 4.3.3. The considered binary FTN signaling with the factor K is comparable to the 2^K-PAM Nyquist rate signaling, and for comparisons the 2^K-PAM input-constrained channel capacities at the same spectral efficiencies are also plotted in Figure 4.8. We observe that the proposed FTN system for all simulated range of K can approach the corresponding capacity limits of PAM signaling with no ISI to within 1 dB at the target BER=10^{-4}.

[25] The used Turbo code had a rate 1/2 repetition encoder for the outer code and a rate 1 (memory 4) recursive convolutional code, described by code polynomials (G_r, G)=(037,020) in octal values, for the inner code.

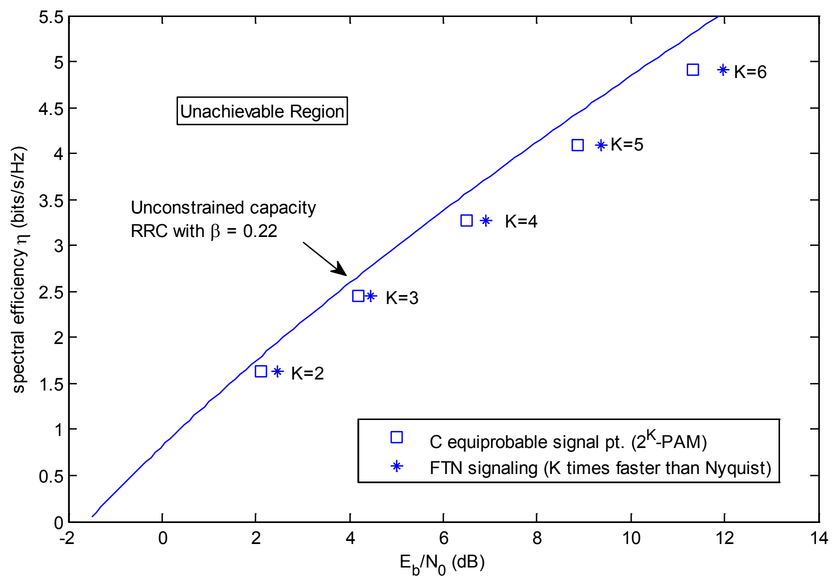

Figure 4.8 Achieved spectral efficiencies (for BER = 10^{-4}) using the proposed FTN transceiver employing *K* times faster than the Nyquist rate transmissions; Capacities of competing Nyquist rate systems with equiprobable PAM transmissions and no ISI are also plotted (as square boxes) for reference

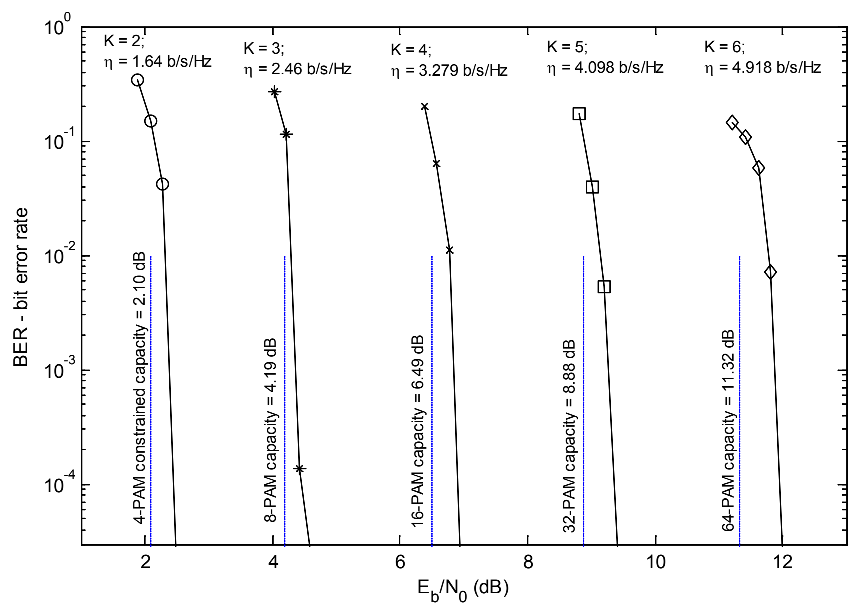

Figure 4.9 BER simulation results of the proposed FTN transceiver in AWGN channel after 100 Turbo iterations; Capacities of competing Nyquist rate systems employing equiprobable *M*-PAM transmission are also plotted for reference

Table 4.1 Power assignments used for the simulations

K	P_1	P_2	P_3	P_4	P_5	P_6
2	0.3283	0.6717	-	-	-	-
3	0.1352	0.2810	0.5838	-	-	-
4	0.0599	0.1264	0.2630	0.5507	-	-
5	0.0273	0.0581	0.1219	0.2554	0.5373	-
6	0.0125	0.0269	0.0568	0.1196	0.2520	0.5322

One of the primary benefits of the considered FTN system is that it can effectively implement very high rate systems with relatively small modulation formats. For example, using only binary antipodal symbols with K=6 FTN signaling, we can implement a system that is equivalent to 64-PAM Nyquist rate system. Furthermore, the proposed low-complexity FTN transceiver design allows practical implementation of these high rate FTN systems with only linear computational complexity at the receiver. This directly contrasts with the earlier FTN coding designs where the implementation complexity of the equalizer grows exponentially with the length of the ISI and hence severely hinders the design.

On the other hand, one potential drawback of the presented design is a non-zero error propagation in the multistage decoding. Amount of error propagation depends on number of stages K and performance of utilized error-correcting-codes. Figure 4.10 plots the expected converging E_b/N_0 of FTN multistage decoder, which is calculated by solving for σ_z^2, the noise power at which the system is expected to converge, in (4.38). The parameter ρ in Figure 4.10 denotes converging E_b/N_0 of utilized Turbo code in AWGN channel (e.g., ρ = 0.7 dB for Berrou's rate 1/2 parallel Turbo code with N = 65,536 bits from [18] and ρ = 0.3 dB for ten Brink's rate 1/2 serial Turbo code with $N = 10^6$ bits from [142]). We considered BPSK modulation formats and square-root raised cosine (RRC) pulse with roll-off factor β = 0.22. We can observe from Figure 4.10 that the converging E_b/N_0 diverges from the capacity with increasing number of stages (or FTN rate factor) K, which is a direct consequence of non-zero error propagation in the multistage decoder.

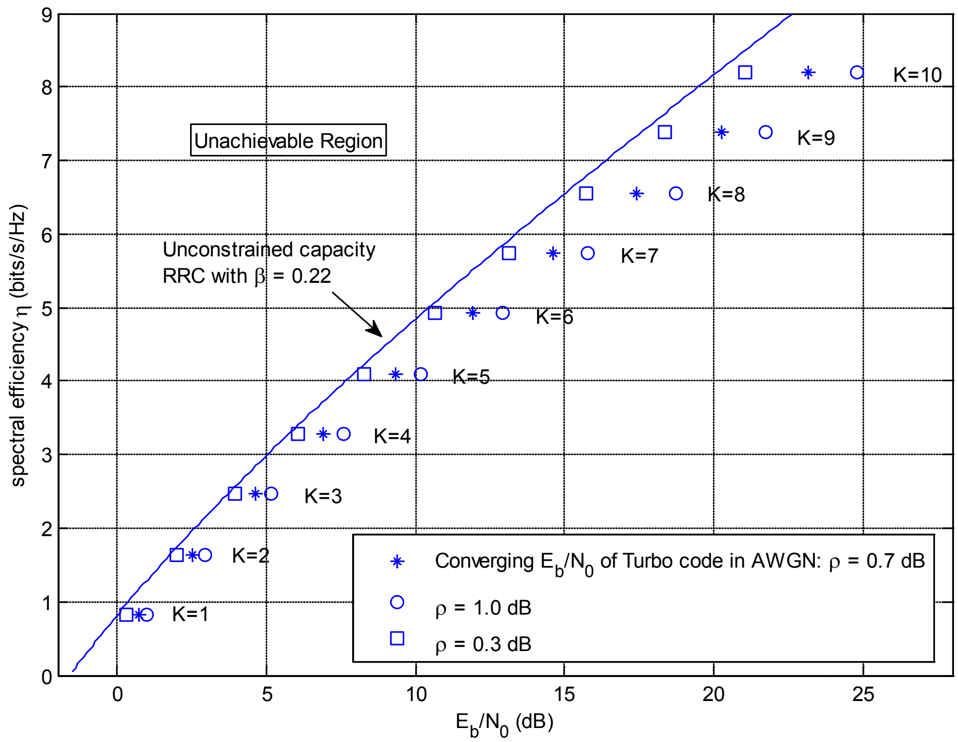

Figure 4.10 Expected converging E_b/N_0 of the FTN multistage decoder with varying number of stages (or FTN rate factor) K; The parameter ρ represents converging E_b/N_0 of used Turbo code in conventional AWGN channel.

The effect of error propagation can be minimized by using a stronger error-correcting-code. For instance, when ten Brink's serial Turbo code [142] with $\rho = 0.3$ dB and $N = 10^6$ bits can be used, the FTN multistage decoder can perform within fraction of decibals away from the capacity for entire range of spectral efficiencies considered (see square markers in Figure 4.10). Alternatively, one can reduce the number of stages K directly, hence the amount of error propagation, by utilizing higher level modulation format (e.g., 4-PAM or 8-PAM) for each stage at the same FTN rate. For example, binary FTN with $K = 10$ is equivalent to FTN with 4-PAM with $K = 5$, in terms of the information rates.

In addition, we also considered peak-to-average power ratio (PAPR) of FTN signals in time domain, which is defined as [19]:

$$PAPR \equiv \frac{\max_t |x(t)|^2}{E\left\{\lim_{T_0\to\infty} \frac{1}{T_0}\int_{-T_0/2}^{T_0/2} |x(t)|^2\,dt\right\}}. \tag{4.41}$$

Large PAPR is known to saturate power amplifiers at the transmitter and may cause undesired nonlinear distortion in the transmitted signal [113]. Figure 4.11 shows the numerically computed PAPR estimates of FTN signals (obtained by averaging at least 200 instances of FTN signal realizations) that are using either uniform power assignments or the non-uniform power assignments as listed in Table 4.1. For comparison purposes, PAPR estimates of Nyquist rate signals using 2^K-PAM input constellations are also plotted as a reference. All signals were modulated by square-root raised cosine pulse with roll-off factor 0.22.

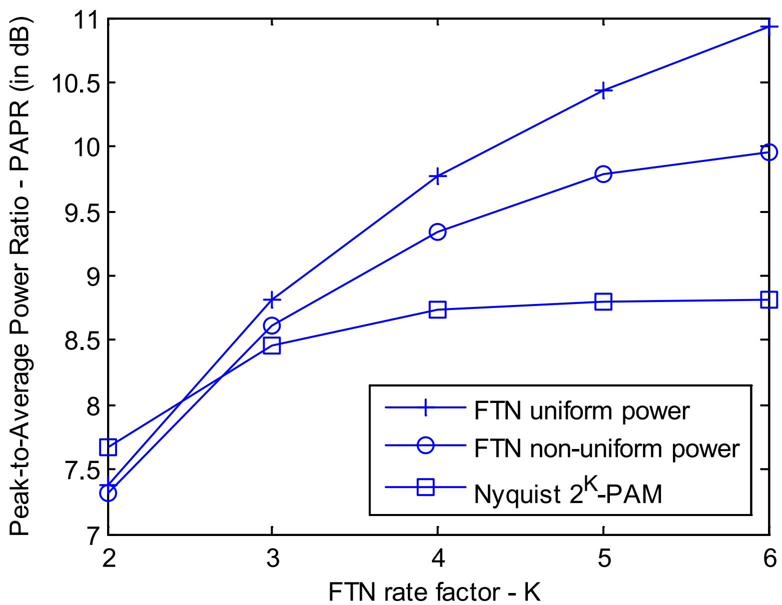

Figure 4.11 Peak-to-average power ratio of FTN signals with uniform or non-uniform power assignments, along with Nyquist rate signal using 2^K-PAM modulation formats; Square-root raised cosine pulse with roll-off factor 0.22 is used.

We first observe from Figure 4.11 that the non-uniform power assignments as compared to uniform power can reduce PAPR of FTN signals for all ranges of FTN rate factor K considered. This implies that reduced PAPR may be an additional benefit to using non-uniform power assignments in FTN signaling. On the other hand, for $K \geq 3$, FTN signals are shown to have higher PAPR than that of Nyquist rate signals using 2^K-PAM input constellations. Consequently, high rate FTN signaling may suffer from increased PAPR, and further research is needed to address this issue. (To the best of our knowledge, PAPR analysis of FTN signals has not been reported in published literature.) Interestingly, at $K = 2$, PAPR of FTN signals are observed to be smaller than that of 4-PAM Nyquist rate signals. This observation may lead to yet another potential research topic in FTN signaling.

Finally, we note that a method of *pipelining* can be used to keep the decoding latency of the multistage decoding to latency associated with only one stage. Pipelining is achieved by feeding a new packet into the first stage while previous packets in each stage are fed to the next − leading to decoding maximum of K packets *in parallel* over K stages.

4.4 Chapter Summary

The main objective of this chapter has been a comprehensive evaluation of *non-precoded* FTN signaling from the capacity and coding perspectives. The review of FTN capacity analysis results in sections 4.1 revealed that the *i.i.d.* (non-precoded) FTN signaling can asymptotically achieve the generalized Shannon capacity of power spectral density of the transmission spectrum (i.e., C_{PSD} from Theorem 2.2) and has an ability to recover information residing in all frequency ranges. Furthermore, binary FTN signaling was shown to achieve the capacity of the high-order (M-ary) Nyquist rate transmission using signal shaping. Based on these observations, we argued that the *i.i.d.* FTN signaling can be seen as an important competing technology to non-binary (M-ary) Nyquist rate communication and could find applications in channels with high SNR, which are frequencly encountered in long-haul optical fiber links, femto cells in wireless systems, DSL channel, etc.

Subsequently in section 4.2, we relaxed the independent and identically distributed (*i.i.d.*) condition on the FTN symbols. We have identified a class of independent but *non-identically distributed* FTN signaling that offers competitive capacity potential when compared to capacity of Nyquist rate systems. Using this FTN signaling approach, a low-complexity FTN-based coding system was designed in section 4.3 which could operate near the FTN capacity and at high spectral efficiencies. The main features of the design include *non-uniform power allocation* over FTN modulation symbols and multistage decoding. This design effectively removes the need for large complexity ISI equalizer and hence significantly reduces the implementation complexity. The obtained simulation results indicated that the low complexity design allows practical implementation of high rate and spectrally efficient FTN systems.

Chapter 5

Benefits of Precoding in FTN Signaling

Precoding and *equalization* have been previously considered as two ways to deal with the intersymbol interference that is inherently introduced by the FTN transmission. Initially, the prior FTN precoding designs primarily aimed to increase the *minimum distance* of the FTN signaling [96], [158], [126], [101], while the recursive precoding design in [125] improved the convergence of serially concatenated FTN coding systems.

In this chapter, we focus on developing an *information-theoretically optimal* precoding strategy that maximizes the mutual information of the FTN channel. In section 5.1, we first consider *convolutional precoding* for the FTN signaling and derive the corresponding closed-form FTN capacity expression. The derived capacity generalizes the capacity analysis in Chapter 4 and further introduces the concept of the (power) water-filling to the FTN signaling through the utilization of convolutional precoding.

In section 5.2, we derive the *universally optimal FTN precoding structure* and show that it can substantially increase the capacity of FTN signaling. This capacity gain would not be possible without utilizing an appropriate precoder at the transmitter. However, this capacity increase comes at a price of either a bandwidth expansion or numerical instability in computing the precoding matrix. These issues are also discussed in section 5.2.

Finally, section 5.3 describes a potential use of the precoded FTN signaling to achieve spread-spectrum communication. We propose an FTN-based spread spectrum architecture and present bit-error-rate (BER) simulation results that indicate feasibility of the proposed FTN-based spread spectrum technique.

5.1 Convolutional Precoding for FTN Signaling

Convolutional precoding has been considered in many digital communication systems, including partial response signaling and trellis coded modulation, due to its practicality in implementation and the tractable computation of power spectral density that results from it [52], [72]. Convolutional precoding has been also considered in the FTN literature (see e.g., [158], [96], [125], [126]) to deal with the FTN-induced intersymbol interference. However, such precoding causes the FTN modulation symbols become non-*i.i.d.* and, to the best of our knowledge, no capacity analysis of precoded FTN transmission has been presented so far.

In this section, we consider *convolutional precoding* for FTN signaling and analyze the corresponding channel capacity (technically, the information rate). It will be shown that convolutional precoding can increase the FTN channel capacity in frequency-selective channels by enabling water-filling over the channel frequency spectrum. In addition, convolutional precoding allows reshaping the transmission spectrum of FTN and achieving the ideal near-flat transmission spectrum while using practical time-limited modulating pulses.

5.1.1 Initial Considerations

First consider a zero-mean *i.i.d.* information sequence $a[0]$, $a[1]$, …, $a[KN-1]$, where N denotes the packet length and K (>1) is the factor by which the Nyquist rate is exceeded. Following the Definition 3.2, the convolutionally precoded FTN modulation symbols are given by $x[n]=\sum_{k=-\infty}^{\infty}\xi_k a[n-k]$ for n = 0, 1, 2, …, $KN-1$, for some *real* precoding coefficients $\{\xi_k\}$ that are assumed to be absolutely summable and it is assumed that $a[n]=0$ for $n<0$ and $n>KN-1$. For mathematical tractability, the real finite precoding coefficients $\{\xi_k\}$ are further assumed to be equal to zero all $|k|>KN-1$ (we will eventually let N tends to infinity in our analysis to allow very long precoding coefficients). Such precoding can be practically achieved by a matrix multiplication or using a filter with a discrete-time finite impulse response (FIR). Note that we only transmit KN data symbols, i.e., $x[n]$ for

$0<n<KN-1$, due to the limited number of symbols that can be transmitted over channels per given time window, although the convolutional precoding $x[n]=\sum_{k=-\infty}^{\infty}\xi_k a[n-k]$ can theoretically output non-zero data symbols for $n<0$ and $n>KN-1$.

Such convolutional precoding can also be conveniently expressed in a matrix equation. Denote the information symbol vector by $\mathbf{a}$ = $[a[0], a[1], \ldots, a[KN\text{-}1]]^T$ and the convolutionally precoded FTN modulation symbol vector by $\mathbf{x} = [x[0], x[1], \ldots, x[KN\text{-}1]]^T$. Then, $\mathbf{x}$ can be expressed as the following the matrix equation:

$$\mathbf{x} = L\mathbf{a}\,, \tag{5.1}$$

where L is a Toeplitz *precoding matrix* defined by

$$L=\begin{bmatrix} \xi_0 & \xi_{-1} & \xi_{-2} & \cdots & \xi_{-KN+1} \\ \xi_1 & \xi_0 & \xi_{-1} & \cdots & \xi_{-KN+2} \\ \xi_2 & \xi_1 & \xi_0 & \cdots & \xi_{-KN+3} \\ \vdots & \vdots & \vdots & \ddots & \vdots \\ \xi_{KN-1} & \xi_{KN-2} & \xi_{KN-3} & \cdots & \xi_0 \end{bmatrix}. \tag{5.2}$$

Such precoding of FTN modulation symbols leads to a convolutionally precoded FTN signal $x(t)$ with a well-defined transmission power spectral density $\mathsf{S}_x(f)$ (as derived in Theorem 3.1):

$$\mathsf{S}_x(f)=\frac{\sigma_a^2}{\Delta t}\left|\mathsf{S}_\xi(f)\,\hat{s}(f)\right|^2, \tag{5.3}$$

where $\hat{s}(f)$ is the Fourier transform of the modulating pulse $s(t)$, $\Delta t = T/K$ is the FTN signaling interval, $\sigma_a^{\,2} = E\{|a[n]|^2\}$ is the variance (or PSD) of the *i.i.d.* information sequence $a[n]$, and $\mathsf{S}_\xi(f)$ is the spectrum of the precoding coefficients, defined by

$$\mathsf{S}_\xi(f)\equiv\sum_{k=-\infty}^{\infty}\xi_k e^{+j2\pi fk\Delta t}\ . \tag{5.4}$$

The channel capacities (or the *information rates*) of the convolutionally precoded FTN signaling in AWGN channel and LTI channel are derived in subsection 5.1.2 and 5.1.3, respectively. Recalling from Definition 2.8, the *information rate* gives the maximal achievable rate when the modulation symbol vector $\mathbf{x}$ has some fixed structure (in our case, it is the convolutionally precoded $\mathbf{x}$), and is defined by $\overline{C}=\lim_{N\to\infty}(NT)^{-1}I(\mathbf{x};\mathbf{y})$ in bits per second where **x** is the convolutionally precoded FTN modulation symbol vector and **y** denotes the corresponding FTN channel output.

5.1.2 Convolutional FTN Precoding in AWGN Channels

We first define some relevant terms. The precoding spectrum $\mathsf{S}_\xi(f)$ is defined as in (5.4) with a set of absolutely summable precoding coefficients $\{\xi_k\}$. In addition, the folded pulse spectrum $\hat{s}_{folded}(f)$ from Definition 3.1 is reproduced below for convenience:

$$\hat{s}_{folded}(f) \equiv \sum_{k=-\infty}^{\infty} \left|\hat{s}(f - k/\Delta t)\right|^2, \quad f \in (-1/2\Delta t, 1/2\Delta t), \tag{5.5}$$

where $\hat{s}(f)$ is the Fourier transform of the modulating pulse $s(t)$.

The information rate of the convolutionally precoded FTN signaling in AWGN channel is given in the following theorem.

Theorem 5.1 (Information rate of convolutionally precoded FTN signaling in AWGN channel): *Consider the convolutionally precoded FTN modulation symbols* $\mathbf{x} = L\mathbf{a}$ *with precoding spectrum* $\mathsf{S}_\xi(f)$ *defined in (5.4), where* **a** *is the i.i.d. information symbol vector with a variance* σ_a^2 *and L is a Toeplitz precoding matrix defined in (5.2). Assume that the folded pulse spectrum* $\hat{s}_{folded}(f)$ *is finite for all* $f \in (-1/(2\Delta t), 1/(2\Delta t))$. *Then the information rate of the convolutionally precoded FTN signaling in AWGN channel* $\mathbf{y} = H\mathbf{x} + \mathbf{z}$ *is given by*

$$\bar{C}_{conv\text{-}precoded}^{FTN} \le \int_{-1/(2\Delta t)}^{1/(2\Delta t)} \log_2\left(1 + \frac{1}{N_0/2}\frac{\sigma_a^2}{\Delta t}\left|\mathsf{S}_\xi(f)\right|^2 \hat{s}_{folded}(f)\right) df \ \textit{ bits per second,} \tag{5.6}$$

with equality if the modulation symbols $\{x[n]\}$ *are jointly Gaussian distributed.*

***Proof*:** When the FTN modulation symbols **x** are convolutionally precoded, the covariance matrix of the FTN symbol vector **x** can be expressed as $K_x = \sigma_a^2 LL^\dagger$, where $(\cdot)^\dagger$ denotes conjugate transpose (or Hermitian) of a matrix.

The mutual information between the precoded FTN modulation symbols **x** and the noisy channel observations $\mathbf{y} = H\mathbf{x}+\mathbf{z}$ is given by:

$$I(\mathbf{x};\mathbf{y}) = h(\mathbf{y}) - h(\mathbf{y}|\mathbf{x}) \tag{5.7}$$

$$= h(\mathbf{y}) - h(\mathbf{z}), \tag{5.8}$$

where $h(\cdot)$ denotes the differential entropy (Definition 2.3) and (5.8) follows from $H\mathbf{x}$ being deterministic given $\mathbf{x}$ and the translation invariance of the differential entropy (Lemma 2.5). The covariance matrix of $\mathbf{y}$ is given by

$$K_y = HK_xH^\dagger + (N_0/2)\cdot H, \tag{5.9}$$

due to $E\{\mathbf{z}\mathbf{z}^\dagger\} = (N_0/2)\cdot H$ from (3.23), where K_x is the covariance matrix of $\mathbf{x}$ and $(\cdot)^\dagger$ denotes conjugate transpose (Hermitian) operation.

By Lemma 2.4, the differential entropy of channel output, $h(\mathbf{y})$, is maximized by having $\mathbf{y}$ circularly symmetric complex Gaussian distributed with covariance K_y:

$$h(\mathbf{y}) \le \log_2\left((\pi e)^{KN}\det(K_y)\right) \tag{5.10}$$

$$= \log_2\left((\pi e)^{KN}\det\left(HK_xH^\dagger + (N_0/2)\cdot H\right)\right), \tag{5.11}$$

with equality if $\mathbf{y}$ is a circularly symmetric complex Gaussian. Furthermore, the differential entropy of the Gaussian noise, $h(\mathbf{z})$, is given by (using Lemma 2.3)

$$h(\mathbf{z}) = \log_2\left((\pi e)^{KN}\det\left((N_0/2)\cdot H\right)\right). \tag{5.12}$$

Therefore, the mutual information (5.8) can be upper- bounded as follows:

$$I(\mathbf{x};\mathbf{y}) \le \log_2\left(\frac{\det\left(HK_xH^\dagger + (N_0/2)\cdot H\right)}{\det\left((N_0/2)\cdot H\right)}\right), \tag{5.13}$$

with equality if and only if $\mathbf{y}$ is circularly symmetric complex Gaussian, which is obtained when $\mathbf{x}$ is also circularly symmetric complex Gaussian.

Since H is Hermitian and invertible as proved in Proposition 3.1, (5.13) can be further simplified as follows:

$$I(\mathbf{x};\mathbf{y}) \le \log_2\left(\det\left(\frac{1}{N_0/2}H^{-1}\right)\det\left(HK_xH^\dagger + (N_0/2)\cdot H\right)\right) \tag{5.14}$$

$$= \log_2\left(\det\left(\frac{1}{N_0/2}H^{-1}HK_xH^\dagger + I_{KN}\right)\right) \tag{5.15}$$

$$= \log_2\left(\det\left(\frac{1}{N_0/2}K_x H + I_{KN}\right)\right) \tag{5.16}$$

$$= \log_2\left(\det\left(\frac{\sigma_a^2}{N_0/2}LL^\dagger H + I_{KN}\right)\right), \tag{5.17}$$

where (5.14) is due to $\det(A^{-1}) = \det(A)^{-1}$, (5.15) is by $\det(A)\det(B) = \det(AB)$, (5.16) follows from the conjugate symmetry of H (i.e., $H = H^\dagger$), and (5.17) is due to the covariance matrix of the convolutionally precoded $\mathbf{x}$ being equal to $K_x = \sigma_a^2 LL^\dagger$. Denoting $\lambda_j\{A\}$ by the j-th eigenvalue of the matrix A, the information rate of the convolutionally precoded FTN then becomes:

$$\overline{C}^{FTN}_{conv\text{-}precoded} \equiv \lim_{N\to\infty}(NT)^{-1}I(\mathbf{x};\mathbf{y}) \le \lim_{N\to\infty}\frac{1}{NT}\log_2\left(\det\left(\frac{\sigma_a^2}{N_0/2}LL^\dagger H + I_{KN}\right)\right) \tag{5.18}$$

$$= \lim_{N\to\infty}\frac{1}{NT}\log_2\left(\det\left(\frac{\sigma_a^2}{N_0/2}L^\dagger HL + I_{KN}\right)\right), \tag{5.19}$$

$$= \lim_{N\to\infty}\frac{1}{NT}\sum_{j=0}^{KN-1}\log_2\left(1+\frac{\sigma_a^2}{N_0/2}\lambda_j\left\{L^\dagger HL\right\}\right), \tag{5.20}$$

where (5.19) is due to the identity: $\log\det(AB+I) = \log\det(BA+I)$, and (5.20) is due to the identities: $\det(A) = \prod_j \lambda_j\{A\}$ and $\lambda_j\{I+A\} = 1+\lambda_j\{A\}$ for any Hermitian matrix A (see section 2.4).

In order to further evaluate the above, we invoke Szegö's theorem on the asymptotic eigenvalues of the product of Toeplitz matrices $L^\dagger$, H, and L (using the generalized Szegö's theorem for product of Toeplitz matrices in Theorem D.2 in Appendix D). Consequently, (5.20) converges in the limit $N \to \infty$ to

$$\overline{C}^{FTN}_{conv\text{-}precoded} \le \frac{1}{2\pi\Delta t}\int_{-\pi}^{\pi}\log_2\left(1+\sigma_a^2(N_0/2)^{-1}\left|\xi(\lambda)\right|^2 h(\lambda)\right)d\lambda, \tag{5.21}$$

where

$$\xi(\lambda) \equiv \sum_{k=-\infty}^{\infty}\xi_k e^{jk\lambda} \text{ and } h(\lambda) \equiv \sum_{k=-\infty}^{\infty}h_k e^{jk\lambda}. \tag{5.22}$$

By a change of variable (substituting $\lambda = 2\pi f\Delta t$), (5.21) can be rewritten as

$$\overline{C}^{FTN}_{conv\text{-}precoded} \leq \int_{-1/(2\Delta t)}^{1/(2\Delta t)} \log_2\left(1+\sigma_a^2 (N_0/2)^{-1} \left|\xi(2\pi f \Delta t)\right|^2 h(2\pi f \Delta t)\right) df \tag{5.23}$$

$$= \int_{-1/(2\Delta t)}^{1/(2\Delta t)} \log_2\left(1+\sigma_a^2 (N_0/2)^{-1} \left|\mathsf{S}_\xi(f)\right|^2 h(2\pi f \Delta t)\right) df \tag{5.24}$$

$$= \int_{-1/2\Delta t}^{1/2\Delta t} \log_2\left(1+\sigma_a^2 (N_0/2)^{-1} \left|\mathsf{S}_\xi(f)\right|^2 (\Delta t)^{-1} \hat{s}_{folded}(-f)\right) df\,, \tag{5.25}$$

where (5.24) is due to $\xi(2\pi f\Delta t) = \sum_{k=-\infty}^{\infty} \xi_k e^{jk2\pi f\Delta t}$, which is equal to the precoding spectrum $\mathsf{S}_\xi(f)$ as defined in (5.4), and (5.25) is due to the relationship $\hat{s}_{folded}(f) = \Delta t \cdot h(-2\pi f \Delta t)$ as proved in Lemma 3.3. Finally, applying a change of variable ($f' = -f$) to (5.25), followed by $\mathsf{S}_\xi^*(f) = \mathsf{S}_\xi(-f)$ for real precoding coefficients $\{\xi_k\}$, yields the desired result. This completes the proof of Theorem 5.1. ■

The information rate expression in (5.6) is an integral of a non-negative function over a frequency range $f \in (-1/(2\Delta t),\ 1/(2\Delta t))$. Consequently, as the FTN signaling rate $1/\Delta t$ increases, the wider the integral range becomes. If $\hat{s}_{folded}(f)$ has nonzero frequency component beyond frequency range $f \in (-1/(2T),\ 1/(2T))$, FTN signaling can lead to a higher information rate[26]. (This is similar to the non-precoded *i.i.d.* FTN signaling case in section 4.1.) On the other hand, when compared to the capacity of the *i.i.d.* FTN signaling, i.e., $C^{FTN}_{i.i.d.} = \int_{-1/(2\Delta t)}^{1/(2\Delta t)} \log_2\left(1+P/(N_0/2)\cdot \hat{s}_{folded}(f)\right) df$ in (4.2), convolutional precoding in FTN newly introduces a frequency-dependent term called the precoding spectrum $\mathsf{S}_\xi(f) = \sum_k \xi_k e^{j2\pi fk\Delta t}$ into the information rate expression (5.6). This implies that the information rate of FTN can in general be increased by carefully choosing a convolutional precoder with appropriate precoding coefficients $\{\xi_k\}$.

In order to gain further insights into Theorem 5.1, an upper-bound on the information rate of the convolutionally precoded FTN signaling is established in the following.

[26] We note that the folded pulse spectrum $\hat{s}_{folded}(f)$ has nonzero frequency components beyond the frequency range $f \in (-1/(2T),\ 1/(2T))$ for any practical time-limited modulating pulse shape $s(t)$.

Theorem 5.2 (Upper-bound on the information rate of FTN): *Let* $\mathsf{S}_x(f) = \sigma_a^2 (\Delta t)^{-1} \left| \mathsf{S}_\xi(f) \hat{s}(f) \right|^2$ *be the power spectral density (PSD) of the convolutionally precoded FTN signal* $x(t)$ *as derived in Theorem 3.1. Then, the information rate of the convolutionally precoded FTN signaling,* $\overline{C}_{conv\text{-}precoded}^{FTN}$*, in AWGN channel is upper-bounded by*

$$\overline{C}_{conv\text{-}precoded}^{FTN} \le \int_{-\infty}^{\infty} \log_2 \left(1 + (N_0/2)^{-1} \mathsf{S}_x(f) \right) df , \tag{5.26}$$

which is the generalized Shannon capacity formula C_{PSD} *in Theorem 2.2 for complex AWGN channels.*

Proof: Rewrite the right hand side of (5.26) as follows:

$$\int_{-\infty}^{\infty} \log_2 \left(1 + (N_0/2)^{-1} \mathsf{S}_x(f) \right) df = \int_{-\infty}^{\infty} \log_2 \left(1 + \frac{1}{N_0/2} \frac{\sigma_a^2}{\Delta t} \left| \mathsf{S}_\xi(f) \hat{s}(f) \right|^2 \right) df \tag{5.27}$$

$$= \sum_{k=-\infty}^{\infty} \int_{-k/\Delta t - 1/(2\Delta t)}^{-k/\Delta t + 1/(2\Delta t)} \log_2 \left(1 + \frac{1}{N_0/2} \frac{\sigma_a^2}{\Delta t} \left| \mathsf{S}_\xi(f) \hat{s}(f) \right|^2 \right) df \tag{5.28}$$

$$= \sum_{k=-\infty}^{\infty} \int_{-1/(2\Delta t)}^{1/(2\Delta t)} \log_2 \left(1 + \frac{1}{N_0/2} \frac{\sigma_a^2}{\Delta t} \left| \mathsf{S}_\xi\left(f - \frac{k}{\Delta t}\right) \right|^2 \left| \hat{s}\left(f - \frac{k}{\Delta t}\right) \right|^2 \right) df \tag{5.29}$$

$$= \int_{-1/(2\Delta t)}^{1/(2\Delta t)} \sum_{k=-\infty}^{\infty} \log_2 \left(1 + \frac{1}{N_0/2} \frac{\sigma_a^2}{\Delta t} \left| \mathsf{S}_\xi(f) \right|^2 \left| \hat{s}\left(f - \frac{k}{\Delta t}\right) \right|^2 \right) df \tag{5.30}$$

$$\ge \int_{-1/(2\Delta t)}^{1/(2\Delta t)} \log_2 \left(1 + \frac{1}{N_0/2} \frac{\sigma_a^2}{\Delta t} \left| \mathsf{S}_\xi(f) \right|^2 \sum_{k=-\infty}^{\infty} \left| \hat{s}\left(f - \frac{k}{\Delta t}\right) \right|^2 \right) df \tag{5.31}$$

$$= \int_{-1/(2\Delta t)}^{1/(2\Delta t)} \log_2 \left(1 + \frac{1}{N_0/2} \frac{\sigma_a^2}{\Delta t} \left| \mathsf{S}_\xi(f) \right|^2 \hat{s}_{folded}(f) \right) df , \tag{5.32}$$

where (5.27) is due to $\mathsf{S}_x(f) = \sigma_a^2 (\Delta t)^{-1} \left| \mathsf{S}_\xi(f) \hat{s}(f) \right|^2$, (5.28) is due to the linearity of integral, (5.29) is due to the substitution of variable ($f' = f - k/\Delta t$), (5.30) is due to the periodicity of the precoding spectrum $\mathsf{S}_\xi(f)$ with the period $1/\Delta t$, (5.31) is by using the inequality $\sum_{k=-\infty}^{\infty} \log(1 + x_k) \ge \log\left(1 + \sum_{k=-\infty}^{\infty} x_k\right)$ for $x_k \ge 0$ for all k, and (5.32) is due to the definition of $\hat{s}_{folded}(f)$. Finally, comparing with Theorem 5.1, we obtain the desired result. This completes the proof of Theorem 5.2. ■

Theorem 5.2 states that, regardless of the choice of the convolutional precoding coefficients, the information rate of the convolutionally precoded FTN system is limited by the generalized Shannon capacity formula. This further implies that there exist Nyquist rate systems with appropriate waterfilling that can also achieve the same capacity. Consequently, the FTN capacity benefits due to convolutional precoding can be mainly attributed to inducing a modified transmission PSD $\mathsf{S}_x(f) = \sigma_a^2 (\Delta t)^{-1} \left| \mathsf{S}_\xi(f) \hat{s}(f) \right|^2$. These three observations give a global perspective on the merits of using convolutional precoding for FTN transmission.

Before closing the subsection, as an auxiliary result we present and prove the capacity of *non-precoded* FTN signaling, i.e., when the modulating symbols $\{x[n]\}$ are all *i.i.d.*, originally stated as Theorem 4.1.

Corollary 5.1 (non-precoded i.i.d. FTN capacity [127]): *Let the modulation symbols* $\{x[n]\}$ *be chosen i.i.d. Then the capacity of the i.i.d. FTN signaling in AWGN channel becomes*

$$C_{i.i.d.}^{FTN} = \int_{-1/(2\Delta t)}^{1/(2\Delta t)} \log_2 \left(1 + P/(N_0/2) \cdot \hat{s}_{folded}(f)\right) df \,. \tag{5.33}$$

***Proof*:** The lack of precoding leads to the precoding matrix $L = I_{KN}$, the precoding spectrum $\mathsf{S}_\xi(f) = 1$, and the FTN modulation symbol vector $\mathbf{x} = \mathbf{a}$. Also, the covariance matrix of $\mathbf{x}$ becomes $K_x = \sigma_a^2 L L^\dagger = \sigma_a^2 I_{KN}$. Then, by the transmission power constraint $(NT)^{-1} tr\left(K_x H\right) \le P$ from Proposition 3.3, we get the variance of the information sequence $\sigma_a^2 = E\{|x[n]|^2\} = P\Delta t$. Substituting these to Theorem 5.1 and with jointly Gaussian distributed $\mathbf{x}$, we get the desired result. This completes the proof. ■

5.1.3 Convolutional FTN Precoding in LTI Channels

The purpose of this subsection is to extend the information rate analysis of the convolutionally precoded FTN in AWGN channel in subsection 5.1.2 to linear time-invariant (LTI) channel as shown in Figure 5.1.

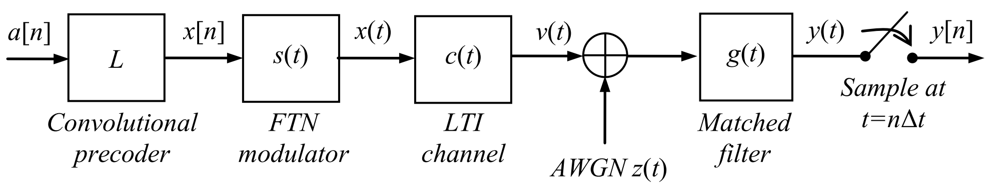

Figure 5.1 Block diagram of the considered convolutionally precoded FTN signaling in LTI channel

Recall that the corresponding discrete-time channel model, developed in section 3.1, is

$$\mathbf{y} = \alpha \tilde{H}\mathbf{x} + \mathbf{z}, \tag{5.34}$$

where

$$\alpha \equiv s(t) * c(t) * g(t)\big|_{t=0}, \tag{5.35}$$

$$\tilde{H} \equiv \begin{bmatrix} 1 & \tilde{h}_{-1} & \tilde{h}_{-2} & \cdots & \tilde{h}_{-(KN-1)} \\ \tilde{h}_{1} & 1 & \tilde{h}_{-1} & \cdots & \tilde{h}_{-(KN-2)} \\ \tilde{h}_{2} & \tilde{h}_{1} & 1 & \cdots & \tilde{h}_{-(KN-3)} \\ \vdots & \vdots & \vdots & \ddots & \vdots \\ \tilde{h}_{KN-1} & \tilde{h}_{KN-2} & \tilde{h}_{KN-3} & \cdots & 1 \end{bmatrix}, \tag{5.36}$$

$$\tilde{h}_k \equiv \alpha^{-1}\, s(t) * c(t) * g(t)\big|_{t=k\Delta t}. \tag{5.37}$$

Note that $\tilde{H}$ is a Toeplitz matrix (not necessarily Hermitian), which represents collective ISI due to the FTN signaling *and* LTI channel response $c(t)$. Furthermore, recall the definitions of the *precoding spectrum* $\mathsf{S}_{\xi}(f) \equiv \sum_n \xi_n e^{+j2\pi f n\Delta t}$ from (5.4) and the *folded-pulse spectrum* $\hat{s}_{folded}(f) \equiv \sum_k \left|\hat{s}(f - k/\Delta t)\right|^2$ from (5.5), where $\{\xi_k\}$ is a set of convolutional precoding coefficients and $\hat{s}(f)$ denotes the Fourier transform of the modulating pulse $s(t)$. In addition, define *folded-receiver spectrum* $\hat{g}_{folded}(f)$ and *folded-pulse-channel-receiver spectrum* $\hat{h}_{folded}(f)$ in a similar fashion as:

$$\hat{g}_{folded}(f) \equiv \sum_{k=-\infty}^{\infty} \left|\hat{g}(f-k/\Delta t)\right|^2 \text{ for } f \in \left(-\frac{1}{2\Delta t}, \frac{1}{2\Delta t}\right), \tag{5.38}$$

$$\hat{h}_{folded}(f) \equiv \sum_{k=-\infty}^{\infty} \hat{s}(f-k/\Delta t)\hat{c}(f-k/\Delta t)\hat{g}(f-k/\Delta t) \text{ for } f \in \left(-\frac{1}{2\Delta t}, \frac{1}{2\Delta t}\right), \tag{5.39}$$

where $\hat{g}(f)$ and $\hat{c}(f)$ denote the Fourier transforms of the receiver matched filter response $g(t)$ and LTI channel impulse response $c(t)$, respectively[27].

With the above definitions, we derive the following theorem about information rate of the convolutionally precoded FTN on a LTI channel:

Theorem 5.3 (Information rate of convolutionally precoded FTN in LTI channel): *Consider the convolutionally precoded FTN modulation symbols* $\mathbf{x} = L\mathbf{a}$ *with precoding spectrum* $\mathsf{S}_\xi(f)$ *defined in (5.4), where* $\mathbf{a}$ *is the i.i.d. information symbol vector with a variance* σ_a^2 *and L is a Toeplitz precoding matrix defined in (5.2). If LTI channel spectrum and the folded-pulse-channel-receiver spectrum are finite, i.e.,* $|\hat{c}(f)| < \infty$ *and* $\hat{h}_{folded}(f) < \infty$ *for all real frequencies f, and if the receiver matched filter response satisfies* $|\hat{g}_{folded}(f)| > 0$ *for* $f \in (-1/(2\Delta t),\ 1/(2\Delta t))$*, then the information rate of the convolutionally precoded FTN signaling in LTI channel is upperbounded by*

$$\bar{C}^{FTN}_{conv\text{-}precoded} \le \int_{-1/(2\Delta t)}^{1/(2\Delta t)} \log_2\left(1+\frac{1}{N_0/2}\frac{\sigma_a^2}{\Delta t}\left|\mathsf{S}_\xi(f)\right|^2 \frac{\left|\hat{h}_{folded}(f)\right|^2}{\hat{g}_{folded}(f)}\right) df \ \ \textit{bits per second,} \tag{5.40}$$

with equality if the convolutionally precoded modulation vector $\mathbf{x}$ *is jointly Gaussian distributed.*

[27] It is interesting to note that note that $\hat{g}_{folded}(f)$ is absolutely integrable if $g(t)$ is a finite energy signal, since $\int_{-1/(2\Delta t)}^{1/(2\Delta t)} \left|\hat{g}_{folded}(f)\right| df = \sum_{k=-\infty}^{\infty}\int_{-1/(2\Delta t)-k/\Delta t}^{1/(2\Delta t)-k/\Delta t} \left|\hat{g}(f)\right|^2 df = \int_{-\infty}^{\infty}\left|\hat{g}(f)\right|^2 df < \infty$. Similarily, $\hat{h}_{folded}(f)$ is also absolutely integrable if $s(t)$ and $g(t)$ are both finite energy signals *and* $|\hat{c}(f)| < \infty$ (which is satisfied for most practical channels of interest). This can be proved by the similar procedure as above and by using the Hölder's inequality.

Proof: Please see subsection 5.1.5 for the proof of this theorem. ■

Theorem 5.3 successfully extends the FTN information rate in AWGN channel in Theorem 5.1 to LTI channels. Comparing to the AWGN channel where the information rate depends on the folded-pulse spectrum $\hat{s}_{folded}(f)$, the information rate expression (5.40) in LTI channel now depends on the ratio $\left|\hat{h}_{folded}(f)\right|^2 / \hat{g}_{folded}(f)$, which takes into account of the modulating pulse response $s(t)$, channel impulse response $c(t)$, and the receiver matched filter response $g(t)$.

We now find the structure of the optimal convolutional precoder that maximizes the information rate (5.40) in an LTI channel. The optimal precoding strategy is shown to have the 'water-filling' or 'water-pouring' [31] interpretation, which is known to be the capacity-achieving strategy in traditional ISI channels, correlated noise channels, correlated MIMO channels, etc., but is shown here for the first time to be capacity-achieving for the convolutionally precoded FTN channels.

Theorem 5.4 (Power water-filling in convolutional precoded FTN signaling): *The information rate of the convolutionally precoded FTN signaling in LTI channel, subject to the average transmission power constraint*

$$\int_{-\infty}^{\infty} \mathsf{S}_x(f)df \le P, \tag{5.41}$$

is maximized by the water-filling strategy:

$$\sup_{\mathsf{S}_\xi(f)} \overline{C}_{conv\text{-}precoded}^{FTN} = \int_{-1/(2\Delta t)}^{1/(2\Delta t)} \log_2\left(\max\left(\mu \frac{2}{N_0}\frac{\left|\hat{h}_{folded}(f)\right|^2}{\hat{s}_{folded}(f)\hat{g}_{folded}(f)},1\right)\right)df, \tag{5.42}$$

where the water-filling parameter μ is chosen such that

$$\int_{-1/(2\Delta t)}^{1/(2\Delta t)} \max\left(\mu - \frac{N_0}{2}\frac{\hat{s}_{folded}(f)\hat{g}_{folded}(f)}{\left|\hat{h}_{folded}(f)\right|^2},0\right)df = P. \tag{5.43}$$

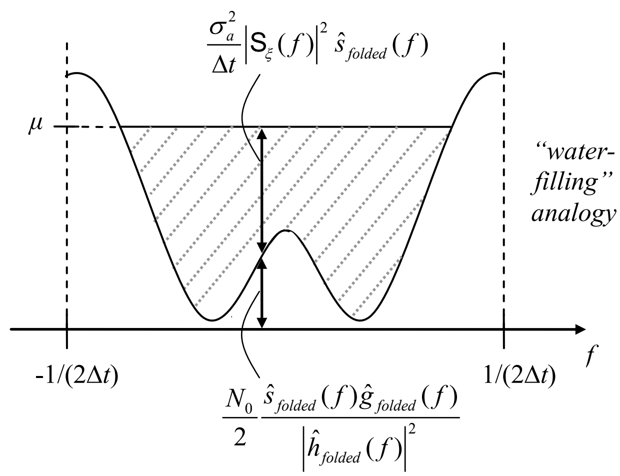

Figure 5.2 Illustrating power water-filling in frequency domain for the convolutionally precoded FTN in LTI channel under the average transmission power constraint

Proof Theorem 5.4: Recall that for convolutionally precoded FTN signal $x(t)$, its power spectral density has the form $\mathsf{S}_x(f)=(\Delta t)^{-1}\sigma_a^2\left|\mathsf{S}_\xi(f)\hat{s}(f)\right|^2$. First write the power constraint (5.41) as:

$$\int_{-\infty}^{\infty}\mathsf{S}_x(f)df=\int_{-\infty}^{\infty}(\Delta t)^{-1}\sigma_a^2\left|\mathsf{S}_\xi(f)\right|^2\left|\hat{s}(f)\right|^2df \tag{5.44}$$

$$=\sum_{k=-\infty}^{\infty}\int_{-1/(2\Delta t)-k/\Delta t}^{1/(2\Delta t)-k/\Delta t}(\Delta t)^{-1}\sigma_a^2\left|\mathsf{S}_\xi(f)\right|^2\left|\hat{s}(f)\right|^2df \tag{5.45}$$

$$=\sum_{k=-\infty}^{\infty}\int_{-1/(2\Delta t)}^{1/(2\Delta t)}(\Delta t)^{-1}\sigma_a^2\left|\mathsf{S}_\xi(f-k/\Delta t)\right|^2\left|\hat{s}(f-k/\Delta t)\right|^2df \tag{5.46}$$

$$=\sum_{k=-\infty}^{\infty}\int_{-1/2\Delta t}^{1/2\Delta t}(\Delta t)^{-1}\sigma_a^2\left|\mathsf{S}_\xi(f)\right|^2\left|\hat{s}(f-k/\Delta t)\right|^2df \tag{5.47}$$

$$=\int_{-1/2\Delta t}^{1/2\Delta t}(\Delta t)^{-1}\sigma_a^2\left|\mathsf{S}_\xi(f)\right|^2\sum_{k=-\infty}^{\infty}\left|\hat{s}(f-k/\Delta t)\right|^2df \tag{5.48}$$

$$=\int_{-1/2\Delta t}^{1/2\Delta t}(\Delta t)^{-1}\sigma_a^2\left|\mathsf{S}_\xi(f)\right|^2\hat{s}_{folded}(f)df \tag{5.49}$$

$$\le P, \tag{5.50}$$

where (5.45) is due to the linearity of integral, (5.46) is due to a change of variable, (5.47) is due to the periodicity of the precoding spectrum $\mathsf{S}_\xi(f)$ with a period $1/\Delta t$, (5.48) is due to Fubini's theorem, (5.49) is by the definition of $\hat{s}_{folded}(f) \equiv \sum_k \left|\hat{s}(f - k/\Delta t)\right|^2$, and (5.50) is due to the transmission power constraint (5.41).

We now find the optimal precoding spectrum $\mathsf{S}_{\xi}(f) \equiv \sum_n \xi_n e^{+j2\pi f n \Delta t}$ that maximizes the information rate of FTN in (5.40), subject to the power constraint (5.49) and (5.50). We first form a Lagrangian function:

$$\begin{aligned} \mathsf{L}(\left|\mathsf{S}_{\xi}(f)\right|^2) \equiv & \int_{-1/(2\Delta t)}^{1/(2\Delta t)} \log_2 \left(1 + \frac{1}{N_0/2} \frac{\sigma_a^2}{\Delta t} \left|\mathsf{S}_{\xi}(f)\right|^2 \frac{\left|\hat{h}_{folded}(f)\right|^2}{\hat{g}_{folded}(f)} \right) df \\ & - \lambda \left(\frac{\sigma_a^2}{\Delta t} \int_{-1/2\Delta t}^{1/2\Delta t} \left|\mathsf{S}_{\xi}(f)\right|^2 \hat{s}_{folded}(f) df - P \right), \end{aligned} \tag{5.51}$$

where λ, the Lagrange multiplier, is a constant (not a function of f) with an integral constraint. Using the Euler-Lagrange equation of the calculus of variations,

$$0 = \frac{\partial \mathsf{L}}{\partial \left|\mathsf{S}_{\xi}(f)\right|^2} = \frac{1}{\ln 2} \frac{\sigma_a^2 \left(\Delta t \cdot N_0/2\right)^{-1} \left|\hat{h}_{folded}(f)\right|^2 \Big/ \hat{g}_{folded}(f)}{1 + \sigma_a^2 \left(\Delta t \cdot N_0/2\right)^{-1} \left|\mathsf{S}_{\xi}(f)\right|^2 \left|\hat{h}_{folded}(f)\right|^2 \Big/ \hat{g}_{folded}(f)} - \lambda \frac{\sigma_a^2}{\Delta t} \hat{s}_{folded}(f) \tag{5.52}$$

which, after some simplifications and by setting $\mu = 1/(\lambda \cdot \ln 2)$, becomes

$$(\Delta t)^{-1} \sigma_a^2 \left|\mathsf{S}_{\xi}(f)\right|^2 \hat{s}_{folded}(f) = \max\left(\mu - \frac{N_0}{2} \frac{\hat{s}_{folded}(f) \hat{g}_{folded}(f)}{\left|\hat{h}_{folded}(f)\right|^2}, 0 \right), \tag{5.53}$$

where μ is chosen such that the power constraint (5.49) and (5.50) is satisfied. Finally, the desired expression is obtained from substituting (5.53) into (5.40). This completes the proof of Theorem 5.4. ■

Figure 5.2 illustrates the power allocation strategy (5.43) by the water-filling analogy. Note that, once the water-filling parameter μ is determined, the optimal convolutional precoding coefficients $\{\xi_k\}$ can then be determined from (5.53) and by noting that $\{\xi_k\}$ is essentially the set of Fourier series coefficients of $\mathsf{S}_{\xi}(f)$ satisfying

$$\mathsf{S}_{\xi}(f) = \sum_{k=-\infty}^{\infty} \xi_k e^{+j2\pi f k \Delta t} \quad \text{and} \tag{5.54}$$

$$\xi_k = \Delta t \int_{-1/(2\Delta t)}^{1/(2\Delta t)} \mathsf{S}_\xi(f) e^{-j2\pi f k \Delta t} df \,. \tag{5.55}$$

We present below two important special cases when the receiver matched filter with the impulse response $g(t)$ is either matched to the modulating pulse response only, i.e., $g(t) = s^*(-t)$, or matched to the combined response of LTI channel and the modulating pulse, i.e., $g(t) = (s(t) * c(t))^*\big|_{t=-t}$. Note that the latter is the optimal matched filtering in the sense of maximizing the received signal-to-noise ratio (SNR), but the former is also being used in practice where adaptive adjustment of the receiver to varying $c(t)$ is not feasible, such as in rapidly changing channels, or where the receiver is "hardwired" and cannot be adjusted.

First define two special cases of the *folded-pulse-channel-receiver spectrum* $\hat{h}_{folded}(f)$:

$$\hat{h}^{(1)}_{folded}(f) \equiv \sum_{k=-\infty}^{\infty} \left|\hat{s}(f - k/\Delta t)\right|^2 \hat{c}(f - k/\Delta t) \text{ and} \tag{5.56}$$

$$\hat{h}^{(2)}_{folded}(f) \equiv \sum_{k=-\infty}^{\infty} \left|\hat{s}(f - k/\Delta t)\right|^2 \left|\hat{c}(f - k/\Delta t)\right|^2 . \tag{5.57}$$

where (5.56) results when $g(t) = s^*(-t)$ and (5.57) results when $g(t) = (s(t) * c(t))^*\big|_{t=-t}$. The following corollary deals with the case with $g(t) = s^*(-t)$.

Corollary 5.2 (Information rate of convolutionally precoded FTN in LTI channel when receiver matched filter is matched only to the transmit modulating pulse): *Let the receiver filter response matched to the transmit modulating pulse* $g(t) = s^*(-t)$ *and define a special case of the folded-pulse-channel-receiver spectrum* $\hat{h}_{folded}(f)$ *as*

$$\hat{h}^{(1)}_{folded}(f) \equiv \sum_{k=-\infty}^{\infty} \left|\hat{s}(f - k/\Delta t)\right|^2 \hat{c}(f - k/\Delta t) \,. \tag{5.58}$$

If LTI channel spectrum is finite, i.e., $|\hat{c}(f)| < \infty$ *for all frequency range f, then the information rate of the convolutionally precoded FTN signaling in an LTI channel is given by*

$$\bar{C}^{FTN}_{conv\text{-}precoded} \le \int_{-1/(2\Delta t)}^{1/(2\Delta t)} \log_2\left(1 + \frac{1}{N_0/2} \frac{\sigma_a^2}{\Delta t} \left|\mathsf{S}_\xi(f)\right|^2 \frac{\left|\hat{h}^{(1)}_{folded}(f)\right|^2}{\hat{s}_{folded}(f)}\right) df \,, \tag{5.59}$$

with equality if the convolutionally precoded modulation vector **x**=L**a** *is jointly Gaussian distributed.*

Proof: Note that $\hat{g}(f) = \hat{s}^*(f)$ and hence $\hat{g}_{folded}(f) = \sum_k \left|\hat{s}(f - k/\Delta t)\right|^2 = \hat{s}_{folded}(f)$. Also, $\hat{h}_{folded}(f) = \sum_{k=-\infty}^{\infty} \left|\hat{s}(f - k/\Delta t)\right|^2 \hat{c}(f - k/\Delta t) = \hat{h}^{(1)}_{folded}(f)$. Substituting $\hat{g}_{folded}(f) = \hat{s}_{folded}(f)$ and $\hat{h}_{folded}(f) = \hat{h}^{(1)}_{folded}(f)$ into Theorem 5.3 yields the expression (5.59).

Furthermore, note that (5.59) is well defined even when the folded-pulse spectrum $\hat{s}_{folded}(f) = 0$ for some $f \in (-1/(2\Delta t), 1/(2\Delta t))$. This is because the ratio $\left|\hat{h}^{(1)}_{folded}(f)\right| / \hat{s}_{folded}(f)$ is always well defined as shown below:

$$\frac{\left|\hat{h}^{(1)}_{folded}(f)\right|}{\hat{s}_{folded}(f)} \leq \frac{\sum_{k=-\infty}^{\infty} \left|\hat{s}(f - k/\Delta t)\right|^2 \left|\hat{c}(f - k/\Delta t)\right|}{\hat{s}_{folded}(f)} \tag{5.60}$$

$$\leq \frac{\left(\max_f \left|\hat{c}(f)\right|\right) \sum_{k=-\infty}^{\infty} \left|\hat{s}(f - k/\Delta t)\right|^2}{\hat{s}_{folded}(f)} \tag{5.61}$$

$$= \max_f \left|\hat{c}(f)\right| \tag{5.62}$$

$$< \infty, \tag{5.63}$$

where (5.61) is due to $\left|\hat{c}(f - k/\Delta t)\right| \leq \max_f \left|\hat{c}(f)\right|$ and (5.62) is by the definition of $\hat{s}_{folded}(f)$. Finally, (5.63) follows from the assumption $|\hat{c}(f)| < \infty$, which holds for most practical channels of interest. This completes the proof of Corollary 5.2. ■

Next corollary deals with the case with $g(t) = (s(t) * c(t))^*\big|_{t=-t}$.

Corollary 5.3 (Information rate of convolutionally precoded FTN in LTI channel when receiver matched filter is matched to the transmitter and the channel): *Let the receiver filter response matched to the modulating pulse and the channel response* $g(t) = (s(t) * c(t))^*\big|_{t=-t}$. *If LTI channel spectrum is finite,* $|\hat{c}(f)| < \infty$ *for all frequency range* f*, the information rate of the convolutionally precoded FTN signaling in LTI channel is given by*

$$\overline{C}^{FTN}_{conv\text{-}precoded} \le \int_{-1/(2\Delta t)}^{1/(2\Delta t)} \log_2\left(1+\frac{1}{N_0/2}\frac{\sigma_a^2}{\Delta t}\left|\mathsf{S}_{\xi}(f)\right|^2 \hat{h}^{(2)}_{folded}(f)\right)df\,, \tag{5.64}$$

with equality if the modulation symbols $\{x[n]\}$ *are jointly Gaussian distributed.*

Proof: Note that the Fourier transform of $g(t)$ can be evaluated as $\hat{g}(f) = \hat{s}^*(f)\hat{c}^*(f)$ using the convolution property of the Fourier transform. Hence the folded-receiver spectrum becomes $\hat{g}_{folded}(f) = \sum_{k=-\infty}^{\infty}\left|\hat{s}(f-k/\Delta t)\right|^2\left|\hat{c}(f-k/\Delta t)\right|^2 = \hat{h}^{(2)}_{folded}(f)$. Similarly, the folded-pulse-channel-receiver spectrum becomes $\hat{h}_{folded}(f) = \sum_{k=-\infty}^{\infty}\left|\hat{s}(f-k/\Delta t)\right|^2\left|\hat{c}(f-k/\Delta t)\right|^2$ $= \hat{h}^{(2)}_{folded}(f)$. Substituting $\hat{g}_{folded}(f) = \hat{h}^{(2)}_{folded}(f)$ and $\hat{h}_{folded}(f) = \hat{h}^{(2)}_{folded}(f)$ into Theorem 5.3 yields the desired result. This completes the proof of Corollary 5.3. ■

5.1.4 Numerical Results on Convolutionally Precoded FTN

Figure 5.3 compares the information rates of the convolutionally precoded FTN using the water-filling strategy (5.42) and the non-precoded FTN using the *i.i.d.* modulation symbols, when

- FTN modulating pulse $s(t) = 1$ for $t \in [0, 1]$ and 0 elsewhere (the rectangular pulse),
- LTI channel response $c(t) = e^{-t}u(t)$ (modeling a simple RC low-pass filter response), where $u(t)$ is the step function, and
- receiver matched filter response $g(t) = s^*(-t)$ (receiver matched to the transmit modulating pulse only).

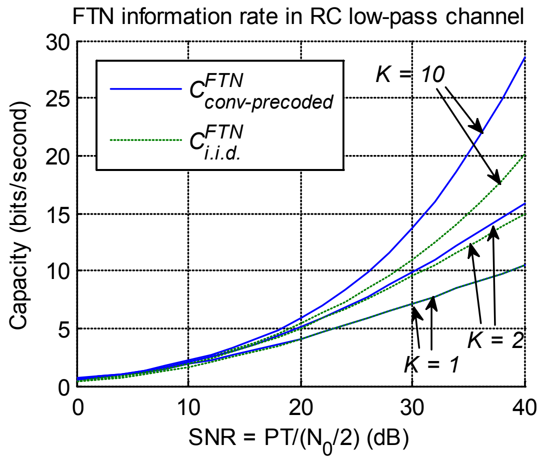

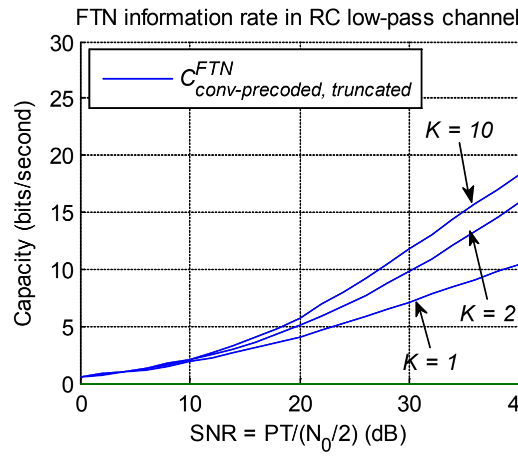

Figure 5.3 FTN information rates in RC low-pass channel with different signaling rates $1/\Delta t = K/T$, using convolutional precoding (waterfilling) (solid) and *i.i.d.* (dashed); Right plot shows the FTN capacity when the power water-filling is restricted to only over a truncated frequency range of [−1, 1] Hertz

Note from the left plot of Figure 5.3 that FTN signaling (K>1) clearly outperforms the conventional Nyquist rate signaling (K=1). In addition, the convolutional precoded FTN signaling with water-filling strategy is clearly better than the *i.i.d.* FTN signaling. As discussed previously, the FTN capacity gain from convolutional precoding is due to reshaping of the transmit signal's PSD to yield ideal near-flat channel spectrum. This approach, however, can also lead to a spectral expansion if the water-filling extends to the outside of the designated channel bandwidth as discussed in section 3.4. If we restrict the water-filling to the main-lobe width of the pulse spectrum $\hat{s}(f)$ (i.e., by truncating the integration limits in (5.42) and (5.43) to only $f \in [-1, 1]$), the FTN information rates are as shown in the right plot of Figure 5.3. Comparing with the left plot, the capacity gains from the FTN signaling are clearly reduced, but still about two-fold gains are possible at 40dB compared to the Nyquist case.

We now investigate the impact of the receiver matched filter response $g(t)$ on the FTN information rates. Figure 5.4 plots the information rates of convolutionally precoded FTN signaling when the utilized receiver matched filter is either matched to the FTN modulating pulse only, i.e., $g(t) = s^*(-t)$, or matched to combined response of LTI channel and the FTN modulating pulse, i.e., $g(t) = (s(t) * c(t))^*\big|_{t=-t}$. We can observe from the figure that there exists non-zero capacity benefit in using the channel-matched filter receiver $g(t)$ $= (s(t) * c(t))^*\big|_{t=-t}$, and this receiver should be used if accurate estimation of the channel response $c(t)$ is possible. In the cases when the channel exhibits rapid variations in time (such as the wireless fading channel) and the adaptive adjustment of the receiver to varying $c(t)$ is not feasible, however, the pulse-matched filter receiver $g(t) = s^*(-t)$ must be used and this will incur a small capacity penalty as seen in Figure 5.4.

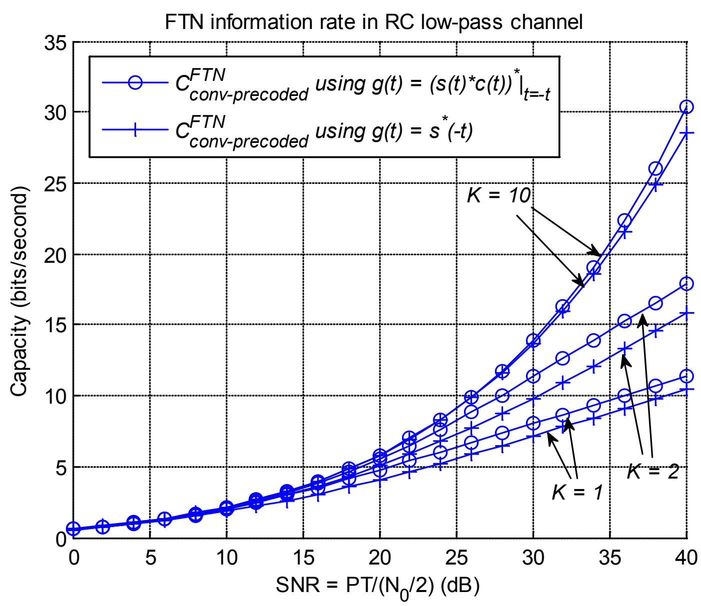

Figure 5.4 Comparing the information rates of convolutionally precoded FTN when the receiver matched filter is matched to the FTN modulating pulse only or to the combined response of LTI channel and the FTN modulating pulse

In Figure 5.5, we consider root-raised cosine pulse $s(t)$ with the roll-off factor $\beta = 0.22$ (used in e.g., WCDMA standard):

- $s(t) = \dfrac{4\beta}{\pi\sqrt{T}} \dfrac{\cos\left((1+\beta)\pi t/T\right) + \left(\sin\left((1-\beta)\pi t/T\right)\right)\big/\left(4\beta t/T\right)}{1-\left(4\beta t/T\right)^2}$ with $T = 1$ μs,

when communicating over a fixed two-path fading channel and using matched filter receiver that is matched only to the modulation pulse:

- $c(t) = \delta(t) + \alpha\cdot\delta(t-\tau)$ (modeling a realization of two-path fading channel), where $\alpha = 0.5$, $\tau = 3.3$ μs, and
- $g(t) = s^*(-t)$ (receiver matched to modulating pulse only).

As can be seen from Figure 5.5, convolutional precoding on FTN signals again improve the capacity when compared to the *i.i.d.* FTN case. This implies that convolutional precoding is beneficial due to its ability to waterfill on the FTN channel spectrum. On the other hand, the capacity gains from increasing the signaling rates beyond the Nyquist rate are only marginal (i.e., no notable differences observed between K=2 and K>2 cases). This is because the root-raised cosine pulse $s(t)$ is strictly band-limited and hence there is little excess bandwidth available for the FTN signaling to utilize by reshaping the transmission PSD.

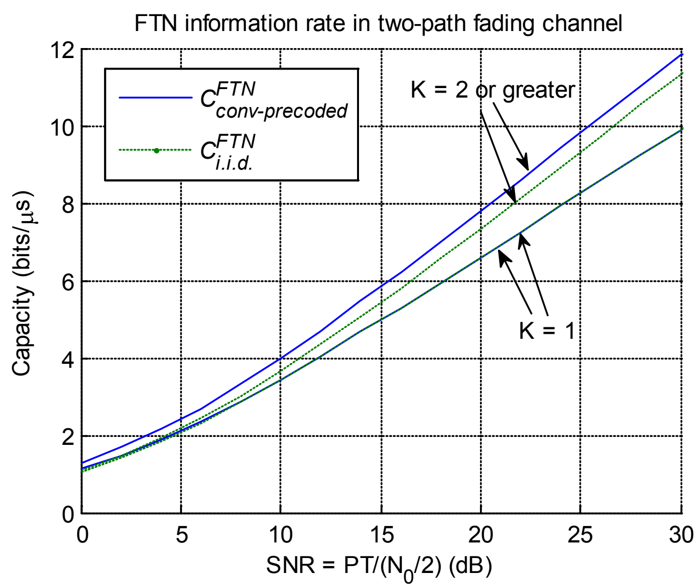

Figure 5.5 FTN information rates in a realization of two-way fading channel using a root-raised cosine modulating pulse *s*(*t*)

5.1.5 Proof of Theorem 5.3

The objective of this subsection is to provide a proof of Theorem 5.3 which gives the information rate of the convolutionally precoded FTN in LTI channel in subsections 5.1.3. The corresponding channel model is reproduced below for convenience:

$$\mathbf{y} = \alpha \tilde{H}\mathbf{x} + \mathbf{z}, \tag{5.65}$$

subject to the FTN transmission power constraint from Corollary 3.1:

$$\frac{1}{NT} tr\left(U^{\dagger} H^{1/2} K_x H^{1/2} U\right) \le P \tag{5.66}$$

for some unitary matrix U and covariance matrix of modulation symbols K_x. Other relevant definitions are also reproduced below for convenience (see section 3.1 for details):

- Normalization factor: $\alpha \equiv s(t) * c(t) * g(t)\big|_{t=0}$, (5.67)

- FTN matrix for LTI channel: $\tilde{H} \equiv \begin{bmatrix} 1 & \tilde{h}_{-1} & \cdots & \tilde{h}_{-(KN-1)} \\ \tilde{h}_1 & 1 & \cdots & \tilde{h}_{-(KN-2)} \\ \vdots & \vdots & \ddots & \vdots \\ \tilde{h}_{KN-1} & \tilde{h}_{KN-2} & \cdots & 1 \end{bmatrix}$, (5.68)

  with the ISI coefficients: $\tilde{h}_k \equiv \alpha^{-1} s(t) * c(t) * g(t)\big|_{t=k\Delta t}$, (5.69)

- Noise covariance matrix: $E\{\mathbf{z}\mathbf{z}^{\dagger}\} = \frac{N_0}{2}\left\|g\left(t\right)\right\|^2 \varPhi$, (5.70)

- Receiver filter correlation matrix: $\varPhi \equiv \begin{bmatrix} 1 & \varphi_{-1} & \cdots & \varphi_{-(KN-1)} \\ \varphi_1 & 1 & \cdots & \varphi_{-(KN-2)} \\ \vdots & \vdots & \ddots & \vdots \\ \varphi_{KN-1} & \varphi_{KN-2} & \cdots & 1 \end{bmatrix}$, (5.71)

  with the receiver filter correlations: $\varphi_k \equiv \left\|g\left(t\right)\right\|^{-2} \int_{-\infty}^{+\infty} g\left(\tau\right) g^{*}\left(\tau - k\Delta t\right) d\tau$. (5.72)

First consider the following two lemmas:

Lemma 5.1 (Upperbound on Mutual Information of FTN in LTI Channel): *If the FTN modulation vector* **x** *has a covariance matrix* K_x, *then the mutual information of FTN signaling in LTI channel can be upperbounded by:*

$$I(\mathbf{x};\mathbf{y}) \le \log_2\left(\det\left(I_{KN} + \frac{|\alpha|^2}{(N_0/2)\|g(t)\|^2}\Phi^{-1/2}\tilde{H}K_x\tilde{H}^{\dagger}\Phi^{-1/2}\right)\right), \tag{5.73}$$

where the upperbound is achieved if **x** *is circularly symmetric Gaussian distributed.*

Proof: Rewrite mutual information between **x** and $\mathbf{y} = \alpha\tilde{H}\mathbf{x} + \mathbf{z}$ as:

$$I(\mathbf{x};\mathbf{y}) = h(\mathbf{y}) - h(\mathbf{y}|\mathbf{x}) \tag{5.74}$$

$$= h(\mathbf{y}) - h(\mathbf{z}) \tag{5.75}$$

$$= h(\mathbf{y}) - \log_2\left((\pi e)^{KN}\det\left(\frac{N_0}{2}\|g(t)\|^2\Phi\right)\right) \tag{5.76}$$

$$\le \log_2\left((\pi e)^{KN}\det(K_y)\right) - \log_2\left((\pi e)^{KN}\det\left(\frac{N_0}{2}\|g(t)\|^2\Phi\right)\right) \tag{5.77}$$

$$= \log_2\left(\frac{\det\left(|\alpha|^2\tilde{H}K_x\tilde{H}^{\dagger} + (N_0/2)\|g(t)\|^2\Phi\right)}{\det\left((N_0/2)\|g(t)\|^2\Phi\right)}\right), \tag{5.78}$$

where $h(\cdot)$ denotes the differential entropy, (5.75) is due to $\alpha\tilde{H}\mathbf{x}$ being deterministic given **x**, followed by the translation invariance of the differential entropy (Lemma 2.5), (5.76) is due to the known differential entropy function of Gaussian vector **z** (Lemma 2.3), and (5.77) is due to upper-bounding the differential entropy by choosing **y** circularly symmetric complex Gaussian distributed with covariance matrix K_y (Lemma 2.4). Moreover, (5.78) is due to the covariance matrix of **y** being equal to $K_y = |\alpha|^2\tilde{H}K_x\tilde{H}^{\dagger} + (N_0/2)\|g(t)\|^2\Phi$. Note that the upperbound in (5.77) is achieved if and only if **y** is circularly symmetric complex Gaussian, which can be obtained when **x** is chosen circularly symmetric complex Gaussian with the covariance matrix K_x.

Due to Proposition 3.1, the receiver filter correlation matrix Φ is Hermitian and invertible, and hence it can be decomposed into $\Phi = \Phi^{1/2}\Phi^{1/2}$, where $\Phi^{1/2}$ is symmetric positive definite. Therefore, (5.78) can be further simplified as follows:

$$I(\mathbf{y};\mathbf{x}) \le \log_2\left(\frac{\det\left(|\alpha|^2 \tilde{H}K_x\tilde{H}^\dagger + (N_0/2)\|g(t)\|^2 \Phi\right)}{(N_0/2)^{KN}\|g(t)\|^{2KN}\det\left(\Phi^{1/2}\right)\det\left(\Phi^{1/2}\right)}\right) \tag{5.79}$$

$$= \log_2\left(\det\left(\Phi^{-1/2}\right)\det\left(\frac{|\alpha|^2}{(N_0/2)\|g(t)\|^2}\tilde{H}K_x\tilde{H}^\dagger + \Phi\right)\det\left(\Phi^{-1/2}\right)\right) \tag{5.80}$$

$$= \log_2\left(\det\left(I_{KN} + \frac{|\alpha|^2}{(N_0/2)\|g(t)\|^2}\Phi^{-1/2}\tilde{H}K_x\tilde{H}^\dagger\Phi^{-1/2}\right)\right), \tag{5.81}$$

where (5.79) and (5.81) are due to det(AB) = det(A)det(B), and (5.80) is due to 1/det(A) = det(A^{-1}) for an invertible matrix A. Note that I_{KN} denotes $KN\times KN$ identity matrix. This completes the proof of Lemma 5.1. ■

Lemma 5.2 (Inverse Fourier series of ISI coefficients and receiver filter correlations): *Denote the inverse Fourier series of the ISI coefficients $\tilde{h}_k$ and the receiver filter correlations φ_k by $\tilde{h}(\lambda) \equiv \sum_{k=-\infty}^{\infty}\tilde{h}_k e^{jk\lambda}$ and $\varphi(\lambda) \equiv \sum_{k=-\infty}^{\infty}\varphi_k e^{jk\lambda}$, respectively. When $\lambda = -2\pi f \Delta t$, these inverse Fourier series can be written as*

$$\tilde{h}(-2\pi f \Delta t) = \alpha^{-1}(\Delta t)^{-1}\hat{h}_{folded}(f), \tag{5.82}$$

$$\varphi(-2\pi f \Delta t) = \|g(t)\|^{-2}(\Delta t)^{-1}\hat{g}_{folded}(f), \tag{5.83}$$

where the folded-pulse-channel-receiver spectrum is defined as $\hat{h}_{folded}(f) \equiv \sum_k \hat{s}(f-k/\Delta t)\hat{c}(f-k/\Delta t)\hat{g}(f-k/\Delta t)$ that is assumed to be finite for all f, and the folded-receiver spectrum is defined as $\hat{g}_{folded}(f) \equiv \sum_k |\hat{g}(f-k/\Delta t)|^2$.

Proof: The term $\tilde{h}(-2\pi f\Delta t)$ can be simplified as follows:

$$\tilde{h}(-2\pi f \Delta t) = \alpha^{-1}\sum_{k=-\infty}^{\infty}\left(\int_{-\infty}^{\infty}\int_{-\infty}^{\infty} s(\tau)g(\lambda-\tau)c(k\Delta t-\lambda)d\tau d\lambda\right)e^{-j2\pi fk\Delta t} \tag{5.84}$$

$$= \alpha^{-1} \sum_{k=-\infty}^{\infty} \left(\int_{-\infty}^{\infty} \hat{s}(\lambda)\hat{g}(\lambda)\hat{c}(\lambda) e^{j2\pi\lambda k\Delta t} d\lambda \right) e^{-j2\pi f k\Delta t} \tag{5.85}$$

$$= \alpha^{-1} \int_{-\infty}^{\infty} \hat{s}(\lambda)\hat{g}(\lambda)\hat{c}(\lambda) \sum_{k=-\infty}^{\infty} e^{j2\pi(\lambda-f)k\Delta t} d\lambda \tag{5.86}$$

$$= \alpha^{-1} \int_{-\infty}^{\infty} \hat{s}(\lambda)\hat{g}(\lambda)\hat{c}(\lambda) \sum_{k=-\infty}^{\infty} \delta\left(\Delta t(\lambda - f) + k\right) d\lambda \tag{5.87}$$

$$= \alpha^{-1} (\Delta t)^{-1} \sum_{k=-\infty}^{\infty} \hat{s}(f - k/\Delta t)\hat{g}(f - k/\Delta t)\hat{c}(f - k/\Delta t), \tag{5.88}$$

where (5.85) is due to the generalized Parseval's theorem $\int_{-\infty}^{\infty} a(t) b^*(t) dt = \int_{-\infty}^{\infty} \hat{a}(f)\hat{b}^*(f) df$ and the delay property of the Fourier transform, (5.86) and (5.88) are due to the Fubini's theorem [28], and (5.87) is due to the Poisson summation formula $\sum_{k=-\infty}^{\infty} e^{jk2\pi t} = \sum_{k=-\infty}^{\infty} \delta(t+k)$. Similarly, the term $\varphi(-2\pi f\Delta t)$ may be written as

$$\varphi(-2\pi f \Delta t) = \left\| g\left(t\right) \right\|^{-2} (\Delta t)^{-1} \sum_{k=-\infty}^{\infty} \left| \hat{g}(f - k/\Delta t) \right|^2 . \tag{5.89}$$

This completes the proof of Lemma 5.2. ■

We are now ready to prove Theorem 5.3 on the information rate of the convolutionally precoded FTN signaling in LTI channel.

Proof of Theorem 5.3 (*information rate of convolutionally precoded FTN in LTI channel*): When the FTN modulation symbol vector $\mathbf{x}$ is convolutionally precoded, i.e., $\mathbf{x} = L\mathbf{a}$, the covariance matrix K_x can be expressed as $K_x = \sigma_a^2 L L^\dagger$, where σ_a^2 is the variance of the *i.i.d.* information sequence $\{a[n]\}$ and L is the *Toeplitz* precoding matrix defined by (5.2). Due to Lemma 5.1, the information rate of the convolutionally precoded FTN signaling can be written as:

[28] To use the Fubini's theorem, we go backwards from (5.88) to (5.86), establishing equalities throughout. First note that (5.88) is by definition equal to $\alpha^{-1}(\Delta t)^{-1} \hat{h}_{folded}(f)$, which was assumed to be finite for all f. Since (5.88) is finite, Fubini's theorem can be applied to obtain (5.87) (by interchanging the order of the integral and the sum), and from (5.87) we can re-apply Fubini to get (5.86).

$$\overline{C}^{FTN}_{conv\text{-}precoded} \le \lim_{N\to\infty}\frac{1}{NT}\log_2\left(\det\left(I_{KN}+\frac{|\alpha|^2}{(N_0/2)\|g(t)\|^2}\Phi^{-1/2}\tilde{H}K_x\tilde{H}^{\dagger}\Phi^{-1/2}\right)\right) \tag{5.90}$$

$$= \lim_{N\to\infty}\frac{1}{NT}\log_2\left(\det\left(I_{KN}+\frac{\sigma_a^2|\alpha|^2}{(N_0/2)\|g(t)\|^2}\Phi^{-1/2}\tilde{H}LL^{\dagger}\tilde{H}^{\dagger}\Phi^{-1/2}\right)\right) \tag{5.91}$$

$$= \lim_{N\to\infty}\frac{1}{NT}\log_2\left(\det\left(I_{KN}+\frac{\sigma_a^2|\alpha|^2}{(N_0/2)\|g(t)\|^2}L^{\dagger}\tilde{H}^{\dagger}\Phi^{-1}\tilde{H}L\right)\right) \tag{5.92}$$

$$= \lim_{N\to\infty}\frac{1}{NT}\sum_{j=0}^{KN-1}\log_2\left(1+\frac{\sigma_a^2|\alpha|^2}{(N_0/2)\|g(t)\|^2}\lambda_j\left\{L^{\dagger}\tilde{H}^{\dagger}\Phi^{-1}\tilde{H}L\right\}\right) \tag{5.93}$$

where (5.90) is due to Lemma 5.1 which becomes equality if **x** is circularly symmetric complex Gaussian distributed with a covariance matrix K_x, (5.91) is due to $K_x=\sigma_a^2LL^{\dagger}$, and (5.92) is due to logdet(AB+I) = logdet(BA+I). Moreover, denoting $\lambda_j\{A\}$ by the j-th eigenvalue of the matrix A, (5.93) follows from the identities: $\det(A)=\prod_j\lambda_j\{A\}$ and $\lambda_j\{I+A\}=1+\lambda_j\{A\}$ for any Hermitian matrix A [55].

We note that Φ^{-1} is not Toeplitz (since inverse of a Toeplitz matrix is not Toeplitz in general) and $\tilde{H}$ is not Hermitian in general by its definition. Therefore, we cannot directly apply Szegö's theorem to (5.93) as we did in the proof of Theorem 5.1. We note, however, that inverse of a Toeplitz matrix is Toeplitz *asymptotically* as $N\to\infty$ [56]. Furthermore, Φ^{-1} is Hermitian since Φ is Hermitian and by $(\Phi^{-1})^{\dagger}=(\Phi^{\dagger})^{-1}$. In addition, a product of Toeplitz matrices is asymptotically Toeplitz [56]. Hence, the *matrix product*, $L^{\dagger}\tilde{H}^{\dagger}\Phi^{-1}\tilde{H}L$, is asymptotically Hermitian Toeplitz and is asymptotically equivalent to an another Toeplitz matrix $T_n(\cdot)$ by the generalized version of Szegö's theorem in Theorem D.2.

By applying Theorem D.2 to the matrix product $L^{\dagger}\tilde{H}^{\dagger}\Phi^{-1}\tilde{H}L$, (5.93) converges in the limit to

$$\overline{C}^{FTN}_{conv\text{-}precoded} \le \frac{1}{2\pi\Delta t}\int_{-\pi}^{\pi}\log_2\left(1+\frac{\sigma_a^2|\alpha|^2}{(N_0/2)\|g(t)\|^2}|\xi(\lambda)|^2\left|\tilde{h}(\lambda)\right|^2\varphi^{-1}(\lambda)\right)d\lambda\,, \tag{5.94}$$

where

$$\xi(\lambda) \equiv \sum_{k=-\infty}^{\infty} \xi_k e^{jk\lambda}\ ,\ \tilde{h}(\lambda) \equiv \sum_{k=-\infty}^{\infty} \tilde{h}_k e^{jk\lambda}\ ,\ \varphi(\lambda) \equiv \sum_{k=-\infty}^{\infty} \varphi_k e^{jk\lambda}\ . \tag{5.95}$$

By a change of variable (setting $\lambda = -2\pi f\Delta t$), (5.94) can be rewritten as

$$\bar{C}^{FTN}_{conv\text{-}precoded} \le \int_{-1/(2\Delta t)}^{1/(2\Delta t)} \log_2\left(1+\frac{\sigma_a^2|\alpha|^2}{(N_0/2)\|g(t)\|^2}\left|\mathsf{S}_\xi(f)\right|^2 \frac{\left|\tilde{h}(-2\pi f\Delta t)\right|^2}{\varphi(-2\pi f\Delta t)}\right)df\,, \tag{5.96}$$

where we made use of the definition of recoding spectrum: $\xi(-2\pi f\Delta t) = \sum_k \xi_k e^{-j2\pi fk\Delta t}$ $= \mathsf{S}_\xi(-f)$, followed by the property $\mathsf{S}_\xi(f) = \mathsf{S}_\xi^*(-f)$ for real convolutional precoding coefficients $\{\xi_k\}$.

Finally by Lemma 5.2, we can substitute into (5.96): $\tilde{h}(-2\pi f\Delta t) = \alpha^{-1}(\Delta t)^{-1}\hat{h}_{folded}(f)$ and $\varphi(-2\pi f\Delta t)\ = \|g(t)\|^{-2}(\Delta t)^{-1}\hat{g}_{folded}(f)$. This completes the proof of Theorem 5.3. ■

5.2 Capacity-wise Optimal Precoding for FTN Signaling

In this section, we further generalize the FTN system model by considering a linear FTN precoding that is not of convolutional nature. We find the *universally optimal* linear precoding strategy that maximizes the mutual information of the FTN channel. Subsection 5.2.1 first derives the optimal precoding strategies and the corresponding channel capacity for the FTN transmissions over AWGN channel. Useful insights into the optimal FTN precoding are highlighted in subsection 5.2.2. The analysis about the optimal FTN precoding is then extended to LTI channel transmissions in subsection 5.2.3. Discussions about the findings and the implementation issues follow in subsection 5.2.4.

5.2.1 Derivation of Optimal FTN Precoding in AWGN Channels

This subsection presents the capacity limit of optimally precoded FTN signaling over AWGN channel when subject to the FTN transmission power constraint from (3.57). Furthermore, the structure of the optimal precoding for the FTN signaling that can achieve the capacity limit is also presented. This is followed by an example of the optimal FTN precoder.

Theorem 5.5 (Capacity of optimally precoded FTN in AWGN channel)**:** *Consider the FTN communication system operating in AWGN channel* $\mathbf{y} = H\mathbf{x}+\mathbf{z}$*, subject to the FTN transmission power constraint (3.57). Furthermore, consider the linear precoding* $\mathbf{x}=L\mathbf{a}$ *of a zero-mean* σ_a^2*-variance i.i.d. information sequence* $\mathbf{a}$ *by a precoding matrix L. Then,*

(a) the capacity of optimally precoded FTN signaling is given by

$$C_{optimally\text{-}precoded}^{FTN} = \frac{K}{T}\log_2\left(1+\frac{PT}{K\cdot N_0/2}\right) \textit{ bits per second,} \tag{5.97}$$

which is achieved by having circularly symmetric complex Gaussian distributed $\mathbf{x}$**,** *and*

(b) the optimal precoding matrix L that maximizes the mutual information on the FTN channel satisfies

$$\sigma_a^2 LL^\dagger = P\Delta t \cdot H^{-1}. \tag{5.98}$$

Proof**:** We start from the mutual information between the precoded FTN modulation symbols $\mathbf{x}$ and the noisy channel observations $\mathbf{y} = H\mathbf{x}+\mathbf{z}$:

$$I(\mathbf{x};\mathbf{y}) = h(\mathbf{y}) - h(\mathbf{y}|\mathbf{x}) \tag{5.99}$$

$$= h(\mathbf{y}) - h(\mathbf{z}), \tag{5.100}$$

where $h(\cdot)$ denotes the differential entropy (Definition 2.3) and (5.100) follows from $H\mathbf{x}$ being deterministic given $\mathbf{x}$ and the translation invariance of the differential entropy (Lemma 2.5). The covariance matrix of $\mathbf{y}$ is given by

$$K_y = HK_xH^\dagger + (N_0/2)\cdot H, \tag{5.101}$$

due to noise correlation $E\{\mathbf{z}\mathbf{z}^\dagger\} = (N_0/2)\cdot H$ from (3.23), where K_x is the covariance matrix of $\mathbf{x}$.

By Lemma 2.4, the differential entropy of channel output, $h(\mathbf{y})$, can be upper-bounded by

$$h(\mathbf{y}) \le \log_2\left((\pi e)^{KN} \det(K_y)\right) \tag{5.102}$$

$$= \log_2\left(\left(\pi e\right)^{KN}\det\left(HK_xH^{\dagger} + \left(N_0/2\right)\cdot H\right)\right), \tag{5.103}$$

with equality if and only if **y** is a circularly symmetric complex Gaussian vector. Also by Lemma 2.3, the differential entropy of the correlated Gaussian noise vector **z** is given by

$$h(\mathbf{z}) = \log_2\left(\left(\pi e\right)^{KN}\det\left(\left(N_0/2\right)\cdot H\right)\right). \tag{5.104}$$

Therefore, the mutual information (5.100) can be upper- bounded as follows:

$$I(\mathbf{x};\mathbf{y}) \le \log_2\left(\frac{\det\left(HK_xH^{\dagger} + \left(N_0/2\right)\cdot H\right)}{\det\left(\left(N_0/2\right)\cdot H\right)}\right), \tag{5.105}$$

with equality if and only if **y** is circularly symmetric complex Gaussian vector, which is obtained when **x** is also circularly symmetric complex Gaussian vector.

Since H is Hermitian and invertible due to Proposition 3.1, (5.105) can be further simplified as follows:

$$I(\mathbf{x};\mathbf{y}) \le \log_2\left(\det\left(\frac{1}{N_0/2}H^{-1}\right)\det\left(HK_xH^{\dagger} + \left(N_0/2\right)\cdot H\right)\right) \tag{5.106}$$

$$= \log_2\left(\det\left(\frac{1}{N_0/2}H^{-1}HK_xH^{\dagger} + I_{KN}\right)\right) \tag{5.107}$$

$$= \log_2\left(\det\left(\frac{1}{N_0/2}K_xH + I_{KN}\right)\right), \tag{5.108}$$

where I_{KN} denotes $KN\times KN$ identity matrix, (5.106) is due to $\det(A^{-1}) = \det(A)^{-1}$, (5.107) is by $\det(A)\det(B) = \det(AB)$, and (5.108) follows from $H = H^{\dagger}$. Furthermore H can be decomposed into $H^{1/2}H^{1/2}$ and by the log-determinant identity $\log\det(AB+I) = \log\det(BA+I)$,

$$I(\mathbf{x};\mathbf{y}) \le \log_2\left(\det\left(\frac{1}{N_0/2}H^{1/2}K_xH^{1/2} + I_{KN}\right)\right). \tag{5.109}$$

The term inside the determinant, i.e., $(cH^{1/2}K_xH^{1/2} + I_{KN})$ for some constant c, is overall Hermitian and non-negative definite (note that K_x is Hermitian and non-negative definite by definition of the covariance matrix). Therefore, we can use Hadamard's inequality from Lemma 2.12 to further upper-bound (5.109) by (denoting $(A)_{ii}$ as $(i,i)^{\text{th}}$ entry of matrix A)

$$I(\mathbf{x};\mathbf{y}) \le \sum_{i=0}^{KN-1} \log_2\left(1+\frac{1}{N_0/2}\left(H^{1/2}K_xH^{1/2}\right)_{ii}\right), \tag{5.110}$$

with an equality if and only if $H^{1/2}K_xH^{1/2}$ is diagonal. This implies that optimal K_x is such that $H^{1/2}K_xH^{1/2}$ is diagonal, say $H^{1/2}K_xH^{1/2} = D$.

Now the problem becomes a constrained maximization of

$$\max_{d_0,d_1,\cdots,d_{KN-1}} \sum_{i=0}^{KN-1} \log_2\left(1+\left(N_0/2\right)^{-1} d_i\right) \tag{5.111}$$

subject to the power constraint from (3.57) simplifying to

$$\frac{1}{NT} tr\left(H^{1/2}K_xH^{1/2}\right) = \frac{1}{NT}\sum_{i=0}^{KN-1} d_i \le P, \tag{5.112}$$

where d_i denotes the i-th diagonal entry of matrix D. We can solve this constrained maximization problem by the method of Lagrange multipliers [20]. First construct a Lagrange function Λ as

$$\mathsf{L}\left(d_i\right) = \sum_{i=0}^{KN-1} \log_2\left(1+\left(N_0/2\right)^{-1} d_i\right) - \lambda\left(\frac{1}{NT}\sum_{i=0}^{KN-1} d_i - P\right), \tag{5.113}$$

where λ is a Lagrange multiplier. Taking a partial derivative with respect to d_i and setting it to zero yields

$$\frac{\partial \mathsf{L}}{\partial d_i} = \frac{1}{\ln 2}\left(\frac{1}{N_0/2+d_i}\right) - \left(\frac{\lambda}{NT}\right) = 0 \tag{5.114}$$

or

$$d_i = \left(\frac{NT}{\lambda \ln 2}\right) - \left(\frac{N_0}{2}\right). \tag{5.115}$$

Substituting (5.115) back to the power constraint (5.112) and solving for λ yields

$$\lambda = \frac{NT}{\ln 2\left(P\Delta t + N_0/2\right)}. \tag{5.116}$$

Finally, substituting (5.116) back to (5.115) and simplifying, we arrive at the solution $d_i = P\Delta t$. In other words, the optimal diagonal matrix is $D = P\Delta t \cdot I_{KN}$, or

$$H^{1/2}K_xH^{1/2} = \left(P\Delta t\right)\cdot I_{KN}. \tag{5.117}$$

By substituting in (5.117) into (5.110) and using the definition of the capacity $C = \lim_{N\to\infty} \sup_{p_x} (NT)^{-1} I(\mathbf{x};\mathbf{y})$ in units of bits per second, we arrive at the desired FTN capacity expression $C^{FTN}_{optimally\text{-}precoded}$ in (5.97).

Furthermore, note that the optimal input covariance K_x that satisfies (5.117) is $P\Delta t{\cdot}H^{-1}$, which is well defined since H is invertible and H^{-1} is Hermitian due to the inverse of an invertible Hermitian matrix is also Hermitian. Finally note that the covariance matrix of the precoded modulation symbols K_x is equal to $\sigma_a^2 LL^{\dagger}$, where σ_a^2 is the variance of **a**. This leads to the desired relation $K_x = \sigma_a^2 LL^{\dagger} = P\Delta t{\cdot}H^{-1}$ for the optimal precoding matrix L. This completes the proof of Theorem 5.5. ■

It is also interesting to note that the capacity of optimally precoded FTN transmission $C^{FTN}_{optimally\text{-}precoded}$ in (5.97) does not depend on the *shape* of the modulating pulse $s(t)$, but it does depend on the pulse bandwidth W=1/(2T). On the other hand, the optimal FTN precoder L does depend on the shape of $s(t)$ through the FTN matrix H as this optimal precoder must satisfy (5.98).

Figure 5.6 shows the capacity of precoded FTN signaling with varying FTN signaling rate factor K. Note that the conventional Nyquist-rate signaling is represented by K = 1 plot. It can be observed that precoding can substantially increase the capacity of the FTN signaling especially for moderate to high SNRs (shown for 20 dB to 50 dB range in the figure). This numerical result indicates a significant potential in using the optimally precoded FTN signaling.

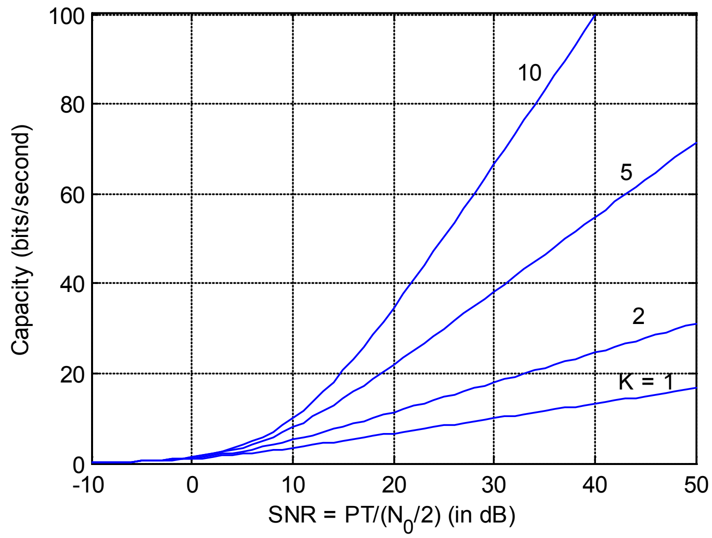

Figure 5.6 Capacity of optimally precoded FTN signaling versus SNR with varying *K* with *T* = 1

An example of the optimal precoding matrix L that satisfies Theorem 5.5 is presented below and illustrated in Figure 5.7. First, since H is fixed and known to the transmitter, H^{-1} can be derived before the communication commences. Then we can apply the Choleski factorization on H^{-1}: $H^{-1}=LL^{\dagger}$, where L is a lower triangular matrix. Consider an *i.i.d.* information sequence $\{a[n]\}$ (or $\mathbf{a} = [a[0], a[1], \ldots, a[KN\text{-}1]]^T$ in a vector notation) with a variance $\sigma_a^2 = P\Delta t$ for all n. We can linearly precode $\mathbf{a}$ by the lower triangular matrix L and set it equal to $\mathbf{x}$, i.e. $\mathbf{x} = L\mathbf{a}$. Note that this linear precoding matrix L satisfies the optimality condition (5.98), hence is capacity-wise optimal. Also, the lower triangular structure of L is favorable for real-time communication since the resulting $x[n]$ depends only on the current and the past information sequence: $a[n]$, $a[n\text{-}1]$, …, $a[0]$.

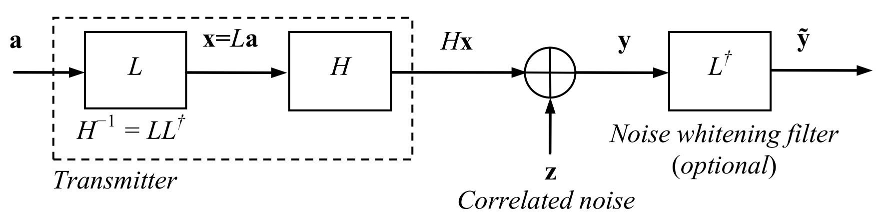

Figure 5.7 FTN signaling with the optimal precoding and an optional noise whitening filter in vector notations

Also illustrated in Figure 5.7 is an optional noise whitening filter at the receiving end. The effect of this filter on the signal component of **y** is described in the following. The filtered output $\tilde{\mathbf{y}} = L^{\dagger}\mathbf{y}$ can be expressed as (by substituting $\mathbf{x} = L\mathbf{a}$)

$$\tilde{\mathbf{y}} = L^{\dagger}\left(H\mathbf{x} + \mathbf{z}\right) = L^{\dagger} HL\mathbf{a} + \tilde{\mathbf{z}}\,, \tag{5.118}$$

where $\tilde{\mathbf{z}} = L^{\dagger}\mathbf{z}$ is a *whitened* Gaussian noise vector with zero mean and $(N_0/2)\cdot I_{KN}$ covariance. Finally, by $H^{-1}=LL^{\dagger}$, (5.118) can be written as

$$\tilde{\mathbf{y}} = \mathbf{a} + \tilde{\mathbf{z}}\,, \tag{5.119}$$

which is commonly referred to as parallel Gaussian channels in the literature.

In the following, the capacity of optimally precoded FTN in the limit $K \to \infty$ is derived.

Corollary 5.4 (Asymptotic capacity of optimally precoded FTN)**:** *The asymptotic capacity of optimally precoded FTN is given by*

$$\lim_{K\to\infty} C^{FTN}_{optimally\text{-}precoded} = \frac{1}{\ln 2}\frac{P}{N_0/2} \text{ bits per second,} \tag{5.120}$$

as FTN signaling rate factor $K \to \infty$.

Proof**:** This corollary can be proved by applying l'Hôpital's rule to the capacity expression from (5.97). ■

The asymptotic capacity expression (5.120) scales linearly in the signal-to-noise ratio (SNR). Furthermore, note that this linear capacity gain is achieved with the optimally precoded FTN signaling without increasing the transmission bandwidth (when the modulating pulse $s(t)$ is strictly band-limited). More insights into the capacity of this optimally precoded FTN signaling is given in subsection 5.2.2.

We note that the above capacity analysis derives the Shannon capacity for FTN transmission as opposed to traditionally considered capacity of Nyquist transmission. Our results seem to be consistent with that of Ash [5], [6], [7], who also arrived at a similar capacity expression while using a different (Fortet) channel model without using the FTN signaling framework.

5.2.2 Insights into Capacity of Optimally Precoded FTN

The objective of this subsection is to take a signal processing point of view to illustrate FTN transmission and the optimal FTN precoder from Theorem 5.5. For this, it is convenient to decompose the FTN communication channel model $\mathbf{y} = H\mathbf{x} + \mathbf{z}$ derived in (3.21) into a set of parallel channels. First, the FTN matrix H can be decomposed into $H = U\Lambda U^{\dagger}$ by the eigendecomposition (Theorem 2.3) where U is the unitary matrix whose columns are the eigenvectors of H and Λ is the diagonal matrix whose diagonal entries λ_i are the corresponding eigenvalues (such eigenvalue decomposition is possible since H is a Hermitian). Furthermore, recall from section 3.1 that the Gaussian noise vector $\mathbf{z}$ in the FTN model is correlated with the covariance matrix $K_z = E\{\mathbf{z}\mathbf{z}^{\dagger}\} = (N_0/2)H$ (see section 3.1 for the details).

We first consider *non-precoded* modulation symbols $\mathbf{x}$, i.e., statistically independent modulation symbols $\mathbf{x}$. In this case, $\mathbf{y} = (U\Lambda U^{\dagger})\mathbf{x} + \mathbf{z}$, or

$$\tilde{\mathbf{y}} = \Lambda\tilde{\mathbf{x}} + \tilde{\mathbf{z}} \tag{5.121}$$

where $\tilde{\mathbf{y}} \equiv U^{\dagger}\mathbf{y}$, $\tilde{\mathbf{x}} \equiv U^{\dagger}\mathbf{x}$, and the noise $\tilde{\mathbf{z}} \equiv U^{\dagger}\mathbf{z}$ is an uncorrelated Gaussian vector with zero mean and $(N_0/2)\Lambda$ covariance. Once we decode $\tilde{\mathbf{x}}$, the original modulation symbols $\mathbf{x}$ can be obtained by $\mathbf{x} = U\tilde{\mathbf{x}}$. Note that the formulation (5.121) is equivalent to KN parallel channels as shown in Figure 5.8.

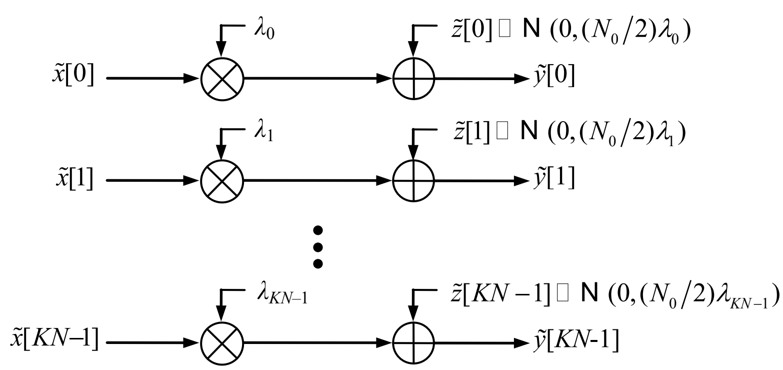

Figure 5.8 ***KN*** **parallel channels formulation of FTN transmission when using independent modulation symbols x**

The capacity of the i-th parallel channel is given by maximizing

$$I(\lambda_i \tilde{x}[i] + \tilde{z}[i]; \tilde{x}[i]) = \log_2\left(\frac{\lambda_i^2 P_i T + (N_0/2)\lambda_i}{(N_0/2)\lambda_i}\right) = \log_2\left(1 + \lambda_i SNR_i\right) \qquad (5.122)$$

where $I(\cdot;\cdot)$ denotes mutual information as defined in Definition 2.5 and $SNR_i \equiv P_i T/(N_0/2)$ with P_i being the power allocated to the i-th channel (and $P_i T$ is the energy). Therefore, the capacity of the KN parallel channels is simply

$$C_{i.i.d.}^{FTN} = \max_{P_0,\cdots,P_{KN-1}} \sum_{i=0}^{KN-1} \log_2\left(1 + \lambda_i SNR_i\right), \qquad (5.123)$$

and the optimal power allocation is given by the classical water-filling algorithm [31].

Note that if a particular λ_i is small, i.e., $\lambda_i \approx 0$, then the i-th parallel channel is essentially useless as it contributes little to the capacity. Recalling that the λ_i are the eigenvalues of the FTN matrix H, we see that the capacity depends heavily on the eigenvalue distribution of H. As discussed in section 3.2, for FTN signals that are strictly bandlimited to $(-W, W)$ Hertz, only about $2WNT$ eigenvalues are significant and the rest are arbitrarily small as N tends to infinity. In other words, the number of parallel channels reduces to only N (by replacing $T = 1/(2W)$ by the Nyquist theorem), which is exactly how many parallel channels the conventional Nyquist rate signaling would give. Therefore, without precoding, when independent modulation symbols $\mathbf{x}$ are sent and when strictly bandlimited modulating pulse is used, the FTN capacity gain over the Nyquist rate signaling is marginal and reduces to zero as the block length N goes to infinity.

On the other hand, consider sending *linearly precoded* modulation symbols $\mathbf{x} = H^{-1/2}\mathbf{a}$, where $\mathbf{a}$ is an *i.i.d.* information symbol vector with covariance $(P\Delta t)\cdot I_{KN}$. Note that this linear precoding satisfies the optimality criterion (5.98) from Theorem 5.5 and hence is capacity-wise optimal. Furthermore, sending such precoded modulation symbols $\mathbf{x}$ does not violate the FTN transmission power constraint (3.56). Noting that $H^{-1/2} = U\Lambda^{-1/2}$ (since $H^{-1} = U\Lambda^{-1}U^{\dagger}$ and $H^{-1} = H^{-1/2}H^{-1/2}$), the corresponding parallel channels are

$$\tilde{\mathbf{y}} = \Lambda^{1/2}\mathbf{a} + \tilde{\mathbf{z}}, \qquad (5.124)$$

where $\tilde{\mathbf{y}} = U^{\dagger}\mathbf{y}$, and the noise $\tilde{\mathbf{z}} = U^{\dagger}\mathbf{z}$ is again an uncorrelated Gaussian vector with zero mean and $(N_0/2)\Lambda$ covariance. These parallel channels are depicted in Figure 5.9.

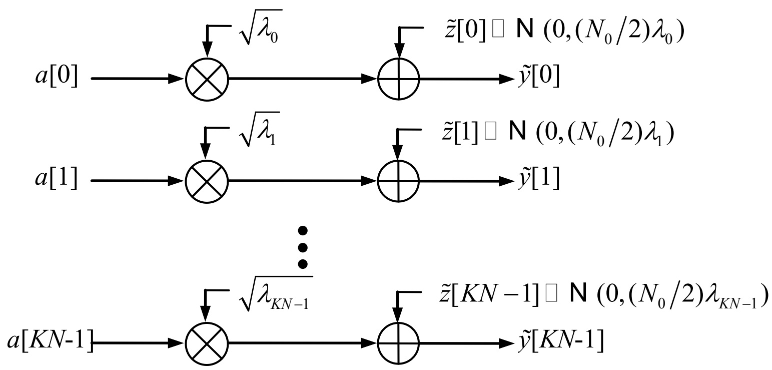

Figure 5.9 ***KN*** **parallel channel formulation using precoded FTN modulation symbols x =** $\boldsymbol{H^{-1/2}}$**a**

The only difference from the parallel channels in Figure 5.8 is the square roots appearing in the channel gains. However this seemingly small change makes rather significant impact on the capacity. The *i*-th channel capacity is now given by maximizing

$$I\left(\sqrt{\lambda_i}a[i]+\tilde{z}[i];a[i]\right)=\log_2\left(\frac{\lambda_i P_i T+\left(N_0/2\right)\lambda_i}{\left(N_0/2\right)\lambda_i}\right)=\log_2\left(1+SNR_i\right), \tag{5.125}$$

where $I(\cdot;\cdot)$ denotes the mutual information. The capacity of the *KN* parallel channels is then

$$C^{FTN}_{optimally\text{-}precoded}=\max_{P_0,\cdots,P_{KN-1}}\sum_{i=0}^{KN-1}\log_2\left(1+SNR_i\right), \tag{5.126}$$

which is no longer dependent on the eigenvalues λ_i of *H*. This capacity is equivalent to that of the *KN* parallel AWGN channels as shown in Figure 5.10. This implies that no matter how small the channel gains $\sqrt{\lambda_i}$ are, as long as they are strictly nonzero[29], the particular *i-th* parallel channel is equally good as the conventional AWGN channel. This is because the noise variance $(N_0/2)\lambda_i$ is also small if channel gains are small, leading to a fixed SNR_i.

[29] The eigenvalues of *H*, λ_i, are indeed nonzero for any finite *N*. This is a direct consequence of the invertibility of the matrix *H* as proved in Proposition 3.1.

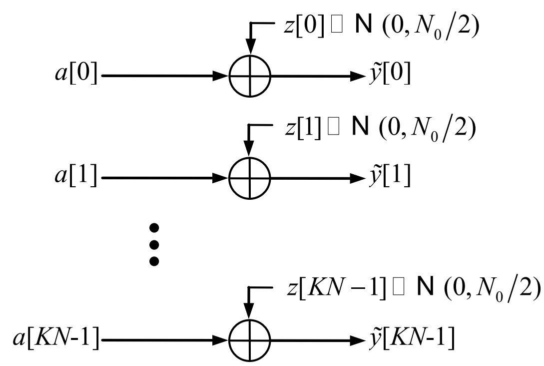

Figure 5.10 Parallel AWGN channels equivalent to Figure 5.9 in terms of overall channel capacity

Considering that the Nyquist signaling gives N parallel channels only, the FTN signaling using precoded modulation symbols $\mathbf{x} = H^{-1/2}\mathbf{a}$ increases the capacity by providing additional channels in total of KN channels (this is consistent with our Hilbert space argument in section 2.6).

Before closing the subsection, we point out an important issue about the computer precision (or range) versus the capacity. When the i-th channel gain $\sqrt{\lambda_i}$ is very small (but nonzero), the received value $\tilde{y} = \sqrt{\lambda_i}\tilde{a}[i] + \tilde{z}[i]$ will also be scaled down to a small value. If the value falls below the range of data-type representation of the computing platform, the received value will simply be truncated down to zero and hence the corresponding channel cannot be utilized by the decoder. Consequently, the practically attainable capacity of FTN depends on the available precision of the computing platform. We discuss this issue in a greater detail in subsection 5.2.4.

5.2.3 Optimal FTN Precoding in LTI Channels

The objective of this subsection is to extend the analysis of the optimal FTN precoding from subsection 5.2.1 for AWGN channel to linear time-invariant (LTI) channel setup as shown in Figure 5.11.

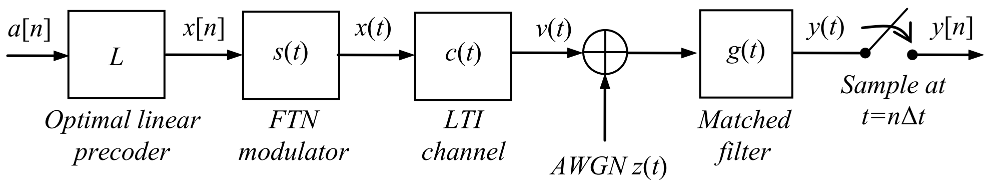

Figure 5.11 Block diagram of the optimally precoded FTN signaling in LTI channel

Recall that the corresponding discrete-time channel model is (as developed in section 3.1)

$$\mathbf{y} = \alpha \tilde{H} \mathbf{x} + \mathbf{z}, \tag{5.127}$$

under the transmission power constraint (3.57):

$$\frac{1}{NT} tr\left(U^{\dagger} H^{1/2} K_x H^{1/2} U\right) \leq P, \tag{5.128}$$

for some unitary matrix U and covariance matrix of precoded modulation symbols K_x. The relevant definitions are also reproduced below for convenience (see section 3.1 for details):

- Normalization factor: $\alpha \equiv s(t) * c(t) * g(t)\big|_{t=0}$, (5.129)

- FTN matrix for LTI channel: $\tilde{H} \equiv \begin{bmatrix} 1 & \tilde{h}_{-1} & \cdots & \tilde{h}_{-(KN-1)} \\ \tilde{h}_1 & 1 & \cdots & \tilde{h}_{-(KN-2)} \\ \vdots & \vdots & \ddots & \vdots \\ \tilde{h}_{KN-1} & \tilde{h}_{KN-2} & \cdots & 1 \end{bmatrix}$, (5.130)

- ISI coefficients: $\tilde{h}_k \equiv \alpha^{-1} s(t) * c(t) * g(t)\big|_{t=k\Delta t}$, (5.131)

- Noise covariance matrix: $E\{\mathbf{z}\mathbf{z}^{\dagger}\} = \frac{N_0}{2} \left\| g(t) \right\|^2 \Phi$, (5.132)

- Receiver filter correlation matrix: $\Phi \equiv \begin{bmatrix} 1 & \varphi_{-1} & \cdots & \varphi_{-(KN-1)} \\ \varphi_1 & 1 & \cdots & \varphi_{-(KN-2)} \\ \vdots & \vdots & \ddots & \vdots \\ \varphi_{KN-1} & \varphi_{KN-2} & \cdots & 1 \end{bmatrix}$, (5.133)

- Receiver filter correlations: $\varphi_k \equiv \left\| g(t) \right\|^{-2} \int_{-\infty}^{+\infty} g(\tau) g^*(\tau - k\Delta t) \, d\tau$. (5.134)

Furthermore, the data symbol vector **x** is assumed to be linearly precoded, i.e., **x**=L**a**, where **a** is an *i.i.d.* information sequence with a variance σ_a^2.

The resulting precoding strategies have 'water-filling' or 'water-pouring' interpretations.

Theorem 5.6 (Optimal precoder for FTN signaling in LTI channel)**:** *Consider the FTN communication system operating in LTI channel using linear precoding* **x**=L**a** *of zero-mean* σ_a^2*-variance i.i.d. information sequence* **a** *by a precoding matrix L. Furthermore let, by the eigenvalue decomposition,*

$$\left(\Phi^{-1/2}\tilde{H}H^{-1/2}\right)^{\dagger}\left(\Phi^{-1/2}\tilde{H}H^{-1/2}\right)=U\Lambda U^{\dagger}, \tag{5.135}$$

where H is the FTN matrix as defined in (3.22), U is a unitary matrix, and Λ is a diagonal matrix with eigenvalues on the diagonal. Also define a diagonal matrix D with the i-th diagonal entry given by the water-filling algorithm (see Figure 5.12)

$$d_i = \max\left(\mu-\left(\frac{(N_0/2)\|g(t)\|^2}{|\alpha|^2}\right)\lambda_i^{-1},\ 0\right), \tag{5.136}$$

where λ_i *is the i-th diagonal entry of Λ and μ is the water-filling parameter chosen to satisfy the following power constraint*

$$\frac{1}{NT}\sum_{i=0}^{KN-1} d_i \le P. \tag{5.137}$$

Then

(a) the capacity of the optimally precoded FTN signaling subject to the FTN transmission power constraint (3.57) is given by

$$C_{optimally\text{-}precoded}^{FTN}=\lim_{N\to\infty}\frac{1}{NT}\sum_{i=0}^{KN-1}\log_2\left(\max\left(\frac{|\alpha|^2}{(N_0/2)\|g(t)\|^2}\mu\lambda_i,\ 1\right)\right) \text{ bits per second,} \tag{5.138}$$

which is achieved by having circularly symmetric Gaussian distributed **x***, and*

(b) the precoding matrix L that maximizes the mutual information of the FTN channel satisfies

$$\sigma_a^2 LL^{\dagger} = H^{-1/2}UDU^{\dagger}H^{-1/2}. \tag{5.139}$$

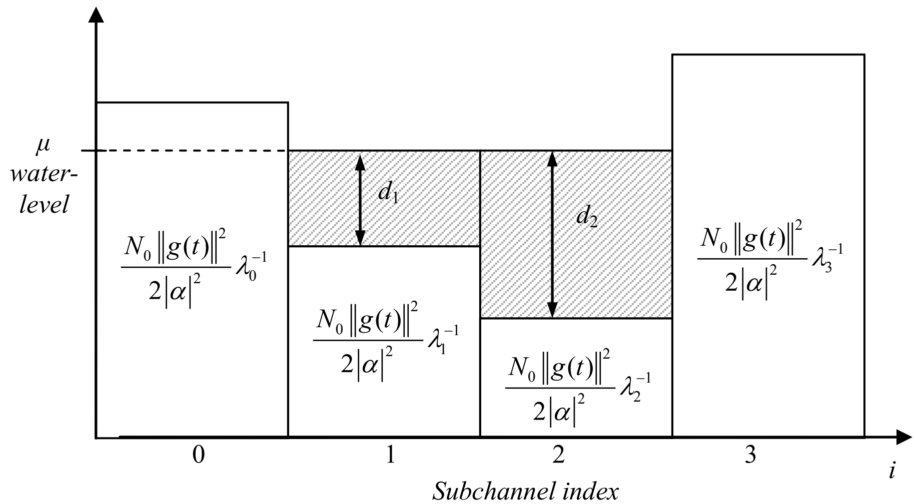

Figure 5.12 Water-filling algorithm: The water-filling parameter μ is chosen such that the area of the shaded region divided by NT is exactly P

***Proof of Theorem 5.6*:** We begin with the mutual information between the precoded modulation symbol vector $\mathbf{x}$ and LTI channel observation vector $\mathbf{y}$ (from Lemma 5.1)

$$I(\mathbf{y};\mathbf{x}) \le \log_2\left(\det\left(\frac{|\alpha|^2}{(N_0/2)\|g(t)\|^2}\Phi^{-1/2}\tilde{H}K_x\tilde{H}^{\dagger}\Phi^{-1/2} + I_{KN}\right)\right), \tag{5.140}$$

which, due to Lemma 5.1, becomes equality if $\mathbf{x}$ is circularly symmetric complex Gaussian distributed with a covariance matrix K_x. The next step is to re-express above as a function of $H^{1/2}K_xH^{1/2}$, trace of which appears in the transmission power constraint (5.128). Consider the following series of equalities:

$$\Phi^{-1/2}\tilde{H}K_x\tilde{H}^{\dagger}\Phi^{-1/2} = \Phi^{-1/2}\tilde{H}\left(H^{-1/2}H^{1/2}\right)K_x\left(H^{1/2}H^{-1/2}\right)\tilde{H}^{\dagger}\Phi^{-1/2} \tag{5.141}$$

$$= \left(\Phi^{-1/2}\tilde{H}H^{-1/2}\right)\left(H^{1/2}K_xH^{1/2}\right)\left(H^{-1/2}\tilde{H}^{\dagger}\Phi^{-1/2}\right) \tag{5.142}$$

$$= \left(\Phi^{-1/2}\tilde{H}H^{-1/2}\right)\left(H^{1/2}K_xH^{1/2}\right)\left(\Phi^{-1/2}\tilde{H}H^{-1/2}\right)^{\dagger}. \tag{5.143}$$

We now substitute (5.143) back into the mutual information (5.140) for further simplifications:

$$I(\mathbf{y};\mathbf{x}) \le \log_2\left(\det\left(\frac{|\alpha|^2}{(N_0/2)\|g(t)\|^2}\left(\Phi^{-1/2}\tilde{H}H^{-1/2}\right)\left(H^{1/2}K_xH^{1/2}\right)\left(\Phi^{-1/2}\tilde{H}H^{-1/2}\right)^{\dagger}+I_{KN}\right)\right) \tag{5.144}$$

$$=\log_2\left(\det\left(\frac{|\alpha|^2}{(N_0/2)\|g(t)\|^2}\left(H^{1/2}K_xH^{1/2}\right)\left(\Phi^{-1/2}\tilde{H}H^{-1/2}\right)^{\dagger}\left(\Phi^{-1/2}\tilde{H}H^{-1/2}\right)+I_{KN}\right)\right) \tag{5.145}$$

$$=\log_2\left(\det\left(\frac{|\alpha|^2}{(N_0/2)\|g(t)\|^2}\left(H^{1/2}K_xH^{1/2}\right)\left(U\Lambda U^{\dagger}\right)+I_{KN}\right)\right) \tag{5.146}$$

$$=\log_2\left(\det\left(\frac{|\alpha|^2}{(N_0/2)\|g(t)\|^2}\Lambda^{1/2}U^{\dagger}\left(H^{1/2}K_xH^{1/2}\right)U\Lambda^{1/2}+I_{KN}\right)\right) \tag{5.147}$$

where (5.145) follows from the determinant identity det($AB+I$) = det($BA+I$), and U and Λ in (5.146) are $KN\times KN$ unitary and diagonal matrices, respectively, obtained by the following eigenvalue decomposition:

$$\left(\Phi^{-1/2}\tilde{H}H^{-1/2}\right)^{\dagger}\left(\Phi^{-1/2}\tilde{H}H^{-1/2}\right)=U\Lambda U^{\dagger}. \tag{5.148}$$

Moreover, (5.147) is due to the decomposition $\Lambda=\Lambda^{1/2}\Lambda^{1/2}$ (which is possible since the matrix product $\left(\Phi^{-1/2}\tilde{H}H^{-1/2}\right)^{\dagger}\left(\Phi^{-1/2}\tilde{H}H^{-1/2}\right)$ is Hermitian), followed by the determinant identity det($AB+I$) = det($BA+I$).

Using Hadamard's inequality from Lemma 2.12 and denoting $(A)_{ij}$ as the (i, j)-th entry of matrix A:

$$I(\mathbf{y};\mathbf{x}) \le \sum_{i=0}^{KN-1}\log_2\left(1+\frac{|\alpha|^2}{(N_0/2)\|g(t)\|^2}\left(U^{\dagger}H^{1/2}K_xH^{1/2}U\right)_{ii}\lambda_i\right), \tag{5.149}$$

which becomes an equality if and only if $U^{\dagger}H^{1/2}K_xH^{1/2}U$ is diagonal. This implies that the optimal K_x is such that $D\equiv U^{\dagger}H^{1/2}K_xH^{1/2}U$ is diagonal and its diagonal entries d_i satisfy the constraint

$$\frac{1}{NT}\sum_{i=0}^{KN-1}d_i \le P, \tag{5.150}$$

due to the transmission power constraint (5.128). The solution to this constrained optimization problem is then found via the water-filling, which is given by:

$$d_i = \left(U^\dagger H^{1/2} K_x H^{1/2} U\right)_{ii} = \max\left(\mu - \left(\frac{(N_0/2)\|g(t)\|^2}{|\alpha|^2}\right)\lambda_i^{-1},\ 0\right), \tag{5.151}$$

where μ is chosen to satisfy the constraint (5.150). Substituting this back into (5.149) yields

$$I(\mathbf{y};\mathbf{x}) \le \sum_{i=0}^{KN-1} \log_2\left(\max\left(\frac{|\alpha|^2}{(N_0/2)\|g(t)\|^2}\mu\lambda_i,\ 1\right)\right) \tag{5.152}$$

The above (5.152) becomes equality if the water-filling solution (5.151) is used. That is, the covariance matrix K_x must satisfy

$$K_x = H^{-1/2} U D U^\dagger H^{-1/2}, \tag{5.153}$$

where D is the diagonal matrix with entries given by the water-filling solution (5.151).

The desired capacity expression (5.138) is then obtained by substituting the mutual information expression from (5.152) into the definition of the capacity $C = \lim_{N\to\infty} \sup_{p_x} (NT)^{-1} I(\mathbf{x};\mathbf{y})$ in units of bits per second. Furthermore, due to (5.153) and by noting that the covariance matrix K_x of a linearly precoded data symbols $\mathbf{x}=L\mathbf{a}$ is $K_x = \sigma_a^2 LL^\dagger$, we arrive at the desired relation $K_x = \sigma_a^2 LL^\dagger = H^{-1/2} U D U^\dagger H^{-1/2}$ for the optimal precoding matrix L. This completes the proof of Theorem 5.6. ■

An example of an optimal precoding matrix that satisfies (5.139) is shown in Figure 5.13. First, since the matrices $\tilde{H}$, Φ, and H are known to the transmitter, we can apply the eigenvalue decomposition $\left(\Phi^{-1/2}\tilde{H}H^{-1/2}\right)^\dagger \left(\Phi^{-1/2}\tilde{H}H^{-1/2}\right) = U\Lambda U^\dagger$ prior to the communication commences. The diagonal entries of the optimal diagonal matrix D are determined by the water-filling algorithm (5.136). A precoding matrix is then computed offline by $L=H^{-1/2}UD^{1/2}$ and stored in a lookup table. Note that this particular linear precoding matrix L satisfies the optimality condition (5.139). At the time of communication, generate an *independent* information sequence $\{a[n]\}$, or $\mathbf{a} \equiv [a[0], a[1],$

…, $a[KN\text{-}1]]^T$ in a vector form, with a covariance matrix $K_a \equiv E\{\mathbf{aa}^\dagger\} = I_{KN}$. Finally, precode $\mathbf{a}$ by the precoding matrix L and set it equal to $\mathbf{x}$, i.e., $\mathbf{x} = L\mathbf{a}$.

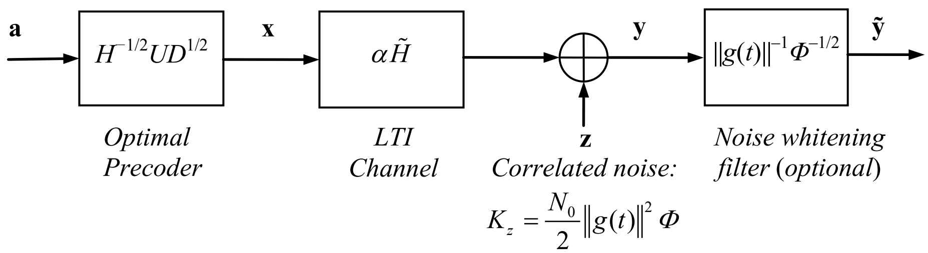

Figure 5.13 FTN signaling in LTI channels with the optimal precoding and optional noise whitening filter in discrete-time (vector) notations

Also illustrated in Figure 5.13 is an optional noise whitening filter at the receiving end. The filtered output $\tilde{\mathbf{y}}$ can be expressed as (by substituting $\mathbf{x} = H^{-1/2}UD^{1/2}\mathbf{a}$)

$$\tilde{\mathbf{y}} = \|g(t)\|^{-1}\Phi^{-1/2}\left(\alpha\tilde{H}\mathbf{x}\right) + \tilde{\mathbf{z}} = \alpha\|g(t)\|^{-1}\left(\Phi^{-1/2}\tilde{H}H^{-1/2}\right)UD^{1/2}\mathbf{a} + \tilde{\mathbf{z}}, \tag{5.154}$$

where $\tilde{\mathbf{z}} \equiv \|g(t)\|^{-1}\Phi^{-1/2}\mathbf{z}$ is a *whitened* Gaussian noise with zero mean and $(N_0/2)\cdot I_{KN}$ covariance. But due to the eigenvalue decomposition $(\Phi^{-1/2}\tilde{H}H^{-1/2})^\dagger(\Phi^{-1/2}\tilde{H}H^{-1/2}) = U\Lambda U^\dagger$, we have

$$\Phi^{-1/2}\tilde{H}H^{-1/2} = \Lambda^{1/2}U^\dagger . \tag{5.155}$$

Substitution this into (5.154) and by $U^\dagger U = I_{KN}$, we obtain

$$\tilde{\mathbf{y}} = \alpha\|g(t)\|^{-1}\left(\Lambda D\right)^{1/2}\mathbf{a} + \tilde{\mathbf{z}}, \tag{5.156}$$

which is known as the set of parallel Gaussian channels in the literature. Note that $\Lambda^{1/2}$ carries eigenvalues (or so called eigen-channels) of the matrix product $\Phi^{-1/2}\tilde{H}H^{-1/2}$ which entails contributions from the transmit pulse response $s(t)$ (via H), LTI channel response $c(t)$ (via $\tilde{H}$), and the receiver filter response $g(t)$ (via Φ). On the other hand, the entries of $D^{1/2}$ are determined by the water-filling algorithm, purpose of which is to combat the imperfect channel responses *and* the FTN-induced ISI. When the channel $c(t)$ is well-behaving, i.e., its eigenvalues become close to unity, $\Lambda^{1/2}D^{1/2}$ becomes approximately I_{KN} since $D^{1/2}$ will be chosen by the water-filling algorithm to be almost $\Lambda^{-1/2}$ under the allowances of the transmission power constraint. In such case, we simply obtain KN

number of parallel Gaussian channels, of which both capacities and practical performances are well understood.

5.2.4 Discussion on Implementation Issues: Precision Versus Capacity

Subsections 5.2.1 to 5.2.3 showed the merits of precoding and the substantial capacity potential in the optimally precoded FTN transmission. The information theoretic analysis in subsections 5.2.1 to 5.2.3, however, assumes perfect computing precision and ideal computing environments, and we examine the impact of finite computing precision on the optimal precoding in this subsection.

Recall from Theorem 5.5 that the optimal precoding matrix L must satisfy $\sigma_a^2 LL^\dagger = P\Delta t \cdot H^{-1}$. Generating this matrix L involves a *matrix inversion* of the FTN matrix H, which becomes ill-conditioned when the modulating pulse $s(t)$ is strictly bandlimited. Example 5.1 below illustrates this issue:

Example 5.1 (Bandlimited modulating pulse): *The FTN matrix H when the modulating pulse is* $s(t) = (2W)^{1/2}\text{sinc}(2Wt)$ *(which has a constant frequency response over* $f \in (-W, W)$ *and zero everywhere else) is given by* $H = [\text{sinc}((i-j)/K)]_{i,\, j=0,1,\ldots,KN-1}$*, for* $K>0$ *and* $N>0$*. This is a Toeplitz matrix with a size KN×KN. Although this matrix is theoretically invertible for every finite K and N, it quickly becomes ill-conditioned with increasing K or N. Figure 5.14a plots the condition numbers[30] of this matrix in logarithmic scale when K = 2 and N is varied from 1 to 10 (note that condition numbers near 1 indicate a well-conditioned matrix).*

From Figure 5.14*a*, we can readily see that the condition numbers increase exponentially with increasing FTN packet length N. With the IEEE standard double-precision floating-point-numbers using 64 bits (used in MATLAB), computing matrix inversions or solving linear equations is accurate for condition numbers up to around 10^{16}. (This corresponds to N = 11 or 12 for the considered Example 5.1.) If a matrix has a condition number larger than 10^{16}, then the inverse of the matrix can contain very large

[30] Condition number is defined in section 2.4. It gives an indication of the accuracy of the results from matrix inversion and the linear equation solution.

values (in the order of 10^{16}) and may not be accurate. As a consequence, the computing precision needs to be increased accordingly in order to accurately implement the optimally precoded FTN systems with larger K and N. For instance, *quadrature*-precision floating-point-number formats (using 128 bits) can push the condition number limit to around 10^{34}. Moreover, extended precision formats and variable precision arithmetic can push this limit even further.

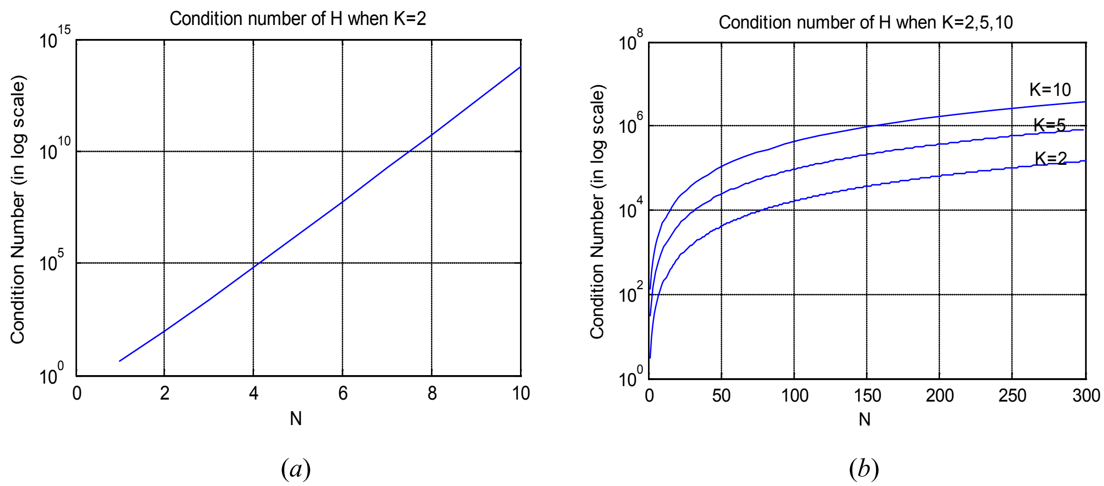

Figure 5.14 Condition numbers of the FTN matrix *H* when (a) sinc-type modulating pulse is used as in Example 5.1 or when (b) rectangular modulating pulse is used as in Example 5.2; (condition numbers are estimated by MATLAB built-in function *cond*)

On the other hand, when $s(t)$ is a time-limited pulse (hence not bandlimited) the corresponding matrix H turns out to be much more well-conditioned. This is demonstrated in the following example.

Example 5.2 (Non-bandlimited modulating pulse): *The FTN matrix H when the $s(t)$ is a rectangular pulse, i.e., $s(t) = T^{-1/2}$ within $t \in (0, T)$ and zero everywhere else, is given by $H = [max(0, 1-|i-j|/K)]_{i,j=0,1,\ldots,KN-1}$, for $K>0$, $N>0$. Note that this is a banded Toeplitz matrix with size $KN \times KN$. As before, we plot the condition numbers of this matrix with varying N in Figure 5.14b, which reveals that the condition numbers of H increase only linearly with N, in contrast to the exponential increase from Example 5.1. This implies that standard software such as MATLAB can simulate very large K and N without loss in the accuracy. Unfortunately, using non-bandlimited modulating pulse in optimally precoded FTN* *signaling may cause spectral broadening as discussed in subsection 3.4.3 and shown in Table 3.1, and hence is typically not suitable for the optimal precoding.*

From the previous two examples, we see that the condition numbers of matrix H are strongly tied to the bandlimited-ness of the modulating pulse $s(t)$. We can make this relationship precise by making a following connection with the eigenvalue analysis of H from section 3.2. Recall from Lemma 2.14 that the condition number $\kappa(H)$ for Hermitian matrices can be expressed as

$$\kappa(H) = \left|\lambda_{\max}(H)/\lambda_{\min}(H)\right|, \tag{5.157}$$

where $\lambda_{\max}(H)$ and $\lambda_{\min}(H)$ are the maximal and the minimal (by moduli) eigenvalues of H, respectively. This shows that the condition numbers are inversely proportional to the minimum eigenvalue of the matrix. Therefore, the exponential increase in the condition numbers from using strictly band-limited pulses can be attributed to the quickly decaying minimum eigenvalue of H with increasing N (see section 3.2 for the eigenvalue analysis of H).

Consequently, the more bandlimited the modulating pulses are, the more eigenvalues of H quickly converges to zero; leading to more rapidly increasing condition numbers of H as its size $KN \times KN$ increases. This makes the computation of the matrix inverse H^{-1} increasingly difficult for bandlimited FTN transmission and consequently obtaining the optimal precoding matrix L.[31]

Fortunately, there exist powerful techniques such as extended-precision formats and arbitrary precision arithmetic with which the precision is limited only by the available memory of the computing system. With these techniques, one can explore precoding gain versus available computing precision: i.e., the more precision is available, the longer packets with length N or the faster FTN with larger K can be implemented with the optimal

[31] One may also explain this phenomenon from the parallel channel argument from subsection 5.2.2. Recall that with the optimal precoding, the parallel channels are scaled by square-root of eigenvalues of the FTN matrix H (see subsection 5.2.2 for details). When a particular eigenvalue of H is so small in magnitude such that it falls below the range of data-type representation of the computing platform, the corresponding parallel channel cannot be recognized and no data can be recovered from this channel. Consequently, the full capacity benefits from the optimal precoding can only be realized if the computing system has enough computing precision so that it can recognize and process very small real numbers.

precoding. With the exponential growth in the memory size (following the Moore's law [103]), the true capacity potentials of the precoded FTN signaling may be realized in near future.[32]

5.3 Using Precoded FTN for Spread-Spectrum Communication

It is interesting to note that the precoded FTN signaling described in this chapter so far may find an application as a new type of spread-spectrum communication. Traditional spread spectrum communication systems rely on either direct sequence spreading, time/frequency hopping or a combination of these [108]. Alternatively, the considered FTN signaling with appropriate precoding at the transmitter can also generate signals that have a spread spectrum when compared to the bandwidth of the original signal. This idea stems from the observation that optimally precoded FTN signals based on non-bandlimited modulating pulses can undergo spectral broadening, as shown in Table 3.1. If the degree of broadening can be precisely controlled (e.g., by using a wideband frequency filter front-end), precoding of FTN signals can be used to spread the signal spectrum "unconventionally". Consequently, the FTN based spread-spectrum technique can potentially be used to allow secure communication and/or improve resistance to jamming and interference.

The FTN system model and design of appropriate spectrum spreading precoders and corresponding receivers are first presented in subsection 5.3.1. Numerical power spectral density estimates as well as bit-error-rate simulation results are then provided in subsection 5.3.2 which show that spread spectrum communication using precoded FTN signaling can be a feasible alternative to traditional spread spectrum methods.

[32] An additional interesting problem is to determine the pulse shape that is maximally bandlimited (or has minimal out-of-band energy) for a given eigenvalue decay rate. This leads to a new subproblem of pulse design for FTN systems.

5.3.1 System Setup for FTN- based Spread-spectrum Signaling

The system block diagram of the considered spread spectrum FTN model is shown in Figure 5.15. An *i.i.d.* data vector **a** of size $KN\times 1$ is first linearly precoded to form a set of modulation symbol vector $\mathbf{x} = L\mathbf{a}$ by a matrix precoder L. The FTN modulator generates an FTN signal $x(t)$, which is frequency-filtered by a wideband filter to suppress spectral side-lobes and subsequently transmitted onto a wideband channel. At the receiving-end, a noisy version of the transmitted FTN signal is first matched filtered and sampled at the FTN rate of $1/\Delta t$ times per second. Finally, a decorrelator produces a vector of estimates $\hat{\mathbf{a}}$ about the data vector **a**.

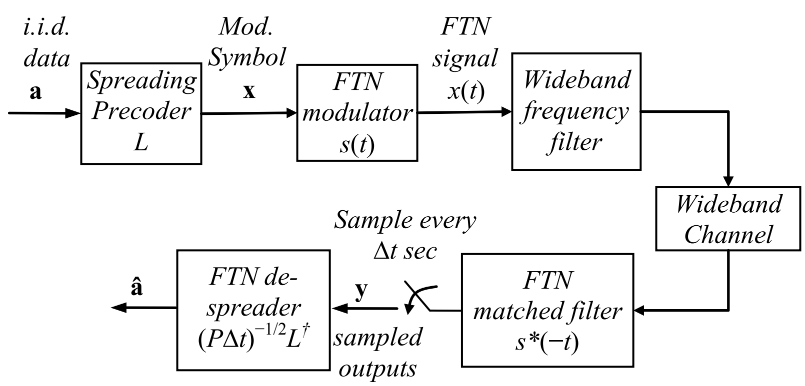

Figure 5.15 Schematic block diagram of the proposed spread spectrum FTN communication system

The purpose of the FTN spreading precoder is to achieve broadband nature of the signal transmitted over the channel. The FTN de-spreader module in Figure 5.15 aims to recover the data from the matched filter output by joint removal of the FTN interference. Towards this goal, we consider a matrix precoder L designed to compute $\mathbf{x} = L\mathbf{a}$, where **a** is assumed to be normalized to have zero mean and unit variance. The spreading matrix L satisfies

$$LL^{\dagger} = (P\Delta t)\cdot H^{-1}, \tag{5.158}$$

which maximizes the mutual information on the FTN channel, as proved in Theorem 5.5. On the other hand, the FTN de-spreader in Figure 5.15 implements $\hat{\mathbf{a}} = (P\Delta t)^{-1/2}L^{\dagger}\mathbf{y}$ which, with the precoder L, yields

$$\hat{\mathbf{a}} = \left(P\Delta t\right)^{-1/2} L^{\dagger}\mathbf{y} = \left(P\Delta t\right)^{-1/2} (L^{\dagger} H L\mathbf{a} + L^{\dagger}\mathbf{z}) = \mathbf{a} + \tilde{\mathbf{z}}, \tag{5.159}$$

where $\tilde{\mathbf{z}}$ is a *whitened* Gaussian vector with zero mean and $N_0/2$ variance. As discussed in section 3.4, such FTN precoding does broaden the transmission spectrum, if $s(t)$ is not strictly bandlimited.

5.3.2 Numerical Power Spectral Density Estimates and BER Simulation

The spread-spectrum FTN communication system shown in Figure 5.15 was simulated with the following system parameters:

- $T = 10$ ms; $K = 100$; $\Delta t = T/K = 0.1$ ms;
- Modulating pulse $s(t)$: Square-root raised cosine with a roll-off factor β=0.22 (used in e.g., WCDMA standard), delayed in time by $T/2$ and time-truncated to $t \in [0, T]$;
- Precoder: $L = (P\Delta t)^{1/2} \cdot H^{-1/2}$ (satisfies (5.158));
- Ideal brick-wall wideband frequency filter with $W = 10$ kHz.

Figure 5.16 plots the modulating pulse $s(t)$ and the spread-spectrum precoded FTN signal $x(t)$ from the simulation. Figure 5.17 shows the numerical power spectral density (PSD) estimates of the precoded FTN signal $x(t)$, plotted using the Welch method from [160] (which is a variant of the periodogram-based spectral estimation technique). When compared to the conventional Nyquist rate narrowband signal (in the left plot of Figure 5.17), the precoded FTN signal clearly exhibits significant spectrum spreading by a factor of 25 in this case. Plotted at the right of Figure 5.17 is the PSD estimate of randomly precoded FTN signal with an *i.i.d.* Gaussian precoding matrix (i.e., when entries of L are *i.i.d.* Gaussian distributed). It can be seen that randomly chosen precoding matrix does not provide spectral broadening and hence specific precoding matrices such as L from (5.158) should be used for spreading.

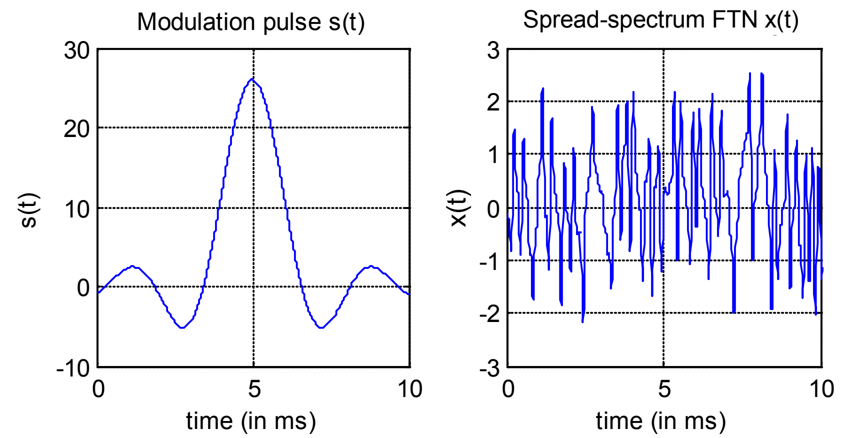

Figure 5.16 Plots of modulating pulse *s*(*t*) (time-truncated root raised cosine) (left) and a snapshot of the wideband precoded FTN signal *x*(*t*) in a small time window (right)

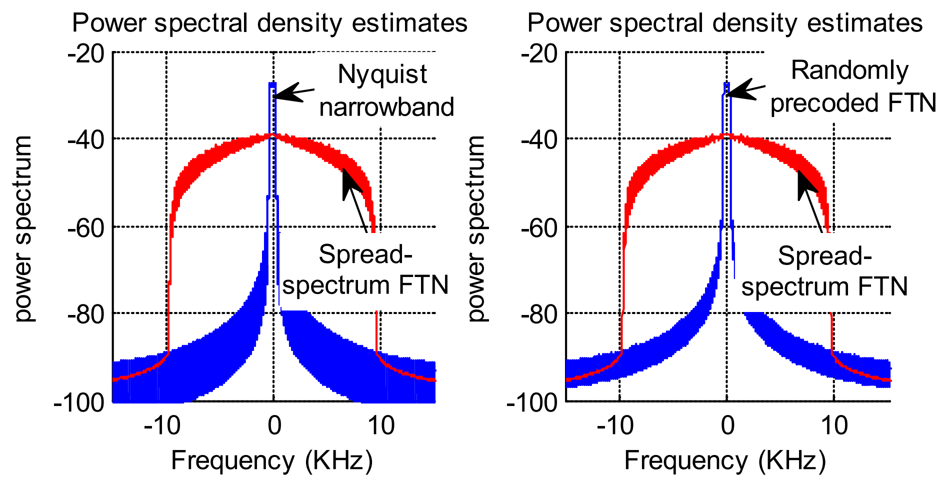

Figure 5.17 Power spectral density estimates of the generated spread-spectrum FTN signal (red), as compared to the original Nyquist narrowband signal and a randomly precoded FTN signal (both in blue). See text for details.

In Figure 5.18, we show bit error rate (BER) performance of the spread-spectrum FTN signal using hard decision demodulation after the FTN de-spreader in Figure 5.15. The definition of the signal-to-noise ratio (SNR) was $SNR = P/N_0$ where P is the available power and the information rate was computed by $KN/((N+1)T)$ (in bits/second). Figure 5.18 shows that the spread-spectrum FTN signal has nearly the same performance as the narrowband Nyquist counterpart; thus demonstrating feasibility of the proposed scheme.

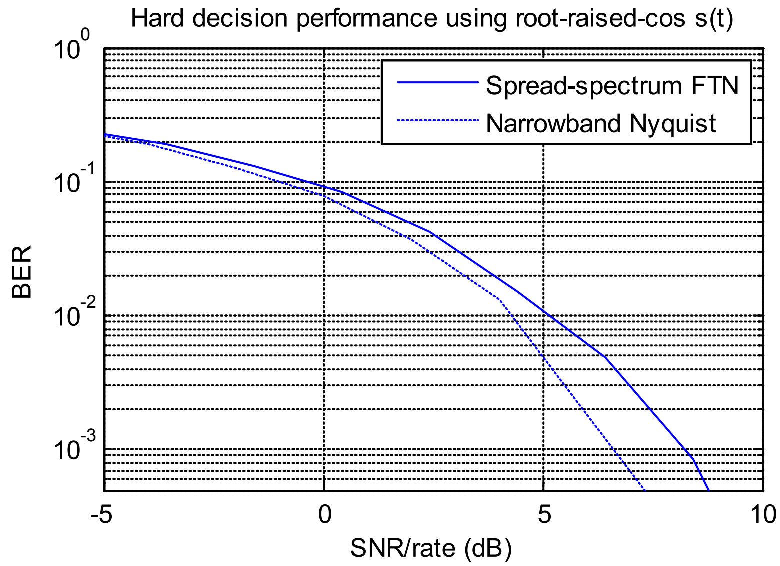

Figure 5.18 Hard decision bit error rate performances of the proposed spread-spectrum FTN system compared to the BER performance of the conventional (narrowband) Nyquist system.

5.4 Chapter Summary

The main objective of this chapter was to study, evaluate and optimize the merits of precoding in FTN-based data communication. We considered two types of precoding, namely, previously proposed convolutional FTN precoding in section 5.1 and the information-theoretically optimal FTN precoding derived in section 5.2. Furthermore, we also proposed an application of the pre-coded FTN signalling to achieve spread-spectrum digital communication in section 5.3.

In particular, it was first shown that convolutional FTN precoding can increase the capacity of the non-precoded FTN signaling by spectrum reshaping. Consequently, the optimal (non-convolutional) FTN precoding, derived in section 5.2, yielded substantial capacity gains when compared to the non-precoded FTN transmission. However, this FTN capacity increase occurred at a price of either a large bandwidth expansion for strictly non-bandlimited pulses or a significant numerical instability encountered for strictly-bandlimited modulating pulses. We further explored in section 5.3 a potential application of the precoded FTN signaling to generate spread-spectrum signals. Specific system architecture was proposed and its BER performance evaluated.

Chapter 6

Faster than Nyquist Broadcasting

This chapter describes a novel concept of using the faster than Nyquist (FTN) signaling to achieve transmission over broadcast channels, by multiplexing signals corresponding to multiple users' messages using different time-offsets in the *continuous-time domain*. This method is further shown to be *capacity-wise optimal* in the Gaussian broadcast channel, which implies that the described FTN broadcasting technique can be a viable alternative to the currently known capacity-achieving techniques in the Gaussian broadcast channel, e.g., superposition coding [28] and dirty paper coding [27]. Consequently, two FTN-based broadcast transceiver architectures are proposed that can perform close to the capacity boundaries of the Gaussian broadcast channels. In the FTN broadcasting, the users' data are completely separated in the coding stage and are explicitly transmitted over the channel. This alleviates the definition of auxiliary random variables in the channel coding theorems and eliminates joint encoding, which is required in the previously proposed capacity-achieving techniques.

Section 6.1 first gives a general overview of the Gaussian broadcast channel model and its capacity region. The concept of the FTN broadcasting in the continuous-time Gaussian broadcast channels is then formulated in section 6.2 and its information-theoretic optimality in the Gaussian broadcast channel is established in section 6.3. Subsequently, two FTN-based broadcasting receiver architectures are presented in section 6.4. The simulation results presented in section 6.5 show that the FTN broadcasting can perform close to the capacity boundaries of the broadcast channels.

6.1 Introduction to Gaussian Broadcast Channels

Figure 6.1 illustrates a wireless downlink channel with two receivers accepting two separate streams of data (e.g., two separate phone calls, music files, or streaming videos). Widely employed broadcasting strategy in practice is transmission of the two messages one after the other in a *time-sharing* fashion, or separating the messages in the frequency domain.

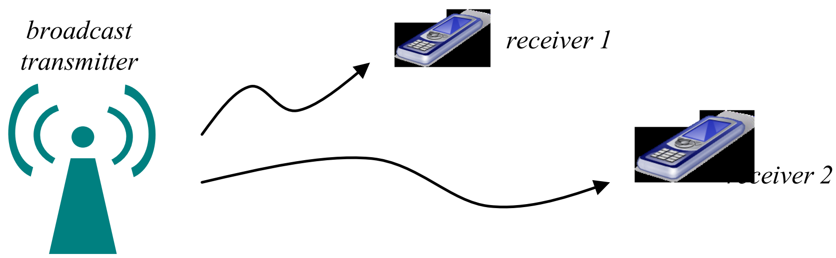

Figure 6.1 Two-user wireless downlink channel with private messages

From an information theoretic perspective, the primary question in broadcast channel is how much capacity gain the broadcast channel coding can provide upon traditional time-sharing or the frequency-division broadcasting. In 1972, Cover showed that the broadcast channel coding can in general yield superior capacity than the time-sharing or frequency-division broadcasting [28]. Coding in broadcast channel involves multiplexing messages of multiple users into one stream of channel symbols, such that the messages can be reliably recovered at the receivers.

In this chapter, we focus on an important class of broadcast channels known as the Gaussian broadcast channel. In particular, we consider the continuous-time Gaussian broadcast channel with one broadcasting transmitter and K receivers, as shown in Figure 6.2.

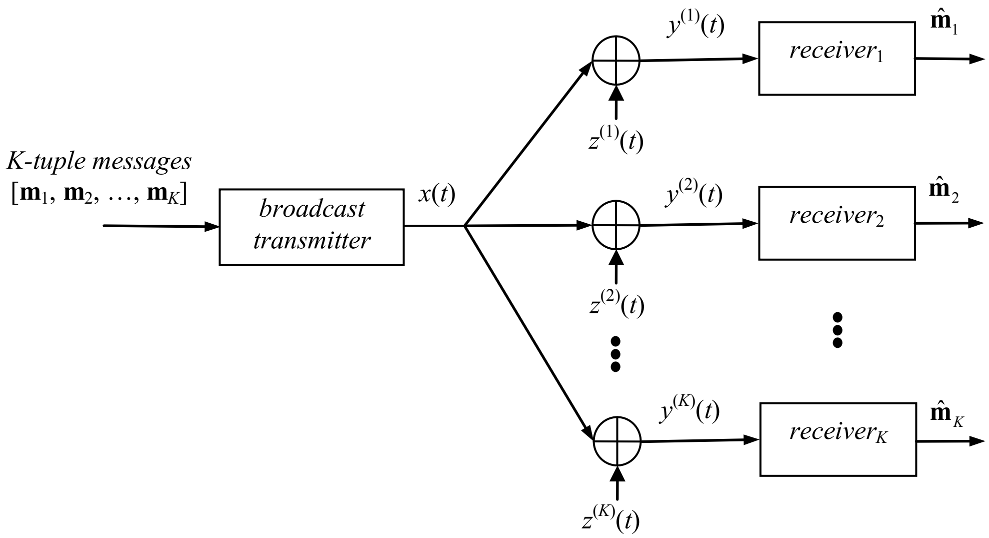

Figure 6.2 *K*-user continuous-time Gaussian broadcast channel

This model may represent certain wireless downlink channels, e.g., K wireless devices downloading separate data streams from a base station transmitter. The transmitter encodes the K *independent* message vectors of length N, $\mathbf{m}_1, \mathbf{m}_2, \ldots, \mathbf{m}_K$, which are intended for the respective K receivers, into a continuous-time bandlimited signal $x(t)$ with a bandwidth of W Hz. The signal $x(t)$ is then broadcast to K receivers, where it gets perturbed by independent additive white Gaussian noise (AWGN) signals $z^{(1)}(t), z^{(2)}(t), \ldots, z^{(K)}(t)$ with zero mean and two-sided power spectral densities $N_0^{(1)}/2$, $N_0^{(2)}/2$, …, $N_0^{(K)}/2$, respectively. Without loss of generality, we will assume that $N_0^{(1)} \le N_0^{(2)} \le \ldots \le N_0^{(K)}$, meaning that the receivers are indexed according to increasing noise strengths and decreasing quality of signal receptions. The broadcasting transmitter is further assumed to know this ordering (but not necessarily the precise noise value of each receiver) through channel sounding or periodic feedbacks from receivers.

Furthermore, all K communication links in the broadcast channel are assumed to have a common channel bandwidth of W Hz, and hence, the corresponding Nyquist signaling rate is given by $1/T = 2W$ symbols per second. Finally, the channel signal-to-noise ratio (SNR) at the k-th receiver will be defined by $SNR_k = PT/(N_0^{(k)}/2)$, where P is the available transmission power in watts.

The capacity region of the K-user continuous-time bandlimited Gaussian broadcast channel is known and is given by a set of K-tuple spectral efficiencies (η_1, η_2, …, η_K) in bits per second per Hz, such that [28], [16]

$$\eta_k \leq \log_2\left(1+\frac{P_k}{\sum_{j=1}^{k-1} P_j + N_0^{(k)} W}\right) \text{ for } k \in \{1, 2, \ldots, K\}. \tag{6.1}$$

Note that in (6.1), the available transmit power P is split to K non-negative parts, P_1, P_2, …, P_K such that $\sum_{k=1}^{K} P_k = P$, for encoding of the K users' messages (i.e., P_1 is used to encode user 1's message, P_2 is used to encode user 2's messages, etc.). The achievability of the capacity region (6.1) assumes that these power assignments P_1, P_2, …, P_K are known at all receivers. The capacity region (6.1) is also derived with the assumption that the conventional Nyquist rate transmission and standard matched filtering are used at the transmitter and the receivers, respectively.

The two widely-known techniques in the literature that can achieve the capacity boundaries of Gaussian broadcast channel (6.1) are the superposition coding [28], [16] and the dirty paper coding [27]. Recently, near-capacity performances using these two coding techniques are reported in the literature (see e.g., [138], [17], [152], [114], [3], [166]). Although these two coding schemes are conceptually well-understood, applying them in practical systems turned out to be challenging and many of the presently used broadcasting standards still operate using the suboptimal time-sharing and frequency-division broadcasting techniques.

The capacity region (6.1) of the two-user (K=2) Gaussian broadcast channel is plotted in Figure 6.3 for various SNR pairs of the two receivers. For comparison purposes, the maximum achievable rate regions when the two-user messages are broadcasted using the *time-sharing* strategy are also plotted in dashed lines in Figure 6.3. One can observe that when $SNR_1 = SNR_2$ (as in Figure 6.3a), the time-sharing broadcasting achieves the capacity of the Gaussian broadcast channel, making the broadcast channel coding unnecessary in this case. As the differences of the two channel SNRs increase (as in Figure 6.3b through Figure 6.3d), however, the broadcast channel coding starts dominating the time-sharing strategy. Consequently, the coding should be used if the broadcast channel is asymmetrical as in typical *wireless downlink channels* where mobile receivers are in different locations and thus have different SNR characteristics.

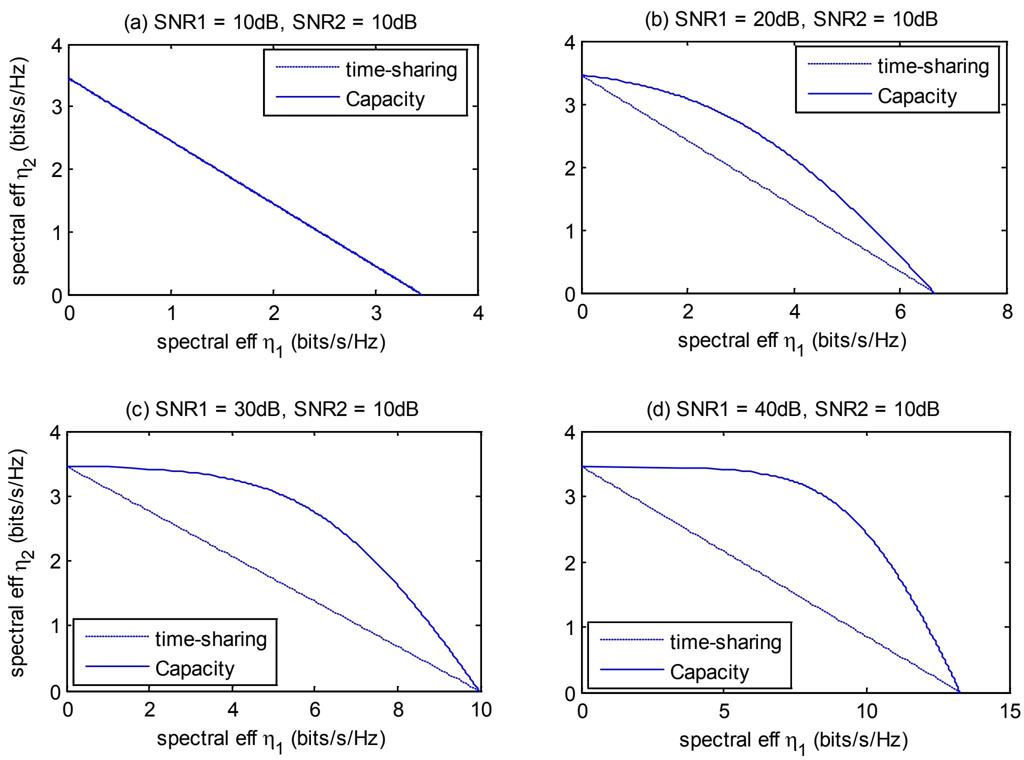

Figure 6.3 Capacity regions of two-user Gaussian broadcast channel and the time-sharing rate regions for various *SNR* pairs; *SNR*$_1$ is 10dB through 40dB, and *SNR*$_2$ is 10dB

The capacity region (6.1) is achieved by transmitting Gaussian-distributed input symbols. On the other hand, when the practical finite symbol constellations such as PAM, QAM or PSK are used, the corresponding achievable throughput (or the input-constellation constrained capacity region) is smaller and can be derived as follows. First let X_1, X_2, …, X_K be the symbol constellations used by the K receivers, respectively. Due to the power splitting (i.e., splitting P into P_1, P_2, …, P_K), the input constellations should be chosen such that X_1 uses power P_1 and X_2 uses power P_2, etc. (e.g., for 4-PAM equi-probable modulation formats, $\mathsf{X}_k \in \{-3A_k, -A_k, +A_k, +3A_k\}$, where $A_k = \sqrt{P_k T/5}$). Then, the input-constellation constrained capacity region is given by [17], [114]

$$\eta_k \le (TW)^{-1} C_{\mathsf{X}_k}\left(\sum\nolimits_{j=1}^{k-1} P_j T + N_0^{(k)}/2\right) \text{ for } k \in \{1,2,\ldots,K\}, \tag{6.2}$$

where

$$C_{\mathsf{X}_k}(\sigma^2) = \log_2|\mathsf{X}_k| - \frac{1}{|\mathsf{X}_k|}\sum_{x\in\mathsf{X}_k} E_{Y|X}\left\{\log_2 \sum_{x'\in\mathsf{X}_k} \exp\left(\frac{(y-x)^2-(y-x')^2}{2\sigma^2}\right)\right\}. \tag{6.3}$$

In (6.3), $Y = X + Z$ with $Z \sim \mathsf{N}(0,\sigma^2)$ and the conditional expectation $E_{Y|X}\{\cdot\}$ can be computed numerically. The expression (6.2) further allows numerical computation of the minimum allowable $SNR_k = PT/(N_0^{(k)}/2)$ for a given spectral efficiency η_k under the symbol constellation constraints.

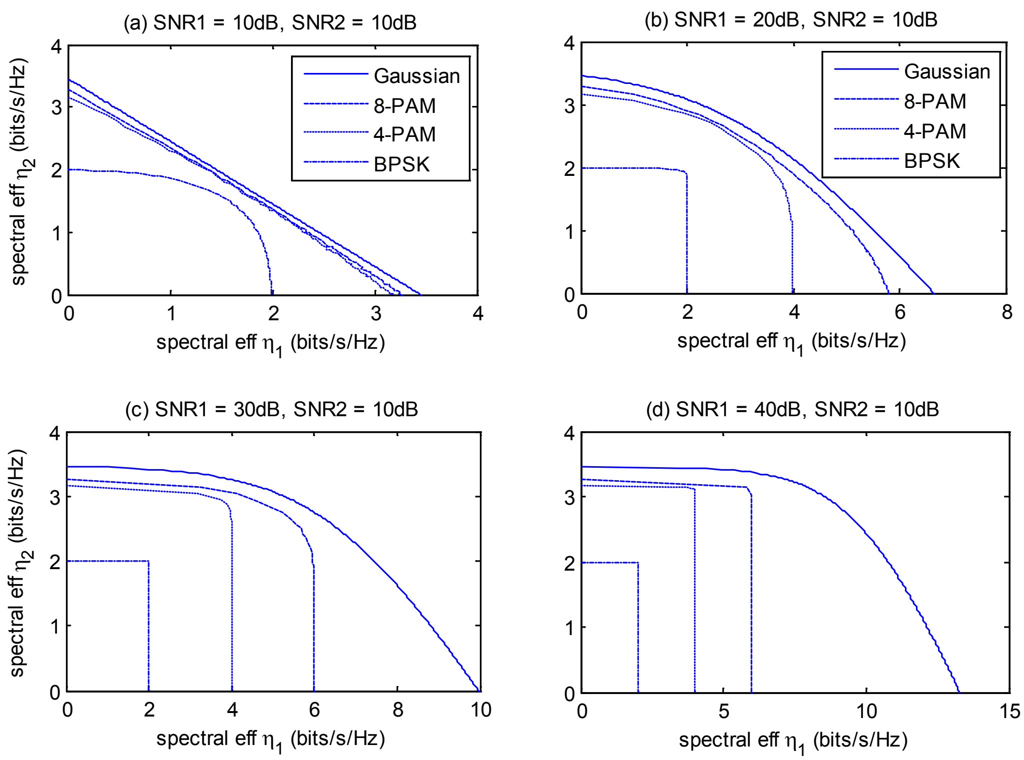

Figure 6.4 Input-constellation constrained capacity regions of two-user Gaussian broadcast channel for various *SNR* pairs; SNR_1 is 10dB through 40dB, and SNR_2 is 10dB

Figure 6.4 plots BPSK, 4-PAM, and 8-PAM input constrained capacity regions of two-user Gaussian broadcast channel for varying SNR pairs. In addition, the unconstrained Gaussian-input capacity regions are also plotted for comparison purposes. Due to the limited symbol constellations, BPSK, 4-PAM, and 8-PAM limit the maximum achievable spectral efficiencies to 2 bits/s/Hz, 4 bits/s/Hz, and 6 bits/s/Hz respectively. As practical digital communication systems use finite inpute constellations, we will use the input-contellation constrained capacity region (6.2) as an appropriate capacity benchmark for our simulated broadcast coding systems in section 6.5.

6.2 Proposed FTN Broadcasting and its Channel Model

This section describes a new method of using FTN signaling to achieve transmission over Gaussian broadcast channels. First, a system block diagram of the FTN signaling over K-user continuous-time Gaussian broadcast channel is shown in Figure 6.5.

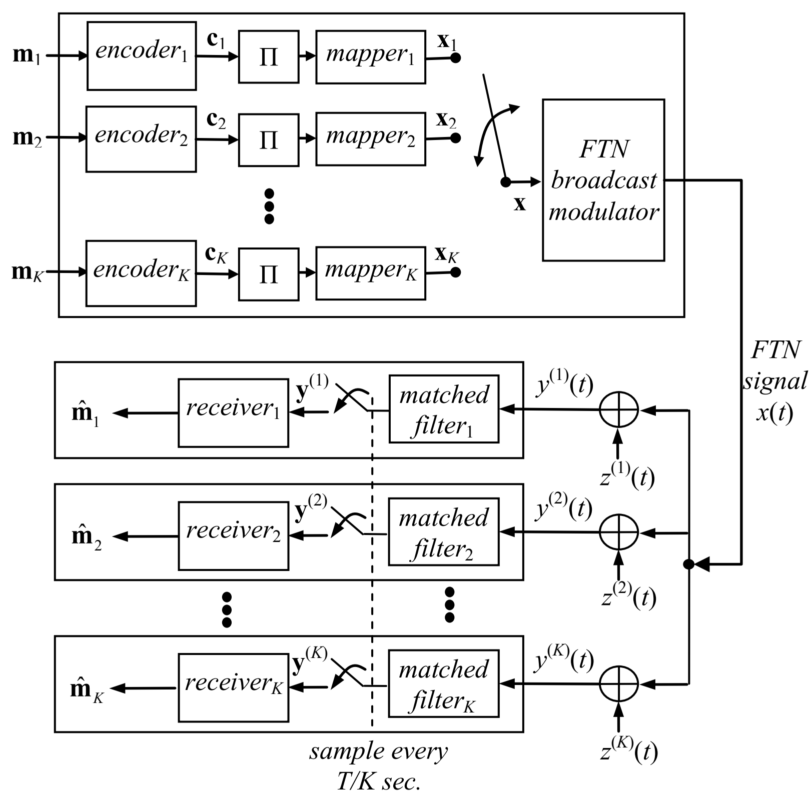

Figure 6.5 System block diagram of faster than Nyquist broadcasting over a *K*-user continuous-time Gaussian broadcast channel

At the FTN broadcast transmitter, the K users' message vectors $\mathbf{m}_1$, $\mathbf{m}_2$, …, $\mathbf{m}_K$ are *separately* encoded by user-specific error control encoders, interleaved, and subsequently mapped onto separate user-specific signal constellations (e.g., PAM, QAM, or PSK) by the mapping devices. The resulting K-user data symbol vectors $\mathbf{x}_1$, $\mathbf{x}_2$, …, $\mathbf{x}_K$ are then passed to the FTN broadcast modulator which generates the FTN signal $x(t)$ given by

$$x(t) = \sum_{k=1}^{K}\sum_{n=0}^{N-1} x_k[n]s\left(t - nT - (k-1)T/K\right), \tag{6.4}$$

where $x_k[n]$ denotes the n-th data symbol of k-th user data symbol vector $\mathbf{x}_k = \left[x_k[0], x_k[1], \cdots, x_k[N-1]\right]$, $1/T$ is the Nyquist rate of the channel, and $s(t)$ is a T-orthogonal unit energy modulating pulse[33] (assumed to be real valued for brevity). The available average transmit power P is split to K non-negative parts P_1, P_2, …, P_K such that $P = \sum_{k=1}^{K} P_k$, for transmission of each user's data symbols $x_k[n]$. The FTN signal $x(t)$ is also illustrated in Figure 6.6 for the case of three users $K = 3$.

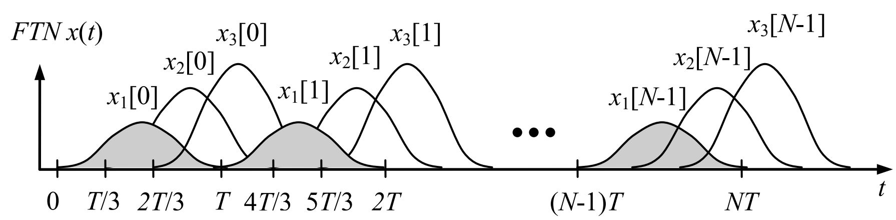

Figure 6.6 Illustration of faster than Nyquist broadcast signal $x(t)$ carrying three-user messages (signals corresponding to user 1's message is shaded for an illustration)

Note that the modulation symbols are transmitted in the following order: $x_1[0]$, $x_2[0]$, …, $x_K[0]$, $x_1[1]$, $x_2[1]$, …, $x_K[1]$, …, $x_1[N\text{-}1]$, $x_2[N\text{-}1]$, …, $x_K[N\text{-}1]$. Accordingly, we define a combined data symbol vector by $\mathbf{x}$ = [$x_1[0], x_2[0], \cdots, x_K[0]$, $x_1[1], x_2[1], \cdots, x_K[0]$, …, $x_1[N-1], x_2[N-1], \cdots, x_K[N-1]$], and hence

$$x_k[n] = x[Kn + (k-1)], \text{ for } n = 0, 1, \ldots, N-1 \text{ and } k = 1, 2, \ldots, K. \tag{6.5}$$

Using this definition, we may rewrite (6.4) simply as

$$x(t) = \sum_{n=0}^{KN-1} x[n]s\left(t - nT/K\right), \tag{6.6}$$

---

[33] The T-orthogonal modulating pulses $s(t)$ refer to pulses that are orthogonal T-seconds apart, i.e., $\int_{-\infty}^{\infty} s(t)s^*(t-nT)dt = 0$ for all integer $n \neq 0$.

where $\mathbf{x} = [x[0], x[1], \ldots, x[KN\text{-}1]]^T$ represents the combined data symbol vector (note the resemblance of (6.6) with the definition of the FTN signal $x(t)$ from the earlier chapters).

We note that unlike in traditional broadcast channel coding where K messages must be *jointly* encoded to produce one data symbol at each symbol interval, FTN can transmit the all K data symbols $x_1[n]$, $x_2[n]$, …, $x_K[n]$ *explicitly* and *separately* over the channel by increasing the number of channel uses per second. Furthermore, the considered FTN broadcasting does not incur any bandwidth expansion for *i.i.d.* data symbols $x[n]$ as proved in section 3.4.

The transmitted FTN signal $x(t)$ is then broadcast to K separate receivers as shown in Figure 6.5, where $x(t)$ gets perturbed by K independent additive white Gaussian noise (AWGN) signals $z^{(1)}(t)$, $z^{(2)}(t)$, …, $z^{(K)}(t)$ with zero mean and two-sided power spectral densities $N_0^{(1)}/2$, $N_0^{(2)}/2$, …, $N_0^{(K)}/2$, respectively. Without loss of generality, we assume that $N_0^{(1)} \le N_0^{(2)} \le \ldots \le N_0^{(K)}$, meaning that the receivers are indexed according to increasing noise strengths and decreasing quality of signal receptions. As before, the broadcasting transmitter is further assumed to know this ordering (but not necessarily the precise noise value of each receiver) through channel sounding or periodic feedbacks from receivers.

At the K individual receivers (see Figure 6.5), the noisy signals $y^{(1)}(t)$, $y^{(2)}(t)$, …, $y^{(K)}(t)$ are passed to respective matched filters with the impulse response $s(-t)$ and then sampled at every T/K seconds (i.e., at the FTN signaling rate). With the convention that $x[n] = 0$ for $n < 0$ and $n > KN\text{-}1$, the n-th sample at the k-th receiver, $y^{(k)}[n]$, can be written as

$$y^{(k)}[n] = \sum_{l=-L}^{L} h_l x[n-l] + z^{(k)}[n], \; n = 0,1,\ldots,KN-1, \tag{6.7}$$

where the integer parameter L determines the memory length of the FTN-induced intersymbol interference (ISI), which can be appropriately chosen depending on the support of the pulse correlation coefficients $\{h_l\}$:

$$h_l = \int_{-\infty}^{+\infty} s(t)\, s(t - l \cdot T/K)\, dt, \; l \in \{-L, -L+1, \cdots, 0, \cdots, L\}. \tag{6.8}$$

The noise sample after the k-th receiver matched filter, $z^{(k)}[n] = \int_{-\infty}^{\infty} z^{(k)}(t) s(t - nT/K) dt$, is Gaussian distributed with a zero mean and an autocorrelation

$$E\left\{z^{(k)}[n]z^{(k)}[m]\right\} = (N_0^{(k)}/2)\cdot h_{m-n},\ m,n \in \mathbb{Z}\ . \tag{6.9}$$

For convenience, the equation (6.7) can also be expressed in a matrix form:

$$\mathbf{y}^{(k)} = H\mathbf{x} + \mathbf{z}^{(k)},\ \text{for } k = 1,2,\ldots,K, \tag{6.10}$$

where $\mathbf{y}^{(k)} = [y^{(k)}[0], y^{(k)}[1], \cdots, y^{(k)}[KN{-}1]]^T$, $\mathbf{x} = [x[0], x[1], \ldots, x[KN-1]]^T$ with $x[n]$ as in (6.5). Note that H is a symmetric Toeplitz matrix defined by $H = [h_{i-j}]_{i,j=0,1,\cdots,KN-1}$, i.e.,

$$H \equiv \begin{bmatrix} 1 & h_{-1} & h_{-2} & \cdots & h_{-(KN-1)} \\ h_1 & 1 & h_{-1} & \cdots & h_{-(KN-2)} \\ h_2 & h_1 & 1 & \cdots & h_{-(KN-3)} \\ \vdots & \vdots & \vdots & \ddots & \vdots \\ h_{KN-1} & h_{KN-2} & h_{KN-3} & \cdots & 1 \end{bmatrix}, \tag{6.11}$$

where h_{i-j} is as defined in (6.8). Finally, the zero mean additive Gaussian noise vector $\mathbf{z}^{(k)} = [z^{(k)}[0], z^{(k)}[1], \cdots, z^{(k)}[KN{-}1]]^T$ is *correlated* as seen in (6.9) and has a covariance matrix:

$$E\left\{\mathbf{z}^{(k)}(\mathbf{z}^{(k)})^T\right\} = (N_0^{(k)}/2)H\ . \tag{6.12}$$

Note that the above correlation occurs due to the sampling of the filtered noise faster than the Nyquist rate at the receivers.

6.3 Optimality of the Proposed FTN Broadcast Signaling

In this section, we prove that the considered FTN broadcasting allows achieving the capacity boundary of K-user continuous-time Gaussian broadcast channel[34]. Throughout this section, we will assume that the K-user data symbol vector $\mathbf{x}$ is zero mean Gaussian distributed. We will show that the capacity of the Gaussian broadcast channel is achieved with this choice of $\mathbf{x}$, meaning that there is no loss in assuming such an $\mathbf{x}$. We will also assume that the strictly bandlimited modulating pulse $s(t) = (2W)^{1/2}\text{sinc}(2Wt)$ is being used throughout. Furthermore, $\mathbf{x}$ has the following $KN{\times}KN$ *diagonal* covariance matrix K_x:

[34] We have reported a special case of *2-user* Gaussian broadcast channel in [78], which has a simpler and more compact proof.

$$K_x = I_N \otimes diag(P_1T, P_2T, \cdots, P_KT), \tag{6.13}$$

where $\otimes$ denotes the Kronecker product of matrices (Definition 2.14), and $diag(\cdot)$ denotes a diagonal matrix with the diagonal entries given by its arguments. Note also that the maximum available power P is split into K non-negative parts, P_1, P_2, …, P_K such that $\sum_{k=1}^{K} P_k = P$, for encoding of the K users' messages.

We first present and prove the following two lemmas.

Lemma 6.1 (Mutual information of partial user input given the rest): *Consider the discrete-time FTN channel model (6.10) with independent data symbols* $\mathbf{x} \sim \mathcal{N}(\mathbf{0}, K_x)$ *and diagonal covariance matrix* K_x *given by (6.13). Then, the mutual information between random vectors* $\mathbf{y}^{(k)}$ *and* ($\mathbf{x}_1$, $\mathbf{x}_2$, …, $\mathbf{x}_i$), *conditioned on* ($\mathbf{x}_{i+1}$, $\mathbf{x}_{i+2}$, …, $\mathbf{x}_K$)*, is given by the following*[35] *for* $i = 1, 2, \cdots, K$:

$$\lim_{N\to\infty} \frac{1}{NT} I\left(\mathbf{y}^{(k)}; (\mathbf{x}_1, \cdots, \mathbf{x}_i) \middle| \mathbf{x}_{i+1}, \cdots, \mathbf{x}_K\right) = W \log_2\left(1 + \frac{\sum_{j=1}^{i} P_j}{N_0^{(k)} W}\right). \tag{6.14}$$

Proof: The proof of Lemma 6.1 can be found in Subsection 6.3.1. ■

Lemma 6.2 (Mutual information of i^{th} user input given partial information): *Consider the discrete-time FTN channel model (6.10) with independent data symbols* $\mathbf{x} \sim \mathcal{N}(\mathbf{0}, K_x)$ *and diagonal covariance matrix* K_x *given by (6.13). Then, for* i=1, 2, ⋯, K−1, *the mutual information between random vectors* $\mathbf{y}^{(k)}$ *and* $\mathbf{x}_i$, *conditioned on* ($\mathbf{x}_{i+1}$, $\mathbf{x}_{i+2}$, …, $\mathbf{x}_K$)*, is given by the following:*

$$\lim_{N\to\infty} \frac{1}{NT} I\left(\mathbf{y}^{(k)}; \mathbf{x}_i \middle| \mathbf{x}_{i+1}, \cdots, \mathbf{x}_K\right) = W \log_2\left(1 + \frac{P_i}{\sum_{j=1}^{i-1} P_j + N_0^{(k)} W}\right). \tag{6.15}$$

Proof: Applying multiple times the chain rule of mutual information from Lemma 2.2 to (6.15), we have the following series of equalities:

[35] When $i = K$, (6.14) is interpreted as $\lim_{N\to\infty} (NT)^{-1} I\left(\mathbf{y}^{(k)}; \mathbf{x}\right) = W \log_2\left(1 + P/(N_0^{(k)} W)\right)$.

$$\lim_{N\to\infty}\frac{1}{NT}I\left(\mathbf{y}^{(k)};\mathbf{x}_i\middle|\mathbf{x}_{i+1},\cdots,\mathbf{x}_K\right)$$
$$=\lim_{N\to\infty}\frac{1}{NT}\left[I\left(\mathbf{y}^{(k)};\left(\mathbf{x}_i,\cdots,\mathbf{x}_K\right)\right)-I\left(\mathbf{y}^{(k)};\left(\mathbf{x}_{i+1},\cdots,\mathbf{x}_K\right)\right)\right] \tag{6.16}$$

$$\begin{aligned}=\lim_{N\to\infty}\frac{1}{NT}\Big[&I\left(\mathbf{y}^{(k)};\left(\mathbf{x}_1,\cdots,\mathbf{x}_K\right)\right)-I\left(\mathbf{y}^{(k)};\left(\mathbf{x}_1,\cdots,\mathbf{x}_{i-1}\right)\middle|\mathbf{x}_i,\cdots,\mathbf{x}_K\right)\\&-\left(I\left(\mathbf{y}^{(k)};\left(\mathbf{x}_1,\cdots,\mathbf{x}_K\right)\right)-I\left(\mathbf{y}^{(k)};\left(\mathbf{x}_1,\cdots,\mathbf{x}_i\right)\middle|\mathbf{x}_{i+1},\cdots,\mathbf{x}_K\right)\right)\Big]\end{aligned} \tag{6.17}$$

$$=\lim_{N\to\infty}\frac{1}{NT}\left[I\left(\mathbf{y}^{(k)};\left(\mathbf{x}_1,\cdots,\mathbf{x}_i\right)\middle|\mathbf{x}_{i+1},\cdots,\mathbf{x}_K\right)-I\left(\mathbf{y}^{(k)};\left(\mathbf{x}_1,\cdots,\mathbf{x}_{i-1}\right)\middle|\mathbf{x}_i,\cdots,\mathbf{x}_K\right)\right] \tag{6.18}$$

$$=W\log_2\left(1+\frac{\sum_{j=1}^{i}P_j}{N_0^{(k)}W}\right)-W\log_2\left(1+\frac{\sum_{j=1}^{i-1}P_j}{N_0^{(k)}W}\right) \tag{6.19}$$

$$=W\log_2\left(1+\frac{P_i}{\sum_{j=1}^{i-1}P_j+N_0^{(k)}W}\right), \tag{6.20}$$

where (6.16)-(6.18) are due to applying multiple times the chain rule of mutual information from Lemma 2.2, (6.19) is due to Lemma 6.1, and (6.20) follows from combining the logarithms. This completes the proof of Lemma 6.2. ■

Using the two preceding lemmas, we now prove the optimality of FTN broadcasting over *K*-user Gaussian broadcast channel.

Theorem 6.1 (Optimality of faster than Nyquist broadcasting): *The FTN transmission can achieve the capacity boundaries of the continuous-time K-user Gaussian broadcast channel with Nyquist rate signaling that is given by:*

$$\eta_k\le\log_2\left(1+\frac{P_k}{\sum_{j=1}^{k-1}P_j+N_0^{(k)}W}\right)\ \textit{for}\ k=1,2,\ldots,K. \tag{6.21}$$

Proof: An *achievable spectral-efficiency region* of the FTN signaling on K-user Gaussian broadcast channel (in bits per second per Hz)[36] is the set of spectral-efficiency tuples (η_1, η_2, …, η_K) such that

$$\eta_k \leq \lim_{N\to\infty} \frac{1}{NTW} I\left(\mathbf{y}^{(k)}; \mathbf{x}_k \middle| \mathbf{x}_{k+1}, \cdots, \mathbf{x}_K\right) \text{ for } k = 1, 2, \ldots, K. \tag{6.22}$$

The achievability of the region above follows from the Cover's coding principle of the degraded broadcast channel [28], which can be stated as follows:

1. The K^{th} receiver, with the worst SNR among all receivers[37], decodes its own message $\mathbf{x}_K$ from its channel observation $\mathbf{y}^{(K)}$ while treating all the other users' messages $\mathbf{x}_1$, …, $\mathbf{x}_{K-1}$ as another source of noise. Consequently, due to the channel coding theorem, $\mathbf{x}_K$ can be decoded with arbitrarily small probability of error as long as $\eta_K \leq \lim_{N\to\infty}(NTW)^{-1} I(\mathbf{y}^{(K)}; \mathbf{x}_K)$.
2. On the other hand, the $(K-1)^{\text{th}}$ receiver first decodes the K^{th} user message $\mathbf{x}_K$ from its channel observation $\mathbf{y}^{(K-1)}$, before decoding its own message $\mathbf{x}_{K-1}$. Note that this receiver can successfully decode $\mathbf{x}_K$ with arbitrary small probability of error due to having a higher SNR than the K^{th} receiver (in other words, if the K^{th} receiver with the worst SNR can decode $\mathbf{x}_K$, the $(K\text{-}1)^{\text{th}}$ receiver with better SNR can also decode $\mathbf{x}_K$). Consequently, the $(K\text{-}1)^{\text{th}}$ receiver can decode its own message $\mathbf{x}_{K-1}$ with the complete knowledge of $\mathbf{x}_K$, leading to the requirement: $\eta_{K-1} \leq \lim_{N\to\infty}(NTW)^{-1} I(\mathbf{y}^{(K-1)}; \mathbf{x}_{K-1} | \mathbf{x}_K)$.
3. Successively applying the concept of step 2, i.e., decoding $\mathbf{x}_K$, $\mathbf{x}_{K-1}$, …, $\mathbf{x}_{k+1}$ first before decoding $\mathbf{x}_k$ at k-th receiver, leads to the requirements (6.22) for all $k = 1, 2, \ldots, K$.

We will now show that the achievable region (6.22) is precisely equal to the capacity region of the K-user Gaussian broadcast channel (6.21). This means that the achievable region is in fact the capacity region of FTN and the FTN transmission is *optimal* in the K-

[36] Note that the mutual information in bits per second per Hz needs to be normalized by NTW seconds. This is because the total time duration of the FTN signal $x(t)$ is about NT seconds (see Figure 6.6), plus $(K\text{-}1)T/K$ which is negligible compared to NT for N sufficiently large.

[37] This is due to the assumption $N_0^{(1)} \leq N_0^{(2)} \leq \cdots \leq N_0^{(K)}$.

user Gaussian broadcast channel. For the cases $k = 1, 2, \ldots, K-1$, the rate region (6.22) is evaluated to the following expression using Lemma 6.2:

$$\lim_{N\to\infty} \frac{1}{NTW} I\left(\mathbf{y}^{(k)}; \mathbf{x}_k \middle| \mathbf{x}_{k+1}, \cdots, \mathbf{x}_K\right) = \log_2\left(1 + \frac{P_k}{\sum_{j=1}^{k-1} P_j + N_0^{(k)} W}\right), \; k = 1,2,\ldots,K-1, \quad (6.23)$$

which is precisely equal to the capacity region of Gaussian broadcast channel (6.21). In the special case $k = K$, the spectral-efficiency region (6.22) can be evaluated as follows:

$$\lim_{N\to\infty} \frac{1}{NTW} I\left(\mathbf{y}^{(K)}; \mathbf{x}_K\right)$$

$$= \lim_{N\to\infty} \frac{1}{NTW}\left[I\left(\mathbf{y}^{(K)}; (\mathbf{x}_1, \cdots, \mathbf{x}_{K-1}, \mathbf{x}_K)\right) - I\left(\mathbf{y}^{(K)}; (\mathbf{x}_1, \cdots, \mathbf{x}_{K-1}) \middle| \mathbf{x}_K\right)\right] \quad (6.24)$$

$$= \lim_{N\to\infty} \frac{1}{NTW}\left[I\left(\mathbf{y}^{(K)}; \mathbf{x}\right) - I\left(\mathbf{y}^{(K)}; (\mathbf{x}_1, \cdots, \mathbf{x}_{K-1}) \middle| \mathbf{x}_K\right)\right] \quad (6.25)$$

$$= \log_2\left(1 + \frac{P}{N_0^{(K)} W}\right) - \log_2\left(1 + \frac{\sum_{j=1}^{K-1} P_j}{N_0^{(K)} W}\right) \quad (6.26)$$

$$= \log_2\left(\frac{P_K + \sum_{j=1}^{K-1} P_j + N_0^{(K)} W}{\sum_{j=1}^{K-1} P_j + N_0^{(K)} W}\right) \quad (6.27)$$

$$= \log_2\left(1 + \frac{P_K}{\sum_{j=1}^{K-1} P_j + N_0^{(K)} W}\right), \quad (6.28)$$

where (6.24) is due to the chain rule of mutual information from Lemma 2.2, (6.25) is due to the definition of the combined data symbol vector $\mathbf{x}$, (6.26) is by Lemma 6.1, and (6.27) is due to $\sum_{j=1}^{K} P_j = P$. We have therefore established that the capacity region of the FTN broadcasting is precisely equal to that of the K-user Gaussian broadcast channel. This completes the proof of Theorem 6.1. ■

Remark: The expression of the FTN spectral-efficiency regions (6.22) does not involve any auxiliary random variables, in contrast to the conventional capacity regions of the degraded broadcast channels[38]. This is because the number of channel use is increased by the FTN signaling, thus allowing all users' data symbols to explicitly enter the broadcast channel.

6.3.1 Proof of Lemma 6.1

The objective of this subsection is to prove Lemma 6.1, which is needed in establishing the optimality of faster than Nyquist broadcasting in K-user Gaussian broadcast channel. We first state and prove the following two propositions that will be useful in proving Lemma 6.1.

***Proposition 6.1* (*Spectrum of the FTN-induced ISI coefficients h_0, h_1, …, h_{KN-1}*):** *Let h_0, h_1, …, h_{KN-1} be the pulse correlation coefficients defined by $h_l = \int_{-\infty}^{+\infty} s(t)s(t-l\cdot T/K)dt$ for l = 0, 1, …, $KN-1$ and let us consider $s(t)=(2W)^{1/2}\mathrm{sinc}(2Wt)$. Then for $p = -(K-1), -(K-2), \ldots, K-1$, and over a frequency range $f \in [-W, W]$,*

$$\sum_{k=-\infty}^{\infty} h_{kK+p} e^{j2\pi f kT} = e^{j2\pi f\, pT/K}, \tag{6.29}$$

where T=1/(2W) is the Nyquist interval, K is a positive integer, and $j=\sqrt{-1}$ is the imaginary unit.

Proof of Proposition 6.1: By the definition of the pulse correlation coefficients h_l,

$$\sum_{k=-\infty}^{\infty} h_{kK+p} e^{j2\pi fkT} = \sum_{k=-\infty}^{\infty}\left(\int_{-\infty}^{\infty} s(t)s(t-kT-pT/K)dt\right)e^{j2\pi fkT} \tag{6.30}$$

$$= \sum_{k=-\infty}^{\infty}\left(\int_{-\infty}^{\infty} \left|\hat{s}(\lambda)\right|^2 e^{j2\pi\lambda(kT+pT/K)}d\lambda\right)e^{j2\pi fkT}, \tag{6.31}$$

[38] The capacity region of two-user degraded broadcast channel is the set of rate pairs (R_1, R_2) such that $R_1 \le I(X;Y_1|U)$, $R_2 \le I(U;Y_2)$, where U is called *auxiliary* random variable that is never transmitted over the channel [39]. The purpose of U is assist encoding/decoding of two users' messages M_1 and M_2 to/from a single transmission symbol X. In FTN broadcasting, definition of U is not necessary since all users' data symbols are explicitly transmitted over the channel.

where (6.31) is due to the generalized Parseval's theorem $\int_{-\infty}^{\infty} a(t)b^*(t)dt = \int_{-\infty}^{\infty} \hat{a}(f)\hat{b}^*(f)df$ and the delay property of the Fourier transform. For $s(t)=(2W)^{1/2}\text{sinc}(2Wt)$, its Fourier transform is given by $\hat{s}(f) = \sqrt{1/(2W)}$ over the frequency range $f \in [-W, W]$ and zero everywhere else. Hence, (6.31) can be further simplified as

$$\sum_{k=-\infty}^{\infty} h_{kK+p} e^{j2\pi fkT} = \sum_{k=-\infty}^{\infty} \left(\frac{1}{2W} \int_{-W}^{W} e^{j2\pi\lambda(kT+pT/K)} d\lambda \right) e^{j2\pi fkT} \tag{6.32}$$

$$= \frac{1}{2W} \int_{-W}^{W} e^{j2\pi\lambda pT/K} \left(\sum_{k=-\infty}^{\infty} e^{j2\pi(\lambda+f)kT} \right) d\lambda \tag{6.33}$$

$$= \frac{1}{2W} \int_{-W}^{W} e^{j2\pi\lambda pT/K} \left(\sum_{k=-\infty}^{\infty} \delta\big((\lambda+f)T-k\big) \right) d\lambda \tag{6.34}$$

$$= \int_{-1/2}^{1/2} e^{j2\pi\lambda p/K} \left(\sum_{k=-\infty}^{\infty} \delta\big(\lambda-(k-f/(2W))\big) \right) d\lambda, \tag{6.35}$$

where (6.33) is due to changing the order of summation and integral, (6.34) is due to the Poisson summation formula $\sum_{k=-\infty}^{\infty} e^{jk2\pi t} = \sum_{k=-\infty}^{\infty} \delta(t-k)$ and (6.35) is due to a change of variables and $T=1/(2W)$. It is not hard to see that only one impulse centered at $\lambda = -f/(2W)$ falls within the integral range of $\lambda \in [-1/2, 1/2]$ for any $f \in [-W, W]$. This implies that (6.35) can be simplified to

$$\sum_{k=-\infty}^{\infty} h_{kK+p} e^{j2\pi fkT} = \int_{-1/2}^{1/2} e^{j2\pi\lambda p/K} \delta\big(\lambda - f/(2W)\big) d\lambda \tag{6.36}$$

$$= e^{j2\pi fpT/K}. \tag{6.37}$$

This completes the proof of Proposition 6.1. ■

The next proposition deals with the FTN broadcasting scenario when the user data-symbol vectors $\mathbf{x}_{i+1}, \mathbf{x}_{i+2}, \ldots, \mathbf{x}_K$ are all equal to zero for $1 \le i \le K$ (in other words, when the power assignments $P_{i+1}, P_{i+2}, \ldots, P_K$ are all zeros).

Proposition 6.2: *Let Q_i be a (covariance) matrix defined by*

$$Q_i = I_N \otimes diag\left(P_1T, P_2T, \cdots, P_iT, 0, \cdots, 0\right) \text{ for } 1 \le i \le K, \tag{6.38}$$

where $\otimes$ denotes the Kronecker product of matrices, I_N is the $N\times N$ identity matrix, diag$(\cdot)$ denotes a diagonal matrix with diagonal entries given by its arguments, $T=1/(2W)$ is the Nyquist signaling interval, and P_1, P_2, …, P_i are non-negative real numbers. Then for any constant c,

$$\lim_{N\to\infty} \frac{1}{NT}\frac{1}{2}\log_2 \det\left(cQ_iH + I_{KN}\right) = W\log_2\left(1+\frac{c}{2W}\sum_{j=1}^{i}P_j\right), \tag{6.39}$$

where $H = [\text{sinc}((i-j)/K)\text{: } i,j=1,\ldots,KN]$ *using the strictly bandlimited modulating pulse* $s(t) = (2W)^{1/2}\text{sinc}(2Wt)$.

Proof of Proposition 6.2: The proof involves asymptotic analysis on the eigenvalues of Hermitian block Toeplitz matrices [58]. First, denoting $\lambda_j\{A\}$ by the j-th eigenvalue of the matrix A, we rewrite the left-hand-side of (6.39) as

$$\lim_{N\to\infty} \frac{1}{NT}\frac{1}{2}\log_2 \det\left(cQ_iH + I_{KN}\right) = \lim_{N\to\infty} \frac{1}{NT}\frac{1}{2}\log_2 \det\left(cQ_i^{1/2}HQ_i^{1/2} + I_{KN}\right) \tag{6.40}$$

$$= \lim_{N\to\infty} \frac{1}{NT}\frac{1}{2}\sum_{j=0}^{KN-1}\log_2\left(1+c\lambda_j\left\{Q_i^{1/2}HQ_i^{1/2}\right\}\right), \tag{6.41}$$

where (6.40) is due to the decomposition of the block diagonal matrix $Q_i = Q_i^{1/2}Q_i^{1/2}$, followed by the identity: $\log_2\det(AB+I) = \log_2\det(BA+I)$, and (6.41) is due to the identities: $\det(A) = \prod_j \lambda_j\{A\}$ and $\lambda_j\{I+A\} = 1+\lambda_j\{A\}$ for any Hermitian matrix A [55]. Note that H and $Q_i^{1/2}$ are two instances of Hermitian block Toeplitz matrices since they can be written as

$$H = \begin{bmatrix} H^{(0)} & H^{(-1)} & \cdots & H^{(-(N-1))} \\ H^{(1)} & H^{(0)} & \cdots & H^{(-(N-2))} \\ \vdots & \vdots & \ddots & \vdots \\ H^{(N-1)} & H^{(N-2)} & \cdots & H^{(0)} \end{bmatrix}, \quad Q_i^{1/2} = \begin{bmatrix} \left(Q_i^{1/2}\right)^{(0)} & & & \\ & \left(Q_i^{1/2}\right)^{(0)} & & \\ & & \ddots & \\ & & & \left(Q_i^{1/2}\right)^{(0)} \end{bmatrix}, \tag{6.42}$$

where $H^{(m)}$ for $m \in [-(N-1),\ (N-1)]$ are $K\times K$ Toeplitz matrices and $\left(Q_i^{1/2}\right)^{(0)}$ is a $K\times K$ diagonal matrix defined by $\left(Q_i^{1/2}\right)^{(0)} = diag\left(\sqrt{P_1T}, \sqrt{P_2T}, \cdots, \sqrt{P_iT}, 0, \cdots, 0\right)$.

The asymptotic eigenvalues of product of Hermitian block Toeplitz matrices can be characterized by the product of so-called 'spectrum' of the individual Toeplitz matrices [58]. Using this result and again denoting $\lambda_j\{A\}$ by the j-th eigenvalue of the matrix A, (6.41) can be evaluated as

$$\lim_{N\to\infty} \frac{1}{NT}\frac{1}{2}\sum_{j=0}^{KN-1} \log_2\left(1 + c\lambda_j\left\{Q_i^{1/2} H Q_i^{1/2}\right\}\right) = \frac{1}{2}\int_{-W}^{W}\sum_{j=0}^{K-1} \log_2\left(1 + c\lambda_j\left\{F(f)\right\}\right) df\ , \quad (6.43)$$

where $F(f)$ is a $K\times K$ matrix, known as the 'spectrum' of the product of block Toeplitz matrices, defined as

$$F(f) = \left(Q_i^{1/2}\right)^{(0)} \cdot \left(\sum_{m=-\infty}^{\infty} H^{(m)} e^{j2\pi fmT}\right) \cdot \left(Q_i^{1/2}\right)^{(0)}. \quad (6.44)$$

Hence, in order to further evaluate (6.43), we need to determine the eigenvalues of $F(f)$ for $f \in [-W,W]$. First, recall the definition of $H^{(m)}$ as the m-th block matrix of H, i.e.,

$$H^{(m)} = \begin{bmatrix} h_{mK} & h_{mK-1} & \cdots & h_{mK-(K-1)} \\ h_{mK+1} & h_{mK} & \cdots & h_{mK-(K-2)} \\ \vdots & \vdots & \ddots & \vdots \\ h_{mK+K-1} & h_{mK+K-2} & \cdots & h_{mK} \end{bmatrix}. \quad (6.45)$$

By Proposition 6.1, $\sum_m H^{(m)} e^{j2\pi fmT}$ can be evaluated as

$$\sum_{m=-\infty}^{\infty} H^{(m)} e^{j2\pi fmT} = \begin{bmatrix} 1 & Z^{-1} & \cdots & Z^{-(K-1)} \\ Z^{1} & 1 & \cdots & Z^{-(K-2)} \\ \vdots & \vdots & \ddots & \vdots \\ Z^{K-1} & Z^{K-2} & \cdots & 1 \end{bmatrix}, \quad (6.46)$$

where $Z = e^{j2\pi fT/K}$ is a complex exponential. Therefore $F(f)$ can be written as

$$F(f) = \begin{bmatrix} \sqrt{P_1T} & & & & \\ & \ddots & & & \\ & & \sqrt{P_iT} & & \\ & & & 0 & \\ & & & & \ddots \\ & & & & & 0 \end{bmatrix} \begin{bmatrix} 1 & Z^{-1} & \cdots & Z^{-(K-1)} \\ Z^{1} & 1 & \cdots & Z^{-(K-2)} \\ \vdots & \vdots & \ddots & \vdots \\ Z^{K-1} & Z^{K-2} & \cdots & 1 \end{bmatrix} \begin{bmatrix} \sqrt{P_1T} & & & & \\ & \ddots & & & \\ & & \sqrt{P_iT} & & \\ & & & 0 & \\ & & & & \ddots \\ & & & & & 0 \end{bmatrix}. \quad (6.47)$$

We can further show that $F(f)$ is a rank 1 matrix since it can be decomposed as $F(f) = \mathbf{u}\mathbf{u}^{\dagger}$, where $\mathbf{u}$ is a $K\times1$ vector given by

$$\mathbf{u} = \left[\sqrt{P_1 T}Z^1, \sqrt{P_2 T}Z^2, \cdots, \sqrt{P_i T}Z^i, 0, \cdots, 0\right]^T. \tag{6.48}$$

Therefore, $F(f)$ has only *one eigenvalue* and this eigenvalue corresponds to the matrix trace of $F(f)$ since trace of any non-negative definite matrix is the sum of its eigenvalues [55]. That is,

$$\lambda_0\{F(f)\} = tr(F(f)) = \sum_{j=1}^{i} P_j T. \tag{6.49}$$

Finally, we substitute (6.49) back to (6.43) and by noting that $T = 1/(2W)$,

$$\frac{1}{2}\int_{-W}^{W}\sum_{j=0}^{K-1}\log_2\left(1+c\lambda_j\{F(f)\}\right)df = \frac{1}{2}\int_{-W}^{W}\log_2\left(1+c\lambda_0\{F(f)\}\right)df \tag{6.50}$$

$$= \frac{1}{2}\int_{-W}^{W}\log_2\left(1+c\sum_{j=1}^{i}P_j T\right)df \tag{6.51}$$

$$= W\log_2\left(1+\frac{c}{2W}\sum_{j=1}^{i}P_j\right), \tag{6.52}$$

where (6.50) is due to $F(f)$ having only one non-zero eigenvalue λ_0 and (6.51) is due to (6.49). This completes the proof of Proposition 6.2. ■

We are now ready present the proof of Lemma 6.1.

Proof of Lemma 6.1: Let $h(\cdot)$ be the differential entropy and recall that $\mathbf{y}^{(k)} = H\mathbf{x} + \mathbf{z}^{(k)}$. Due to the definition of the mutual information,

$$I\left(\mathbf{y}^{(k)};(\mathbf{x}_1,\cdots,\mathbf{x}_i)\middle|\mathbf{x}_{i+1},\cdots,\mathbf{x}_K\right) = h\left(\mathbf{y}^{(k)}\middle|\mathbf{x}_{i+1},\cdots,\mathbf{x}_K\right) - h\left(\mathbf{y}^{(k)}\middle|\mathbf{x}_1,\cdots,\mathbf{x}_i,\mathbf{x}_{i+1},\cdots,\mathbf{x}_K\right) \tag{6.53}$$

$$= h\left(\mathbf{y}^{(k)}\middle|\mathbf{x}_{i+1},\cdots,\mathbf{x}_K\right) - h\left(H\mathbf{x}+\mathbf{z}^{(k)}\middle|\mathbf{x}\right) \tag{6.54}$$

$$= h\left(\mathbf{y}^{(k)}\middle|\mathbf{x}_{i+1},\cdots,\mathbf{x}_K\right) - h\left(\mathbf{z}^{(k)}\right) \tag{6.55}$$

$$= h\left(\mathbf{y}^{(k)}\middle|\mathbf{x}_{i+1},\cdots,\mathbf{x}_K\right) - \frac{1}{2}\log_2\left((2\pi e)^{KN}\det\left(\frac{N_0^{(k)}}{2}H\right)\right), \tag{6.56}$$

where (6.54) is due to having ($\mathbf{x}_1$, $\mathbf{x}_2$, …, $\mathbf{x}_K$) is equivalent to having given $\mathbf{x}$, (6.55) is due to $H\mathbf{x}$ being deterministic when $\mathbf{x}$ is known, followed by the translation invariance of the differential entropy (Lemma 2.5), and (6.56) is by the known differential entropy expression of Gaussian random vector with a covariance matrix $(N_0^{(k)}/2)\cdot H$.

Now denoting m-th column vector of the FTN matrix H by $\mathbf{h}_m$ and n-th data symbol of the user m's message by $x_m[n]$, we express $\mathbf{y}^{(k)}$ as:

$$\mathbf{y}^{(k)} = \sum_{m=1}^{K}\mathbf{h}_m x_m[0] + \sum_{m=1}^{K}\mathbf{h}_{K+m} x_m[1] + \cdots + \sum_{m=1}^{K}\mathbf{h}_{(N-1)K+m} x_m[N-1] + \mathbf{z}^{(k)} \tag{6.57}$$

$$= \sum_{m=1}^{K}\sum_{n=0}^{N-1}\mathbf{h}_{nK+m} x_m[n] + \mathbf{z}^{(k)}. \tag{6.58}$$

Hence, the conditional differential entropy in (6.56) can be completely written as

$$h\left(\mathbf{y}^{(k)}\middle|\mathbf{x}_{i+1},\cdots,\mathbf{x}_K\right) = h\left(\sum_{m=1}^{K}\sum_{n=0}^{N-1}\mathbf{h}_{nK+m} x_m[n] + \mathbf{z}^{(k)}\middle|\mathbf{x}_{i+1},\cdots,\mathbf{x}_K\right) \tag{6.59}$$

$$= h\left(\sum_{m=1}^{i}\sum_{n=0}^{N-1}\mathbf{h}_{nK+m} x_m[n] + \mathbf{z}^{(k)}\right) \tag{6.60}$$

$$= h\left(\mathbf{y}^{(k)}\middle|\mathbf{x}_{i+1} = \cdots = \mathbf{x}_K = 0\right), \tag{6.61}$$

where (6.60) is again due to the translation invariance of the differential entropy (Lemma 2.5) and (6.61) follows since (6.60) no longer depends on the input terms $\mathbf{x}_{i+1}$, $\mathbf{x}_{i+2}$, …, $\mathbf{x}_K$. Hence, the conditional differential entropy can be written as

$$h\left(\mathbf{y}^{(k)}\middle|\mathbf{x}_{i+1},\cdots,\mathbf{x}_K\right) = \frac{1}{2}\log_2 \det\left((2\pi e)^{KN}\operatorname{cov}\left(\mathbf{y}^{(k)}\middle|\mathbf{x}_{i+1} = \cdots = \mathbf{x}_K = 0\right)\right), \tag{6.62}$$

where $\operatorname{cov}(\mathbf{y}^{(k)}|\mathbf{x}_{i+1} = \cdots = \mathbf{x}_K = 0)$ denotes the covariance of $\mathbf{y}^{(k)}$ when $\mathbf{x}_{i+1}$, $\mathbf{x}_{i+2}$, …, $\mathbf{x}_K$ are all zeros, i.e.,

$$\operatorname{cov}\left(\mathbf{y}^{(k)}\middle|\mathbf{x}_{i+1} = \cdots = \mathbf{x}_K = 0\right) = HQ_iH^T + (N_0^{(k)}/2)H, \tag{6.63}$$

with Q_i as defined as

$$Q_i = I_N \otimes diag\left(P_1T, P_2T, \cdots, P_iT, 0, \cdots, 0\right). \tag{6.64}$$

Substituting (6.62) back to (6.56) and simplifying, we obtain

$$\frac{1}{NT} I\left(\mathbf{y}^{(k)};\left(\mathbf{x}_1,\cdots,\mathbf{x}_i\right)\middle|\mathbf{x}_{i+1},\cdots,\mathbf{x}_K\right)=\frac{1}{NT}\frac{1}{2}\log_2\left(\frac{\det\left(HQ_iH^T+(N_0^{(k)}/2)H\right)}{\det\left((N_0^{(k)}/2)H\right)}\right) \tag{6.65}$$

$$=\frac{1}{NT}\frac{1}{2}\log_2\det\left((N_0^{(k)}/2)^{-1}Q_iH+I_{KN}\right). \tag{6.66}$$

Finally using Proposition 6.2 with $c = (N_0^{(k)}/2)^{-1}$, we obtain the desired expression. This completes the proof of Lemma 6.1. ■

6.4 Proposed FTN Broadcast Receiver Architectures

In this section, we propose two FTN broadcast receiver architectures that can be used to recover the FTN transmitted data intended for K respective receivers. One receiver architecture, described in subsection 6.4.1, is based on the optimal *maximum a posteriori* (MAP) equalizer followed by an iterative Turbo equalization. An alternative receiver architecture, described in subsection 6.4.2, is based on a Gaussian approximation of the intersymbol interference (ISI) followed by successive ISI cancellation.

6.4.1 FTN Receiver Architecture with MAP-based Turbo Equalization

In this subsection, FTN broadcast receiver architecture that is based on Turbo equalization principle is described. The k-th receiver architecture of the K-user broadcast channel is shown in Figure 6.7 and is described in the following.

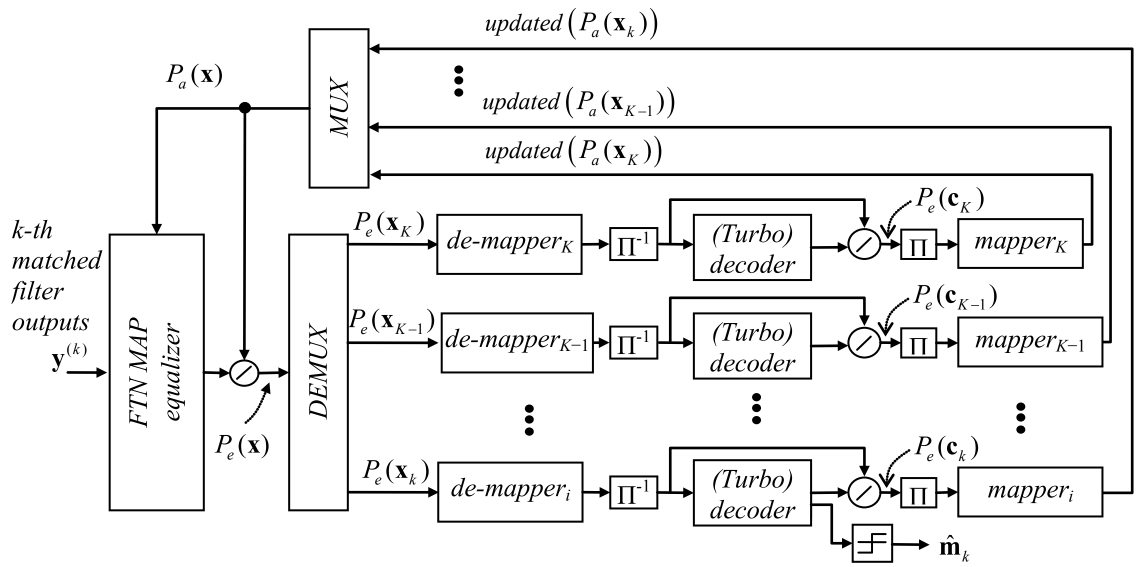

Figure 6.7 Proposed FTN broadcast receiver architecture based on Turbo equalization principle

The matched filter outputs $\mathbf{y}^{(k)}$ are first passed to a *maximum a posteriori* (MAP) equalizer, along with a priori information about the data symbols $\mathbf{x}$ (denoted by $P_a(\mathbf{x})$ in probabilities). It is assumed that mapping constellations of $\mathbf{x}_1$, $\mathbf{x}_2$, …, $\mathbf{x}_K$, and power assignments P_1, P_2, …, P_K are known at all receivers of the broadcast channel. Initially all $\mathbf{x}$ are assumed to be equi-probable. The MAP equalizer provides soft outputs (or reliability values) about the data symbols $\mathbf{x}$ given $\mathbf{y}^{(k)}$. The detailed description of the MAP equalizer will be given at the end of this subsection.

From the soft outputs of the MAP equalizer, the contributions from a priori information $P_a(\mathbf{x})$ are removed to obtain an extrinsic information $P_e(\mathbf{x})$ about the data symbols $\mathbf{x}$. Subsequently, $P_e(\mathbf{x})$ is de-multiplexed into K users' data symbols, $P_e(\mathbf{x}_K)$, $P_e(\mathbf{x}_{K-1})$, …, $P_e(\mathbf{x}_1)$, by following the definition of $\mathbf{x}$ in (6.5). Of these, only $P_e(\mathbf{x}_i)$ for $i \in \{k, k+1, \ldots, K\}$ needs to be processed since the remaining data $\mathbf{x}_1$, $\mathbf{x}_2$, …, $\mathbf{x}_{k-1}$ cannot be properly decoded by the k-th receiver due to the degraded broadcast channel setup, as described in Cover's degraded broadcast coding principle [28]. The extrinsic information about the i-th user data symbols $P_e(\mathbf{x}_i)$ are then de-mapped into binary bit format, which are further de-interleaved and (Turbo) decoded. The decoder provides reliability values about the codewords $\mathbf{c}_i$ and the corresponding message bits $\mathbf{m}_i$ for $i = \{k, k+1, \ldots, K\}$.

In the second and subsequent iterations of Turbo-equalization, the extrinsic information $P_e(\mathbf{c}_i)$ for $i = \{k, k+1, \ldots, K\}$ are re-interleaved, re-mapped, and multiplexed together to form an updated a-priori information $P_a(\mathbf{x})$ about the data symbols $\mathbf{x}$. The a-priori information $P_a(\mathbf{x})$ is then fed back to the MAP equalizer for improved estimates about the data symbols $\mathbf{x}$. These steps continue for a prescribed number of iterations or until some convergence is reached.

We now fully describe the maximum a posteriori (MAP) equalizer in Figure 6.7 that is suitable for the considered FTN broadcast system. The MAP equalizer described herein is not standard in the sense that it must 1) handle the nonzero correlations of the noise samples $\mathbf{z}^{(k)}$ and 2) handle (possibly) different modulation formats of each user's data symbols.

We start from the FTN broadcast channel model (6.7) at the k-th receiver; reproduced below for convenience:

$$y^{(k)}[n] = \sum_{l=-L}^{L} h_l x[n-l] + z^{(k)}[n],\ n = 0,1,\ldots,KN-1, \tag{6.67}$$

where $x[n]$ is the n^{th} symbol of the combined data symbol vector $\mathbf{x}$ and L is the ISI memory length that is equal to or larger than K. This channel model is an instance of the *Ungerboeck observation model* as discussed in subsection 2.3.2, and the a-posteriori probabilities $p(x[n]|\mathbf{y}^{(k)})$ are given by

$$p(x[n]|\mathbf{y}^{(k)}) \propto \sum_{\substack{\mathbf{x} \\ excluding\ x[n]}} \prod_i \Pr(x[i]) \exp\left(\frac{2}{N_0}\left(x[i]y^{(k)}[i] - \frac{1}{2}x^2[i]h_0 - \sum_{l=1}^{L} x[i]x[i-l]h_l\right)\right), \tag{6.68}$$

where $\propto$ denotes 'proportional to'.

For the purpose of building a MAP equalizer that can efficiently compute (6.68), an appropriate trellis diagram is first constructed from a block diagram shown in Figure 6.8. The block diagram admits K-tuple of input symbols $[x[n], x[n+1], \ldots, x[n+K-1]]$ and the corresponding states are the all possible combinations of L consecutive input $x[n]$. Note that only L registers are needed in the block diagram (as opposed to $2L+1$, which is the full memory of the observation model) since the expression (6.68) does not depend on h_l for

$l<0$ by accounting for the symmetry of h_l (i.e., $h_l = h_{-l}$). For example, the trellis diagrams for two users (K=2) when both users are using antipodal modulations and the ISI memory length L = 2~4 are shown in Figure 6.9.

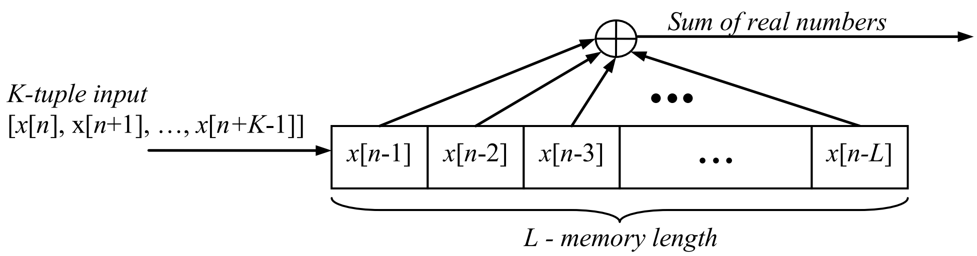

Figure 6.8 A block diagram for constructing an appropriate trellis diagram of the FTN broadcast channel model; Only L registers are needed (and not 2L+1) due to the symmetry of h_l and the a-posteriori probabilities in (6.68) depending only on h_0, h_1, …, h_L

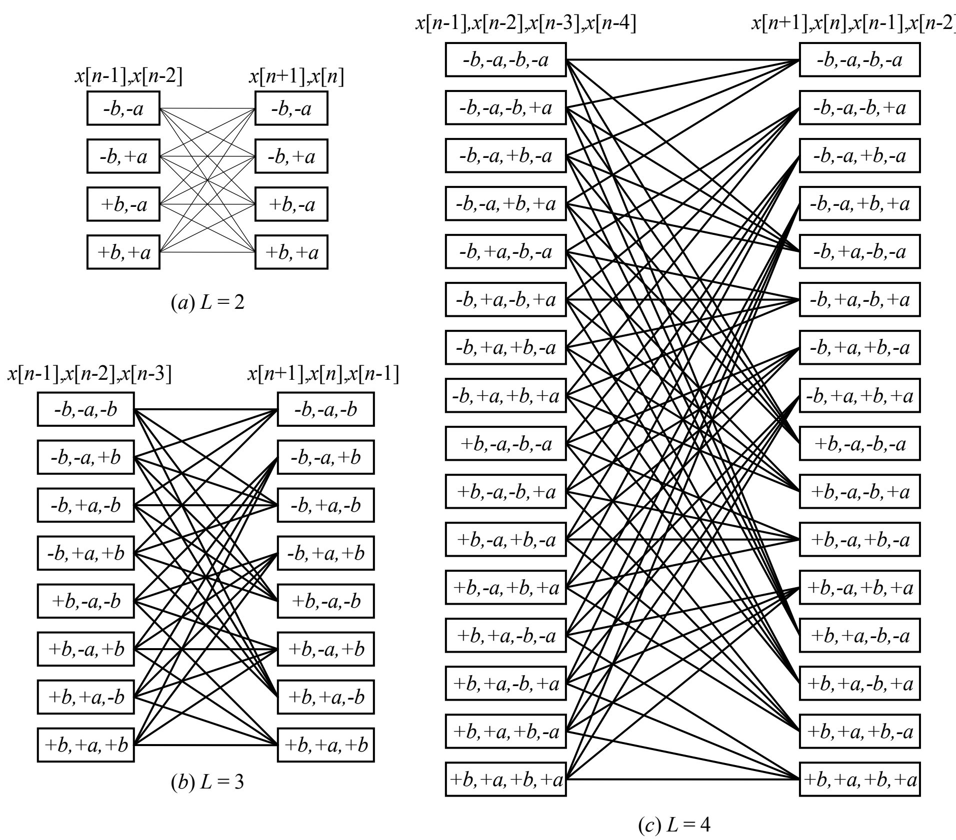

Figure 6.9 Trellis diagram of the FTN broadcast channel model (6.67) for 2 users (K=2) where both users are using antipodal modulations $x_1[n]$=±a and $x_2[n]$=±b, and ISI memory lengths are (a) L=2, (b) L=3, or (c) L=4; Input to each trellis edge is the pair ($x[n]$,$x[n+1]$)

Given the trellis representation, the MAP symbol detection of the FTN broadcast channel model (6.67) can be accomplished using the BCJR algorithm with suitable trellis edge metrics (see subsection 2.3.2 for more details). First let S be a set of states in a trellis stage. Then the edge-metric of the trellis-edge connecting the two states $s \in \mathsf{S}$ and $s' \in \mathsf{S}$ at the m-th trellis-stage is given by[39]

$$\gamma_m(s,s') = \prod_{i=Km}^{Km+(K-1)} \Pr(x[i]) \exp\left(\frac{2}{N_0} \left(x[i]y^{(k)}[i] - \frac{1}{2}x^2[i]h_0 - \sum_{l=1}^{L} x[i]x[i-l]h_l \right) \right), \qquad (6.69)$$

for $m \in \{0, 1, \ldots, N\text{-}1\}$, where each trellis-stage accounts for the FTN signal transmission over T seconds (i.e., time duration for K data symbol transmissions).

The computational complexity of the described MAP symbol detection scales quadratically with the total number of states of a trellis stage, $|\mathsf{S}|$, and is given by the following *Big-O* notation: $O(KN\cdot|\mathsf{S}|^2)$. The total number of states of a trellis stage $|\mathsf{S}|$ can be derived as follows. First let k-th user's data symbols $x_k[n]$ use symbol constellation X_k, i.e., $x_k[n] \in \mathsf{X}_k$. Referring to the block diagram in Figure 6.8, the states of a trellis stage are the all possible combinations of L consecutive inputs $x[n]$. Therefore, the total numbers of states for $L \geq K$ are given by

$$|\mathsf{S}| = \begin{cases} |\mathsf{X}|^L, & \text{if } |\mathsf{X}_1| = \cdots = |\mathsf{X}_K| = |\mathsf{X}| \\ \left(\prod_{k=1}^{K} |\mathsf{X}_k| \right)^{L/K}, & \text{if } L = nK \text{ for } n \text{ integer} \\ \left(\prod_{k=1}^{K} |\mathsf{X}_k| \right)^{(L-1)/K} \max\{|\mathsf{X}_1|, |\mathsf{X}_2|, \cdots, |\mathsf{X}_K|\}, & \text{if } L = nK+1 \text{ for } n \text{ integer} \\ \left(\prod_{k=1}^{K} |\mathsf{X}_k| \right)^{(L-2)/K} \max\{|\mathsf{X}_1||\mathsf{X}_2|, \cdots, |\mathsf{X}_{K-1}||\mathsf{X}_K|\}, & \text{if } L = nK+2 \text{ for } n \text{ integer} \\ \vdots & \vdots \end{cases} \qquad (6.70)$$

In other words, $|\mathsf{S}|$ scales *exponentially* with the length of the ISI memory L.

[39] The only difference of (6.69) compared to (2.34) of the single user case is the appearance of the product over index i. This product is needed to account for the K-tuple inputs in the trellis diagrams.

For example, for two-user broadcast channel (K=2) with ISI memory length L=6, when first user and second user are using BPSK and 4-PAM, respectively ($|\mathsf{X}_1|$=2 and $|\mathsf{X}_2|$=4), the number of states is given by (2·4)·(2·4)·(2·4) = 512. The overall computational complexity of the MAP equalizer then becomes $O(KN\cdot 512^2) \approx O(5\times 10^5\cdot N)$, which may be prohibitively large for practical implementations in the current state-of-the-art VLSI or FPGA based communication system hardware. Consequently, the presented MAP equalizer design is appropriate only for small K and L. For moderate to large K and L, the Gaussian-approximation based receiver architecture proposed in the following subsection 6.4.2 is more appropriate due to its *linear* computational-complexity.

6.4.2 Using Successive Interference Cancellation and Gaussian Approximation

The FTN broadcast receiver architecture we propose in this subsection is based on the Gaussian approximation and successive cancellation of the FTN-induced ISI. The k-th receiver architecture of the K-user broadcast channel and the detailed descriptions of the individual components are shown Figure 6.10.

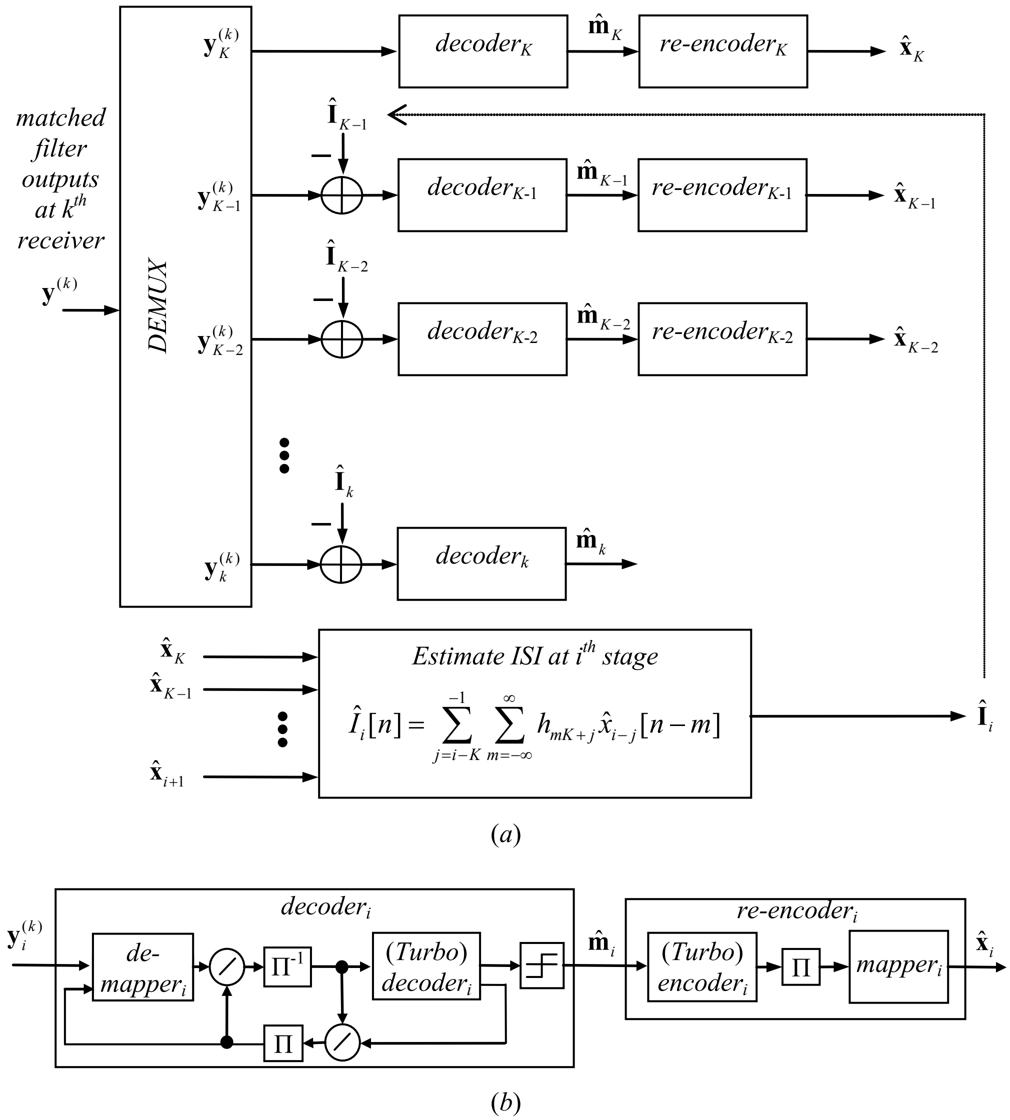

Figure 6.10 Proposed FTN broadcast Turbo receiver architecture based on a Gaussian approximation and a successive cancellation of intersymbol interference; (*a*) the overall structure of the Turbo receiver architecture; (*b*) detailed description of the *decoder$_i$* and *re-encoder$_i$* modules

First, the matched filter outputs at the *k*-th receiver $\mathbf{y}^{(k)}$ are de-multiplexed into *K* sub-vectors, $\mathbf{y}_K^{(k)}$, $\mathbf{y}_{K-1}^{(k)}$, …, $\mathbf{y}_1^{(k)}$, where $\mathbf{y}_i^{(k)}$ is defined for $i \in \{1, 2, \ldots, K\}$ by

$$\mathbf{y}_i^{(k)} = \left[y_i^{(k)}[0], \quad y_i^{(k)}[1], \quad y_i^{(k)}[2], \quad \cdots, \quad y_i^{(k)}[N-1] \right] \tag{6.71}$$

$$= \left[y^{(k)}[i-1], \quad y^{(k)}[K+i-1], \quad y^{(k)}[2K+i-1], \quad \cdots, \quad y^{(k)}[K(N-1)+i-1] \right]. \tag{6.72}$$

The sub-vector $\mathbf{y}_i^{(k)}$ represents noisy observation about the data symbol vector $\mathbf{x}_i$ that is intended for the i^{th} receiver. Furthermore, the term $y_i^{(k)}[n]$ can be expressed explicitly as a function of $x_i[n]$ as

$$y_i^{(k)}[n] = \sum_{j=i-K}^{i-1} \sum_{m=-\infty}^{\infty} h_{mK+j} x_{i-j}[n-m] + z^{(k)}\left[Kn+i-1\right], \tag{6.73}$$

for $i \in \{1, 2, \ldots, K\}$ and $n \in \{0, 1, \ldots, N-1\}$, which is due to the expression of $y^{(k)}[n]$ in (6.7) and the definition of $x_i[n]$ in (6.5). But for any T-orthogonal unit energy modulating pulses $s(t)$,

$$h_{mK} = \begin{cases} 1 & \mathit{if}\ m = 0 \\ 0 & \mathit{if}\ m \neq 0, \end{cases} \tag{6.74}$$

by the definition $h_l = \int_{-\infty}^{+\infty} s(t)\, s\left(t - l \cdot T/K\right) dt$. Therefore, (6.73) can be rewritten as

$$y_i^{(k)}[n] = x_i[n] + \sum_{j=i-K}^{-1} \sum_{m=-\infty}^{\infty} h_{mK+j} x_{i-j}[n-m] + \sum_{j=1}^{i-1} \sum_{m=-\infty}^{\infty} h_{mK+j} x_{i-j}[n-m] + z^{(k)}\left[Kn+i-1\right]. \tag{6.75}$$

Furthermore, due to (6.74), the noise samples $z^{(k)}[Kn+i-1]$ for $n \in \{0, 1, \ldots, N\text{-}1\}$ are *independent* zero mean Gaussian distributed with variance of $N_0^{(k)}/2$.

In Figure 6.10a, the proposed k-th FTN receiver in the K-user broadcast channel proceeds in multiple decoding stages, decoding from the most powerful FTN sub-stream vector $\mathbf{y}_K^{(k)}$ in the top branch and gradually working its way down to the desired FTN sub-stream vector $\mathbf{y}_k^{(k)}$ in the bottom branch. (Without loss of generality, the depicted decoding structure assumes that the assigned powers are chosen such that $P_K \geq P_{K\text{-}1} \geq \ldots \geq P_1$.) It is further assumed that power assignments $P_1, P_2, \ldots, P_K$ are known at all K receivers of the broadcast channel.

The k-th FTN receiver first processes $\mathbf{y}_K^{(k)}$ (in the top branch after the de-multiplexer in Figure 6.10a), which represents a noisy observation about the data symbol vector $\mathbf{x}_K$ that is intended for the K-th receiver. Due to (6.75), the n-th element of $\mathbf{y}_K^{(k)}$ is given by

$$y_K^{(k)}[n] = x_K[n] + \sum_{j=1}^{K-1} \sum_{m=-\infty}^{\infty} h_{mK+j} x_{K-j}[n-m] + z^{(k)}\left[Kn+i-1\right]. \tag{6.76}$$

The term $\sum_{j=1}^{K-1}\sum_{m=-\infty}^{\infty} h_{mK+j}x_{K-j}[n-m]$ on the right-hand-side of (6.76) represents the ISI to the desired symbol $x_K[n]$ and is approximated by a Gaussian random variable using the *Central Limit Theorem*. Consequently, the receiver treats the ISI term as additional noise and approximates it by a Gaussian random variable with zero mean and $\sum_{j=1}^{K-1}\sum_{m=-\infty}^{\infty} \left|h_{mK+j}\right|^2 P_{K-j}T$ variance (due to the variance of $x_k[n]$ being P_kT). Therefore, a posteriori probabilities of K-th user's data symbols $x_K[n]$ can be approximated by

$$\Pr\left(x_K[n]\,\middle|\,y_K^{(k)}[n]\right) \cong c\cdot\Pr\left(x_K[n]\right)\exp\left(-\frac{(y_K^{(k)}[n]-x_K[n])^2}{2\sigma_K^2}\right), \tag{6.77}$$

where $\sigma_K{}^2$ denotes the variance of noise plus ISI, i.e., $\sigma_K^2 = N_0^{(k)}/2 + \sum_{j=1}^{K-1}\sum_{m=-\infty}^{\infty}\left|h_{mK+j}\right|^2 P_{K-j}T$, $\Pr(x_K[n])$ is a priori probability of $x_K[n]$, and c is a normalization constant that can be easily computed by the law of total probability. Using this Gaussian approximation (6.77), the *decoder*$_K$ in Figure 6.10 computes estimates about K-th user messages $\hat{\mathbf{m}}_K$ by taking a hard decision, and these are then re-encoded to produce estimates about K-th user's data symbols $\hat{\mathbf{x}}_K$.

Next, the receiver processes $\mathbf{y}_{K-1}^{(k)}$ (in the second branch after the de-multiplexer in Figure 6.10). The estimates $\hat{\mathbf{x}}_K$ in the last step are used to recreate an ISI term $\sum_m h_{mK-1}\hat{x}_K[n-m]$, which is then subtracted from $y_{K-1}^{(k)}[n]$ to obtain

$$y_{K-1}^{(k)}[n] - \sum_{m=-\infty}^{\infty} h_{mK-1}\hat{x}_K[n-m] \cong x_{K-1}[n] + \sum_{j=1}^{K-2}\sum_{m=-\infty}^{\infty} h_{mK+j}x_{K-1-j}[n-m] + z^{(k)}\left[Kn{+}i{-}1\right]. \tag{6.78}$$

Note that if the estimates $\hat{\mathbf{x}}_K$ from the last step were without any error, (6.78) becomes an equality. Subsequently, $x_{K\text{-}1}[n]$ is decoded while approximating the rest of the terms in (6.78) as a Gaussian distributed noise with $\sigma_{K-1}^2 = N_0^{(k)}/2 + \sum_{j=1}^{K-2}\sum_{m=-\infty}^{\infty}\left|h_{mK+j}\right|^2 P_{K-1-j}T$ variance. The estimates about the message intended for $(K\text{-}1)^{\text{th}}$ receiver, $\hat{\mathbf{m}}_{K-1}$, are then obtained by taking a hard decision, which are further re-encoded to produce $\hat{\mathbf{x}}_{K-1}$ for later processing.

Generally, consider the step when $\mathbf{y}_i^{(k)}$ is being processed with regard to the i-th user data $\mathbf{x}_i$. At this time, the symbol estimates $\hat{\mathbf{x}}_K$, $\hat{\mathbf{x}}_{K-1}$, …, $\hat{\mathbf{x}}_{i+1}$ are already available from the previous steps and the corresponding ISI terms can be estimated as $\sum_{j=i-K}^{-1}\sum_{m=-\infty}^{\infty} h_{mK+j}\hat{x}_{i-j}[n-m]$. These are then subtracted from $y_i^{(k)}[n]$ to yield (using (6.75))

$$y_i^{(k)}[n]-\sum_{j=i-K}^{-1}\sum_{m=-\infty}^{\infty} h_{mK+j}\hat{x}_{i-j}[n-m]\cong x_i[n]+\sum_{j=1}^{i-1}\sum_{m=-\infty}^{\infty} h_{mK+j}x_{i-j}[n-m]+z^{(k)}\left[Kn+i-1\right], \quad (6.79)$$

which becomes an equality if the estimates $\hat{\mathbf{x}}_K$, $\hat{\mathbf{x}}_{K-1}$, …, $\hat{\mathbf{x}}_{i+1}$ are all without errors. Again, due to the *Central Limit Theorem*, the residual ISI term $\sum_{j=1}^{i-1}\sum_{m=-\infty}^{\infty} h_{mK+j}x_{i-j}[n-m]$ is approximated by a zero mean Gaussian random variable with a variance $\sum_{j=1}^{i-1}\sum_{m=-\infty}^{\infty}\left|h_{mK+j}\right|^2 P_{i-j}T$. Consequently, a posteriori probabilities of data symbols intended to i-th receiver $x_i[n]$ can be approximated by

$$\Pr\left(x_i[n]\,\middle|\,y_i^{(k)}[n]\right)\cong c\cdot\Pr\left(x_i[n]\right)\exp\left(-\frac{(y_i^{(k)}[n]-x_i[n])^2}{2\sigma_i^2}\right), \quad (6.80)$$

where σ_i^2 denotes the variance of noise plus ISI, i.e., $\sigma_i^2 = N_0^{(k)}/2+\sum_{j=1}^{i-1}\sum_{m=-\infty}^{\infty}\left|h_{mK+j}\right|^2 P_{i-j}T$, $\Pr(x_i[n])$ is a priori probability of $x_i[n]$, and c is a normalization constant. Using the Gaussian approximation (6.80), the *decoder*$_i$ computes estimates about i-th user messages $\hat{\mathbf{m}}_i$ by taking a hard decision. These estimated i-th user messages $\hat{\mathbf{m}}_i$ are then re-encoded to produce estimates about i-th user's data symbols $\hat{\mathbf{x}}_i$. These steps continue from $i = K$ all the way down to $i = k$, where the *decoder*$_k$ simply takes the hard decision $\hat{\mathbf{m}}_k$ since it is the message intended for the considered k-th receiver.

We note that the K-th receiver in the K-user broadcast channel simply apply a single user decoding of its own message $\hat{\mathbf{m}}_K$. On the other hand, the receiver 1 in the K-user broadcast channel performs the decoding of all K users' messages while successive canceling the corresponding ISIs, in order to obtain an ISI-free AWGN channel observation of the desired symbols $x_1[n]$.

From the implementation point of view, only one *decoder* and *re-encoder* would be needed if all user data are encoded using the same error-control-codes. Furthermore, each *de-mapper* in the proposed FTN receivers needs to only operate on the signal constellation of individual user symbols (e.g., binary constellation if all users are using BPSK symbols) and *not* on the expanded *joint* constellation of all users' symbols (e.g., 2^K-ary constellation if all K users are using BPSK symbols). This significantly reduces the implementation complexity and allows supporting a large number of receivers in the broadcast channel.

6.5 Simulation Results

In this section, we report simulation performances of the FTN broadcast receiver architectures proposed in subsection 6.4.1 and subsection 6.4.2. These simulation results will be compared to the capacity limits of the Gaussian broadcast channel.

In all simulations throughout this section, the modulating pulses $s(t)$ were chosen to be the square-root raised cosine with the roll-off factor β=0.22, used in, e.g., WCDMA standard (with time-truncation to $\pm 6T$ about t=0, signaling interval $T=(1+\beta)/(2W)$, and W = 1 kHz). Figure 6.11 depicts the modulating pulse $s(t)$ in time domain and the corresponding pulse correlation coefficients $h_l = \int_{-\infty}^{+\infty} s(t)\, s(t - l \cdot T/K)\, dt$. We can observe that h_l for $|l| > 5$ are small in magnitude (less than 0.05) and hence can be ignored by setting L=5 at the receiver. It was also verified by simulations that fixing L=5 indeed caused only negligible performance loss.

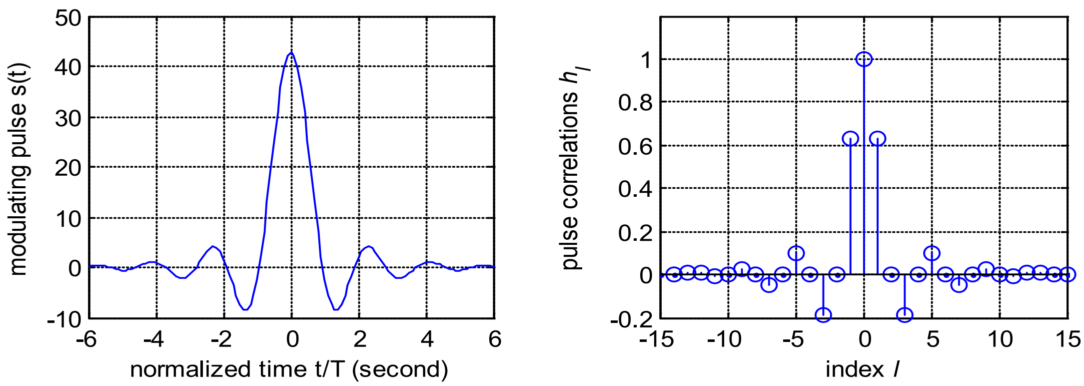

(*a*) (*b*)

Figure 6.11 Characteristics of the time-truncated square-root raised cosine modulating pulse $s(t)$ with the roll-off factor β=0.22; (*a*) plotting in normalized time t/T in seconds where $T=(1+\beta)/(2W)$; (*b*) plotting the corresponding pulse correlations h_l

6.5.1 Simulation Results of Turbo Equalization based FTN Architecture

First, we report the simulation results of the Turbo-equalization based FTN broadcast architecture that was presented in subsection 6.4.1, for 2-user Gaussian broadcast channel. All interleavers were pseudorandom with packet length $N=2\times10^4$ and both users were using binary antipodal signaling. The power assignments were P_1=0.2 and P_2=0.8 (about 6 dB difference between the two). Different power ratios were also tested and yielded similar results.

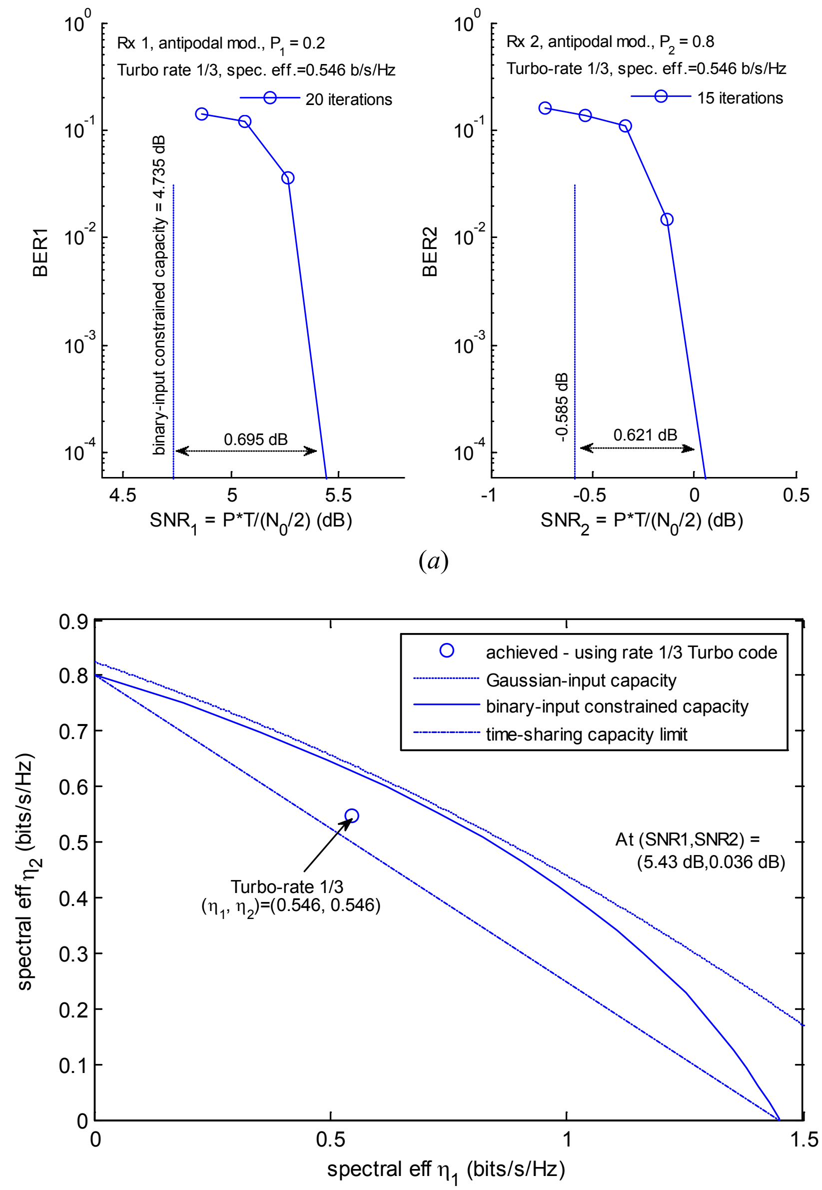

(*a*)

(*b*)

Figure 6.12 Simulated performances of Turbo-equalization based receiver architecture at 2 receivers of the broadcast channel using rate 1/3 Turbo encoders with power assignments P_1=0.2 and P_2=0.8; (*a*) BER curves with respect to the binary-input constrained capacities of the Gaussian broadcast channel (in dotted lines); (*b*) Achieved spectral efficiency pairs at the converging SNRs (i.e., SNR at the BER = 10^{-4})

Figure 6.12 shows the simulated BER performances and the corresponding achieved spectral-efficiency pairs when the 2 encoders at the FTN broadcast transmitter were the rate 1/3 UMTS parallel Turbo codes [153]. All BER curves of the simulated FTN broadcast systems (see Figure 6.12a) reached the target BER=10^{-4} within 1 dB from the corresponding binary-input constrained capacities of the Gaussian broadcast channel. Figure 6.12b shows the corresponding achieved spectral-efficiency pairs with respect to the binary-input constrained capacity region at the converging SNR pairs. The results demonstrate that the designed FTN broadcast system can be superior to the time-sharing based broadcasting system and can perform close to the capacity boundaries of the Gaussian broadcast channel.

Moreover, a higher rate FTN broadcasting system has been also simulated by using the rate 1/2 parallel Turbo codes by Berrou *et al.* [18] at the FTN broadcast transmitter. Figure 6.13 shows the corresponding simulated BER performances and the achieved spectral-efficiency pairs. These results again demonstrate the near-capacity performances of the designed FTN broadcast system.

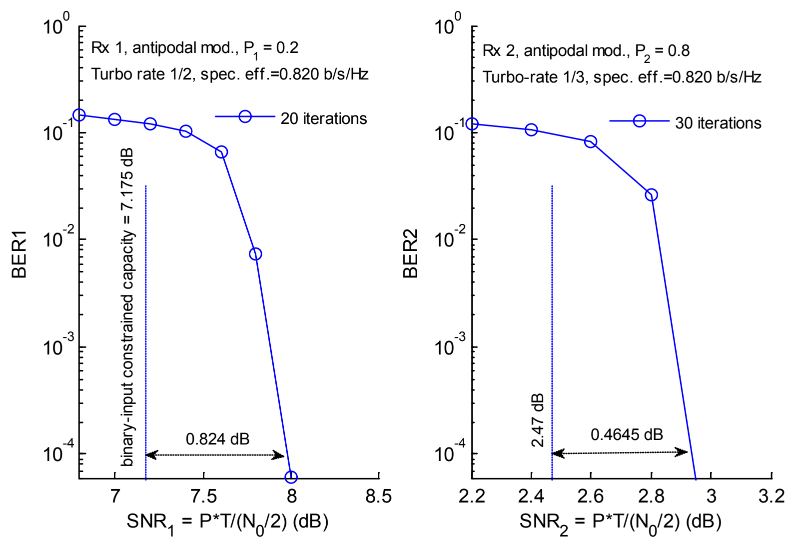

(*a*)

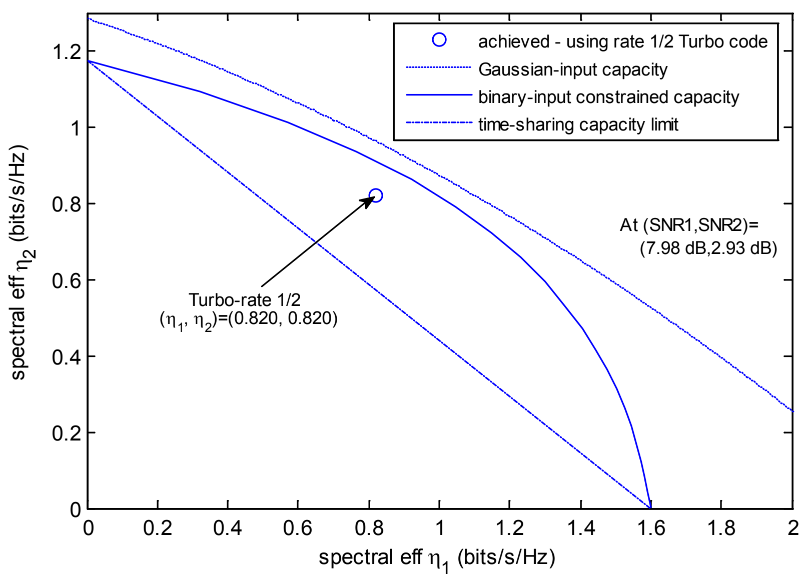

(*b*)

Figure 6.13 Simulated performances of Turbo-equalization based receiver architecture at 2 receivers of the broadcast channel when the Turbo encoders are now rate 1/2; (*a*) BER curves with respect to the binary-input constrained capacities of the Gaussian broadcast channel (in dotted lines); (*b*) Achieved spectral efficiency pairs at the converging SNRs (i.e., SNR at the BER = 10^{-4})

6.5.2 Simulation Results of Gaussian-approximation based FTN Architecture

We now report the simulated performances of the Gaussian-approximation based FTN broadcast architecture that was presented in subsection 6.4.2, in 2-user Gaussian broadcast channel (K=2). The system setup is described below:

- Both users were using binary antipodal modulations ($\mathsf{X}_k \in \{-\sqrt{P_k T}, +\sqrt{P_k T}\}$ where k = 1, 2), and P_1=0.02 and P_2=0.98 were the power assignments between the users (about 17 dB difference)[40].
- All interleavers were pseudorandom and the packet lengths were $N = 10^5$.
- Stephan ten Brink's rate 1/2 serial Turbo code [142] is known to perform very close to the capacity limit of the AWGN channel. This Turbo encoder (without the doping) has been used at the FTN broadcast transmitter.
- The achieved spectral efficiency for each user was $\eta_k = R_{coding} \cdot R_{modulation} \cdot R_{signaling} / W$ = $(1/2)\cdot(1)\cdot(1/T)/W = (1/2)\cdot 2/(1+\beta) = 0.8197$ bits/s/Hz.

As shown in Figure 6.14a, the BER curves at the 2 receivers reach the target performance BER=10^{-4} at SNR_1 = 17.64 dB and SNR_2 = 0.826 dB, respectively, which are less than 0.5 dB away from the respective binary-input constrained capacities. Figure 6.14b plots the achieved spectral efficiency pair (η_1, η_2) with respect to the capacity region of the Gaussian broadcast channel. We observe that the designed FTN broadcast system significantly outperforms to the time-sharing broadcasting in this case and can operate very close to the capacity boundary of the Gaussian broadcast channel.

[40] We simulated heavily asymmetrical channel conditions between the receivers, which led to the heavily skewed power splitting (e.g., P_1=0.02, P_2=0.98). This was motivated by observing that when the two channel qualities are the same (i.e., $N_0^{(1)}=N_0^{(2)}$), coding in Gaussian broadcast channel is unnecessary as time-sharing also achieves the capacity, as discussed in section 6.1. Nevertheless, more balanced power assignments such as P_1=0.2 and P_2=0.8 were also tested and yielded near capacity results.

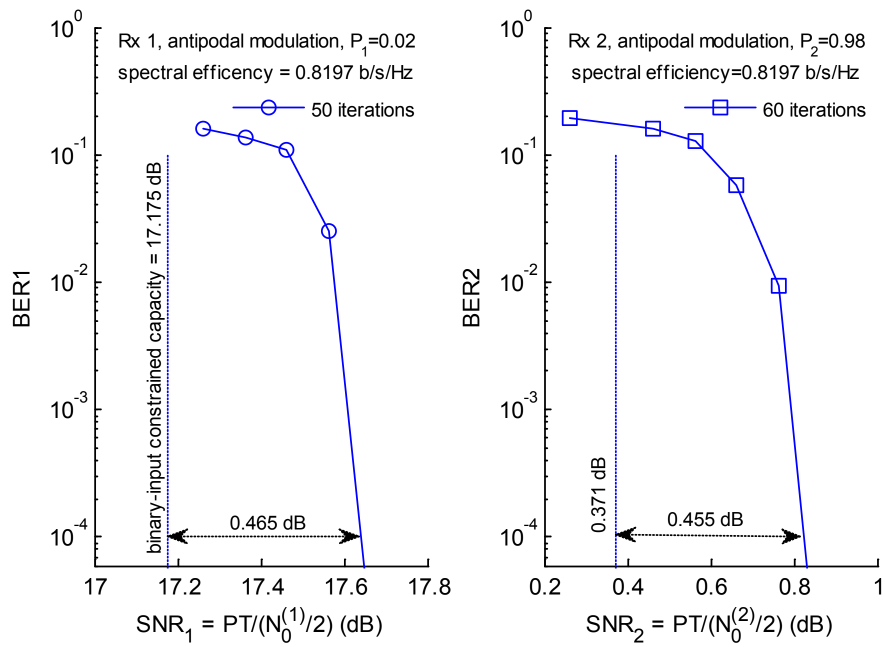

(*a*)

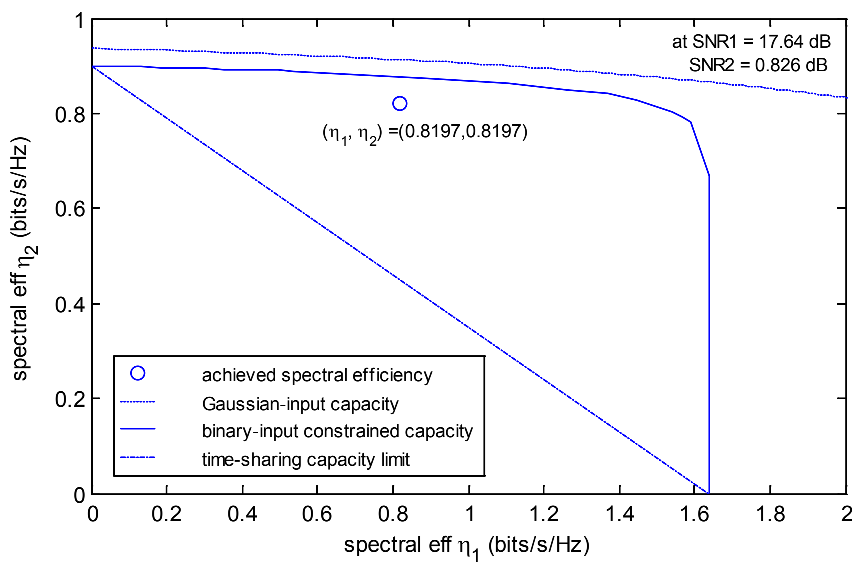

(*b*)

Figure 6.14 Simulated performances of the Gaussian approximation based receiver architecture in 2-user Gaussian broadcast channel, where both users using binary antipodal modulation with power assignments P_1=0.02 and P_2=0.98; (*a*) BER curves at 2 receivers with respect to the binary-input constrained capacities of the Gaussian broadcast channel (in dotted lines); (*b*) Achieved spectral efficiency pairs at the converging SNRs (i.e., SNR at the BER=10^{-4})

We also simulated the Gaussian-approximation based FTN broadcast architecture using a higher order modulation (first user message is now mapped to 8-PAM constellation with 'd21' mapping [143] whereas the second user message is still mapped to the binary antipodal constellation). The system setup is described below:

- The power allocations were P_1=0.03 and P_2=0.97 (about 15 dB difference) and packet lengths were N=5×10^4.
- The *encoder*$_1$ at the transmitter was a rate 1/2 recursive systematic convolutional code with memory 2, described by code polynomials (G_r,G)=(07,05) in octal values [143], where G_r stands for the recursive feedback polynomial[41].
- The *encoder*$_2$ was still the rate 1/2 serial Turbo code (without the doping) [142].
- The spectral efficiencies of the first and second users were $\eta_1 = (1/2)\cdot\log_2(8)\cdot(1/T)/W$ = 2.459 and $\eta_2 = (1/2)\cdot(1)\cdot(1/T)/W$ = 0.8197 in bits/s/Hz.

Figure 6.15 shows simulated BER curves of the FTN broadcast receivers[42] and the corresponding achieved spectral efficiency pair with respect to the Gaussian broadcast capacity region. Again, we can observe that the simulated FTN broadcast system clearly outperforms the *time-sharing* broadcasting, while the results also indicate a potential of closely approaching the capacity boundary of the Gaussian broadcast channel at high spectral efficiencies.

---

[41] Stephan ten Brink, using the EXIT chart analysis, showed that this memory-2 code matches well with 8-PAM with 'd21' mapping [143]. However, it still performs 1.8 dB away from the AWGN capacity limit.

[42] The 1.592 dB gap between the receiver 1's BER performance and the corresponding 8-PAM input constrained capacity in Figure 6.15 is mainly due to the inherent limitations in the Turbo decoder design (i.e., memory-2 (G_r,G)=(07,05) in concatenation with 8-PAM constellation with 'd21' mapping is known to perform about 1.8 dB away from the AWGN capacity [143]). One way to improve this performance further is by utilizing the Turbo-trellis coded modulation [117], which is known to perform very close to the capacity limits at high spectral efficiencies.

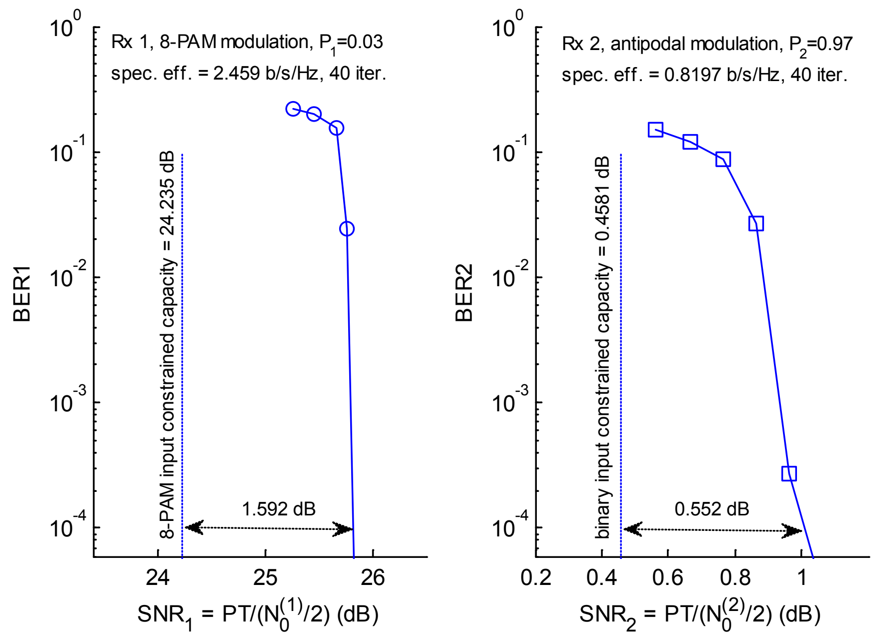

(*a*)

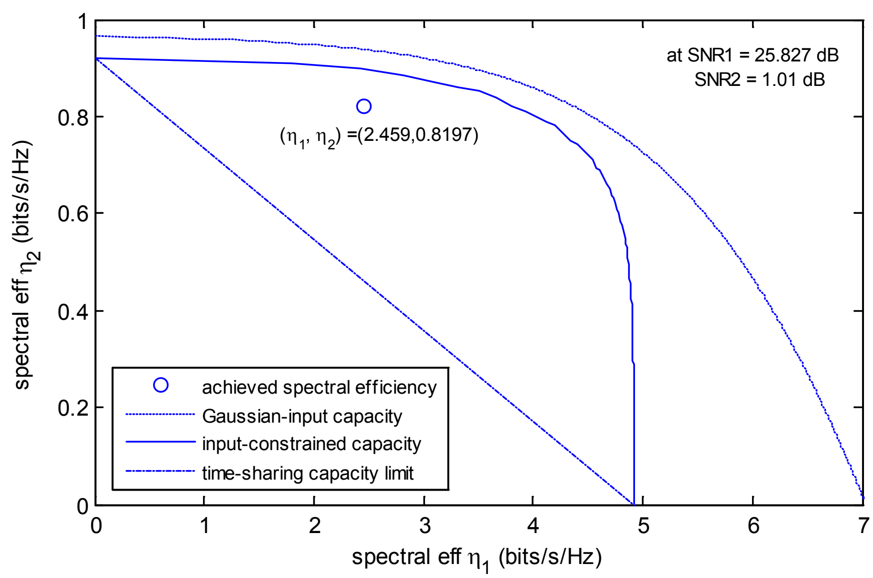

(*b*)

Figure 6.15 Simulated performances of Gaussian-approximation based receiver architecture when the first user is now using 8-PAM modulation (with 'd21' mapping) and the second user is still using binary antipodal modulation, with power assignments P_1=0.03 and P_2=0.97; (*a*) BER curves at 2 receivers with respect to the 8-PAM and binary-input constrained capacities (in dotted lines); (*b*) Achieved spectral efficiency pairs at the converging SNRs

6.6 Chapter Summary

In this chapter, we proposed using the faster than Nyquist (FTN) signaling to achieve transmission over continuous-time broadcast channels. Furthermore, we have shown that the FTN broadcasting is capacity-wise optimal in the Gaussian broadcast channel, proving that FTN can be a viable alternative to other capacity-achieving techniques in broadcast channels (e.g., superposition coding and dirty paper coding). Consequently, two Turbo-coded FTN broadcast transceiver architectures have been designed, which are based on the Turbo equalization and Gaussian-approximation of ISI, respectively. Simulation results indicated that the designed FTN broadcast systems can outperform traditional *time*-or *frequency division* broadcasting and have the potential to perform close to the capacity boundaries of the Gaussian broadcast channel. The results in this chapter open a potential avenue for future research on the FTN signaling in various network settings involving multiple users and/or nodes.

Chapter 7

Conclusion

This work has been motivated by an explosive growth of data intensive applications over spectrally confined networks, such as video on demand, ubiquitous social networking and streaming live video services. These applications create a need for more spectrally efficient communication designs. To improve traditional Nyquist rate digital transmission systems, this dissertation studied the faster than Nyquist (FTN) rate signaling over continuous-time bandlimited channels as a means to trade processing complexity for improved spectral efficiency. The main goal of this work has been to develop a comprehensive treatment of the FTN signaling with a strong emphasis on its information-theoretic analysis in various channel setups and corresponding coding design to allow approaching the FTN capacity limits.

7.1 Research Contributions

This research has mainly contributed to advancing the knowledge on how digital information rates scale with the signaling rates in various communication settings over continuous-time channels. The three major research contributions have been the identification of the potential capacity benefits in precoded FTN signaling (Chapter 5), the establishment of the optimality of FTN signaling over Gaussian broadcast channels (Chapter 6), and the proposal of near-capacity FTN coding architectures (Chapter 4 and Chapter 6).

The research was mainly divided up into the following five parts:

- Formulation of discrete-time FTN channel models;
- Power spectral analysis of various FTN signals;
- Capacity analysis and coding designs for non-precoded FTN;
- Analysis of precoded FTN and identifying its merits;
- Exploration of FTN signaling over broadcast channels.

Furthermore, Table 7.1 summarizes the individual research contributions.

Table 7.1 Summary of presented research contributions

Objective	*Research Contributions*
Formulation of FTN channel models (Chapter 3)	- Formulated discrete-time FTN channel models for AWGN and linear Gaussian channel transmissions with generalized waveforms - Developed power transmission constraints in matrix equations that is suitable for any general FTN signals - Analyzed properties of FTN through the eigenvalue analysis of the FTN matrix H
Spectral analysis of various FTN signals (Chapter 3)	- Derived exact power spectral density (PSD) expressions of convolutionally precoded FTN signals - Studied PSD of more general, linearly precoded FTN signals - Identified sufficient conditions on FTN to prevent spectral broadening
Analysis of non-precoded FTN signaling (Chapter 4)	- Analyzed capacity of independent non-identically distributed FTN signaling - Proposed a low-complexity non-precoded FTN system architecture that offers significant implementation complexity savings at high spectral efficiencies
Analysis of precoded FTN signaling (Chapter 5)	- Derived the capacity-wise optimal precoding structure for FTN signaling - Analyzed the capacity of optimally precoded FTN signaling, which revealed significant capacity potentials in the FTN signaling - Formulated capacity versus computer precision tradeoffs for FTN - Analyzed capacity of convolutional precoded FTN signaling - Extended capacity analysis to LTI Gaussian channel setup, in which the capacity admits the classical water-filling solution

FTN broadcasting (Chapter 6)	- Proposed the novel concept of FTN broadcasting, which extends the FTN concept to a network setting for the first time - Showed FTN signaling over Gaussian broadcast channel is capacity-wise optimal - Proposed two transceiver architectures based on the FTN broadcasting, which showed the potential to perform close to the capacity boundaries of Gaussian broadcast channel

7.2 Directions for Future Work

This dissertation has revealed that there is a significant potential to the FTN signaling and opened an avenue for more exciting research in new directions. Future research work related to the presented FTN research results are listed below:

- The capacity potential in the optimally precoded FTN signaling can be further exploited with the technological advancements in the computer memory.
- The proposed FTN system can be implemented in hardware for actual field-tests. Two of the most attractive applications for the FTN systems wireless broadcast networks and fiber-optic communications systems.
- With its ability to multiplex more than one user's data in the time-domain, the proposed FTN broadcasting technique can be further exploited in various other network settings involving multiple users. For instance, the concept of FTN broadcasting can be applied to the interference channels or relay networks that involve multiple transmitters and receivers.
- The FTN channel model resembles many other practical digital communication setups including, but not limited to, inter-symbol interference channels, multiple-access channels with asynchronous transmitters, MIMO channels with asynchronous signal transmissions between antennas, and signal transmission over channels with time-varying channel bandwidths. Due to the similarities in these channel models, the analysis from this dissertation can be used to study these important, but non-trivial, communication scenarios.

(This page is intentionally left blank)

Appendix A

Proofs of Selected Information Theory Results

For completeness purposes, objective of this appendix is to provide proofs to selected (well-known) information theoretic results on the differential entropy function − namely, the differential entropy of a Gaussian random vector in Lemma 2.3, entropy maximizing distribution under the average power constraint in Lemma 2.4, and translation invariance of differential entropy in Lemma 2.5 − as well as the capacity of bandlimited Gaussian channel in Theorem 2.1. These results are used throughout the information theoretic analysis in Chapter 4, Chapter 5, and Chapter 6.

Lemma 2.3 (Differential entropy of Gaussian): *The differential entropy of a circularly symmetric complex Gaussian vector* $\mathbf{z}$ *with invertible covariance matrix* K_z *is* $h(\mathbf{z}) = \log_2((\pi e)^n \det K_z)$.

***Proof*:** The differential entropy of n-by-1 vector $\mathbf{z}$ is (by Definition 2.2 and Definition 2.3)

$$h(\mathbf{z}) = -E_{\mathbf{z}}\left\{\log_2 p(\mathbf{z})\right\} = -\frac{1}{\ln 2} E_{\mathbf{z}}\left\{-(\mathbf{z}-\boldsymbol{\mu})^{\dagger} K_z^{-1}(\mathbf{z}-\boldsymbol{\mu}) - \ln\left(\pi^n \det K_z\right)\right\} \quad \text{(A.1)}$$

$$= \frac{1}{\ln 2} E_{\mathbf{z}}\left\{tr\left((\mathbf{z}-\boldsymbol{\mu})^{\dagger} K_z^{-1}(\mathbf{z}-\boldsymbol{\mu})\right)\right\} + \log_2\left(\pi^n \det K_z\right) \quad \text{(A.2)}$$

$$= \frac{1}{\ln 2} E_{\mathbf{z}}\left\{tr\left(K_z^{-1}(\mathbf{z}-\boldsymbol{\mu})(\mathbf{z}-\boldsymbol{\mu})^{\dagger}\right)\right\} + \log_2\left(\pi^n \det K_z\right) \quad \text{(A.3)}$$

$$= \frac{1}{\ln 2} tr\left(K_z^{-1} E_{\mathbf{z}}\left\{(\mathbf{z}-\boldsymbol{\mu})(\mathbf{z}-\boldsymbol{\mu})^{\dagger}\right\}\right) + \log_2\left(\pi^n \det K_z\right) \quad \text{(A.4)}$$

$$= \frac{1}{\ln 2} tr\left(K_z^{-1} K_z\right) + \log_2\left(\pi^n \det K_z\right) \tag{A.5}$$

$$= \log_2 e^n + \log_2\left(\pi^n \det K_z\right) = \log_2\left(\left(\pi e\right)^n \det K_z\right), \tag{A.6}$$

where (A.2) is due to trace of a constant is the constant, (A.3) is by the trace identity tr(AB) = tr(BA), (A.4) is by exchanging order of trace and expectation operators, and (A.5) follows from the definition of the covariance matrix. This completes the proof. ■

Lemma 2.4 (Gaussian as entropy maximizing distribution): *Let* **x** *be a circularly symmetric complex Gaussian vector with* $n \times n$ *covariance matrix* K_x. *Also let* **y** *be another random vector, not necessarily Gaussian, with the same covariance. Then* $h(\mathbf{y}) \le h(\mathbf{x})$ *with equality if and only if* **y** *is also circularly symmetric Gaussian.*

***Proof*:** We start by evaluating the difference in the differential entropies:

$$h(\mathbf{x}) - h(\mathbf{y}) = -E_{\mathbf{x}}\left\{\log_2 p_{\mathbf{x}}(\mathbf{x})\right\} + E_{\mathbf{y}}\left\{\log_2 p_{\mathbf{y}}(\mathbf{y})\right\}. \tag{A.7}$$

But since $Cov(\mathbf{x}) = Cov(\mathbf{y}) = K_x$, for a nonsingular K_x,

$$-E_{\mathbf{x}}\left\{\log_2 p_{\mathbf{x}}(\mathbf{x})\right\} = \left(\log_2 e\right) tr\left(K_x^{-1} Cov(\mathbf{x})\right) + \log_2\left(\pi^n \det K_x\right) \tag{A.8}$$

$$= \left(\log_2 e\right) tr\left(K_x^{-1} Cov(\mathbf{y})\right) + \log_2\left(\pi^n \det K_x\right) \tag{A.9}$$

$$= -E_{\mathbf{y}}\left\{\log_2 p_{\mathbf{x}}(\mathbf{y})\right\}. \tag{A.10}$$

Therefore, (A.7) can be written as

$$h(\mathbf{x}) - h(\mathbf{y}) = E_{\mathbf{y}}\left\{\log_2 \frac{p_{\mathbf{y}}(\mathbf{y})}{p_{\mathbf{x}}(\mathbf{y})}\right\} \tag{A.11}$$

$$\ge \frac{1}{\ln(2)} E_{\mathbf{y}}\left\{1 - \frac{p_{\mathbf{x}}(\mathbf{y})}{p_{\mathbf{y}}(\mathbf{y})}\right\} \tag{A.12}$$

$$= \frac{1}{\ln(2)}\left(1 - \int p_{\mathbf{x}}(\mathbf{y})\, d\mathbf{y}\right) = 0, \tag{A.13}$$

where the inequality in (A.12) is due to the log-inequality: $\ln(x) \ge 1 - (1/x)$ for $x > 0$. This completes the proof. ■

Lemma 2.5 (Translation invariance of differential entropy): *Let* $\mathbf{x}$ *be any* $n\times 1$ *complex random vector and* $\mathbf{c}$ *be any deterministic (non-random) vector. Then* $h(\mathbf{x}+\mathbf{c}) = h(\mathbf{x})$.

***Proof*:** Let $\mathbf{y} = \mathbf{x} + \mathbf{c}$. Then $p_{\mathbf{y}}(\mathbf{y}) = p_{\mathbf{x}}(\mathbf{y}-\mathbf{c})$, and

$$h(\mathbf{x}+\mathbf{c}) = -\int_{\mathbf{y}\in\mathbb{C}^n} p_{\mathbf{y}}(\mathbf{y})\log_2 p_{\mathbf{y}}(\mathbf{y})\,d\mathbf{y} \tag{A.14}$$

$$= -\int_{\mathbf{y}\in\mathbb{C}^n} p_{\mathbf{x}}(\mathbf{y}-\mathbf{c})\log_2 p_{\mathbf{x}}(\mathbf{y}-\mathbf{c})\,d\mathbf{y} \tag{A.15}$$

$$= -\int_{\mathbf{x}\in\mathbb{C}^n} p_{\mathbf{x}}(\mathbf{x})\log_2 p_{\mathbf{x}}(\mathbf{x})\,d\mathbf{x} \tag{A.16}$$

$$= h(\mathbf{x}), \tag{A.17}$$

where (A.16) is due to a change of variables in the integral. This completes the proof. ■

A proof of the capacity expression of bandlimited AWGN channel is given below:

Theorem 2.1 (Capacity of bandlimited Gaussian channel [132], [31]): *The capacity of an additive white Gaussian noise (AWGN) channel with noise power spectral density N0/2 watts/Hertz, and transmission power P watts is given by*

$$C_{AWGN} = \frac{1}{2T}\log_2\left(1+\frac{PT}{N_0/2}\right) \text{ bits per second,} \tag{A.18}$$

where T is the symbol period in seconds. When the Gaussian channel is strictly bandlimited to [−W, W] Hertz with the Nyquist rate signaling of 1/T = 2W, the corresponding capacity of the bandlimited Gaussian channel is given by

$$C_{AWGN} = W\log_2\left(1+\frac{P}{N_0 W}\right) \text{ bits per second.} \tag{A.19}$$

***Proof*:** Consider the channel input vector $\mathbf{x}$ and channel output vector $\mathbf{y} = \mathbf{x} + \mathbf{z}$ of sizes $n\times 1$, where $\mathbf{z}$ is an *i.i.d.* Gaussian noise vector with zero mean and diagonal covariance $K_z = (N_0/2)I_n$. The input vector $\mathbf{x}$ is subject to the conventional average power constraint $n^{-1}\sum_{i=1}^{n} E\{|x_i|^2\} \le PT$ where P is available power in watts (and PT corresponds to energy in Joules per symbol).

Following the definition of the channel capacity formula from Definition 2.7, we evaluate the mutual information between $\mathbf{x}$ and $\mathbf{y}$ as follows:

$$n^{-1}I(\mathbf{x};\mathbf{y}) = n^{-1}\left(h(\mathbf{y}) - h(\mathbf{y}|\mathbf{x})\right) \tag{A.20}$$

$$= n^{-1}\left(h(\mathbf{y}) - h(\mathbf{z}|\mathbf{x})\right) \tag{A.21}$$

$$= n^{-1}\left(h(\mathbf{y}) - h(\mathbf{z})\right) \tag{A.22}$$

$$= n^{-1}\left(h(\mathbf{y}) - \log_2\left((\pi e)^n \det K_z\right)\right) \tag{A.23}$$

$$\leq n^{-1}\left(\log_2\left((\pi e)^n \det(K_x + K_z)\right) - \log_2\left((\pi e)^n \det K_z\right)\right) \tag{A.24}$$

$$= n^{-1}\log_2\left(\frac{\det(K_x + K_z)}{\det K_z}\right) \tag{A.25}$$

$$= n^{-1}\log_2\left(\det\left(I_n + \left(\frac{N_0}{2}\right)^{-1} K_x\right)\right) \tag{A.26}$$

$$\leq n^{-1}\log_2\left(\prod_{i=1}^{n}\left(1 + \frac{E\{|x_i|^2\}}{N_0/2}\right)\right) \tag{A.27}$$

$$= n^{-1}\sum_{i=1}^{n}\log_2\left(1 + \frac{E\{|x_i|^2\}}{N_0/2}\right) \tag{A.28}$$

$$\leq \log_2\left(1 + \frac{PT}{N_0/2}\right), \tag{A.29}$$

where (A.20) is due to the definition of mutual information where $h(\cdot)$ denotes the differential entropy, (A.21) is due to the translation invariance of the differential entropy by Lemma 2.5, (A.22) is due to statistical independence of the channel input **x** and the AWGN noise **z**, (A.23) is due to the known differential entropy expression of the Gaussian vector by Lemma 2.3, and (A.24) is due to differential entropy maximizing distribution being Gaussian by Lemma 2.4, followed by **y** having a covariance matrix K_x+K_z, where K_x and K_z are the covariance matrices of **x** and **z**, respectively. Furthermore, (A.26) is obtained after substituting the covariance matrix of noise $K_z = (N_0/2)I_n$, and (A.27) is due to Hadamard's inequality [30] where $E\{|x_i|^2\}$ is i-th diagonal entry of K_x. Finally, (A.28) can be further maximized by using the method of Lagrange multipliers under the power constraint $n^{-1}\sum_{i=1}^{n} E\{|x_i|^2\} \le PT$, leading to (A.29) with an equal power distribution being optimal, i.e., $E\{|x_i|^2\} = PT$ for all i = 1, 2, …, n.

Therefore, we have the following capacity expression:

$$C = \lim_{n\to\infty} \sup_{p(\mathbf{x})\in S} \frac{1}{n} I(\mathbf{x};\mathbf{y}) = \frac{1}{2}\log_2\left(1+\frac{PT}{N_0/2}\right) \textit{ in bits/channel use,} \tag{A.30}$$

where the factor 1/2 is accounts for non-complex (real) AWGN channel transmissions, and the capacity is achieved by choosing **x** Gaussian distributed with zero mean and covariance matrix $K_x = (PT)\cdot I_n$. Finally, assuming the *Nyquist rate transmission*, each data symbol is sent every T seconds (i.e., one channel use per T seconds). This leads to the following capacity expression in units of bits per second:

$$C_{AWGN} = \frac{1}{2T}\log_2\left(1+\frac{PT}{N_0/2}\right) \textit{ in bits/second.} \tag{A.31}$$

Furthermore, substituting $1/T = 2W$ for the *Nyquist rate transmission* leads to (A.19). This completes the proof of Theorem 2.1. ■

Appendix B

Simultaneously Time- and Frequency-Limited Signals

The objective of this appendix is to give a simple plausibility argument to why no signals can be both strictly band-limited and strictly time-limited, except the zero energy signals. First, it is trivial to show that zero energy signals have zero Fourier transforms, and hence the zero energy signals are both time-limited and band-limited in the strict sense.

Now for non-zero energy signals, consider the following argument. Let a non-zero energy signal $x(t)$ be strictly time-limited to the time range $t_1 < t < t_2$. Then the signal can be multiplied by a rectangle function $r(t)$ whose value is equal to one in the time range $t_1 < t < t_2$ and zero everywhere else, without effecting the signal $x(t)$. That is, $x(t) = x(t)r(t)$. Taking the Fourier transform of this product $x(t)r(t)$ yields a *convolution* of $\hat{x}(f)$, denoting the Fourier transform of $x(t)$, and a sinc function which is the Fourier transform of the rectangle function. That is,

$$\hat{x}(f) = \hat{x}(f) * \left[e^{-j\pi f (t_1 + t_2)} (t_2 - t_1) \mathrm{sinc}\left((t_2 - t_1) f \right) \right],$$

where * denotes the convolution. Now suppose that $\hat{x}(f)$ is also strictly band-limited to some frequency range. But due to the infinite support of the sinc function, the convolution of $\hat{x}(f)$ and the sinc function cannot have a finite support. Hence we have a contradiction and conclude that $\hat{x}(f)$ could not have been strictly band-limited when $x(t)$ is strictly time-limited. The converse, i.e., a strictly band-limited signal cannot be also strictly time-limited, may be proven by a similar argument.

Appendix C

Nonsingularity of a Class of Toeplitz Matrices

The goal of this appendix is to prove our own result, Lemma 3.2, which derives a sufficient condition for invertibility of a class of Toeplitz matrices including the FTN matrix H and the noise covariance matrix Φ. The invertibility of these Toeplitz matrices has several important consequences in the analysis of FTN signaling, including the existence of the capacity-achieving precoding for the FTN signaling in Chapter 5.

Lemma 3.2: *Let q_k be defined by:*

$$q_k \equiv \int_{-\infty}^{+\infty} q(\tau) q^*(\tau - k\Delta t)\, d\tau, \quad k \in \mathbb{Z},$$

where $\Delta t > 0$ and $q(t)$ is any non-zero finite energy signal that is either strictly band-limited or time-limited. If $q_k \to 0$ as $k \to \infty$ then the $n \times n$ matrix sequence Q_n defined by $Q_n = [q_{(i-j)}]_{i,\, j=0,\, 1,\, \ldots,\, n-1}$ is non-singular for every n. [43]

Proof: The proof is obtained by modifying the proof of Proposition 5.1.1 in [21] to fit the problem considered here. Without loss of generality, let us assume that $q(t)$ has a unit energy[44], leading to $q_0 = 1$. Now, suppose that Q_n is singular for some n. Then there exists

---

[43] Note that $Q_1 = q_0$, $Q_2 = \begin{bmatrix} q_0 & q_{-1} \\ q_1 & q_0 \end{bmatrix}$, $Q_3 = \begin{bmatrix} q_0 & q_{-1} & q_{-2} \\ q_1 & q_0 & q_{-1} \\ q_2 & q_1 & q_0 \end{bmatrix}$, etc.

[44] This assumption corresponds to normalizing the matrix Q_n by a constant non-zero scalar. This does not affect the non-singularity of the matrices.

an integer $r \geq 1$ such that Q_r is nonsingular but Q_{r+1} is singular (note that Q_1 is always nonsingular since $Q_1 = 1 = Q_1^{-1}$). We will prove the lemma by a contradiction. By Lemma 3.1, singular Q_{r+1} implies that there exist $a_0, \ldots, a_{r-1} \in \square$ not all zero such that

$$q(t - r\Delta t) = \sum_{j=0}^{r-1} a_j q(t - j\Delta t),$$

i.e., $q(t-r\Delta t)$ is linearly dependent to the set $\{q(t), q(t-\Delta t), q(t-2\Delta t), \ldots, q(t-(r-1)\Delta t)\}$ to yield Q_{r+1} singular. (Note that in this appendix, for the brevity of the following proof steps, we will use j to refer to an index of the summation and not to an imaginary unit). We also have, by delaying time by $k\Delta t$,

$$q(t - (r+k)\Delta t) = \sum_{j=0}^{r-1} a_j q(t - (j+k)\Delta t).$$

This implies that $q(t - n\Delta t)$ for all $n \geq r$ are also linearly dependent to the set $\{q(t-k\Delta t)\}_{k = 0, \ldots, r-1}$. Consequently, for all $n \geq r$, there exist constants $a_0^{(n)}, \cdots, a_{r-1}^{(n)}$ not all zero such that

$$\begin{aligned} q(t - n\Delta t) &= \sum_{j=0}^{r-1} a_j^{(n)} q(t - j\Delta t) \\ &= \left(\mathbf{a}^{(n)}\right)^T \mathbf{q}_r(t), \end{aligned} \tag{C.1}$$

where $\mathbf{a}^{(n)} = [a_0^{(n)}, \ \cdots, \ a_{r-1}^{(n)}]^T$ and $\mathbf{q}_r(t) = [q(t), \ \cdots, \ q(t-(r-1)\Delta t)]^T$. In order words, if Q_{r+1} is singular, $Q_{r+2}, Q_{r+3}, \cdots$ are all singular.

Using (C.1), we can derive square of the norm of $q(t)$ as follows:

$$\begin{aligned} 1 &= \int_{-\infty}^{+\infty} q(t - n\Delta t) q^*(t - n\Delta t)\, dt \\ &= \sum_{i=0}^{r-1} \sum_{j=0}^{r-1} a_j^{(n)} \left(a_i^{(n)}\right)^* \int_{-\infty}^{+\infty} q(t - j\Delta t) q^*(t - i\Delta t)\, dt \\ &= \sum_{i=0}^{r-1} \sum_{j=0}^{r-1} a_j^{(n)} \left(a_i^{(n)}\right)^* q_{(i-j)}. \end{aligned}$$

In matrix notations,

$$\begin{aligned} 1 &= \sum_{i=0}^{r-1}\sum_{j=0}^{r-1} a_j^{(n)} q_{(i-j)} \left(a_i^{(n)}\right)^* = \left(\mathbf{a}^{(n)}\right)^\dagger Q_r \mathbf{a}^{(n)} \\ &= \left(\mathbf{a}^{(n)}\right)^\dagger U_r^\dagger \Lambda_r U_r \mathbf{a}^{(n)}, \end{aligned} \tag{C.2}$$

where $(\cdot)^\dagger$ denotes conjugate transpose (Hermitian) operator and $Q_r = U_r^\dagger \Lambda_r U_r$ by eigenvalue decomposition (recall that Q_r is non-singular and is Hermitian positive definite). The $r \times r$ diagonal matrix Λ_r has its diagonal entries strictly positive real eigenvalues $\lambda_0 \geq \lambda_1 \geq \cdots \geq \lambda_{r-1} > 0$ of Q_r, and U_r is an $r \times r$ unitary matrix satisfying $U_r^\dagger U_r = I_r$ where I_r is an $r \times r$ identity matrix.

But note that for some $\mathbf{x} \neq 0$,

$$\begin{aligned} \mathbf{x}^T \Lambda_r \mathbf{x} &= \lambda_0 x_0^2 + \lambda_1 x_1^2 + \cdots + \lambda_{r-1} x_{r-1}^2 \\ &\geq \lambda_{r-1}\left(x_0^2 + x_1^2 + \cdots + x_{r-1}^2\right) = \lambda_{r-1} \mathbf{x}^T \mathbf{x}. \end{aligned}$$

Applying this inequality to (C.2) yields

$$\begin{aligned} 1 = \left(\mathbf{a}^{(n)}\right)^\dagger U_r^\dagger \Lambda_r U_r \mathbf{a}^{(n)} &\geq \lambda_{r-1} \left(\mathbf{a}^{(n)}\right)^\dagger U_r^\dagger U_r \mathbf{a}^{(n)} \\ &= \lambda_{r-1} \left(\mathbf{a}^{(n)}\right)^\dagger \mathbf{a}^{(n)} \\ &= \lambda_{r-1} \sum_{j=0}^{r-1} \left| a_j^{(n)} \right|^2. \end{aligned}$$

Since $\lambda_{r-1} > 0$, dividing by λ_{r-1} to both sides gives

$$\sum_{j=0}^{r-1} \left| a_j^{(n)} \right|^2 \leq \frac{1}{\lambda_{r-1}} < \infty .$$

In other words, for any fixed j,

$$\left| a_j^{(n)} \right| < \infty \text{, for } n \geq r. \tag{C.3}$$

We can also write using (C.1)

$$\begin{aligned}
1 &= \int_{-\infty}^{+\infty} q\left(t-n\Delta t\right) q^*\left(t-n\Delta t\right) dt \\
&= \int_{-\infty}^{+\infty} \left(\sum_{j=0}^{r-1} a_j^{(n)} q\left(t-j\Delta t\right) \right) q^*\left(t-n\Delta t\right) dt \\
&= \sum_{j=0}^{r-1} a_j^{(n)} \int_{-\infty}^{+\infty} q\left(t-j\Delta t\right) q^*\left(t-n\Delta t\right) dt \\
&= \sum_{j=0}^{r-1} a_j^{(n)} q_{(n-j)}.
\end{aligned}$$

We then establish the following inequality (by the triangular inequality):

$$1 = \sum_{j=0}^{r-1} a_j^{(n)} q_{(n-j)} \leq \sum_{j=0}^{r-1} \left|a_j^{(n)}\right| \left|q_{(n-j)}\right| .$$

From our assumption that $q_k \to 0$ as $k \to \infty$ and by $|a_j^{(n)}| < \infty$ from (C.3),

$$1 \leq \sum_{j=0}^{r-1} \left|a_j^{(n)}\right| \left|q_{(n-j)}\right| \to 0 \ \text{ as } n \to \infty,$$

which clearly fails for n large enough. Hence, it is not possible to have $q_k \to 0$ as $k \to \infty$ if Q_n is singular for some n. This completes the proof of Lemma 3.2. ■

Appendix D

Szegö's Theorem on Eigenvalues of Toeplitz Matrices

The objective of this Appendix is to review Szegö's theorem on the asymptotic eigenvalue distribution of Toeplitz matrices and some of its generalizations (please refer to [56] for the proofs).

First we introduce some notations. A sequence of $n \times n$ Hermitian Toeplitz matrices $T_n(p) = [t_{i-j}; i, j = 0, 1, \ldots, n-1]$ is

$$T_n(p) = \begin{bmatrix} t_0 & t_{-1} & t_{-2} & \cdots & t_{-(n-1)} \\ t_1 & t_0 & t_{-1} & & t_{-(n-2)} \\ t_2 & t_1 & t_0 & & t_{-(n-3)} \\ \vdots & & & \ddots & \vdots \\ t_{n-1} & t_{n-2} & t_{n-3} & \cdots & t_0 \end{bmatrix},$$

where $t_k = t_{-k}^*$ due to Hermitianity and $\{t_k\}$ are assumed to be absolutely summable and hence the following inverse Fourier series of $\{t_k\}$ exists:

$$p(\lambda) = \sum_{k=-\infty}^{\infty} t_k e^{jk\lambda}, \tag{D.1}$$

$$t_k = \frac{1}{2\pi} \int_0^{2\pi} p(\lambda) e^{-jk\lambda} d\lambda. \tag{D.2}$$

Furthermore, we let $m_p \equiv \operatorname{ess\,inf}_\lambda p(\lambda)$ (essential infimum) and $M_p \equiv \operatorname{ess\,sup}_\lambda p(\lambda)$ (essential supremum). The asymptotic eigenvalues of $T_n(p)$ as n tends to infinity is given by the following celebrated theorem known as Szegö's theorem [57].

Theorem D.1 (Szegö's theorem [57], [56]): *Let $\tau_{n,k}$ be the eigenvalues of $T_n(p)$. Then for any function $F(x)$ continuous on $[m_p, M_p]$*

$$\lim_{n\to\infty}\frac{1}{n}\sum_{k=0}^{n-1}F(\tau_{n,k})=\frac{1}{2\pi}\int_{-\pi}^{\pi}F(p(\lambda))d\lambda . \tag{D.3}$$

(In other words, sum of eigenvalues converges to integral of inverse Fourier series of the matrix entries.)

Next theorem shows that Szegö's theorem can be applied to a product of Toeplitz matrices, although the product of two Toeplitz matrices is not necessarily Toeplitz.

Theorem D.2 (Product of two Hermitian Toeplitz matrices [56]): *Let $T_n(p) = [t_{i-j}]$ be an $n\times n$ Toeplitz matrix with $p(\lambda)$ as the inverse Fourier series of $\{t_k\}$. Similarly, $T_n(q) = [r_{i-j}]$ is defined as another Toeplitz matrix with $q(\lambda)$ as the inverse Fourier series of $\{r_k\}$. If both $T_n(p)$ and $T_n(q)$ are Hermitian and $\rho_{n,k}$ denote the eigenvalues of the matrix product $T_n(p)T_n(q)$, then for any function, $F(x)$, continuous on $[m_pm_q, M_pM_q]$*

$$\lim_{n\to\infty}\frac{1}{n}\sum_{k=0}^{n-1}F(\rho_{n,k})=\frac{1}{2\pi}\int_{-\pi}^{\pi}F\left(p(\lambda)q(\lambda)\right)d\lambda . \tag{D.4}$$

Next theorem deals with Szegö's theorem for an inverse of a Toeplitz matrix.

Theorem D.3 (Inverse of Toeplitz matrix is asymptotically Toeplitz [56]): *As before, let $T_n(p) = [t_{i-j}]$ be an $n\times n$ Hermitian Toeplitz matrix with $p(\lambda)$ as the inverse Fourier series of $\{t_k\}$. Let $\rho_{n,k}$ be the eigenvalues of $T_n(p)^{-1}$. If $p(\lambda) \geq m_p > 0$, then for any continuous function, $F(x)$ on $[1/M_p, 1/m_p]$*

$$\lim_{n\to\infty}\frac{1}{n}\sum_{k=0}^{n-1}F(\rho_{n,k})=\frac{1}{2\pi}\int_{-\pi}^{\pi}F\left(1/p(\lambda)\right)d\lambda . \tag{D.5}$$

The eigenvalues of Hermitian Toeplitz $T_n(p)$ are characterized below:

Lemma D.1 (Bounds on the eigenvalues [56]): *Let $\tau_{n,k}$ be the eigenvalues of $T_n(p)$ and let m_p and M_p denote the essential infimum and the essential supremum of $p(\lambda)$, respectively. Then*

$$m_p \leq \tau_{n,k} \leq M_p . \tag{D.6}$$

Also, in the limit as n tends to infinity,

$$\lim_{n\to\infty} \max_k \tau_{n,k} = M_p , \tag{D.7}$$

$$\lim_{n\to\infty} \min_k \tau_{n,k} = m_p . \tag{D.8}$$

Finally, the asymptotic eigenvalue distribution of Hermitian Toeplitz $T_n(p)$, as n tends to infinity, is given below:

Lemma D.2 (Asymptotic eigenvalue distribution [56]): *Let $\tau_{n,k}$ be the eigenvalues of $T_n(p)$ and define the eigenvalue distribution function $D_n(x)$ = (number of $\tau_{n,k} \le x$)/n. Assume furthermore that*

$$\int_{\lambda:p(\lambda)=x} d\lambda = 0 . \tag{D.9}$$

Then the limiting distribution $D(x) = \lim_{n\to\infty} D_n(x)$ exists and is given by

$$D(x) = \frac{1}{2\pi}\int_{p(\lambda)\le x} d\lambda . \tag{D.10}$$

(Note that fraction of eigenvalues between two values a and b (b>a) is then D(b) – D(a). The definition D(x) is similar to the cumulative distribution function (CDF) in probability theory.)

Appendix E

BER Results for Some Optimally Precoded FTN Systems

The optimal FTN precoding that we derived in section 5.2 can lead to substantial capacity gains over capacity of non-precoded FTN signaling. As discussed in subsection 5.2.4, however, ill-conditioning of the optimal FTN precoding poses a significant challenge in practical system implementation. Figure E.1 shows our initial BER simulation results of this optimally precoded FTN signaling with varying FTN rate factor K = 1, 2, 3 for short packet lengths N = ceil(20/K), where ceil(·) refers to the smallest interger not less than its argument.

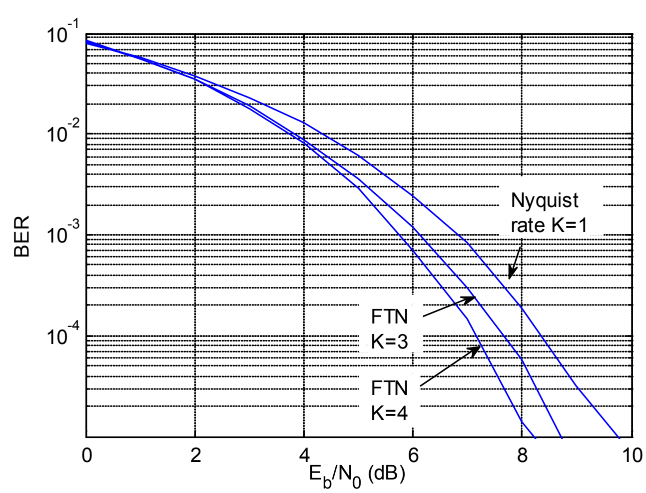

Figure E.1 Simulated bit-error-rate (BER) performances of the optimally precoded FTN signaling as compared to the Nyquist rate signaling for short packet length

In Figure E.1, binary antipodal modulation and strictly bandlimited sinc modulating pulse were used in all cases. Hard decision decoding was used for the K=1 Nyquist rate case, whereas single parity check coding was applied across 2 and 3 consecutive data bits in K = 3 and K = 4 FTN cases, respectively, thereby exploiting the increased symbol rates in FTN.

We also explored fractional-rate FTN signaling by letting the FTN rate factor K to be any positive real number (i.e., allowing $0 < K < 1$). Figure E.2 demonstrates such possibility: By inserting 5 additional sinc pulses into a Nyquist rate of block of size N = 100, up to 5% fractional rate increase over the Nyquist rate was obtained without noticeable loss on BER and bandwidth. These additional FTN pulses can be used to carry extra information such as control data, watermarks, etc.

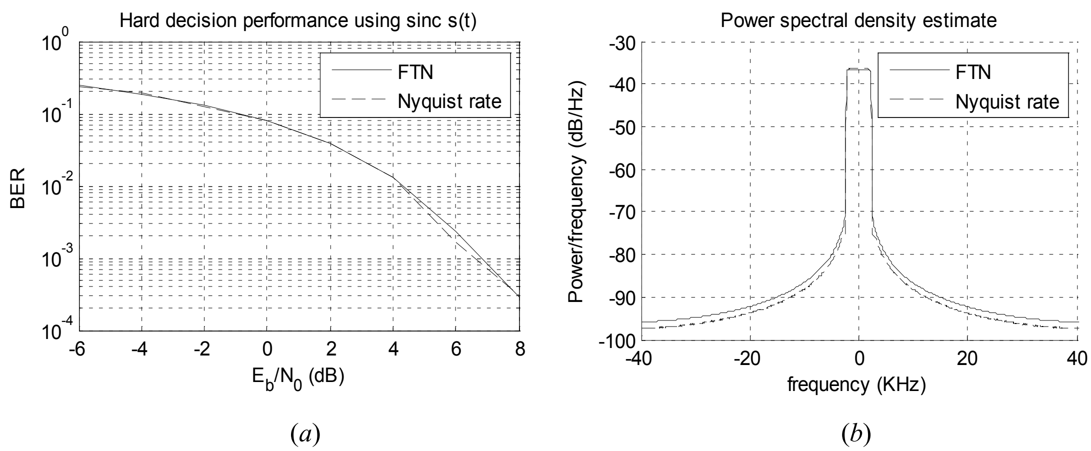

Figure E.2 Fractional-rate FTN signaling (for 5% rate increase over Nyquist rate); (a) showing hard decision performance of FTN compared to the Nyquist rate signaling; (b) the power spectral density estimates for the FTN signal compared to the Nyquist rate signal

References

[1] J. B. Allen and L. R. Rabiner, “A unified approach to short-time Fourier analysis and synthesis,” *Proceedings of the IEEE*, vol. 65, pp. 1558-1564, Nov. 1977.

[2] F. Amoroso, “The bandwidth of digital data signals,” *IEEE Communications Magazine*, vol. 18, pp. 13-24, Nov. 1980.

[3] A. Amraoui, G. Kramer, and S. Shamai (Shitz), “Coding for the MIMO broadcast channel,” in *Proc. IEEE International Symposium on Information Theory*, Yokohama, Japan, pp. 296, Jun./Jul. 2003.

[4] M. Armand and J.-M. Tarascon, “Building better batteries,” *Nature*, vol. 451, pp. 652-657, Feb. 2008.

[5] R. B. Ash, “Capacity and error bounds for a time-continuous Gaussian channel,” *Information and Control*, vol. 6, pp. 14-27, Mar. 1963.

[6] R. B. Ash, “Further discussion of a time-continuous Gaussian channel,” *Information and Control*, vol. 7, pp. 78-83, Mar. 1964.

[7] R. B. Ash, *Information Theory*. New York: Dover, 1990.

[8] E. Ayanoglu, “Data transmission when the sampling frequency exceeds the Nyquist rate,” *IEEE Communications Letters*, vol. 1, pp. 157-159, Nov. 1997.

[9] E. Ayanoglu, N. R. Dagdeviren, G. D. Golden, and J. E. Mazo, “An equalizer design technique for the PCM modem: A new modem for the Digital Public Switched Network,” *IEEE Transactions on Communications*, vol. 46, pp. 763-774, June 1998.

[10] L. Bahl, J. Cocke, F. Jelinek, and J. Raviv, “Optimal decoding of linear codes for minimizing symbol error rate,” *IEEE Transactions on Information Theory*, vol. 20, pp. 284-287, Mar. 1974.

[11] J. Bajcsy and H. Kobayashi, “On obtaining the BCJR algorithm via path counting,” in *Proc. IEEE International Symposium on Information Theory and its Applications*, Honolulu, HI, pp. 192-194, Nov. 2000.

[12] K. Barman and O. Dabeer, “Capacity of MIMO systems with asynchronous PAM,” *IEEE Transactions of Communications*, vol. 57, pp. 3366-3375, Nov. 2009.

[13] N. C. Beaulieu, “Introduction to ‘Certain Topics in Telegraph Transmission Theory’,” *Proceedings of the IEEE*, vol. 90, pp. 276-279, Feb. 2002.

[14] S. Benedetto, D. Divsalar, G. Montorsi, and F. Pollara, “Serial concatenation of interleaved codes: Performance analysis, design, and iterative decoding,” *IEEE Transactions on Information Theory*, vol. 44, pp.909-926, May 1998.

[15] S. Benedetto and G. Montorsi, “Unveiling Turbo codes: Some results on parallel concatenated coding schemes,” *IEEE Transactions on Information Theory*, vol. 42, pp. 409-428, Mar 1996.

[16] P. P. Bergmans, “A simple converse for broadcast channels with additive white Gaussian noise,” *IEEE Transactions on Information Theory*, vol. 20, pp. 279-290, Mar. 1974.

[17] P. Berlin and D. Tuninetti, “LDPC codes for fading Gaussian broadcast channels,” *IEEE Transactions on Information Theory*, vol. 51, pp. 2173-2182, June 2005.

[18] C. Berrou, A. Glavieux, and P. Thitmajshima, “Near Shannon limit error-correcting coding and decoding: Turbo-codes,” in *Proc. IEEE International Conference on Communications*, Geneva, Switzerland, pp. 1064-1070, May 1993.

[19] S. Boyd, “Multitone signals with low crest factor,” *IEEE Transactions on Circuits and Systems*, vol. 33, pp. 1018-1022, Oct. 1986.

[20] S. Boyd and L. Vandenberghe, *Convex Optimization.* Cambridge University Press, 2004.

[21] P. J. Brockwell and R. A. Davis, *Time Series: Theory and Methods,* 2nd ed. New York: Springer-Verlag, 1991.

[22] J.-X. Cai, C. R. Davidson, A. Lucero, H. Zhang, D. G. Foursa, O. V. Sinkin, W. W. Patterson, A. N. Pilipetskii, G. Mohs, and N. S. Bergano, “20 Tbits/s transmission over 6860 km with sub-Nyquist channel spacing,” *IEEE/OSA Journal of Lightwave Technology*, vol. 30, pp. 651-657, Feb. 2012.

[23] P. Chen and F. Alajaji, “Lecture notes in information theory volume II,” Sept. 2009, http://shannon.cm.nctu.edu.tw/it/itvol22004.pdf.

[24] G. Colavolpe and A. Barbieri, “On MAP symbol detection for ISI channels using Ungerboeck observation model,” *IEEE Communications Letters*, vol. 9, pp. 720-722, Aug. 2005.

[25] G. Colavolpe, T. Foggi, A. Modenini, and A. Piemontese, “Faster-than-Nyquist and beyond: How to improve spectral efficiency by accepting interference,” *Optics Express*, vol. 19, pp. 26600-26609, Dec. 2011.

[26] G. R. Cooper and C. D. McGillem, *Probabilistic Methods of Signal and System Analysis,* 3rd ed. Oxford University Press, 1999.

[27] M. H. M. Costa, “Writing on dirty paper,” *IEEE Transactions on Information Theory*, vol. 29, pp. 439-441, May 1983.

[28] T. M. Cover, “Broadcast channels,” *IEEE Transactions on Information Theory*, vol. IT-18, pp. 2-14, Jan. 1972.

[29] T. M. Cover, “Comments on broadcast channels,” *IEEE Transactions on Information Theory*, vol. 44, pp. 2524-2530, Oct. 1998.

[30] T. M. Cover and A. El Gamal, “An information theoretic proof of Hadamard’s inequality,” *IEEE Transactions on Information Theory*,” vol. IT-29, pp. 930-931, Nov. 1983.

[31] T. M. Cover and J. A. Thomas, *Elements of Information Theory*. New York: Wiley-Interscience, 1991.

[32] D. Dasalukunte, F. Rusek, J. B. Anderson, and V. Öwall, “A 0.8mm^2 9.6mW implementation of a multicarrier faster-than-Nyquist signaling iterative decoder in 65nm CMOS,” in *Proc. European Solid State Circuits Conference*, Bordeaux, France, pp. 173-176, Sept. 2012.

[33] D. Dasalukunte, F. Rusek, and V. Öwall, “Multicarrier faster-than-Nyquist transceivers: Hardware architecture and performance analysis,” *IEEE Transactions on Circuits and Systems-I: Regular papers*, vol. 58, pp. 827-838, April 2011.

[34] D. Dasalukunte, F. Rusek, V. Öwall, K. Ananthanarayanan, and M. Kandasamy, “Hardware implementation of mapper for faster-than-Nyquist signaling transmitter,” in *Proc. IEEE NORCHIP*, Trondheim, Norway, 5 pages, Nov. 2009.

[35] Digital video broadcasting (DVB): Interaction channel for satellite distribution systems, ETSI EN 301 790, V1.5.1, European Standard (Telecommunication series), May 2009.

[36] D. Divsalar and F. Pollara, “Turbo codes for PCS applications,” in *Proc. International Conference on Communications*, Seattle, WA, pp. 54-59, June 1995.

[37] C. Douillard, M. Jézéquel, and C. Berrou, “Iterative correction of intersymbol-interference: Turbo equalization,” *European Transactions on Telecommunications*, vol. 6, pp. 507-511, Sept.-Oct. 1995.

[38] C. Douillard, M. Jézéquel, C. Berrou, N. Bengarth, J. Tousch, and N. Pham, "The Turbo code standard for DVB-RCS," in *Proc. International Symposium on Turbo Codes & Related Topics*, Brest, France, pp. 535-538, Sept. 2000.

[39] A. El Gamal and Y.-H. Kim, "Lecture notes on network information theory," 2010. [Online]. Available: http://arxiv.org/abs/1001.3404.

[40] C. Eoff, "The discrete nature of the Paley-Wiener spaces," *Proceedings of the American Mathematical Society*, vol. 123, pp. 505-512, Feb. 1995.

[41] U. Erez and G. W. Wornell, "A super-Nyquist architecture for reliable underwater acoustic communication," in *Proc. Annual Allerton Conference on Communication, Control, and Computing*, Monticello, IL, pp. 469-476, Sept. 2011.

[42] U. Erez and G. W. Wornell, "Super-Nyquist rateless coding for intersymbol interference channels," in *Proc. International Zurich Seminar on Communications*, Zurich, Switzerland, 4 pages, Mar. 2012.

[43] U. Erez, G. W. Wornell, and M. D. Trott, "Faster-than-Nyquist coding: The merits of regime change," in *Proc. Allerton Conference on Communication*, *Control, and Computing*, Monticello, IL, pp. 933-942, Oct. 2004.

[44] G. Fettweis, "Roadways for advancing cellular communications," *Plenary Talk at SYTACom Annual Research Workshop*, Quebec City, QC, Sept. 2012.

[45] A. Fihel and H. Sari, "Performance of reduced-bandwidth 16 QAM with decision-feedback equalization," *IEEE Transactions on Communications*, vol. 35, pp. 715-723, July 1987.

[46] G. D. Forney Jr., "Maximum-likelihood sequence estimation of digital sequences in the presence of intersymbol interference," *IEEE Transactions on Information Theory*, vol. IT-18, pp. 363-378, May 1972.

[47] G. D. Forney Jr. and D. J. Costello, Jr., “Channel coding: The road to channel capacity,” *Proceedings of the IEEE*, vol. 95, pp. 1150-1177, June 2007.

[48] G. D. Forney Jr. and L.-F. Wei, “Multidimensional constellations-Part I: Introduction, figures of merit, and generalized cross constellations,” *IEEE Journal on Selected Areas in Communications,* vol. 7, pp. 877-892, Aug. 1989.

[49] G. J. Foschini, “Contrasting performance of faster binary signaling with QAM,” *AT&T Bell Labs Technical Journal*, vol. 63, pp. 1419-1445, Oct. 1984.

[50] J. B. Fraleigh and R. A. Beauregard, *Linear Algebra*, 3rd ed. United States of America: Addison-Wesley Publishing Co., 1995.

[51] F. R. Gantmacher, *The Theory of Matrices*. *Vol. 1*. Translated by K. A. Hirsch. New York: Chelsea Publishing Co., 1959.

[52] W. A. Gardner, *Cyclostationarity in Communications and Signal Processing.* New York: IEEE Press, 1993.

[53] D. Gesbert, M. Shafi, D. S. Shiu, P. J. Smith, and A. Naguib, “From theory to practice: An overview of MIMO space-time coded wireless systems,” *IEEE Journal on Selected Areas in Communications,* vol. 21, pp. 281-302, Apr. 2003.

[54] *Global Internet phenomena report*, Fall 2011, Sandvine Inc., Retrieved June 2012.

[55] G. H. Golub and C. F. van Loan, *Matrix Computations*, 3rd ed. Baltimore, MD: Johns Hopkins University Press, 1996.

[56] R. M. Gray, “On the asymptotic eigenvalue distribution of Toeplitz matrices,” *IEEE Transactions on Information Theory*, vol. IT-18, pp. 725-730, June 1972.

[57] U. Grenander and G. Szegö, *Toeplitz Forms and Their Applications*, Berkeley, California: University of California Press, 1958.

[58] J. Gutiérrez-Gutiérrez and P. M. Crespo, “Asymptotically equivalent sequences of matrices and Hermitian block Toeplitz matrices with continuous symbols: Applications to MIMO systems,” *IEEE Transactions on Information Theory*, vol. 54, pp. 5671-5680, Dec. 2008.

[59] D. Hajela, “Some new results on faster than Nyquist signaling,” in *Proc. Conference on Information Sciences and Systems*, Baltimore, MD, pp. 399-403, Mar. 1987.

[60] D. Hajela, “Exponential sums and faster than Nyquist signaling,” in *Proc. New York Number Theory Seminar*, New York City, NY, pp. 64-75, 1989.

[61] D. Hajela, “On computing the minimum distance for faster than Nyquist signaling,” *IEEE Transactions on Information Theory*, vol. 36, pp. 289-295, Mar. 1990.

[62] D. Hajela, “On faster than Nyquist signaling: Computing the minimum distance,” *Journal of Approximation Theory*, vol. 63, pp. 108-120, Oct. 1990.

[63] D. Hajela, “On faster than Nyquist signaling: Further estimations on the minimum distance,” *SIAM Journal on Applied Mathematics*, vol. 52, pp. 900-907, June 1992.

[64] M. Hamamura and S. Tachikawa, “Bandwidth efficiency improvement for multi-carrier systems,” in *Proc. IEEE International Symposium on Personal, Indoor and Mobile Radio Communications,* Barcelona, Spain, pp. 48-52, Sept. 2004.

[65] F.-M. Han and X.-D. Zhang, “Wireless multicarrier digital transmission via Weyl-Heisenberg frames over time-frequency dispersive channels,” *IEEE Transactions on Communications*, vol. 57, pp. 1721-1733, June 2009.

[66] W. Hirt and J. L. Massey, “Capacity of the discrete-time Gaussian channel with intersymbol interference,” *IEEE Transactions on Information Theory*, vol. 34, pp. 380-388, May 1988.

[67] H. Imai and S. Hirakawa, "A new multilevel coding method using error correcting codes," *IEEE Transactions on Information Theory*, vol. IT-23, pp. 371-377, May 1977.

[68] International Telecommunications Union, "Key ICT indicators for developed and developing countries and the world (totals and penetration rates)," 2012. [Online]. Available: http://www.itu.int/ITU-D/ict/statistics/at_glance/KeyTelecom.html.

[69] S. Isam and I. Darwazeh, "Precoded spectrally efficient FDM system," in *Proc. IEEE International Symposium on Personal, Indoor and Mobile Radio Communications*, Istanbul, Turkey, pp. 99-104, Sept. 2010.

[70] A. J. Jerri, "The Shannon sampling theorem – its various extensions and applications: A tutorial review," *Proceedings of the IEEE*, vol. 65, pp.1565-1596, Nov. 1977.

[71] W. Jian, Y. Xun, Z. Xi-Lin, and D. Li, "The prefix design and performance analysis of DFT-based overlapped frequency division multiplexing (OvFDM-DFT) system," in *Proc. International Workshop on Signal Design and Its Applications in Communications*, pp. 361-364, Sept. 2007.

[72] P. Kabal and S. Pasupathy, "Partial-response signaling," *IEEE Transactions on Communication*, vol. COM-23, pp. 921-934, Sept. 1975.

[73] I. Kanaras, A. Chorti, M. Rodrigues, and I. Darwazeh, "Spectrally efficient FDM signals: Bandwidth gain at the expense of receiver complexity," in *Proc. IEEE International Conference on Communications*, Dresden, Germany, pp. 3701-3706, June 2009.

[74] Y. J. D. Kim and J. Bajcsy, "Spectral analysis of pre-coded faster than Nyquist signaling," in *Proc. Summer School on Communication and Information Theory*, Banff, AB, pp. 47-48, Aug. 2009.

[75] Y. J. D. Kim and J. Bajcsy, “Achieving spread spectrum signal generation & reception using faster than Nyquist signaling,” in *Proc. Summer School on Communication and Information Theory*, Banff, AB, pp. 15-16, Aug. 2010.

[76] Y. J. D. Kim and J. Bajcsy, “On spectrum broadening of pre-coded faster-than-Nyquist signaling,” in *Proc. IEEE Vehicular Technology Conference Fall*, Ottawa, ON, 5 pages, Sept. 2010.

[77] Y. J. D. Kim and J. Bajcsy, “Information rates of cyclostationary faster-than-Nyquist signaling,” in *Proc. Canadian Workshop on Information Theory*, Kelowna, BC, pp 1-4, May 2011.

[78] Y. J. D. Kim and J. Bajcsy, “Faster than Nyquist broadcast signaling,” in *Proc. Queen's Biennial Symposium on Communications*, Kingston, Ontario, pp. 186-189, May 2012.

[79] Y. J. D. Kim and J. Bajcsy, “An architecture for faster than Nyquist Turbo broadcasting,” in *Proc. International Symposium on Turbo Codes & Iterative Information Processing*, Gothenburg, Sweden, pp. 170-175, Aug. 2012.

[80] Y. J. D. Kim and J. Bajcsy, “An iterative receiver for faster-than-Nyquist broadcasting,” *IET Electronics Letters*, vol. 48, pp. 1561-1562, Nov. 2012.

[81] Y. J .D. Kim and J. Bajcsy, “Binary faster than Nyquist optical transmission via non-uniform power allocation,” in *Proc. Canadian Workshop on Information Theory*, Toronto, ON, pp. 191-196, June 2013.

[82] Y. J. D. Kim, J. Bajcsy, and A. A. Garba, “A method and apparatus for increasing data transmission rates over continuous-time communication channels,” *Report of Invention, Invention No. 09043*, McGill University, Oct. 2008.

[83] Y. J. D. Kim, J. Bajcsy, and A. A. Garba, “Multiplied rate data transmission system,” *US Provisional Patents, US 61359134, US 61501806, US 61639137*, filed on June 2010, June 2011, and Apr. 2012.

[84] Y. J. D. Kim, J. Bajcsy, and A. A. Garba, “Methods and devices for communications systems using multiplied rate transmission,” *PCT International Patent Application filed through the Patent Cooperation Treaty* on Apr. 29, 2013.

[85] Y. J. D. Kim, S. El-Dabbagh, and J. Bajcsy, “Towards real-time faster-than-Nyquist transmission,” *Poster Presentation at SYTACom Annual Research Workshop*, Quebec City, QC, Sept. 2012.

[86] Y. J. D. Kim and J. Bajcsy, “Spectral analysis and applications of precoded faster than Nyquist signals,” in preparation for submission to the *IEEE Transactions on Communications*.

[87] Y. J. D. Kim and J. Bajcsy, “A faster-than-Nyquist approach to transmission over K-user Gaussian broadcast channels,” in preparation for submission to the *IEEE Transactions on Communications.*

[88] R. Koetter, A. C. Singer, and M. Tüchler, “Turbo equalization,” *IEEE Signal Processing Magazine*, vol. 20, pp. 67-80, Jan. 2004.

[89] V. A. Kotel’nikov, “On the transmission capacity of ‘ether’ and wire in electrocommunications,” (material for the first all-union conference on questions of communications), *Izd. Red. Upr. Svyazi RKKA*, Moscow, Russia, 1933.

[90] F. R. Kschischang and S. Pasupathy, “Optimal nonuniform signaling for Gaussian channels,” *IEEE Transactions on Information Theory*, vol. 39, pp. 913-929, May 1993.

[91] H. J. Landau, “Sampling, data transmission, and Nyquist rate,” *Proceedings of the IEEE*, vol. 55, pp. 1701-1706, Oct. 1967.

[92] I. Lee, “The effect of a pre-coder on serially concatenated coding systems with an ISI channel,” *IEEE Transactions on Communications*, vol. 49, pp. 1168-1175, July 2001.

[93] J.-H. Lee and Y.-H. Lee, “Design of multiple MMSE subequalizers for faster-than-Nyquist-rate transmission,” *IEEE Transactions on Communications*, vol. 52, pp. 1257-1264, Aug. 2004.

[94] J. Li, E. Tipsuwannakul, M. Karlsson, and P. A. Andrekson, “Exploiting the faster-than-Nyquist concept in Wavelength-Division Multiplexing systems using duobinary shaping,” *ZTE Communications,* vol. 10, pp. 23-29, Mar. 2012.

[95] S. Lin and D. J. Costello, Jr., *Error Control Coding,* 2nd ed. Englewood Cliffs, NJ: Prentice Hall, 2004.

[96] A. D. Liveris and C. N. Georghiades, “Exploiting faster-than-Nyquist signaling,” *IEEE Transactions on Communications*, vol. 51, pp. 1502−1511, Sept. 2003.

[97] R. M. Loynes, “On the concept of the spectrum for nonstationary processes,” *Journal of the Royal Statistical Society: Series B*, vol. 30, pp. 1-20, 1968.

[98] R. W. Lucky, “Decision feedback and faster-than-Nyquist transmission,” in *Proc. IEEE International Symposium on Information Theory*, Noordwijk, the Netherlands, Paper 7.6, June 1970.

[99] J. E. Mazo, “Faster-than-Nyquist signaling,” *The Bell System Technical Journal*, vol. 54, pp. 1451-1462, Oct. 1975.

[100] J. E. Mazo and H. J. Landau, “On the minimum distance problem for faster-than-Nyquist signaling,” *IEEE Transactions on Information Theory*, vol. 34, pp. 1420-1427, Nov. 1988.

[101] M. McGuire and M. Sima, “Discrete time faster-than-Nyquist signalling,” in *Proc. IEEE Global Telecommunications Conference*, Miami, Florida, 5 pages, Dec. 2010.

[102] L. Mirsky, “A trace inequality of John von Neumann,” *Monatshefte für Mathematik*, vol. 79, pp. 303-306, 1975.

[103] G. E. Moore, “Cramming more components onto integrated circuits,” *Electronics Magazine*, vol. 38, 4 pages, Apr. 1965.

[104] K. R. Narayanan, “Effect of pre-coding on the convergence of Turbo equalization for partial response channels,” *IEEE Journal on Selected Areas in Communications*, vol. 19, pp. 686-698, Apr. 2001.

[105] H. Nyquist, “Certain factors affecting telegraph speed,” *The Bell System Technical Journal*, vol. 3, pp. 324-346, Apr. 1924.

[106] H. Nyquist, “Certain topics in telegraph transmission theory,” *Transactions of the American Institute of Electrical Engineers,* vol. 47, pp. 617-644, Feb. 1928.

[107] A. V. Oppenheim, A. S. Wilsky, and S. H. Nawab, *Signals and Systems*, 2nd ed. Prentice Hall, 1997.

[108] R. L. Pickholtz, D. L. Schilling, and L. B. Milstein, “Theory of spread-spectrum communications − a tutorial,” *IEEE Transactions on Communications*, vol. COM-30, pp. 855-884, May 1982.

[109] M. S. Pinsker, *Information and Information Stability of Random Variables and Processes*, San Francisco, CA: Holden-Day, 1964.

[110] M. Plumb, “Fantastic 4G,” *IEEE Spectrum,* vol. 49, pp. 51-53, January 2012.

[111] M. B. Priestley, “Evolutionary spectra and non-stationary processes,” *Journal of the Royal Statistical Society: Series B*, vol. 27, pp. 204-229, 1965.

[112] A. Prlja, J. B. Anderson, and F. Rusek, “Receivers for faster-than-Nyquist signaling with and without Turbo equalization,” in *Proc. IEEE International Symposium on Information Theory*, Toronto, ON, pp. 464-468, July 2008.

[113] J. G. Proakis and M. Salehi, *Communication Systems Engineering*, 2nd ed. Upper Saddle River, NJ: Prentice Hall, 2002.

[114] M. Ramezani and M. Ardakani, "Disjoint LDPC coding for Gaussian broadcast channels," in *Proc. IEEE International Symposium on Information Theory*, Seoul, Korea, pp. 938-942, July 2009.

[115] C. R. Rao and S. K. Mitra, *Generalized Inverse of Matrices and its Applications*, New York: Wiley, 1971.

[116] D. Raphaeli and Y. Zarai, "Combined Turbo equalization and Turbo decoding," *IEEE Communications Letter*, vol. 2, pp. 107-109, Apr. 1998.

[117] P. Robertson and T. Wörz, "Bandwidth-efficient Turbo trellis-coded modulation using punctured component codes," *IEEE Journal on Selected Areas in Communications*, vol. 16, pp. 206–218, Feb. 1998.

[118] M. R. D. Rodrigues and I. Darwazeh, "A spectrally efficient frequency division multiplexing based communication system," in *Proc. International OFDM Workshop*, Hamburg, Germany, pp. 70-74, 2003.

[119] W. Rudin, *Real and Complex Analysis*. 3rd ed. New York: McGraw-Hill, 1987.

[120] W. D. Rummler, R. P. Coutts, and M. Liniger, "Multipath fading channel models for microwave digital radio," *IEEE Communications Magazine*, vol. 24, pp. 30-42, Nov. 1986.

[121] M. Rumney, "IMT-Advanced: 4G wireless takes shape in an Olympic year," *Agilent Measurement Journal*, pp. 51-60, Sept. 2008. [Online] Available: http://www.agilent.com/go/journal.

[122] F. Rusek, "Partial response and faster-than-Nyquist signaling," Ph.D. dissertation, Lund University, Lund, Sweden, Sept. 2007.

[123] F. Rusek and J. B. Anderson, "The two dimensional Mazo limit," in *Proc. IEEE International Symposium on Information Theory*, Adelaide, Australia, pp. 970-974, Sept. 2005.

[124] F. Rusek and J. B. Anderson, "Successive interference cancellation in multistream faster-than-Nyquist signaling," in *Proc. the International Conference on Wireless Communications and Mobile Computing*, Vancouver, BC, pp. 1021-1026, July 2006.

[125] F. Rusek and J. B. Anderson, "Serial and parallel concatenations based on faster than Nyquist signaling," in *Proc. IEEE International Symposium on Information Theory*, Seattle, WA, pp. 1993-1997, July 2006.

[126] F. Rusek and J. B. Anderson, "Non binary and pre-coded faster than Nyquist signaling," *IEEE Transactions on Communications*, vol. 56, pp. 808−817, May 2008.

[127] F. Rusek and J. B. Anderson, "Constrained capacities for faster-than-Nyquist signaling," *IEEE Transactions on Information Theory*, vol. 55, pp. 764-775, Feb. 2009.

[128] F. Rusek and J. B. Anderson, "Multistream faster than Nyquist signaling," *IEEE Transactions on Communications*, vol. 57, pp. 1329-1340, May 2009.

[129] B. R. Saltzberg, "Intersymbol interference error bounds with application to ideal bandlimited signaling," *IEEE Transactions on Information Theory*, vol. 14, pp. 563-568, July 1968.

[130] J. Salz, "Optimum mean-square decision feedback equalization," *The Bell System Technical Journal*, vol. 52, pp. 1341-1373, Oct. 1973.

[131] S. Shamai, L. H. Ozarow, and A. D. Wyner, "Information rates for a discrete-time Gaussian channel with intersymbol interference and stationary inputs," *IEEE Transactions on Information Theory*, vol. 37, pp. 1527-1539, Nov. 1991.

[132] C. E. Shannon, "A mathematical theory of communication," *The Bell System Technical Journal*, vol. 27, pp. 379-423, 623-656, July and October 1948.

[133] C. E. Shannon, "Communication in the presence of noise," *Proceedings of the IRE*, vol. 37, pp. 10-21, Jan. 1949.

[134] D. Slepian, H. J. Landau, and H. Pollak, "Prolate spheroidal wave functions, Fourier analysis and uncertainty − I", *The Bell System Technical Journal*, vol. 40, pp. 43-64, Jan. 1961.

[135] D. Slepian, H. J. Landau, and H. Pollak, "Prolate spheroidal wave functions, Fourier analysis and uncertainty − II", *The Bell System Technical Journal*, vol. 40, pp. 65-84, Jan. 1961.

[136] B. P. Smith and F. R. Kschischang, "Future prospects for FEC in fiber-optic communications," *IEEE Journal of Selected Topics in Quantum Electronics*, vol. 16, pp.1245-1257, Sept./Oct. 2010.

[137] J. Spero, "The time for mobile is now," presented at Think Mobile with Google, New York, NY, Feb. 2011. [Online] Available: http://www.google.com/events/thinkmobile2011/presentations.html.

[138] T. W. Sun, R. D. Wesel, M. R. Shane, and K. Jarett, "Superposition Turbo TCM for multirate broadcast," *IEEE Transactions on Communications*, vol. 52, pp. 368-371, Mar. 2004.

[139] O. Y. Takeshita and D. J. Costello, Jr., "New deterministic interleaver designs for Turbo codes," *IEEE Transactions on Information Theory*, vol. 46, pp. 1988-2006, Sept. 2000.

[140] *Technical White Paper: Long Term Evolution (LTE): A Technical Overview*, Motorola, Inc., retrieved June 2012.

[141] İ. E. Telatar, "Capacity of multi-antenna Gaussian channels," *European Transactions on Telecommunications*, vol. 10, pp. 585-595, Nov.-Dec. 1999.

[142] S. ten Brink, "Rate one-half code for approaching the Shannon limit by 0.1 dB," *IET Electronics Letters*, vol. 36, pp. 1293-2394, July 2000.

[143] S. ten Brink, "Designing iterative decoding schemes with the Extrinsic Information Transfer Chart," *AEÜ International Journal of Electronics and Communications*, vol. 54, pp. 389-398, Nov. 2000.

[144] S. ten Brink, "Convergence behavior of iteratively decoded parallel concatenated codes," *IEEE Transactions on Communications*, vol. 49, pp. 1727-1737, Oct. 2001.

[145] Third Generation Partnership Project, "3GPP home page," http://www.3gpp.org.

[146] Third Generation Partnership Project, "Technical specification group radio access network; Multiplexing and channel coding (FDD)," *Technical Specification,* 3GPP TS 25.212, ver. 7.0.0, Mar. 2006.

[147] *Transmission Performance Characteristics of Pulse Code Modulation*, ITU-T Recommendation G.712, Sept. 1992.

[148] L. N. Trefethen and D. Bau, III, *Numerical Linear Algebra*, SIAM, 1997.

[149] D. W. Tufts, "Nyquist's problem − the joint optimization of transmitter and receiver in pulse amplitude modulation," *Proceedings of the IEEE*, vol. 53, pp. 248-259, Mar. 1965.

[150] D. W. Tufts, "On 'Sampling, Data Transmission, and the Nyquist Rate' and adaptive communication using randomly time-varying channels," *Proceedings of the IEEE*, vol. 56, pp. 889, May 1968.

[151] G. Ungerboeck, "Adaptive maximum likelihood receiver for carrier-modulated data-transmission systems," *IEEE Transactions on Communications*, vol. 22, pp. 624–636, May 1974.

[152] M. Uppal, V. Stanković, and Z. Xiong, "Code design for MIMO broadcast channels," *IEEE Transactions on Communications*, vol. 57, pp. 986-996, Apr. 2009.

[153] M. C. Valenti and J. Sun, "The UMTS turbo code and an efficient decoder implementation suitable for software-defined radio," *International Journal of Wireless Information Networks*, vol. 8, pp. 203-215, Oct. 2001.

[154] J. M. Varah, "The prolate matrix," *Linear Algebra and its Applications*, vol. 187, pp. 169-278, July 1993.

[155] A. J. Viterbi, "Convolutional codes and their performance in communication systems," *IEEE Transactions on Communications*, vol. COM-19, pp. 751-772, Oct. 1971.

[156] U. Wachsmann, R. F. H. Fischer, and J. B. Huber, "Multilevel codes: Theoretical concepts and practical design rules," *IEEE Transactions on Information Theory*, vol. 45, pp. 1361-1391, July 1999.

[157] C. Walter, "Kryder's law," *Scientific American*, vol. 293, pp. 32-33, Aug. 2005.

[158] C.-K. Wang and L.-S. Lee, "Practically realizable digital transmission significantly below the Nyquist bandwidth," *IEEE Transactions on Communications*, vol. 43, pp. 166−169, Feb./Mar./Apr. 1995.

[159] J. Wang, S. X. Ng, A. Wolfgang, L. L. Yang, S. Chen, and L. Hanzo, "Near-capacity three-stage MMSE Turbo equalization using irregular convolutional codes," in *Proc. ITG Turbo Coding Conference*, Munich, Germany, 6 pages, Apr. 2006.

[160] P. D. Welch, "The use of Fast Fourier Transform for the estimation of power spectra: A method based on time averaging over short, modified periodograms," *IEEE Transactions on Audio and Electroacoustics*, vol. 15, pp. 70-73, June 1967.

[161] E. T. Whittaker, "On the functions which are represented by the expansion of interpolating theory," *Proceedings of the Royal Society of Edinburgh*, vol. 35, pp. 181-194, 1915.

[162] R. Wooding, "The multivariate distribution of complex normal variables," *Biometrika*, vol. 43, pp. 212-215, 1956.

[163] J. M. Wozencraft and I. M. Jacobs, *Principles of Communication Engineering*. New York: Wiley, 1965.

[164] K.-T. Wu and K. Feher, "Multilevel PRS/QPRS above the Nyquist rate," *IEEE Transactions on Communications*, vol. 33, pp. 735-739, July 1985.

[165] Y. G. Yoo and J. H. Cho, "Asymptotic optimality of binary faster-than-Nyquist signaling," *IEEE Communications Letters,* vol. 14, pp. 788-790, Sept. 2010.

[166] R. Zamir, S. Shamai (Shitz), and U. Erez, "Nested linear/lattice codes for structured multiterminal binning," *IEEE Transactions on Information Theory*, vol. 48, pp. 1250-1276, June 2002.